

Hip simulator wear testing of the taper-trunnion junction and bearing surfaces of modular hip prostheses

Rohan Mangesh Bhalekar

**This thesis is submitted in partial fulfilment of the requirements for the
Degree of Doctor of Philosophy**

**Newcastle University
School of Engineering**

January 2020

Abstract

Adverse reaction to metal debris (ARMD) released from the taper-trunnion junction of modular total hip replacements (THR) is an issue of contemporary concern, not only in metal-on-metal (MoM) but in ceramic-on-ceramic (CoC) and metal-on-cross linked polyethylene (MoP) THR. Moreover, there is no consensus in the literature regarding the mechanisms behind material loss at the taper-trunnion junction.

The aim of this research work to investigate the material loss, if any, at the taper-trunnion junction of modular CoC and MoP THR under physiological walking cycles. Following ISO-14242, material loss from the bearing surfaces was also quantified alongside surface topographical and microscopic analysis.

After 5 million cycles, the mean material loss from the ceramic bearing surfaces was 0.25mm^3 , and from the metallic trunnions, it was 0.29mm^3 in the CoC hip simulator test. The three-dimensional surface roughness (Sa) of the trunnions on the unworn and worn areas showed a statistically significant decrease from 0.558 ± 0.060 to $0.312 \pm 0.028\mu\text{m}$ respectively ($p < 0.001$). In the MoP hip simulator test, the mean material loss from the polymeric liners, metallic tapers and trunnions were 14.28 , 0.22 and 0.24mm^3 respectively. The Sa of the femoral tapers on the unworn and worn areas showed a statistically significant increase from 0.510 ± 0.068 to $0.867 \pm 0.233\mu\text{m}$ respectively ($p < 0.001$).

Until this research, no long-term hip simulator tests had quantified material loss from the taper-trunnion junction of commercially available modular CoC and MoP THR. Metallic material loss from the taper-trunnion junctions of CoC and MoP THR may explain the ARMD reported in the literature for these THR. Material loss at the taper-trunnion junction needs to be measured in preclinical testing using the hip simulator to avoid ARMD and further increase the longevity of modular THR. Based on the results, the mechanisms responsible for the material loss at the metallic taper still a multivariable process.

List of Publications

Bhalekar RM, Smith SL, Joyce TJ. “Wear at the taper-trunnion junction of contemporary ceramic-on-ceramic hips shown in a multistation hip simulator.” *Journal of Biomedical Materials Research Part B Applied Biomaterials*. 2019;107(4):1199-209.

Bhalekar RM, Smith SL, Joyce TJ. “Hip simulator testing of the taper-trunnion junction and bearing surfaces of contemporary metal-on-cross-linked-polyethylene hip prostheses.” *Journal of Biomedical Materials Research Part B Applied Biomaterials*. 2019;0(0). (in press)

Bhalekar RM, Stewart TJ, Dell’Aquila C, Smith SL, Joyce TJ. “Evaluation of the material loss from the cobalt-chromium-molybdenum femoral taper of modular metal-on-polyethylene hip prostheses subject to a controlled hip simulator test.” (in preparation)

List of Major Presentations

Bhalekar RM, Smith, SL, Langton DJ, Joyce TJ. “Quantification of Material Loss from the Femoral Taper of Modular Metal-on-Polyethylene Hips tested in a Hip Simulator.” *Society for Biomaterials (SFB) Annual Meeting and Exposition*, Seattle, USA, 2019.

Bhalekar RM, Smith SL, Joyce TJ. “Taper-trunnion junction and bearing surface wear measurement of metal-on-cross-linked polyethylene total hip arthroplasties in a hip joint simulator.” *Orthopaedic Proceedings* 2019;101-B(SUPP_5):17-17. *International Society for Technology in Arthroplasty (ISTA) 31st annual conference*, London, UK, 2018.

Bhalekar RM, Smith, SL, Joyce TJ. “In vitro wear at the taper-trunnion junction of biolox delta hips shown in a multi-station hip simulator.” *Orthopaedic Proceedings* 2019;101-B(SUPP_5):16-16. *International Society for Technology in Arthroplasty (ISTA) 31st annual conference*, London, UK, 2018.

Acknowledgements

First and foremost, I would like to deeply thank my supervisor, Prof Tom Joyce for taking a chance on me. I greatly appreciate that you always had time for me (even during holidays), encouraged me with your priceless ideas and motivated to write research papers. Words cannot ‘quantify’ how helpful your guidance, advice and support has been.

To Dr Simon Smith, my co-supervisor, thank you for being a good mentor and training me on the hip simulator. Thank you for all the support, encouragement and mainly for sharing many mantras such as ‘7 Ps’ and ‘KISS principle’, I will always keep that in mind.

I give my sincere thanks to the School of Engineering, Newcastle University, for providing PhD studentship. I would like to acknowledge Dr Theodora Stewart and Dr Caterina Dell’Aquila from London Metallomics Facility (Kings College London) and Mark Minta (University of Surrey) for conducting metal debris analysis. Special thanks to Mr Michael Foster for acquiring data from the scanning electron microscope. I also thank Mr Christopher Aylott for cutting the femoral heads. I am truly grateful to the Peter Jost Travel Fund for their support towards attending SFB conference.

To Dr Susan Scholes, my ex-co-supervisor, thank you for being a good mentor and always being there to listen. Special thanks to Dr David Langton for generously sharing your time and expertise on the taper-trunnion junction as well as exchanging emails during cricket matches. I also thank Stephen Wells for training me on the CMM and helping me whenever I needed. I would like to thank Mr James Holland for inviting me to see the THR surgery at Freeman Hospital. I am truly grateful to mechanical workshop technicians Messrs. Stuart Baker, Stephen Charlton, Stephen Harrison, Stephen Moore, James Rose, Lewis Sholder, and Brian Stoker for technical assistance throughout my research and sharing thoughts on every MCU movies. I am also grateful to many members of the Bioengineering group for providing feedback on my research during group meetings as well as PGR conferences.

I would like to appreciate Geebee Education, mainly my study abroad counsellor Kapil Dedhia for supporting me and sharing the email of this PhD studentship which changed my life. I also thank Krina Vira for always helping me with Visa applications. To Kartik Poojari, thank you for coming to the airport to receive a stranger (me) and helping me to settle down in the “Toon”. I also thank Prasanna for accommodating me when I first arrived. I am also grateful to Arathi for delicious food and continued friendship.

I am thankful to all my M55 office mates Ben, Shannen, James, Emma, Alex, Lewis, Wan, Xiaoyan for their friendship, insights, and support. To Nilly, it was unbelievable to meet you again here after MSc and thank for giving neck massage, especially while writing up this thesis. Special thanks to my Mexican brother, Israel for accommodating me in your room during ISTA and always having my back.

To Mrs Kathryn Chamberlain, my ‘the’ best friend, I do not have words to say thank you. I would not have finished this PhD journey without you: Iron Man and GK- the inseparable coffee buddies. Still, a big thank you for driving me in, proofreading, ‘there there’ after meetings, Krispy Kreme’s and always being there for me.

Last but not least, I would like to express my warmest thanks to my parents Mangesh and Lata, my sister Ashwini, my cousins, to all Bhalekar’s and my in-laws Chemburkar’s for their unwavering support, love, and faith. Special thanks to my Papa for always pushing me for higher education, without your encouragement and support, this would not have been possible. I also thank Shende Guruji for your blessings and for looking out for me.

And to my wife, Dnyanda, my friend since kindergarten, thanks for always listening me talking about research (although you had no clue), supporting me, understanding me, encouraging me and taking care of me. But more than that, thank you for trusting and believing in me even when I could not. You are a true friend.

Table of Contents

CHAPTER 1:INTRODUCTION	1
1.1 Overview	1
1.2 Aim and Objectives	3
1.2.1 Aim	4
1.2.2 Objectives	4
1.2.3 Research questions	6
1.3 The organisation of the thesis	6
1.4 Declaration	7
CHAPTER 2:LITERATURE REVIEW	8
2.1 Nomenclature for the anatomy of the hip joint	8
2.2 The natural hip joint	9
2.2.1 Anatomy of the natural hip joint ^{46,47}	10
2.2.2 Hip joint disorders and the need for hip arthroplasty	15
2.3 Total hip replacement (THR)	18
2.3.1 An introduction to THR prostheses	18
2.3.2 A brief history of hip arthroplasty	23
2.3.3 Types of THR prostheses	24
2.3.4 Materials in THR	26
2.3.5 Potential causes of failure of primary THR and revision THR	35
2.4 Biotribology and <i>in vitro</i> wear testing of THRs	39
2.4.1 Wear	40
2.4.2 Wear screening devices	42
2.4.3 The human gait cycle and hip joint wear simulators	43
2.4.4 Ceramic-on-ceramic (CoC) THR	54
2.4.5 Metal-on-polyethylene (MoP) THR	56
2.4.6 Friction	58

2.4.7	Lubrication	58
2.4.8	Wettability and THR	62
2.5	Head-neck modularity for total hip replacement: taper-trunnion junction	66
2.5.1	The taper-trunnion junction of the modular hip prostheses	66
2.5.2	Contact mechanics	69
2.5.3	Material loss from the taper-taper trunnion junction of modular hip prostheses	71
2.6	Mechanism responsible for the material loss released from the taper-taper trunnion junction of modular hip prostheses	72
2.6.1	Various theories for the material loss from the metallic taper-trunnion junction reported in the literature	72
2.6.2	Factors affecting the material loss from the taper- trunnion junction of modular hip prostheses	78
2.6.3	Quantification and evaluation of the material loss from the taper-trunnion junction.	81
2.7	What can <i>in vitro</i> studies tell us about what happens <i>in vivo</i>?	87
2.8	Summary	89
CHAPTER 3:	MATERIALS AND METHODS	91
3.1	Hip simulator wear testing of the taper-trunnion junction and bearing surfaces of modular CoC hip prostheses	91
3.1.1	Materials	91
3.1.2	Hip simulator wear test	94
3.1.3	Quantification of the material loss from the taper-trunnion junction and bearing surfaces	97
3.1.4	Visual and microscopic analysis of Ti trunnions	98
3.1.5	Surface roughness measurement	99
3.2	Dynamic loading (DL) but no articulating motion testing of CoC hip prosthesis	99
3.2.1	Materials	99
3.2.2	Test summary	99

3.3	Impaction test of CoC hip prosthesis	101
3.3.1	Materials	101
3.3.2	Test summary	101
3.4	Hip simulator wear testing of the taper-trunnion junction and bearing surfaces of modular metal-on-cross-linked polyethylene hip prostheses	101
3.4.1	Materials	102
3.4.2	Hip simulator wear test	105
3.4.3	Quantification of the material loss from the taper-trunnion junction and bearing surfaces	107
3.4.4	Visual and microscopic analysis of CoCrMo femoral tapers	108
3.4.5	Surface roughness measurement	109
3.4.6	Microscopic inspection of the backside of the XLPE liner	109
3.5	Metal debris analysis	109
3.6	Lubricant pH measurement	110
3.7	Wettability measurement	111
3.8	The six-station anatomical hip simulator	112
3.8.1	Installation of the hip prostheses on the hip simulator	112
3.8.2	Description of the hip simulator loading and motions	115
3.8.3	Assembly and disassembly procedures	118
3.9	Quantification of the material loss from the taper-trunnion junction of hip prostheses using geometric wear measurement	119
3.9.1	Materials	119
3.9.2	Methods	121
3.10	Surface roughness analyses	125
3.10.1	Two-dimensional (2D) surface roughness (Ra) measurements	125
3.10.2	Three-dimensional (3D) surface roughness (Sa) measurements	127
3.11	Statistical methods	128
CHAPTER 4:	RESULTS	129

4.1 Hip simulator wear testing of the taper-trunnion junction and bearing surfaces of modular CoC hip prostheses	129
4.1.1 Quantification of the material loss from the taper-trunnion junction	129
4.1.2 Visual and microscopic inspection of the taper-trunnion junction	131
4.1.3 Two-dimensional (2D) surface roughness (Ra) of ceramic femoral tapers and Ti trunnions	136
4.1.4 Three-dimensional (3D) surface roughness (Sa) of Ti trunnions	137
4.1.5 Quantification of the material loss from the bearing surfaces	139
4.1.6 Three-dimensional (3D) surface roughness (Sa) of the bearing surfaces	142
4.2 Dynamic loading (DL) but no articulating motion testing of ceramic-on-ceramic (CoC) hip prosthesis	144
4.2.1 Quantification of the material loss from ceramic femoral head, acetabular liner and Ti trunnion	145
4.2.2 Two-dimensional (2D) surface roughness (Ra) of ceramic femoral taper and Ti trunnion	146
4.2.3 Three-dimensional (3D) surface roughness (Sa) of the CoC bearing surfaces	147
4.2.4 Comparison of the material loss from Ti trunnions used in CoC hip simulator wear test and DL test.	148
4.3 Impaction test	149
4.4 Hip simulator wear testing of the taper-trunnion junction and bearing surfaces of modular metal-on-cross-linked polyethylene (MoXLPE) hip prostheses	151
4.4.1 Quantification of the material loss from the taper-trunnion junction	152
4.4.2 Two-dimensional (2D) surface roughness (Ra) of the CoCrMo femoral tapers	154
4.4.3 Three-dimensional (3D) surface roughness (Sa) of the CoCrMo femoral tapers	155
4.4.4 Visual and microscopic inspection of the CoCrMo femoral tapers	156
4.4.5 Energy-dispersive X-ray spectroscopy (EDX) analysis of the CoCrMo femoral tapers	158
4.4.6 Quantification of the material loss from the bearing surfaces	165
4.4.7 Three-dimensional (3D) surface roughness (Sa) of the bearing surfaces	168
4.4.8 Microscopic inspection of the backside of the XLPE liner	171
4.5 Metal debris analysis	171

4.5.1	Ceramic-on-ceramic (CoC) hip simulator wear test	171
4.5.2	Metal-on-cross-linked polyethylene (MoXLPE) hip simulator wear test	172
4.6	Lubricant pH measurement	173
4.7	Wettability measurement	175
CHAPTER 5:DISCUSSION		176
5.1	Hip simulator wear testing of the taper-trunnion junction and bearing surfaces of modular CoC hip prostheses	176
5.1.1	Wear at the taper-trunnion junction of CoC prostheses used in the hip simulator wear test: ceramic-on-metal contact.	177
5.1.2	A possible explanation for adverse reaction to metal debris (ARMD) in CoC hip implants	179
5.1.3	Wear at the bearing surfaces of CoC joints used in the hip simulator wear test	180
5.2	Importance of the DL test	182
5.3	Importance of the impaction test	182
5.3.1	Metal debris analysis: CoC hip simulator wear test	183
5.4	Hip simulator wear testing of the taper-trunnion junction and bearing surfaces of modular MoXLPE hip prostheses	183
5.4.1	Wear of the CoCrMo femoral head: is it primarily from the bearing surface or the internal taper of the femoral head?	185
5.4.2	Metal release from the taper-trunnion junction of modular MoXLPE THRs.	187
5.4.3	Metal ion analysis: MoP hip simulator wear test	189
5.4.4	Radial clearance and its effect on the wear	189
5.4.5	The SEM coupled with EDX analysis of the CoCrMo femoral tapers	190
5.4.6	The appearance of imprint damage on the CoCrMo femoral tapers.	192
5.4.7	A possible explanation for the material loss from the CoCrMo femoral taper	192
5.4.8	Wear at the bearing surfaces of cross-linked polyethylene liners	194
5.5	Metal debris analysis	194
5.6	Importance of lubricant pH measurement	196

5.7 Comparison of the metallic material loss from the taper-trunnion junction of contemporary CoC and MoXLPE THRs subject to a controlled hip simulator tests	197
5.8 Importance of wettability measurement of the femoral heads	197
5.9 Limitations	198
CHAPTER 6: CONCLUSIONS AND SUGGESTIONS FOR FURTHER WORK	200
6.1 Conclusions	200
6.1.1 The material loss at the taper-trunnion junction of contemporary CoC hips shown in a multistation hip simulator	200
6.1.2 The necessity of employing articulating motion for the quantification of material loss from the taper-trunnion junction	201
6.1.3 The material loss at the taper-trunnion junction of contemporary MoXLPE hips shown in a multistation hip simulator	201
6.1.4 Summary	202
6.2 Implications	203
6.3 Suggestions for further work	203
REFERENCES	205
APPENDIX A	232
APPENDIX B	233
APPENDIX C	234
APPENDIX D	235

List of Figures

Figure 1 Taper-trunnion junction of modular ceramic femoral head mounted on the metallic trunnion.	2
Figure 2 Anatomical planes of the human body showing coronal/frontal plane, sagittal plane and transverse/axial plane. Image from Drake (2010) ⁴⁶ .	8
Figure 3 The natural hip joint a) anterior view and b) posterior view. Images from Gray (2000) ⁴⁸ .	10
Figure 4 Acetabulum. Image from Drake (2010) ⁴⁶ .	11
Figure 5 The normal hip joint: Cross-sectional view showing the femoral neck angle. Image from Byrne et al. (2010) ⁵⁰ .	11
Figure 6 The femoral neck angle, a) normal, b) coxa vara and c) coxa valga. Image from Byrne et al. (2010) ⁵⁰ .	12
Figure 7 a) Synovial membrane and b) fibrous membrane of the hip joint. Image from Drake (2010) ⁴⁶ .	13
Figure 8 Ligaments of the hip joint a) Iliofemoral and pubofemoral ligament, and b) ischiofemoral ligament. Image from Drake (2010) ⁴⁶ .	13
Figure 9 The motions at the hip joint a) flexion-extension (FE), b) abduction-adduction (AA) and c) internal-external rotation (IER). Image from Drake (2010) ⁴⁶ .	14
Figure 10 X-rays (from left to right) showing the joint space narrowing (inside the red circle) due to osteoarthritis. Image from Altman and Gold (2007) ⁶³ .	15
Figure 11 Fractured neck of femur shown in the red circle. Image from Miller et al. (2005) ⁶⁹ .	16
Figure 12 The CONQUEST FN™ system launched by Smith & Nephew in June 2019. Image from Smith & Nephew (2019) ⁷² .	17
Figure 13 X-ray of a healthy femoral head (left) and collapsed femoral head (right) due to avascular necrosis. Image from OrthoInfo ⁷⁷ .	17
Figure 14 Total hip replacement and hip resurfacing prostheses. Image from Mattei et al. (2011) ⁸¹ .	19
Figure 15 Modularity at the neck-stem junction of commercially available femoral stems. Images from manufacturers websites respectively ^{84,85} .	20
Figure 16 Main components of total hip replacement prostheses showing CoC THR (left) and MoP THR (right).	21

Figure 17 Charnley's low friction THR a) the stainless-steel femoral component and b), c) and d) high-molecular-weight polyethylene acetabular component. Image from Campbell and Rothman (1971) ⁹⁸ .	24
Figure 18 Femoral heads with different diameters. Image from Affatato (2014) ¹⁰¹ .	25
Figure 19 The change in the hip bearing material combinations since 2009 recorded by the NJR. Image from the NJR 15 th Annual Report 2017/18 ⁵ .	26
Figure 20 Detailed timeline in terms of the NJR monitoring of ASR TM hip prostheses ¹²⁹ . (MHRA: Medicines and Healthcare products Regulatory Agency of the Department of Health and Social Care in the United Kingdom).	30
Figure 21 Generations of alumina ceramics used in hip replacement. Image from Ceramtec website.	31
Figure 22 Development of alumina ceramic. Image from Masson (2009) ¹³¹ .	31
Figure 23 Prevention mechanisms for the crack propagation (shown by the continuous red arrow) in BIOLOX ^{®delta} ceramic: a) transformation toughening and b) platelet reinforcement. 1. Alumina grain, 2. Zirconia grain and 3. Plate-like crystal. Image from Zimmer ¹³⁴ .	32
Figure 24 Chemical structure of ethylene and polyethylene. Image from Kurtz (2009) ¹³⁷ .	33
Figure 25 Processing of UHMWPE acetabular liners. a) UHMWPE resin powder, b) semi-finished UHMWPE rods that have been consolidated from the UHMWPE resin powder, c) Machining of the UHMWPE rods on a lathe, and d) UHMWPE acetabular liners after machining. Image from Kurtz (2009) ¹³⁷ .	33
Figure 26 Gamma (γ) or electron beam (Eb) radiation of UHMWPE. Image from Campbell et al. (2004) ¹⁴¹ .	35
Figure 27 Aseptic loosening at the femoral stem indicated by black arrows. Image from Vanrusselt et al. (2015) ¹⁴⁵ .	36
Figure 28 Risk of revision in a) cemented and b) uncemented prostheses by bearing surface as recorded by the NJR. Images from the NJR's 15 th Annual Report 2017/18 ⁵ .	39
Figure 29 a) and b) shows top and side views of pin-on-plate wear testing rig respectively and c) shows pin-on-disk rig from the Biotribology lab, Newcastle University.	43
Figure 30 Seven events in a Gait cycle. Image from Whittle (2014) ¹⁸³ .	45
Figure 31 Normal gait cycle. Image from Rajčúková et al. (2014) ¹⁸⁴ .	46
Figure 32 Comparison of the normal gait cycle with the hip simulator motion and forces: a) the three components of the hip force (W_x , W_y and W_z), scaled with respect to the	

body weight (BW) and corresponding hip angles taken from the ISO 14242-1 and c) normal gait cycle. Image from Mattei et al. (2011) ⁸¹ .	49
Figure 33 Vertical load (W_y) and FE angular velocity (ω_x) for BW= 750N according to ISO 14242-1. Image from Mattei et al. (2011) ⁸¹ .	50
Figure 34 Commercially available hip simulators. Images from manufacturers websites, respectively.	52
Figure 35 Different lubrication regimes. Image from Jin et al. 2006 ¹⁶⁵ .	59
Figure 36 An Idealised Stribeck curve showing different lubrication regimes. Image from Smith and Joyce (2017) ⁴¹ .	60
Figure 37 The Young's contact angle (Θ_Y), formed at the intersection of three interfacial forces: Y_{sv} : surface free energy of the solid, Y_{lv} : surface tension of the liquid and Y_{sl} : interfacial tension between solid and liquid interface.	63
Figure 38 Schematic views of a) superhydrophobic, b) hydrophobic, c) hydrophilic and d) superhydrophilic surfaces. Image from Asmatulu (2016) ²²⁶ .	64
Figure 39 The basic goniometer/ contact angle measurement instrument.	64
Figure 40 Schematic showing dimensions used for describing femoral tapers: D1= proximal diameter, D2= distal diameter, Θ = femoral taper angle Image from Triantafyllopoulos et al. (2015) ²³¹ .	67
Figure 41 Femoral taper and trunnion cone angles and associated mismatches: a) Tip locked, b) Matched and c) Base locked. Image adapted from Ashkanfar et al. (2017) ²³³ .	68
Figure 42 Smooth and rough trunnion with evaluation profile obtained using two-dimensional contacting profilometer, respectively. a) Smooth trunnion ($R_a = 0.520 \mu\text{m}$) and b) Rough trunnion ($R_a = 3.281 \mu\text{m}$).	69
Figure 43 Loading mechanics for the taper-trunnion junctions. M_B = bending moment due to friction at the bearing surfaces, F_J = joint force, F_C = axial compressive joint force along taper axis, F_B = bending component of the joint force, T = torsional moment due to friction at the bearing surfaces, x = axial distance from the femoral head center to the point of taper support. Taper axes are: A-P: anterior-posterior, and Sup-Inf: superior-inferior. Image adapted from Gilbert et al. (2015) ²³⁸ .	70
Figure 44 Mechanically Assisted Crevice Corrosion (MACC). Image adapted from Gilbert and Jacobs (1997) ²⁴⁹ .	74
Figure 45 Summary of Factors affecting the material loss from the taper-trunnion junction or neck-stem junction of modular hip prostheses. Image from Sultan et al. (2018) ²⁶⁹ .	78

Figure 46 From left to right: range of motion (in degrees) increases as the femoral head diameter (\varnothing) size (in mm) increases. Image from Altimed JSC ²⁷⁴ .	79
Figure 47 A sample image of ‘Goldberg score’ criteria. Examples of fretting and corrosion scores for metallic trunnions mounted on CoCrMo femoral heads. Image from Kurtz et al. (2013) ²⁵⁷ .	83
Figure 48 a) Ceramic femoral head (BIOLOX [®] <i>delta</i>), b) ceramic acetabular liner (BIOLOX [®] <i>delta</i>) and c) 12/14 Ti6Al4V trunnions.	91
Figure 49 Engineering drawing of the trunnion used in tests involving CoC THR.	93
Figure 50 The six-station anatomical hip joint simulator showing three CoC test components immersed in diluted new-born-calf serum ²⁹⁵ .	94
Figure 51 a) A test station from the hip simulator and b) schematic of the ceramic femoral head, ceramic acetabular liner, and Ti trunnion in the hip simulator wear test set up. All prostheses were subject to dynamic loading and articulating motion.	95
Figure 52 Surfaces of the BIOLOX [®] <i>delta ceramic liner</i> .	96
Figure 53 Gravimetric measurement of a ceramic acetabular liner using an analytical balance.	97
Figure 54 An example of a wear plot used for the wear rate calculations.	98
Figure 55 a) A DL station and b) schematic of the ceramic femoral head, ceramic acetabular liner, and Ti trunnion in the DL test set up	100
Figure 56 a) CoCrMo femoral head b) XLPE acetabular liner and c) 12/14 Ti6Al4V trunnion.	102
Figure 57 Engineering drawing of the trunnion used in tests involving MoXLPE THR.	104
Figure 58 The six-station anatomical hip joint simulator showing five MoXLPE test components immersed in diluted new-born-calf serum ³⁰⁰ .	105
Figure 59 a) A test station, b) schematic of CoCrMo femoral head, XLPE acetabular liner, and Ti trunnion in test and control station setup, and c) the control station.	106
Figure 60 A cut CoCrMo femoral head showing a) before polishing and b) after polishing the surface.	108
Figure 61 Contact angle measurement of BIOLOX [®] <i>delta</i> femoral head using Theta Lite Optical Tensiometer	111
Figure 62 Screenshot of the OneAttension [™] software window.	112
Figure 63 Various components used for carrying a hip prosthesis.	113

Figure 64 a) A positioning disc, b) a femoral head holder fixed on the positioning discs, and c) markings on the femoral head carrier casing and the base plate for the exact location after disassembly.	114
Figure 65 a) Femoral head and trunnion assembly on the femoral head carrier of the hip simulator and b) Markings were made on the trunnion and the femoral head holder for exact repositioning after cleaning/measurement intervals.	114
Figure 66 Schematic diagram showing the self-centring alignment of the components.	115
Figure 67 a) Variation with time of flexion-extension (FE) and abduction-adduction (AA) angles, and load (L) measured in the TE-86 hip joint simulator and b) Normal gait cycle [Image adapted from Rajtůková et al. (2014) ¹⁸⁴]	117
Figure 68 a) TE-86 hip simulator and b) Zoomed-in image of the station no. 1 showing the slider of a vertical linear guide.	118
Figure 69 CMM measurement set up of a) ceramic femoral taper, b) metallic femoral taper and b) metallic trunnion.	121
Figure 70 Mounting of the femoral head on the CMM platform	122
Figure 71 Cross-section of an internal femoral taper showing COR to rim value and Depth to finish contour value.	122
Figure 72 Mounting of the trunnion on the CMM platform	124
Figure 73 a) Two-dimensional (2D) surface roughness (Ra) measurements using the Surftest SJ-210 profilometer on, b) femoral taper and c) trunnion.	127
Figure 74 a) Three-dimensional (3D) surface roughness (Sa) measurements using Zygo NewView 5000 on b) an acetabular liner at the pole, c) a femoral head at the pole and d) femoral head at 45° tilt.	128
Figure 75 Mean volumetric measurements of all titanium (Ti) trunnions from CoC hip simulator wear test (measured gravimetrically).	130
Figure 76 Box-plot of volumetric measurement of all titanium (Ti) trunnions from CoC hip simulator wear test (measured gravimetrically). ns: no significant difference with adjusted p-value >0.999 and *: adjusted p-value <0.001.	130
Figure 77 A CMM wear map of the internal taper of a test ceramic head.	131
Figure 78 A femoral head and trunnion assembly showing terminologies used to describe the location of the material loss.	132
Figure 79 Hip simulator wear test trunnions showing wear from the proximal-superior end and distal-inferior end respectively.	132

- Figure 80 a) A femoral head and trunnion assembly showing the different anatomical planes, b) and c) a test trunnion showing wear from the proximal-superior end and distal-inferior end respectively, d) and e) optical microscopic images of a test trunnion captured at $0.65\times$ magnification showing worn and unworn areas of the proximal-superior end and distal-inferior ends, respectively. 133
- Figure 81 a) An optical microscopic image at $2.5\times$ magnification and b) scanning electron microscopy (SEM) image of the test trunnion at $500\times$ magnification showing worn and unworn areas. 134
- Figure 82 a) A femoral head and trunnion assembly showing the different terminologies used to describe the location of the material loss, and b) An internal taper of a test femoral head showing grey coloured ring. Image from Bhalekar et al. (2018)²⁹⁵. 134
- Figure 83 a) A femoral head and trunnion assembly showing the different anatomical planes, b) and c) a test trunnion showing wear from the proximal-superior end and distal-inferior end respectively, d) and e) optical microscopic images of a test trunnion captured at $0.65\times$ magnification showing worn and unworn areas of the proximal-superior end and distal-inferior ends, respectively. In the SEM image f) shows, a worn area and an unworn area with the original machining marks at the proximal-superior end and g) shows, worn area at distal-inferior end of the trunnion. 135
- Figure 84 Mean 2D surface roughness R_a (in μm), of ceramic femoral tapers measured pre and post-CoC hip simulator wear test. Error bars represent \pm standard deviation. 136
- Figure 85 Mean 2D surface roughness R_a (in μm), of titanium (Ti) trunnions measured pre and post-CoC hip simulator wear test. Error bars represent \pm standard deviation. 137
- Figure 86 An evaluation profile obtained over the distal-inferior end of a test trunnion ($R_a = 0.321 \mu\text{m}$). The red arrow indicates the worn area. Image from Bhalekar et al. (2018)²⁹⁵. 137
- Figure 87 Surface topography images of a titanium trunnion a) unworn with machining marks visible ($S_a = 0.565 \mu\text{m}$) and b) worn ($S_a = 0.284 \mu\text{m}$). Image from Bhalekar et al. (2018)²⁹⁵. 138
- Figure 88 Mean 3D surface roughness S_a (in μm), of titanium (Ti) trunnions measured on unworn and worn areas after CoC hip simulator wear test. Error bars represent \pm standard deviation. 138
- Figure 89 Mean volumetric measurements of all ceramic femoral heads from CoC hip simulator wear test (measured gravimetrically). 139

Figure 90 Box-plot of volumetric measurement of all ceramic heads from CoC hip simulator wear test (measured gravimetrically). ns: no significant difference with adjusted p-value >0.999.	140
Figure 91 Mean volumetric measurements of all ceramic acetabular liners from CoC hip simulator wear test (measured gravimetrically).	140
Figure 92 Box-plot of volumetric measurement of all ceramic liners from CoC hip simulator wear test (measured gravimetrically). ns: no significant difference with adjusted p-value >0.999.	141
Figure 93 Mean volumetric measurements of all CoC joints from CoC hip simulator wear test (measured gravimetrically).	141
Figure 94 Box-plot of volumetric measurement of all CoC joints from CoC hip simulator wear test (measured gravimetrically). ns: no significant difference with adjusted p-value >0.999.	142
Figure 95 Mean volumetric measurements of CoC joints and titanium (Ti) trunnions from CoC hip simulator wear test (measured gravimetrically). Error bars represent \pm standard deviation ²⁹⁵ .	142
Figure 96 Mean 3D surface roughness Sa (in μm), of the ceramic femoral head and acetabular liners measured pre and post-CoC hip simulator wear test. Error bars represent \pm standard deviation.	143
Figure 97 Surface topography images of a ceramic femoral head a) pre-test (Sa = 0.003 μm) and b) post-test (Sa = 0.003 μm).	144
Figure 98 Surface topography images of a ceramic acetabular liner a) pre-test (Sa = 0.006 μm) and b) post-test (Sa = 0.005 μm).	144
Figure 99 Mean volumetric measurements of the ceramic femoral head, ceramic acetabular liner and titanium (Ti) trunnion used in the DL test (measured gravimetrically).	145
Figure 100 Mean 2D surface roughness Ra (in μm), of ceramic femoral taper measured pre and post-DL test. Error bars represent \pm standard deviation.	146
Figure 101 Mean 2D surface roughness Ra (in μm), of titanium (Ti) trunnions measured pre and post-DL test. Error bars represent \pm standard deviation.	147
Figure 102 Mean 3D surface roughness Sa (in μm), of the ceramic femoral head and acetabular liner measured pre (blue) and post (red)-DL test. Error bars represent \pm standard deviation.	148

- Figure 103 The mean volumetric measurements of titanium trunnions used in CoC hip simulator wear test and the DL test (measured gravimetrically). Error bars represent \pm standard deviation²⁹⁵. 149
- Figure 104 Gravimetric measurement of impaction test trunnions. Error bars represent \pm standard deviation. 150
- Figure 105 An internal taper of an impaction test femoral head showing discolouration prior to cleaning²⁹⁵. 151
- Figure 106 Mean volumetric measurements of all titanium (Ti) trunnions from MoXLPE hip simulator wear test (measured gravimetrically). 152
- Figure 107 Box-plot of volumetric measurement of all titanium (Ti) trunnions from MoXLPE hip simulator wear test (measured gravimetrically). ns: no significant difference with adjeusted p-value >0.999. 153
- Figure 108 A CMM wear map showing the wear pattern of the internal taper of a test CoCrMo head. The circumferential red band at the distal end indicates the worn area. 154
- Figure 109 Mean 2D surface roughness, Ra (in μm), of CoCrMo femoral tapers measured pre and post-MoXLPE hip simulator wear test. Error bars represent \pm standard deviation. 154
- Figure 110 Surface topography images of the internal taper of CoCr femoral heads a) unworn with machining marks visible ($S_a = 0.482 \mu\text{m}$) and b) worn ($S_a = 0.699 \mu\text{m}$). 155
- Figure 111 a) A test CoCrMo femoral head and titanium trunnion assembly, b) the internal taper of cut CoCrMo femoral head showing unworn area at distal end, worn area, and trunnion imprinting, and c) an optical microscopic image of a test femoral taper captured at $0.65\times$ magnification showing unworn area, worn area, and trunnion imprinting. 157
- Figure 112 a) The position of the internal taper of a cut CoCrMo femoral head in the SEM, b) SEM image of the same femoral taper showing the area (red circle) where spot EDX analysis were taken, c), d) and e) SEM images of the undamaged area (U1), damaged area 1 (D1) and damaged area 2 (D2), respectively. The yellow circle on each SEM image represent the spot used for EDX analysis. 159
- Figure 113 SEM image of the same femoral taper showing the area (yellow circle) where spot EDX analysis was taken and Spot EDX spectrum showing undamaged area (U1). 160
- Figure 114 SEM image of the same femoral taper showing the area (yellow circle) where spot EDX analysis were taken and Spot EDX spectrum showing damaged area (D1). The

green arrow indicates an increase in Oxygen, whereas the red arrow indicates a decrease in Cobalt.	161
Figure 115 SEM image of the same femoral taper showing the area (yellow circle) where spot EDX analysis were taken and Spot EDX spectrum showing damaged area 2 (D2). Green arrows indicate an increase in the alloying elements of titanium alloy (Ti6Al4V).	162
Figure 116 The elemental X-ray map taken on the damaged area 1 of a CoCrMo femoral taper subject to hip simulator wear test. The red dotted rectangle shows the presence of mixed oxides.	164
Figure 117 The elemental X-ray map taken on the damaged area 2 of a CoCrMo femoral taper subject to hip simulator wear test. The yellow dotted rectangle showing a strong presence of alloying components of Ti6Al4V trunnion.	165
Figure 118 Mean volumetric measurements of all CoCrMo femoral heads from MoXLPE hip simulator wear test (measured gravimetrically).	166
Figure 119 Box-plot of volumetric measurement of all CoCrMo heads from MoXLPE hip simulator wear test (measured gravimetrically). ns: no significant difference with adjusted p-value >0.999 and *: p<0.001.	166
Figure 120 Mean volumetric measurements of all XLPE acetabular liners from MoXLPE hip simulator wear test (measured gravimetrically).	167
Figure 121 Box-plot of volumetric measurement of all XLPE liners from MoXLPE hip simulator wear test (measured gravimetrically). ns: no significant difference with adjusted p-value >0.999.	167
Figure 122 Mean volumetric wear of CoCrMo femoral heads and titanium trunnions (measured gravimetrically). Error bars represent \pm standard deviation.	168
Figure 123 Mean 3D surface roughness Sa (in μm), of CoCrMo femoral heads measured pre and post-MoXLPE hip simulator wear test. Error bars represent \pm standard deviation.	169
Figure 124 Mean 3D surface roughness Sa (in μm), of XLPE liners, measured pre and post-MoXLPE hip simulator wear test. Error bars represent \pm standard deviation.	169
Figure 125 Surface topography images of a CoCrMo femoral head a) pre-test (Sa = 0.005 μm) and b) post-test (Sa = 0.006 μm).	170
Figure 126. Surface topography images of an XLPE acetabular liner a) pre-test (Sa = 1.080 μm) and b) post-test (Sa = 0.042 μm).	170

- Figure 127 An optical microscopic image at a $3.2\times$ magnification of the backside of XLPE liner taken at the end of hip simulator testing, showing original machining marks, and thus an absence of wear. 171
- Figure 128 a) and b) SEM coupled with EDX analysis of the lubricant samples showing the presence of titanium. Red circles on SEM images represents a spot of EDX analysis. Tables in a) and b) represent spot EDX analysis on the points respectively. 172
- Figure 129 Lubricant cobalt (Co), chromium (Cr) and titanium (Ti) ion concentration at different intervals of the MoXLPE hip simulator wear test. Dotted lines indicate Co, Cr and Ti ions measured from the unused lubricant. Error bar represents \pm standard deviation. 173
- Figure 130 pH of the lubricant measured over every 0.5Mc of the CoC hip simulator test. Error bars represent \pm standard deviation. 174
- Figure 131 pH of the lubricant measured over every 0.5Mc of the MoXLPE hip simulator test. Error bars represent \pm standard deviation. 174
- Figure 132 Contact angle measurement at the pole area of a) ceramic femoral head used in the CoC hip simulator wear test and b) CoCrMo femoral head used in the MoXLPE hip simulator wear test. 175
- Figure 133 A test ceramic femoral head and trunnion assembly with applied load and applied motions, showing toggling and the material loss at two distinct areas (shown in red). Image from Bhalekar et al. (2018)²⁹⁵. 178
- Figure 134 Schematic describing the micromotion, toggling (rocking motion) and entrainment of debris into the taper. The primary mode of damage was corrosion in case 1, and for case 2 it was due to MACC. Image adapted from Cook et al. (2013)⁴⁵. 185
- Figure 135 Box plot from an unpublished work from the McMinn centre indicating statistically significant elevation Ti ion concentration in the patients with CoC THRs mounted on Ti trunnions³⁴⁸. 195

List of Tables

Table 1 Anatomical planes and corresponding directional terms used to define the position of the structures ⁴⁶ .	9
Table 2 Advantages and disadvantages of the modularity at the head-neck interface of the THR ^{27,82,83,86} .	20
Table 3 Terms and definitions for hip prosthesis components as reported in the international standard and NJR glossary.	22
Table 4 ASTM F75 CoCrMo alloy: chemical composition.	28
Table 5 Potential causes of failure of primary THR ¹⁴³ .	35
Table 6 Wear mechanisms and their definitions as per the international standard ASTM G40-17 ¹⁶³ .	40
Table 7 Force acting on the hip joint measured using instrumented prostheses. Adapted from Byrne et al. (2010) ⁵⁰ .	47
Table 8 Testing conditions as per the ISO 14242-1 ¹⁸⁷ .	48
Table 9 Advantages and disadvantages of commonly used lubricants in <i>in vitro</i> studies ⁵⁵ .	51
Table 10 Description of the modern hip simulators.	53
Table 11 Laboratory wear rates found for different CoC hip joints under standard testing conditions.	55
Table 12 Laboratory wear rates found for different MoXLPE hip joints under standard testing conditions	57
Table 13 Typical friction factor values for different bearing surfaces used for THR in the presence of diluted bovine serum ¹⁶⁵ .	58
Table 14 Wettability measurements of different biomaterials reported in the literature	66
Table 15 Dimensions used for describing various femoral tapers. Adapted from Triantafyllopoulos et al. (2015).	67
Table 16 Material properties of various materials used for the taper-trunnion junction. Adapted from Lundberg et al. (2015) ²⁴²	71
Table 17 Standard terminology relating to wear and corrosion described in American Society for Testing and Materials (ASTM) international standards (in alphabetical order) ^{38,163,267}	77
Table 18 The Goldberg scoring system ³⁰ .	82

Table 19 Explant studies involving the quantification of material loss from the taper-trunnion junction of modular hip prostheses.	85
Table 20 Testing conditions as per the ASTM F1875 ³⁸ .	88
Table 21 Summary of CoC components used in CoC hip simulator wear test.	92
Table 22 Summary of all the experimental variables for CoC hip simulator test	96
Table 23 Summary of MoXLPE components used in MoXLPE hip simulator wear test.	103
Table 24 Summary of all the experimental variables for MoXLPE hip simulator test	107
Table 25 Geometric wear measurements on the various components.	120
Table 26 Mean surface roughness of femoral taper and trunnion used for an impaction test.	150
Table 27 The spot EDX results showing norm. C [Wt. %] of polished CoCrMo surface and CoCrMo femoral taper used in the hip simulator wear test.	163
Table 28 Laboratory wear rates found for different CoC hip joints under standard testing conditions compared with this study.	181
Table 29 Laboratory wear rates for different metal-on-cross-linked (MoXLPE) hip joints under standard testing conditions compared with this study. γ : Gamma irradiation, Eb: electron beam irradiation.	186
Table 30 Wear from the taper-trunnion junction of MoP THRs (Ti: titanium alloy, (CoCrMo: cobalt chromium molybdenum alloy).	187

List of Abbreviations

AA	Abduction/Adduction
ALVAL	Aseptic Lymphocytic Vasculitis-Associated Lesions
ALTR	Adverse Local Tissue Reaction
ANOVA	Analysis of variance
AOANJRR	Australian Orthopedic Association National Joint Replacement Registry
ARMD	Adverse Reaction to Metal Debris
ASR	Articular Surface Replacement TM
ASTM	American Society for Testing and Materials
CA	Contact Angle
Co	Cobalt
CoC	Ceramic-on-Ceramic
CoCrMo	Cobalt-Chromium-Molybdenum
CoP	Ceramic-on-Polyethylene
CMM	Co-ordinate Measuring Machine
DL	Dynamic Loading
EDX	Energy Dispersive X-ray spectroscopy
Eb	Electron beam
FE	Flexion/Extension
HRA	Hip Resurfacing Arthroplasty
IER	Internal/External rotation
ICPMS	Inductively Coupled Plasma Mass Spectrometry
ISO	International Organisation for Standardisation
NHS	National Health Service
NICE	National Institute for Clinical Excellence
NIH	National Institute of Health
NJR	National Joint Registry for England, Wales, Northern Ireland and the Isle of Man
MACC	Mechanically Assisted Crevice Corrosion
Mc	Million cycles
Mo	Molybdenum
MoM	Metal-on-Metal
MoP	Metal-on-Polyethylene
PE	Polyethylene
Ppb	Parts per billion
PTFE	Polytetrafluoroethylene
RANKL	Receptor activator of nuclear factor-kappa B ligand
SEM	Scanning Electron Microscope
THR	Total Hip Replacement
Ti	Titanium
TNF	Tumor necrosis factor
UHMWPE	Ultra-High Molecular Weight Polyethylene

UK	United Kingdom
XLPE	Cross-Linked Polyethylene
XPS	X-ray Photoelectron Spectroscopy
XRD	X-ray diffraction

List of terms and definitions

Abrasion	<i>The process by which relative motion between a surface and hard particles or protuberances on an opposing surface produces abrasive wear of that surface</i>
Abrasive wear	<i>Wear due to hard particles or hard protuberances forced against and moving along a solid surface</i>
Acetabular device	<i>A modular acetabular system consisting of a minimum of two components, one of which includes the bearing surface and the second component is a modular acetabular shell intended to contain the bearing liner and contact bone or bone cement</i>
Acetabular shell	<i>The metallic external, hollow structure that provides additional mechanical support or reinforcement for an acetabular liner and whose external features interface directly with the bones of the pelvic socket (for example, through bone cement, intimate press-fit, coatings for attachment to bone cement or tissue, integral screw threads, anchoring screws, pegs, and so forth). The acetabular shell may be solid or contain holes for fixation to the pelvis or attachment of instrumentation</i>
Acetabular liner	<i>Portion of the modular acetabular device with an internal hemispherical socket intended to articulate with the head of a femoral prosthesis. The external geometry of this component interfaces with the acetabular shell through a locking mechanism which may be integral to the design of the liner and shell or may rely upon additional components (for example, metal ring, screws, and so forth)</i>
Adhesive wear	<i>Wear due to localized bonding between contacting solid surfaces leading to material transfer between the two surfaces or loss from either surface</i>
Corrosion	<i>The deterioration of a material, usually a metal, that results from a chemical or electrochemical reaction with its environment</i>
Corrosive wear	<i>Wear in which chemical or electrochemical reaction with the environment is significant</i>
Crevice corrosion	<i>Localized corrosion of a metal or alloy surface at, or immediately adjacent to, an area that is shielded from full exposure to the environment because of close proximity of the metal or alloy to the surface of another material or an adjacent surface of the same metal or alloy</i>
Fatigue wear	<i>wear of a solid surface caused by fracture arising from material fatigue</i>

Femoral head	<i>Convex spherical bearing member for articulation with the natural acetabulum or prosthetic acetabulum</i>
Femoral stem	<i>The part of a modular femoral component inserted into the femur (thigh bone). Has a femoral head mounted on it to form the complete femoral component</i>
Fretting	<i>Small amplitude oscillatory motion, usually tangential, between two solid surfaces in contact” (amplitude range 1 to 100 μm)</i>
Fretting corrosion	<i>The deterioration at the interface between contacting surfaces as the result of corrosion and slight oscillatory slip between the two surfaces</i>
Fretting wear	<i>Wear arising as a result of fretting</i>
Galvanic corrosion	<i>Accelerated corrosion of a metal because of an electrical contact with a more noble metal or non-metallic conductor in a corrosive electrolyte</i>
Sliding wear	<i>Wear due to the relative motion in the tangential plane of contact between two solid bodies</i>
Tribocorrosion (wear-corrosion synergism)	<i>Form of solid surface alteration that involves the joint action of relatively moving mechanical contact with chemical reaction in which the result may be different in effect than either process acting separately</i>
Wear	<i>Alteration of a solid surface by progressive loss or progressive displacement of material due to relative motion between that surface and a contacting substance or substances</i>

Chapter 1: Introduction

1.1 Overview

Total hip replacement (THR), described as “*The Operation of the Century*”¹, is a common orthopaedic surgery. With the increasing life expectancy and growing population, the demand for hip replacement procedures is increasing every year²⁻⁴. More than 100,000 hip replacement procedures were recorded in the National Joint Registry (NJR) for England, Wales, Northern Ireland and the Isle of Man in 2017/18 with an increase of 3.6% from 2016/17⁵. In Australia, there were 47,972 hip replacement procedures recorded by the Australian Orthopaedic Association National Joint Replacement Registry (AOANJRR) in 2017/18 with an increase of 1.1% from 2016/17⁶.

Metal-on-polyethylene (MoP) is the most commonly implanted bearing surface combination with the majority consisting of cobalt-chromium molybdenum (CoCrMo) alloy femoral head articulating against a polyethylene (PE), either cross-linked polyethylene (XLPE) or non-XLPE, acetabular liner⁵. The AOANJRR states, ‘XLPE is classified as UHMWPE that has been irradiated by high dose ($\geq 50\text{kGy}$) gamma or electron beam radiation’. Non-cross-linked ultra-high-molecular-weight polyethylene (UHMWPE) has been used in the majority of THRs for over five decades^{7,8}. However, the articulation of the softer polymeric component against the harder metallic bearing surfaces leads to the production of numerous submicron-sized PE wear particles which can lead to osteolysis⁹⁻¹¹. To reduce PE wear and therefore hopefully increase implant longevity, two approaches have been attempted: the improvement of PE wear resistance by crosslinking^{12,13}, and the introduction of hard-on-hard bearings including metal-on-metal (MoM), and ceramic-on-ceramic (CoC)^{14,15}.

Despite many surgical advantages, explant studies of modular THRs have shown that material loss and debris production is not only restricted to bearing surfaces, it also arises from the taper-trunnion junction with a potential to reduce the longevity of the prosthesis¹⁶⁻²⁰, see Figure 1. The significance of the metal debris released from the modular junction was first extensively recognised with MoM hips, where the material loss from the taper-trunnion junction explained the higher revision rates in MoM THRs compared with hip resurfacings^{21,22}. The term “femoral taper” refers to the internal bore of the femoral head.

The metallic male part of the femoral stem is referred to as the “trunnion”. Thus the head-neck modular junction is referred to as the “taper-trunnion junction”, see Figure 1.

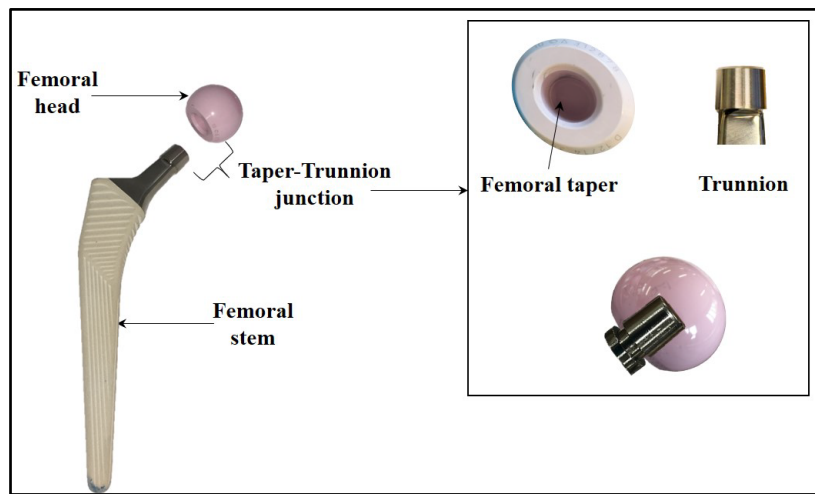


Figure 1 Taper-trunnion junction of modular ceramic femoral head mounted on the metallic trunnion.

Furthermore, the importance of adverse reaction to metal debris (ARMD) released from the taper-trunnion junction of large-diameter ($\geq 36\text{mm}$) MoM THRs, and implant failure is well established¹⁸⁻²³. However, the risk of revision surgery due to ARMD is not only limited to MoM THRs but is also shown in non-MoM [MoP, CoC and ceramic-on-polyethylene (CoP)]²⁴. Langton et al. investigated 369 MoM explants, including THRs and hip resurfacings from patients who had suffered ARMD²⁵. The relationships between total metallic loss and metal ion concentrations and macroscopic and histological tissue appearance of THR patients were compared to those in hip resurfacing patients. Hip resurfacing explants ($10.16 \text{ mm}^3/\text{year}$) were found to have significantly higher ($p < 0.001$) median rates of volumetric material loss than the THRs ($2.25 \text{ mm}^3/\text{year}$). Moreover, when the volumetric material loss from the femoral taper was combined with bearing surface wear in the THR explants this total rate of material loss ($2.52 \text{ mm}^3/\text{year}$) was still significantly less ($p < 0.001$) than in the hip resurfacing explants ($10.16 \text{ mm}^3/\text{year}$). Despite this, the extent of ALVAL (aseptic lymphocyte dominated vasculitis-associated lesion) infiltration and macroscopic tissue destruction was found to be more significant in THR patients. This may suggest that the material loss from the taper-trunnion junction may be more readily trigger a destructive immune cascade than the material loss from bearing surfaces²⁶. Therefore, it is recognised that metal debris released from the taper-trunnion junction of modular THRs may be more biologically active than wear debris released from the bearing surfaces²⁷⁻²⁹.

Various theories have been reported in the literature including mechanical, electrochemical or a combination of both for metal debris formation at the taper-trunnion junction of the modular THRs^{16-19,30-34}. Much of the data for these theories have, appropriately and sensibly, come from explant studies, as these are based on the truest test of all, that in the human body. However, explants come from individuals, each with unique attributes, including loading, motion, and activity. Relatively few *in vitro* studies have evaluated material loss from modular junctions³⁵⁻³⁷. The purpose of these *in vitro* studies includes mainly an assessment of electrochemical characteristics and metallurgy of the implant materials used for the taper-trunnion junction. However, these testing methodologies did not use actual hip prostheses for laboratory testing. In terms of standards, American Society for Testing and Materials (ASTM) F1875 mentions only uniaxial dynamic loading for fretting wear and corrosion testing of modular THRs^{38,39}, which utilises realistic femoral head and trunnion modular of THRs. Note that employment of physiological walking motion was not included in the ASTM F1875. Interestingly, explant analysis of modular THRs demonstrated a toggle effect of the femoral head on the trunnion, a phenomenon responsible for causing damage at the taper-trunnion surfaces by mechanical process and later creating the opening for ingress of corrosive physiological fluid^{18,19}. The toggling is not just superoinferior but appears to involve anteroposterior/posteroanterior direction too. To the authors' best knowledge, no international standard incorporated physiological walking motion for laboratory testing of the taper-trunnion junction of modular THRs.

Hip joint simulators have been built to simulate the biomechanics of the natural hip joint and replicate wear rates, wear patterns and wear debris observed clinically, in controlled laboratory conditions using actual hip prostheses^{40,41}. However, to the authors' best knowledge, no hip simulator tests have quantified metal release from the taper-trunnion junction of modular CoC and MoP THRs.

1.2 Aim and Objectives

1.2.1 Aim

The aim of this research work to quantify the material loss, if any, at the taper-trunnion junction of modular CoC and MoP THRs under standard physiological walking cycle. The purpose of this study was to try and inform the debate around material loss at the taper-trunnion junction. In order to achieve this aim, multi-station hip simulator testing of modular hips mounted on titanium (Ti) alloy trunnions was undertaken under standard physiological walking cycle, replicating the clinical scenario as closely as possible.

1.2.2 Objectives

The objectives of this study are as follows:

- **Quantification of material loss, if any, at the taper-trunnion junction and bearing surfaces of CoC hips mounted on Ti alloy trunnions subject to dynamic loading and articulating motion**

Ceramic-on-ceramic (CoC) THR have a substantially lower wear rate than MoP hips, as shown by hip simulator testing. However, the revision rates of CoC (6.12%) and MoP (6.40%) hips are comparable⁵. It was hypothesised that an explanation could be ARMD from the trunnion led this research to investigate the wear at both the bearing surfaces and the taper-trunnion interface of a contemporary CoC THR in an *in vitro* study. To the authors' best knowledge, no hip simulator tests have assessed and quantified material loss from the taper-trunnion junction of a modular CoC THR. Therefore, to try and explain this discrepancy hip simulator wear test using the latest 4th generation CoC hips was conducted, to investigate the material loss, if any, at the taper-trunnion junction and bearing surfaces of CoC hips mounted on Ti alloy trunnions subject to dynamic loading and articulating motion.

- **Investigate the effect of employing dynamic loading and articulating motion vs dynamic loading on the material loss at the taper trunnion junction of CoC THRs**
Additionally, a CoC sample was employed in a separate dynamically loaded station, with no articulating motion, to investigate the material loss, if any, at the taper-trunnion

junction and bearing surfaces of a CoC hip-mounted on Ti alloy trunnion subject only dynamic loading but no articulating motion.

- **Investigate the effect of impaction on the taper-trunnion junction of CoC THR**

It was appreciated that both the assembly and disassembly of the femoral head from the trunnion could produce wear at the taper-trunnion junction. Therefore, separate impaction test was performed, to investigate the material loss, if any, at the taper-trunnion junction of ceramic femoral head mounted on Ti alloy trunnion.

- **Quantification of material loss, if any, at the taper-trunnion junction and bearing surfaces of CoC hips mounted on Ti alloy trunnions subject to dynamic loading and articulating motion**

Retrieval studies reported ARMD due to debris produced from the taper-trunnion junction of the modular MoP THRs⁴²⁻⁴⁵. Interestingly, retrieval studies showed that the material loss arises mainly from the CoCrMo alloy femoral tapers rather than the Ti alloy trunnions when CoCrMo/Ti alloy combinations are used for the taper-trunnion junction. Therefore, a hip simulator test was performed employing dynamic loading and articulating motions, to assess and quantify material loss from CoCrMo femoral taper of MoP THRs. To the authors' best knowledge, no hip simulator tests assessed and quantified metal release from the taper-trunnion junction of contemporary MoP THRs.

- **Assessment of lubricant after CoC and MoP hip simulator tests**

Metal debris analysis was performed after hip simulator testing of CoC and MoP THRs, to examine the presence of metal debris, if any, within the lubricant.

- **Investigate the effect of wettability on ceramic and metallic femoral heads pre and post hip simulator tests**

The bearing surface research has done in-depth however little known about the wettability of the bearing surfaces subject to hip simulator testing. Therefore, in order to understand pre and, post-test contact angle measurements were performed using the same lubricant used for the hip simulator testing.

1.2.3 Research questions

The major research questions are listed below:

- In CoC articulating components, comprised of ceramic material, where is the metal debris originating from?
- Dynamic loading & articulating motion vs dynamic only loading, does the material loss at the taper-trunnion junction change?
- In MoP articulating components, comprised of metal and softer polymer contact, where is the metal debris originating from?
- What are the mechanisms responsible for the material loss from the taper-trunnion junction of modular MoP THRs, when CoCrMo/Ti alloy combinations are used for the taper-trunnion junction?

1.3 The organisation of the thesis

Following on from this introduction, this thesis contains a literature review (Chapter 2), materials and methods (Chapter 3), results (Chapter 4), discussion (Chapter 5) and conclusion and future work (Chapter 6).

In Chapter 2, a comprehensive literature review was conducted to deliver and establish a relevant background for the chapters to follow. This includes anatomy of the natural hip joint, diseases of the hip, fundamentals of tribology i.e. wear, friction and lubrication, the human gait cycle and *in vitro* hip simulator studies and retrieval studies including quantification of material loss from the bearing surfaces as well as the taper-trunnion junctions of modular THRs, mechanisms responsible for the material loss from the taper-trunnion junctions, *in vitro* testing methods for assessment of the material loss and finally, the summary of the literature review.

In Chapter 3, materials, machines and instruments used for *in vitro* testing of hip prostheses are briefly described. Note that subsections in this chapter have been chosen so as to overlap with future chapters including Results and Discussion.

Chapter 4 shows the experimental results obtained during the *in vitro* studies.

The results are discussed in Chapter 5. This is followed by the limitations of the study and industrial applications of this research work.

Finally, an overall conclusion to this research and suggestions for further work are provided in Chapter 6.

1.4 Declaration

The author performed all work presented in this thesis; apart from the metal debris analysis, which was performed in collaboration with:

- a. The University of Surrey conducted by Mark Minta and
- b. London Metallomics Facility, Kings College London conducted by Dr Theodora Stewart and Dr Caterina Dell'Aquila

Parts of this work have been published in journal papers and conference publications as listed in 'List of Publications' and 'List of Major Presentations' sections respectively.

Chapter 2: Literature Review

In this chapter, the anatomy of the natural hip joint, diseases of the hip, fundamentals of tribology, literature review of THR, *in vitro* hip simulator studies and retrieval studies including quantification of material loss from the bearing surfaces as well as the taper-trunnion junctions of modular THRs are briefly described.

2.1 Nomenclature for the anatomy of the hip joint

This section characterises anatomical planes of the human body and the terms used to describe the location of structures in the human body. The term *anatomy* is derived from the Greek word *ἀνατομή*, meaning dissection or to cut. It is essential to know different anatomical planes and positions of the human body to describe the specific location of the structure. Three principal anatomical planes of the human body are shown in Figure 2 and summarised in Table 1 ⁴⁶.

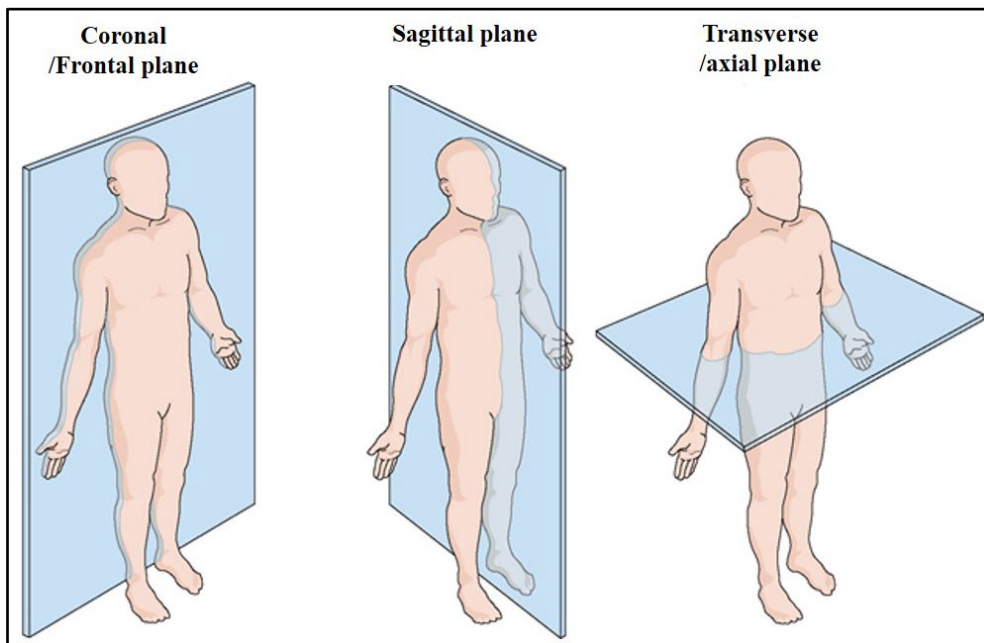


Figure 2 Anatomical planes of the human body showing coronal/frontal plane, sagittal plane and transverse/axial plane. Image from Drake (2010)⁴⁶.

Table 1 Anatomical planes and corresponding directional terms used to define the position of the structures⁴⁶.

Anatomical planes	Orientation of the planes	Body division	Terms used to describe the location of structures
Coronal /Frontal	Vertical	Anterior and posterior parts	Anterior: Towards the front of the body Posterior Towards the back of the body
Sagittal	Vertical but right-angled to coronal planes	Medial and lateral	Medial: Towards the midline of the body Lateral: Away from the midline of the body
Transverse /axial	Horizontal	Superior and inferior parts	Superior: Towards the top of the body Inferior: Towards the bottom of the body

Other terminologies used to describe the location of structures relative to the body or other structures are proximal: the position of the structures located closer to the point of attachment and distal: the position of the structures located farther from the point of attachment.

The natural hip joint is a ball-and-socket joint enclosed by powerful muscles, which provides stability to the joint as well as a wide range of motion in several anatomical planes of the human body. Since the beginning of total hip arthroplasty, surgeons/engineers adapted the anatomy of the natural hip joint in order to design a hip prosthesis. Therefore, to fully understand the causes of hip joint replacement surgery and in order to replicate significant features of the natural hip joint in an artificial hip prosthesis for its long-term success; it is essential to understand the basic anatomy, gait cycle and loads acting on the natural hip joint.

2.2 The natural hip joint

This section illustrates the anatomy of the natural hip joint, followed by a description of the human gait cycle (walking cycle) and biomechanics of the hip joint. To understand hip simulator loading and motion, it is first essential to consider the gait cycle and loads acting on the natural hip joint. Later diseases of the natural hip joint and need for THR surgery are briefly described.

2.2.1 Anatomy of the natural hip joint^{46,47}

The natural hip joint is formed by the articulation of the acetabular cavity of the pelvic bone and the head of the femur, see Figure 3. The hip joint is a typical synovial joint in which the articulating surfaces, i.e. an acetabulum (socket) and head of the femur (ball) are covered with articular cartilage. This assembly is covered with a synovial membrane which produces the synovial fluid which provides lubrication. A capsule of ligaments finally covers the hip joint. The hip joint provides stability during locomotion (walking/running) and is capable of supporting the entire body weight ⁴⁶.

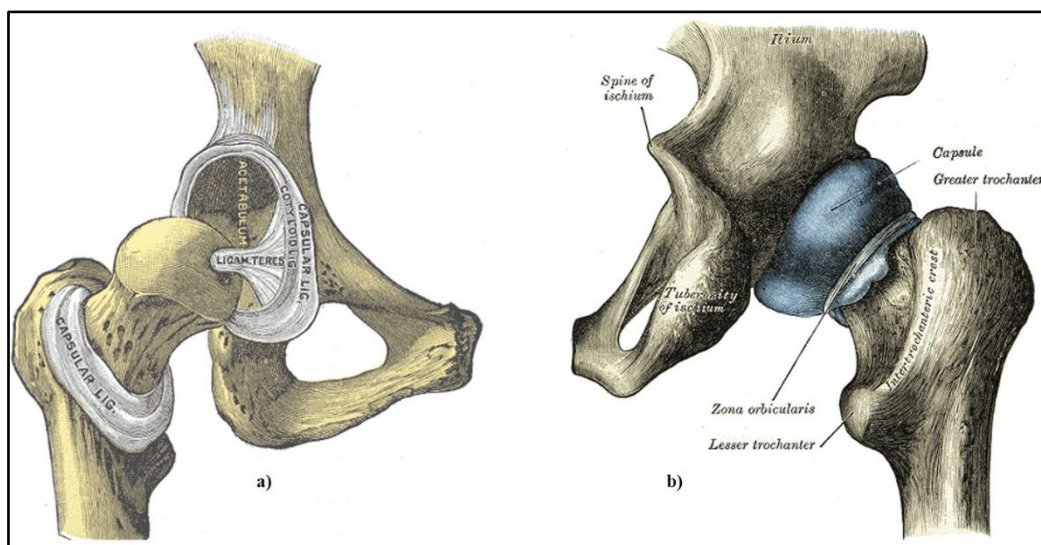


Figure 3 The natural hip joint a) anterior view and b) posterior view. Images from Gray (2000)⁴⁸.

The fusion of the ilium (40%), ischium (40%) and pubis (20%) bones form the single innominate or pelvic bone by adulthood. In childhood, the triradiate cartilage separates these three bones. By the age of 14-16 years, the process of fusion is initiated and is completed by the age of approximately 23 years⁴⁶. The cup-shaped acetabulum or acetabular cavity is formed at the connection of these three bones, see Figure 4. The acetabulum is covered with lunate or horseshoe-shaped hyaline cartilage, usually, 1-7mm thick⁴⁹.

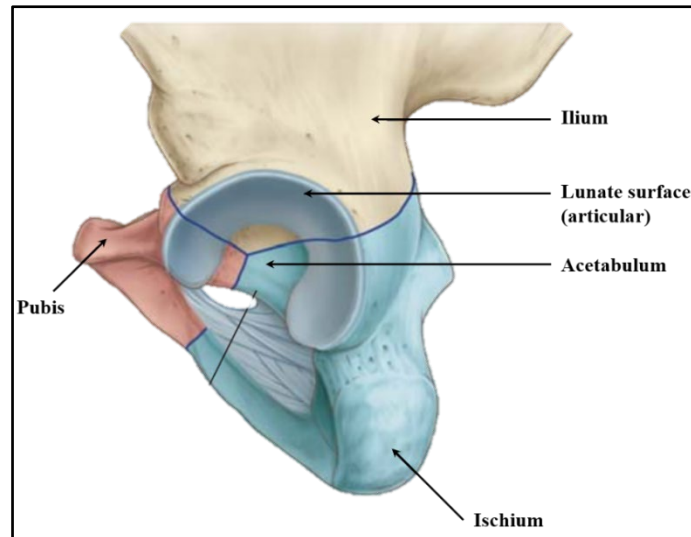


Figure 4 Acetabulum. Image from Drake (2010)⁴⁶.

The femur (or thigh bone) is a long bone, and the head of the femur articulates against the acetabulum of the pelvis at the proximal end forming hip joint, see Figure 5. The femoral head, approximately 60 to 70% of the sphere, is covered with hyaline cartilage⁴⁶. The distal end of the femur forms the knee joint with the tibia of the shinbone. The greater and lesser trochanter projections at the proximal end provide muscle attachment sites⁴⁶.

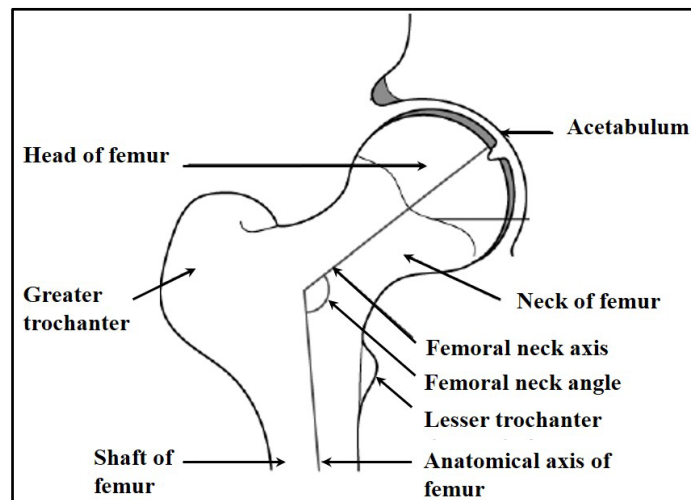


Figure 5 The normal hip joint: Cross-sectional view showing the femoral neck angle. Image from Byrne et al. (2010)⁵⁰.

The femoral neck connects the femoral head with the shaft forming an angle known as femoral neck angle or neck-shaft angle, see Figure 5. The femoral neck angle facilitates an increased range of joint motion without impingement of the femur on the pelvis. In the normal adult, the femoral neck angle is usually $125 \pm 5^\circ$ ⁵⁰. If the inclination angle is less than

120° then it is termed coxa vara and if it is greater than 130° then it is known as coxa valga, see Figure 6.

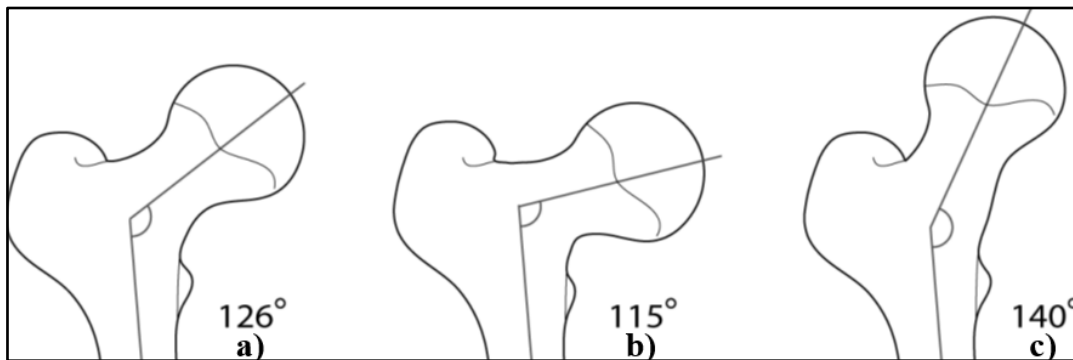


Figure 6 The femoral neck angle, a) normal, b) coxa vara and c) coxa valga. Image from Byrne et al. (2010)⁵⁰.

The synovial membrane encloses the articulating surfaces of the hip joint, see Figure 7 a), and also provides lubrication by secreting synovial fluid. The natural lubricant in the human body is synovial fluid. The synovial fluid is produced inside the synovium, the tissue that envelops the joint space. The synovium is accountable for the synthesis of synovial fluid, along with the production of lubricin and hyaluronic acid⁵¹. The synovial fluid forms a thin layer on the porous surface of articular cartilage and the fluid within the porous cartilage effectively provides a synovial fluid reserve⁵². During normal walking, the synovial fluid retained within the articular cartilage is considered to be squeezed out between the opposing surfaces of the hip joint mechanically to sustain a layer of fluid on the cartilage surface⁵³. In the natural hip joint, the volume of synovial fluid is in the range of 0.2-0.4 mL^{54,55}. The most abundant protein in synovial fluid is albumin (56% of total protein content)⁵⁶. Hyaluronic acid is the largest molecule in synovial fluid⁵⁵. In healthy adults, the protein concentration of synovial fluid has been reported close to 20 g/L^{54,55,57,58}. The protein concentration of synovial fluid has been reported in the range of 30-35 g/L^{54,59} for patients with osteoarthritis whereas for patients with rheumatoid arthritis much higher concentrations with values in the range of 40-45 g/L^{54,59}. In healthy adults, synovial fluid is non-Newtonian, and so the viscosity drops significantly when the shear rate rises⁶⁰.

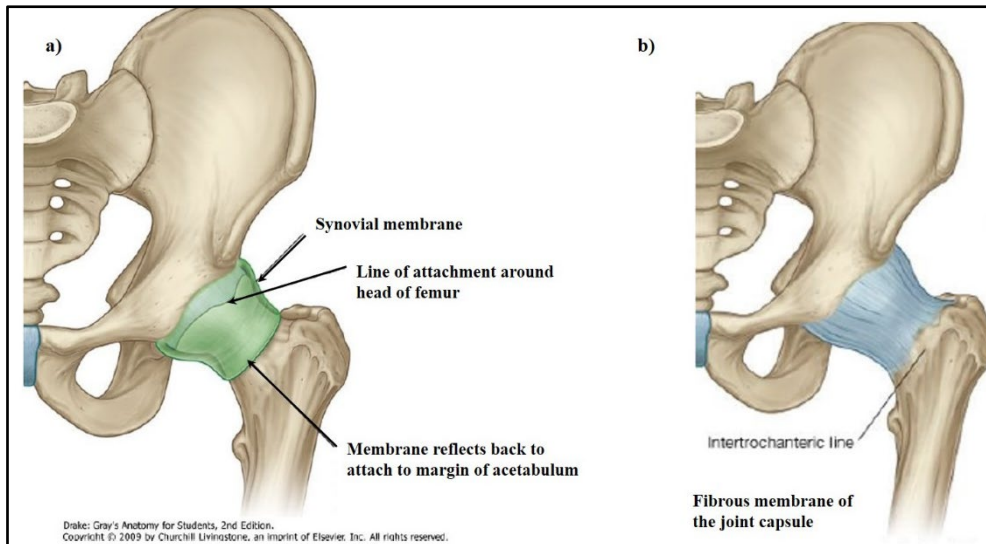


Figure 7 a) Synovial membrane and b) fibrous membrane of the hip joint. Image from Drake (2010)⁴⁶.

Furthermore, the hip joint is covered by a strong and generally thick fibrous membrane, see Figure 7 b). The iliofemoral ligament, pubofemoral ligament and ischiofemoral ligament surround the hip joint spirally forming the joint capsule, which limits the movement of the hip joint providing maximum stability see Figure 8 a) and b) respectively.

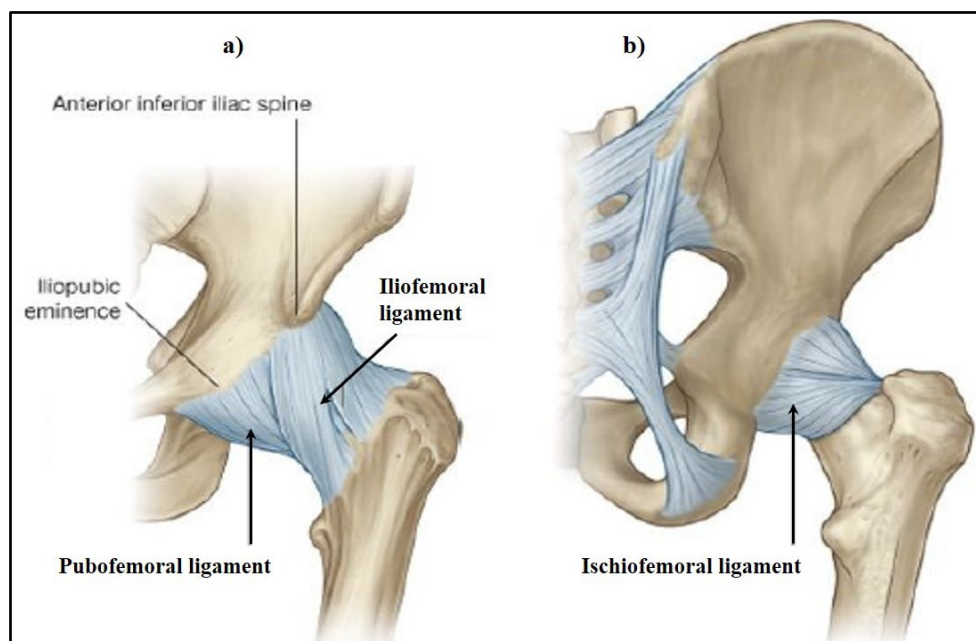


Figure 8 Ligaments of the hip joint a) Iliofemoral and pubofemoral ligament, and b) ischiofemoral ligament. Image from Drake (2010)⁴⁶.

The natural hip joint allows movement in multiple directions. The motions at the hip joint include flexion-extension (FE), abduction-adduction (AA) and internal-external rotation

(IER), see Figure 9 a), b) and c) respectively. These motions are accomplished by a series of various muscles attached to the hip joint.

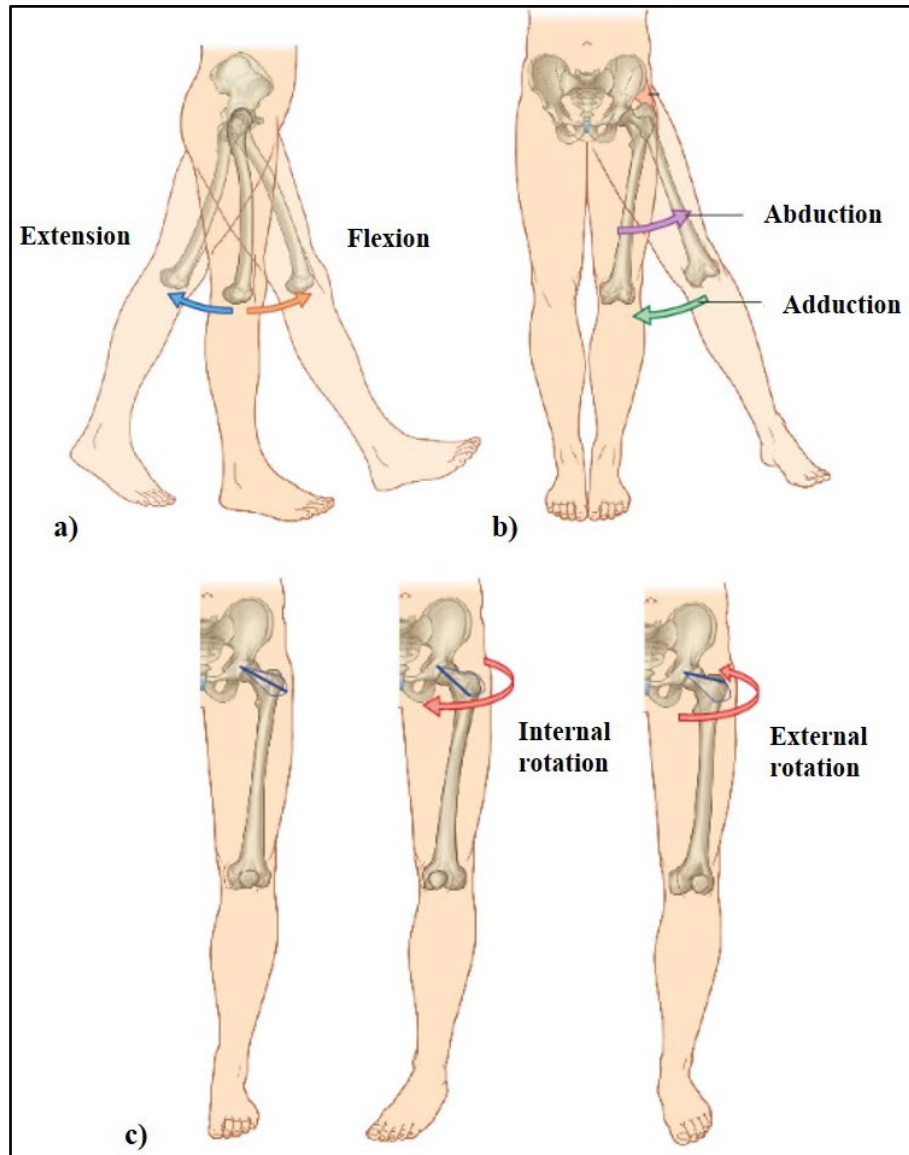


Figure 9 The motions at the hip joint a) flexion-extension (FE), b) abduction-adduction (AA) and c) internal-external rotation (IER). Image from Drake (2010)⁴⁶.

The natural hip joint is covered in a layer of articular cartilage and is lubricated with synovial fluid. The articular cartilage is soft and delicate. However, the loads experienced by the natural hip joints are high. They can exceed several times body weight during normal day-to-day activities e.g. walking, climbing stairs, running, standing up, sitting down etc⁵⁰. When the load is applied to the articular cartilage, it deforms under the applied load and acts to distribute the load over a broad area and consequently reduces contact stress. The deformation of the articular cartilage achieves the fluid film lubrication. The deformation of

articular cartilage also makes contact between the articulating surfaces of the hip more conforming and therefore, facilitating the fluid film lubrication between them. Fluid film lubrication protects the articulating surfaces of the hip from direct contact by separating them with a continuous film of synovial fluid⁶¹.

2.2.2 Hip joint disorders and the need for hip arthroplasty

Hip disorders are disorders that affect the typical healthy hip joint causing pain and discomfort in a person's life. These disorders can arise from injuries, developmental conditions, chronic conditions or infections. There are many possible problems which can arise at the hip joint and give an indication for hip replacement surgery.

Osteoarthritis was responsible for 90% of the primary hip replacement surgeries as per the 15th Annual Report of the National Joint Registry (NJR) for England, Wales, Northern Ireland, and the Isle of Man (2016/17)⁵. In osteoarthritis, the articular cartilage of the load-bearing joints degenerates leading to rubbing of bones against each other, causing distress due to pain, inflammation, swelling and reduced range of motion⁶² see Figure 10.



Figure 10 X-rays (from left to right) showing the joint space narrowing (inside the red circle) due to osteoarthritis. Image from Altman and Gold (2007)⁶³.

Arthritis (from Greek: *arthro* = joint and *itis* = inflammation) is a common joint disorder that causes inflammation and pain in one or more joints, e.g. spine, hips, knees, and ankles. There are over 100 different types of arthritis, but the most common type of arthritis is osteoarthritis⁶⁴. Approximately 9 million people in the UK are affected by osteoarthritis, according to the National Health Service (NHS)⁶⁵. The root cause of osteoarthritis is not

clear, and multiple factors such as age, gender, obesity, joint injury, and gene inheritance can play a role in the development of this degenerative condition⁶⁶. Osteoarthritis primarily affects older people (> 65 years)⁶⁴. At an early stage, painkillers (e.g. ibuprofen) or other non-steroidal anti-inflammatory drugs (NSAIDs) are used for the treatment of osteoarthritis, and if the pain is still persistent, then a viscosupplement (hyaluronic acid) can be injected into the joints. Osteoarthritis degrades the quality of life of a sufferer as well as causing severe pain in performing daily routine activities, alongside limited mobility or immobility. In such cases, then hip replacement surgery may be recommended.

Fractured neck of femur (see Figure 11) was responsible for 5% of the primary hip replacement surgeries as per the NJR. The most common reason for the femoral neck fracture is osteoporosis⁶⁷. Osteoporosis is an age-related disease and characterised by deterioration of the bone and therefore increases the fragility of the bone⁶⁸.

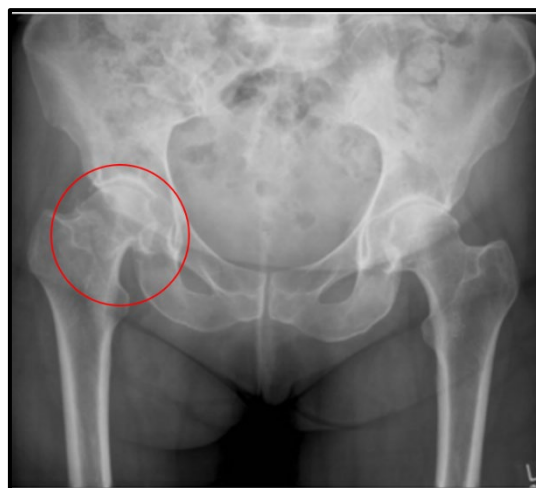


Figure 11 Fractured neck of femur shown in the red circle. Image from Miller et al. (2005)⁶⁹.

Since the year 2000, there were 1.6 million incidents (over 50 years age) of hip fracture occurred due to osteoporosis out of which 70% were women⁷⁰. Sambrook and Cooper estimated that the number of hip fractures worldwide would increase from 1.7 million in 1990 to 6.3 million in 2050⁷¹. Internal fixation devices such as bone screws are typically used for the femoral neck fractures, see Figure 12, but more complicated fractures are treated with hip replacement surgery.



Figure 12 The CONQUEST FNT™ system launched by Smith & Nephew in June 2019. Image from Smith & Nephew (2019)⁷².

Avascular necrosis was responsible for 2% of the primary hip replacement surgeries as per the NJR. Avascular necrosis is caused due to the death of cells in the joint tissue resulting from insufficient blood supply to the bone, see Figure 13. In the natural hip joint, avascular necrosis mainly affects the proximal end of the femur and sometimes the femoral neck. The interruption of blood supply to the femoral head causes cell death (necrosis), therefore resulting in deterioration of the mechanical properties of the bone; eventually leading to the collapse of the joint. Avascular necrosis is a progressive disease caused by factors such as alcoholism or excessive use of corticosteroids⁷³. At early stages, avascular necrosis could be treated with core decompression⁷⁴ and the bone marrow transplantation⁷⁵. However, hip replacement surgery usually is essential after a few months following these procedures^{75,76}.

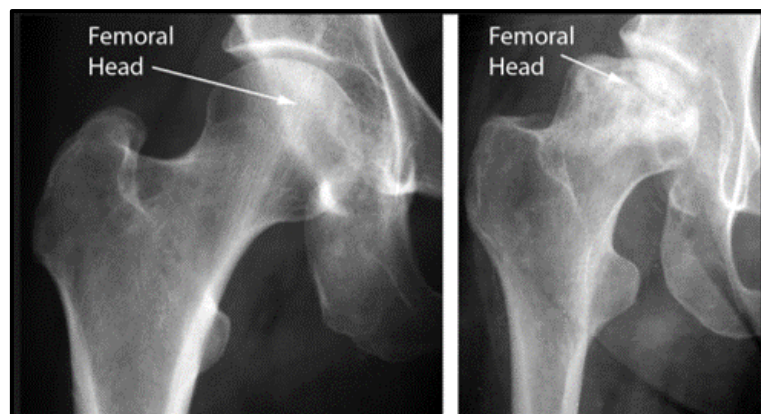


Figure 13 X-ray of a healthy femoral head (left) and collapsed femoral head (right) due to avascular necrosis. Image from OrthoInfo⁷⁷.

Congenital dislocation/dysplasia of the hip (2%), inflammatory arthropathy (1%), chronic trauma (1%) were few other hip joint disorders reported by the NJR for an indication of hip replacement surgeries⁵.

2.3 Total hip replacement (THR)

This section gives a summary of THR prostheses. This includes the terminologies used to describe the prostheses followed by a brief history of THR. Next, the classification of THR is given along with types of biomaterials used for manufacturing the components used in THR prostheses. Finally, various causes responsible for the failure of THR are explained.

2.3.1 *An introduction to THR prostheses*

Total hip replacement (THR) transforms the lives of millions of people who suffer from crippling arthritic diseases. It is an implant to replace/repair the damaged hip joint in order to restore, improve and maintain patient's functionality in day-to-day life. In 2007, The Lancet glorified THR as "*The Operation of the Century*"¹. The life expectancy of well-performing THR ranges between 10 to 15 years^{78,79} but many THRs successfully perform for longer durations.

Total hip replacement (THR) is a common orthopaedic surgery, see Figure 15. With the increasing life expectancy and growing population, the demand for hip replacement procedures is increasing every year²⁻⁴. More than 100,000 hip replacement procedures were recorded in the NJR in 2017/18, an increase of 3.6% from 2016/17⁵. In Australia, there were 47,972 hip replacement procedures recorded by the Australian Orthopedic Association National Joint Replacement Registry (AOANJRR) in 2017/18, an increase of 1.1% from 2016/17⁶.

As per the international standard ASTM F2068-15, THR or total hip arthroplasty is defined as:

*"Replacement of the natural femoral head with a prosthetic femoral head held in place by an implant extending into the shaft of the femur and replacement of the natural acetabulum with a prosthetic acetabulum. The prosthetic femoral head articulates with the bearing surface of the prosthetic acetabulum"*⁸⁰.

Total hip replacement surgery for the first time is known as the primary hip replacement surgery. Whereas surgery performed to remove and replace one or more components of a THR prosthesis is termed revision hip replacement surgery. The NJR reported 96,717 primary and 8,589 revision hip replacement procedures in 2017/18⁵.

An alternative to THR is hip resurfacing arthroplasty (HRA), see Figure 14. Total hip replacement operation requires the complete removal of the natural femoral head, drilling of the femoral medullary canal and insertion of the prosthetic femoral stem whereas the HRA operation includes reshaping of the natural femoral head and positioning a hip resurfacing femoral head without drilling of the femoral medullary canal. Therefore, HRA is a bone-conserving surgery compared to the THR, at least on the femoral side. As per the NJR, of all the primary procedures performed in 2017/18, 0.6% were hip resurfacing procedures⁵.

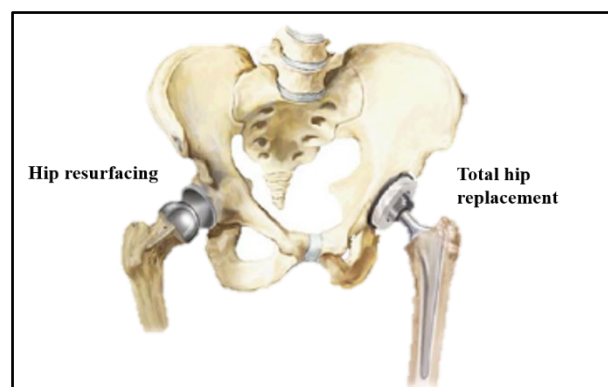


Figure 14 Total hip replacement and hip resurfacing prostheses. Image from Mattei et al. (2011)⁸¹.

Historically, initial designs of THRs comprised of a non-modular - the monobloc femoral component, i.e. femoral head and stem composed of a one-piece with a single neck length option. Therefore, it was difficult to adjust the leg length and offset to restore the natural anatomy of the leg. Hence, the modularity of contemporary THRs was introduced in the 1980s, and it offers various advantages to surgeons, including intraoperative flexibility to restore the natural anatomy of the hip joint^{82,83}. The modular hip component comprised more than one part. The modularity can be exhibited at:

- Head-neck junction between the femoral taper and the trunnion of the femoral stem
- A modular acetabular device which consists of an acetabular shell and acetabular liner

- Neck-stem junction between the trunnion and the body of the femoral stem (modular-neck femoral stems) (See Figure 15)

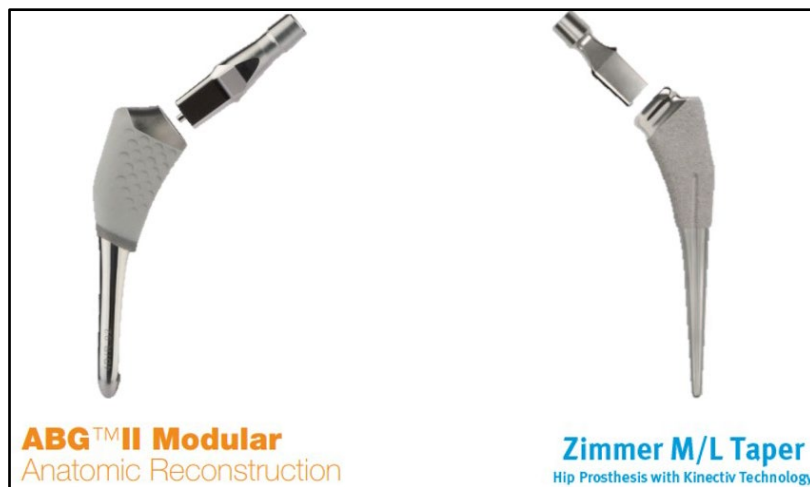


Figure 15 Modularity at the neck-stem junction of commercially available femoral stems. Images from manufacturers websites respectively^{84,85}.

The most common design of modular THR has a single head-neck interface^{27,86}. During the THR operation, the femoral head is placed on the trunnion of the femoral stem. A secure connection between the femoral taper and the trunnion is achieved by the impaction force applied on the femoral head using single or multiple impacts⁸⁷. Advantages and disadvantages of modularity at the taper-trunnion junction of THR are given in Table 2.

Table 2 Advantages and disadvantages of the modularity at the head-neck interface of the THR^{27,82,83,86}.

Advantages	Disadvantages
Allows more straightforward revision surgery without removing the well-fixed femoral stem	Potential site for the material loss in addition to the bearing surfaces
Intraoperative flexibility	Possibility of the fluid ingress at the modular junction
Taper-lock mechanism	Possibility of dislocation of the THR
Allows use of the different material combination, e.g. ceramic femoral head mounted on metallic trunnion	Risk of femoral neck fracture

A THR prosthesis is a ball and socket joint typically consisting of four components: an acetabular shell, acetabular liner, femoral head and femoral stem see Figure 16. The definitions of the hip prostheses' components are given in Table 3.

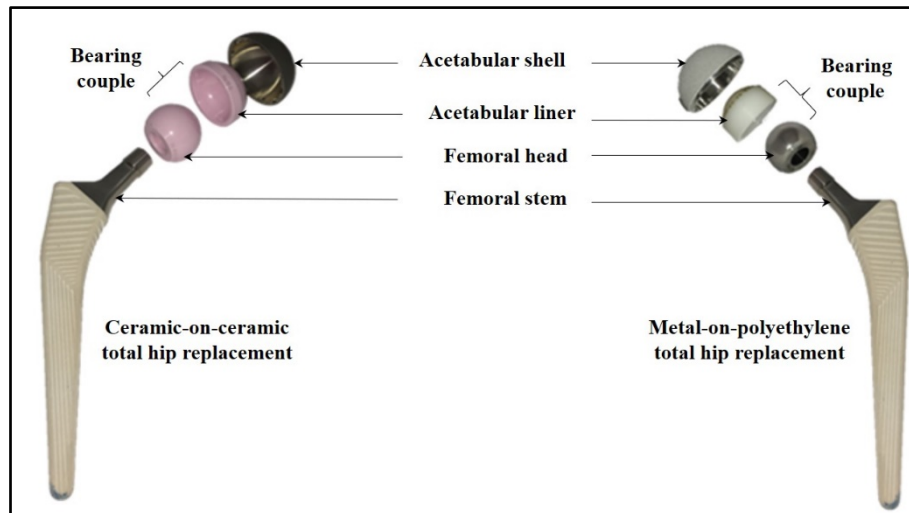


Figure 16 Main components of total hip replacement prostheses showing CoC THR (left) and MoP THR (right).

Table 3 Terms and definitions for hip prosthesis components as reported in the international standard and NJR glossary.

Term	Definition
Acetabular device	<i>“A modular acetabular system consisting of a minimum of two components, one of which includes the bearing surface and the second component is a modular acetabular shell intended to contain the bearing liner and contact bone or bone cement”⁸⁸</i>
Acetabular shell	<i>“The metallic external, hollow structure that provides additional mechanical support or reinforcement for an acetabular liner and whose external features interface directly with the bones of the pelvic socket (for example, through bone cement, intimate press-fit, coatings for attachment to bone cement or tissue, integral screw threads, anchoring screws, pegs, and so forth). The acetabular shell may be solid or contain holes for fixation to the pelvis or attachment of instrumentation”⁸⁸</i>
Acetabular liner	<i>“Portion of the modular acetabular device with an internal hemispherical socket intended to articulate with the head of a femoral prosthesis. The external geometry of this component interfaces with the acetabular shell through a locking mechanism which may be integral to the design of the liner and shell or may rely upon additional components (for example, metal ring, screws, and so forth)”⁸⁸</i>
Femoral head	<i>“Convex spherical bearing member for articulation with the natural acetabulum or prosthetic acetabulum”⁸⁰</i>
Femoral stem	<i>“The part of a modular femoral component inserted into the femur (thigh bone). Has a femoral head mounted on it to form the complete femoral component”⁵</i>

Throughout this study, the term ‘bearing couple’ refers to “a usually spherical ball and cup system intended to articulate against each other as a replacement for the articulating surfaces of the natural hip”⁸⁸, see Figure 16. The surfaces of the bearing couple are termed as the bearing surfaces.

Each component can be made from a variety of materials, in a different range of sizes as per the patient’s requirement. The largest manufacturers in the joint replacement market are Zimmer Biomet, DePuy Synthes, Smith & Nephew, and Stryker. According to the

Orthopaedic Industry Annual Report[®], the global hip joint replacement market increased by 3.2% in 2018 as compared to 2017, achieving revenue of USD 7.6 billion globally with a projection of USD 8.9 billion by 2023⁸⁹.

2.3.2 A brief history of hip arthroplasty

Prof. Themistocles Glück made the first attempt to replace a damaged hip joint of a patient using an ivory ball and socket joint in Germany in 1891⁹⁰. In the late 19th and early 20th centuries, interpositional arthroplasty was experimented by surgeons which involved placing various tissues (fascia lata, skin, pig bladders submucosa) between articulating surfaces of the damaged hip¹. In 1938, Mauris Smith-Petersen implanted a Vitallium (cobalt-chromium) cup as an interpositional device to cover the reshaped femoral head⁹¹. Phillip Wiles developed the first prosthetic THR in 1938 using stainless steel components⁹². Later many efforts at the replacement of damaged hip joints using implants were made; however, most of them were unsuccessful due to the use of inferior materials, poor design and mechanical failure¹. In the 1960s, the late Sir John Charnley revolutionised hip replacement surgery with the introduction of the low friction arthroplasty. Initially Charnley used the combination of stainless steel against polytetrafluorethylene (PTFE)⁹³. Nevertheless, within a year, PTFE implants showed high wear causing adverse soft tissue reactions. In search of low friction and low wear material combination, in 1962 Charnley implanted high-molecular-weight polyethylene as acetabular bearing material replacing PTFE⁹⁴, see Figure 17. This is an example of the MoP prosthesis as the metallic femoral head articulates against the polyethylene cup. The Charnley MoP implants exhibited good long-term survivorship with around 77-81% did not require revision 25 years after primary THR¹. Non-cross-linked UHMWPE has been used in the majority of THRs for over five decades^{7,8}. However, the articulation of the softer polymeric component against the harder metallic bearing surfaces leads to the production of numerous submicron-sized PE wear particles which can lead to osteolysis⁹⁻¹¹. Thus, in order to improve the wear resistance and therefore reduce the number of PE wear particles released, cross-linking of polyethylene was introduced in 1998⁹⁵. Therefore, even after 50 years, today, MoP is a popular choice as compared to other combinations⁵. The triumph of THR has resulted in its indications being expanded to more active and younger (<65 years) patients⁹⁶. Due to the high activity levels and demands in the

younger patients, rates of revisions are higher than those of older patients⁹⁷. Therefore, alternative combination of CoC THR have been used in younger patients¹⁵.

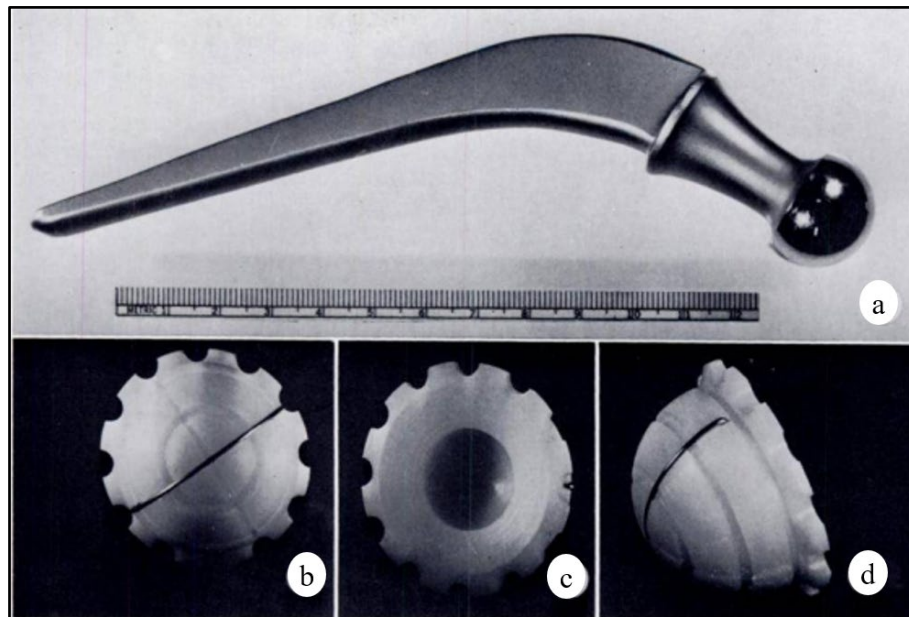


Figure 17 Charnley's low friction THR a) the stainless-steel femoral component and b), c) and d) high-molecular-weight polyethylene acetabular component. Image from Campbell and Rothman (1971)⁹⁸.

2.3.3 Types of THR prostheses

The NJR divided hip arthroplasty in following four types based on unique characteristics of the prostheses: the type of hip replacement, fixation type, materials used for bearing surfaces, and the size of the femoral head or internal diameter of the acetabular bearing⁵.

2.3.3.1 The type of hip replacement

Based on the type of the hip replacement prostheses are divided into THR and HR. These two types are described previously in section 2.3.1.

2.3.3.2 The fixation of THR

Based on the type of fixation used, THRs fall into the following categories: cemented procedure (when both the femoral stem and acetabular component are fixed using bone cement), uncemented procedure (when the femoral stem and acetabular component are fixed without any bone cement), hybrid procedure (when only the femoral stem is fixed using bone cement and not the acetabular liner) and reverse hybrid procedure (when only the acetabular component is fixed using bone cement and not the femoral stem). The bone cement can be defined as “*acrylic resin cements used for fixation of implant components whether with radio-opaque or non-radio-opaque properties and supplied as units containing pre-measured amounts of sterile powder and of sterile liquid in forms suitable for mixing at the time of implantation*”⁹⁹. In the NJR, the most commonly performed THR was an uncemented procedure (38%) in 2017/2018. However, the hybrid procedure (30%) for the first time was more common than the cemented (28%) THRs⁵.

2.3.3.3 The size of femoral head (or internal diameter of the acetabular bearing)

Based on the femoral head diameter size (in mm) used in the surgeries the THR prostheses are divided into following types: 22, 26, 28, 30, 32, 34, 36, 38, 40, 42, 44, 46, 48, 50, 52 and 54+¹⁰⁰. Figure 18 shows different femoral head sizes. The most commonly implanted femoral head size was 32mm in 2017/18 as per the NJR¹⁰⁰.

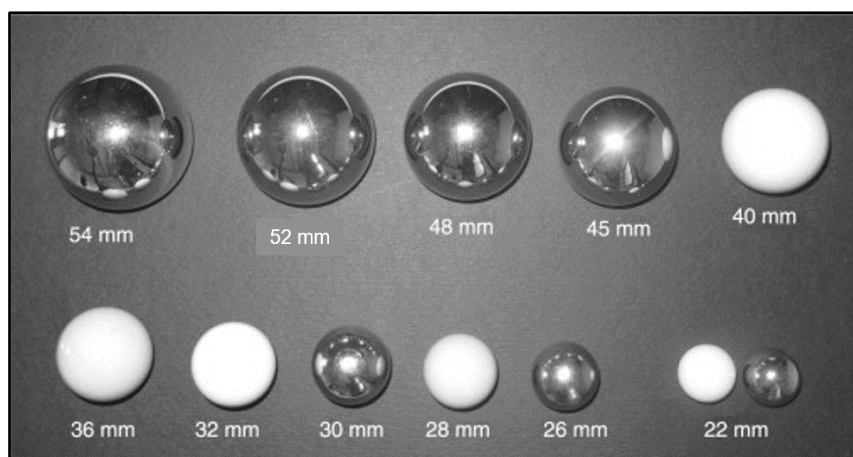


Figure 18 Femoral heads with different diameters. Image from Affatato (2014)¹⁰¹.

2.3.3.4 The bearing surfaces of the hip replacement

Based on materials used for the bearing surfaces, THRs can be divided into the following main categories: metal-on-polyethylene (MoP), ceramic-on-polyethylene (CoP), ceramic-on-ceramic (CoC), and metal-on-metal (MoM). Additionally, ceramic-on-metal (CoM) and metal-on-ceramic (MoC) have been used, but in small numbers⁵. By convention, the femoral head bearing material is listed first, and the acetabular bearing material is second. Metal-on-polyethylene (MoP) and CoC THRs are shown in Figure 16.

Figure 19 shows the change in the hip bearing material combinations since 2009 recorded by the NJR. The most commonly implanted combination is MoP, and the use of CoP bearings has showed a continuous increase². The usage of CoC bearings rose between 2009 and 2012; however, it has declined since then.

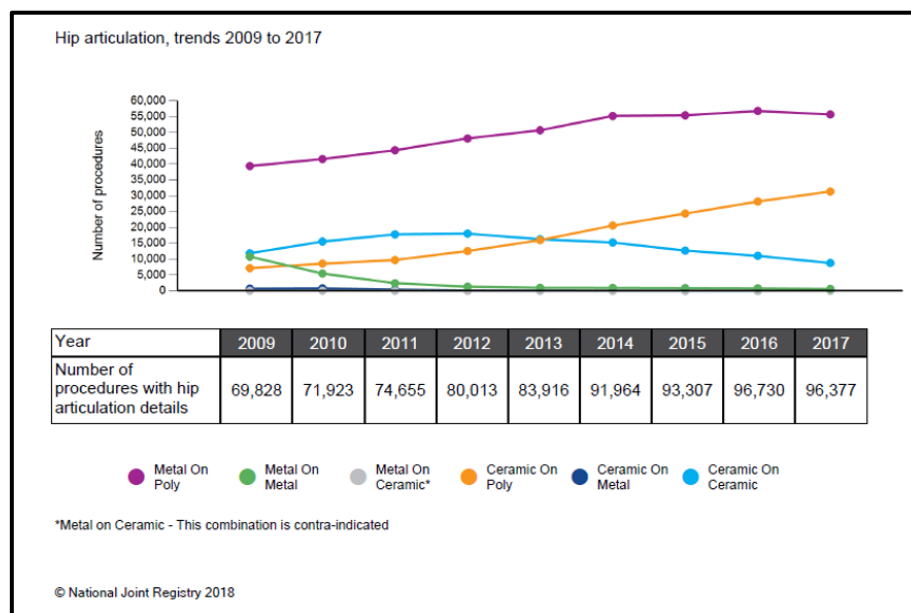


Figure 19 The change in the hip bearing material combinations since 2009 recorded by the NJR. Image from the NJR 15th Annual Report 2017/18⁵.

Metal-on-polyethylene (MoP) is the most commonly implanted bearing surface combination with the majority consisting of a CoCrMo alloy femoral head articulating against a polyethylene, either cross-linked polyethylene (XLPE) or non-XLPE, acetabular liner⁵.

2.3.4 Materials in THR

The American National Institute of Health (NIH) defined the term biomaterial as:

*“any substance or combination of substances, other than drugs, synthetic or natural in origin, which can be used for any period of time, which augments or replaces partially or totally any tissue, organ or function of the body, in order to maintain or improve the quality of life of the individual”*¹⁰². The Williams Dictionary of Biomaterials defined biocompatibility as “the ability of a material to perform with an appropriate host response in a specific application¹⁰³”. However, according to the international standard, no known implant biomaterial has been demonstrated to be completely free from the unfavourable host-immune response by the human body¹⁰⁴. Biomaterials used to replace the damaged hip joint require specific properties such as biocompatible, high strength, hardness, fracture toughness, and excellent corrosion and wear resistance¹⁰⁵. Most commonly used hip implant biomaterials are metals (cobalt alloys, Ti alloys, and stainless steel), ceramics (alumina, zirconia) and polyethylene [non-cross-linked ultra-high-molecular-weight polyethylene (UHMWPE), cross-linked UHMWPE (XLPE)] and XLPE) due to their biocompatibility.

2.3.4.1 Metals

Cobalt chromium molybdenum (CoCrMo) alloys are the most frequently used biomaterials for femoral heads owing to their high hardness, and excellent corrosion and wear resistance properties^{5,106}. Two common types of the CoCrMo alloys are: cast CoCrMo alloy¹⁰⁷ and wrought CoCrMo alloy¹⁰⁸. The American Society for Testing and Materials (ASTM) defined chemical composition for CoCrMo alloys used for surgical implants is given in Table 4.

Table 4 ASTM F75 CoCrMo alloy: chemical composition.

Element	Weight %
Cobalt, Co	Balance
Chromium, Cr	27-30
Molybdenum, Mo	5-7
Carbon, C	<0.35
Nickel, Ni	<0.5
Iron, Fe	<0.75
Silicone, Si	<1
Manganese, Mn	<1
Tungsten, W	<0.2
Phosphorus, P	<0.02
Sulphur, S	<0.01
Nitrogen, N	<0.25
Aluminium, Al	<0.1
Titanium, Ti	<0.1
Boron, B	<0.01

Wrought CoCrMo alloys are available commercially in two categories, ‘high carbon’ (0.15-0.35 wt% carbon) and ‘low carbon’ (less than 0.14 wt% carbon)¹⁰⁸. The increase in carbon content has been demonstrated to encourage the formation of the carbides¹⁰⁹⁻¹¹¹.

Additionally, it has been shown that high carbon CoCrMo alloys have better wear and corrosion resistance properties than low carbon CoCrMo alloys¹¹². Furthermore, the presence of Cr and Mo in the CoCrMo alloy forms spontaneous oxide layer (1-4 nm thick) that provide excellent corrosion resistance properties to these alloys^{32,106}.

One of the critical concerns of modular THRs is the selection of femoral stem material ^{113,114}. If the femoral stem implant material is stronger than the bone, then the femoral stem will carry more of the load. Therefore, the bone is shielded/protected from the applied stress, and this can lead to stress shielding followed by resorption of the bone material and implant failure^{115,116}. The Young's modulus (E) of Ti alloys (E = 110 GPa) is much closer to that of the natural bone (E = 55GPa) compared to CoCrMo alloys (E = 240 GPa) and 316L stainless steel (E = 210 GPa)¹¹⁷. Thus, the femoral stem is commonly composed of Ti alloys rather than stainless steel or CoCrMo alloy^{118,119}.

Furthermore, commercially pure Ti (Cp-Ti) and Ti-based alloys are known to be most biocompatible and corrosion-resistant of all surgical implant materials¹²⁰. This is owing to the spontaneous formation of TiO₂ passive layer (approximately 10 nm thick) on the surface of both materials¹²¹. Commercially Pure Ti (Cp-Ti) and Ti6Al4V alloy have similar corrosion resistance properties; however, the latter has more strength¹²². Moreover, Titanium-12Molybdenum-6Zirconium-2Iron (TMZF) beta Ti alloy (E= 80 GPa) was developed with lower modulus, higher toughness and tensile strength and to enhance osseointegration at the femoral stem-bone interface^{117,123}. Unfortunately, due to poor wear resistance property of Ti alloys compared to the CoCrMo alloys and stainless steel, they are not suitable as a bearing surfaces material^{17,119,124,125}. Thus, Ti alloys are not suitable material for the fabrication of the femoral taper.

The most commonly implanted bearing surface combination is MoP with the femoral head manufactured using CoCrMo alloy ⁵. Furthermore, the use of CoCrMo alloy has been used in the MoM bearings. In MoM prostheses, due to the absence of polymeric components osteolysis caused by PE wear debris is not a concern. However, in the mid-2000s many researchers, surgeons as well as joint implant registries reported high failure rate associated with DePuy Articular Surface Replacement TM (ASR) hip resurfacing system and ASRTM XL acetabular hip system ^{21,126-128}. Detailed timeline in terms of the NJR monitoring of ASRTM hip prostheses is shown in Figure 20.

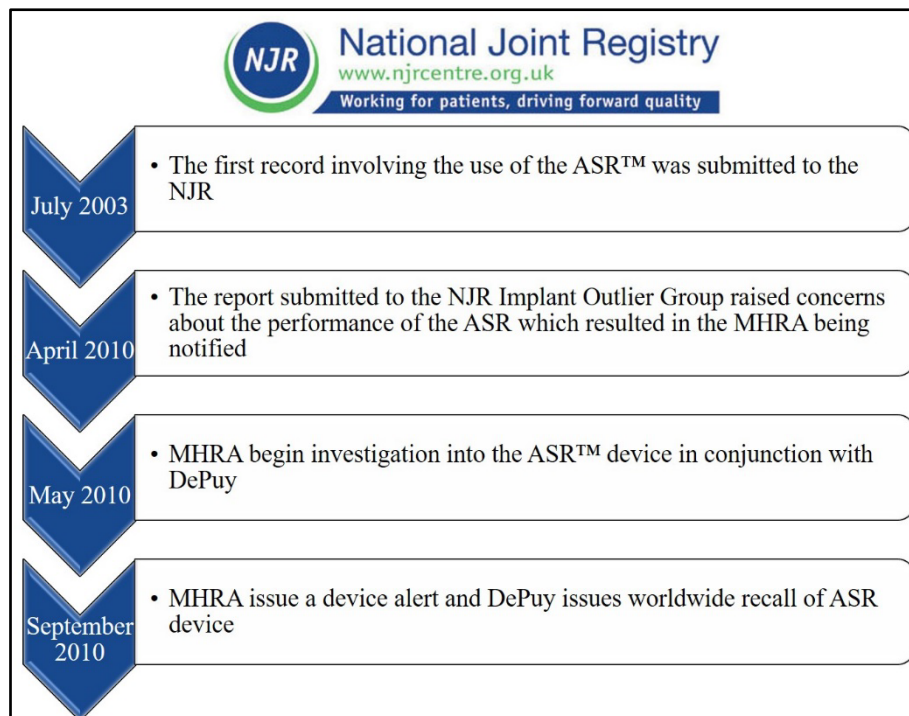


Figure 20 Detailed timeline in terms of the NJR monitoring of ASR™ hip prostheses¹²⁹. (MHRA: Medicines and Healthcare products Regulatory Agency of the Department of Health and Social Care in the United Kingdom).

However, the usage of MoM bearings almost vanished with less than 0.1% THR and 0.6% resurfacing procedures reported by the NJR(2017/18)¹⁰⁰. According to the NJR, metallic materials was used most commonly for the femoral head with 59%¹⁰⁰.

2.3.4.2 Ceramics

Ceramic-on-ceramic THR was introduced in the early 1970s by Boutin¹³⁰, and has gained in popularity with increasing numbers implanted each year⁵. Alumina ceramic has been used owing to excellent biocompatibility, high hardness and strength, inertness, corrosion, and wear resistance properties¹⁵. Over the years, ceramics have been developed to today's fourth-generation BIOLOX®*delta* ceramics, each generation benefiting from enhanced material properties and a corresponding reduction in wear, see Figure 21 and Figure 22. According to the NJR, 41% of hip replacement procedures used ceramic femoral heads¹⁰⁰. Interestingly, in 2017/18, the use of ceramic modular femoral heads increased by 1% compared with the operations performed in 2016/17¹⁰⁰.

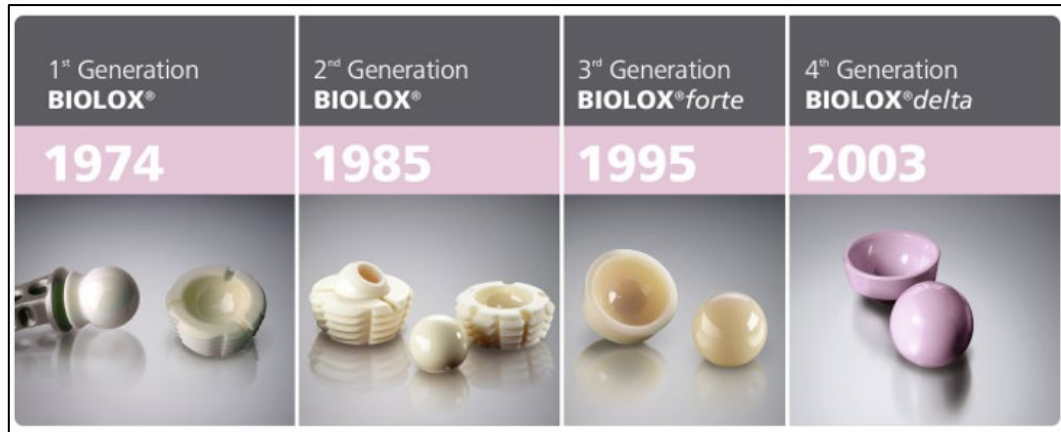


Figure 21 Generations of alumina ceramics used in hip replacement. Image from Ceramtec website.

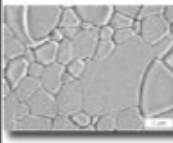
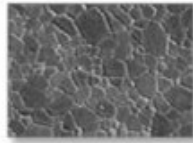
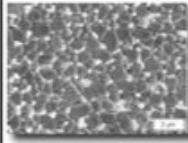
Properties of Ceramics	Alumina Ceramic ISO 6474 1994	1st and 2nd generation Alumina	3rd generation Alumina (Hipped)	Alumina Ceramic Composite
4-point bending strength	400Mpa	500Mpa	580 Mpa	>1000 Mpa
Average Grain Size	< 4.5µm	< 3.2µm	< 1.8µm	< 1,5 µm
Density	3.94g/cm3	3.96g/cm3	3.98g/cm3	4,37g/cm3
Microstructure				

Figure 22 Development of alumina ceramic. Image from Masson (2009)¹³¹.

BIOLOX®*delta* is the latest, fourth-generation ceramic, zirconia toughened alumina (ZTA) and composed of 82% alumina (Al_2O_3), 17% tetragonal zirconia (ZrO_2) particles, 0.5% strontium aluminate and 0.5% chromium oxide (Cr_2O_3)¹³². The strength of BIOLOX®*delta* composite is approximately twice as that of the third generation Alumina, see Figure 22. The excellent toughness of the BIOLOX®*delta* is mainly due to two mechanisms a) transformation toughening and b) platelet reinforcement, see Figure 23 a) and b) respectively¹³³. Firstly, the presence of small zirconia particles dispersed homogeneously is used to stop the propagation of the crack, see Figure 23 a). Secondly, elongated platelet-like structures formed by strontium oxide arrest the crack propagation, see Figure 23 b). Finally, the

alumina matrix is combined with a solid solution of chromium oxide for hardening^{131,133}. Chromium oxide gives the pink colour to BIOLOX®*delta*¹³⁴. More than 3.8 million femoral heads and 1.5 million liners of BIOLOX®*delta* have been implanted worldwide since its launch¹³⁵.

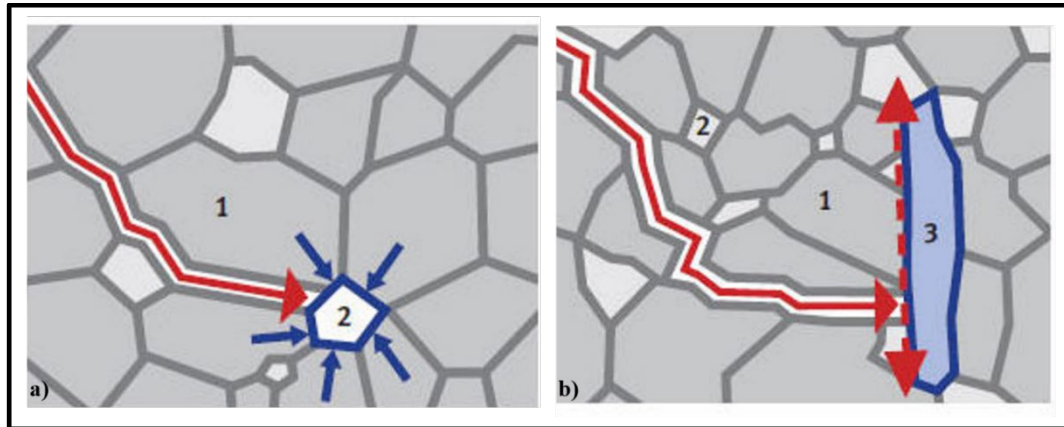


Figure 23 Prevention mechanisms for the crack propagation (shown by the continuous red arrow) in BIOLOX®*delta* ceramic: a) transformation toughening and b) platelet reinforcement. 1.Alumina grain, 2. Zirconia grain and 3. Plate-like crystal. Image from Zimmer¹³⁴.

2.3.4.3 Polymers

Chemical structure of ethylene and PE is shown in Figure 24. The following steps are involved in the manufacturing of non-cross-linked UHMWPE liners: polymerisation of ethylene gas into a resin powder, consolidation of UHMWPE resin powder into rods or sheets and machining of the rods into the desired shape, see Figure 25. After the production of UHMWPE acetabular liners, they must be sterilised, and vacuum packed for distribution. Initially, Charnley acetabular cups were manufactured at Wrightington hospital followed by chemical sterilisation. After 1967, Charnley acetabular cups were manufactured by Chas. F. Thackray Limited of Leeds and were irradiated by gamma (γ) radiation¹³⁶.

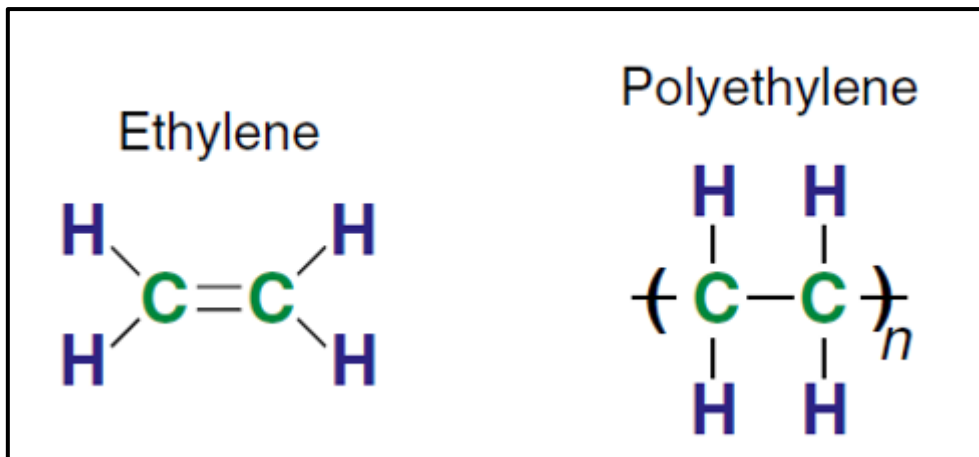


Figure 24 Chemical structure of ethylene and polyethylene. Image from Kurtz (2009)¹³⁷.

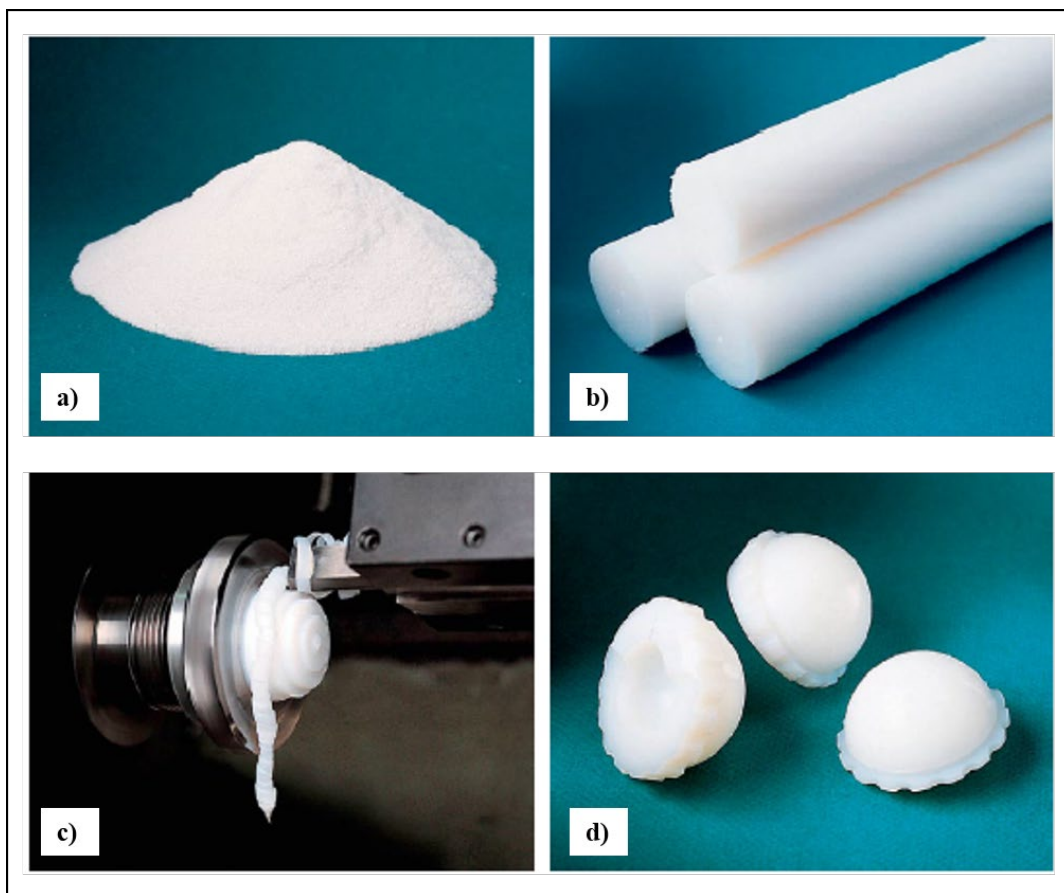


Figure 25 Processing of UHMWPE acetabular liners. a) UHMWPE resin powder, b) semi-finished UHMWPE rods that have been consolidated from the UHMWPE resin powder, c) Machining of the UHMWPE rods on a lathe, and d) UHMWPE acetabular liners after machining. Image from Kurtz (2009)¹³⁷.

Non-cross-linked UHMWPE has been used in the majority of THRs for over five decades^{7,8}. However, the articulation of the softer polymeric component against the harder metallic bearing surfaces leads to the production of numerous submicron-sized PE wear particles which can lead to osteolysis⁹⁻¹¹. Thus, in order to improve the wear resistance and therefore

reduce the number of PE wear particles released, cross-linking of polyethylene was introduced. The AOANJRR states, ‘XLPE is classified as UHMWPE that has been irradiated by high dose (≥ 50 kGy) gamma or electron beam radiation’ and also reported that 97.2% of hip procedures comprising of a PE component utilised XLPE acetabular liners in 2016⁶. Furthermore, the revision rates at 16 years for XLPE (6.4%) is lower than non-XLPE (12.4%) hip replacement procedures⁶.

The cross-linking applied in polymers can be defined as , “*the chemical structure of polyethylene is fundamentally altered by cross-linking, which itself is defined as the joining of two independent polymer molecules by a chemical covalent bond*”⁹⁵. Figure 26 shows the process of cross-linking of UHMWPE by γ or electron beam (Eb) radiation. Gamma or Eb radiation breaks down carbon-hydrogen and carbon-carbon bonds inducing cross-linking, scission of chains or immediate oxidation in the presence of oxidation. Additionally, cross-linking creates free radicals (uncombined electrons), which may cause long-term oxidative degradation of PE by reacting with oxygen molecules¹³⁸. Therefore, XLPE doped with the antioxidant vitamin-E has been developed to prevent long-term oxidative degradation of XLPE, undesirable post-irradiation heat treatments, and improve oxidative stability^{12,139}. The process of cross-linking of UHMWPE, while improving the wear properties of UHMWPE reduces the mechanical ones, making the acetabular liners more at risk of fatigue fracture¹⁴⁰. Furthermore, steep positioning of the acetabular liner that leads to stresses concentration or impingement is considered as a risk factor ¹⁴⁰. Not all XLPEs are the same, considering that apart from γ or EB radiation, annealing and melting technique can also influence the *in vivo* performance of XLPE liners. XLPE liners re-melted after γ or EB radiation exhibit good oxidation resistance but less fatigue resistance. On the other hand, XLPE liners annealed after γ or EB radiation and beneath the melting temperature usually exhibit good fatigue and wear resistance but poor oxidation resistance due to failure in the neutralization of all free radicals in this process.

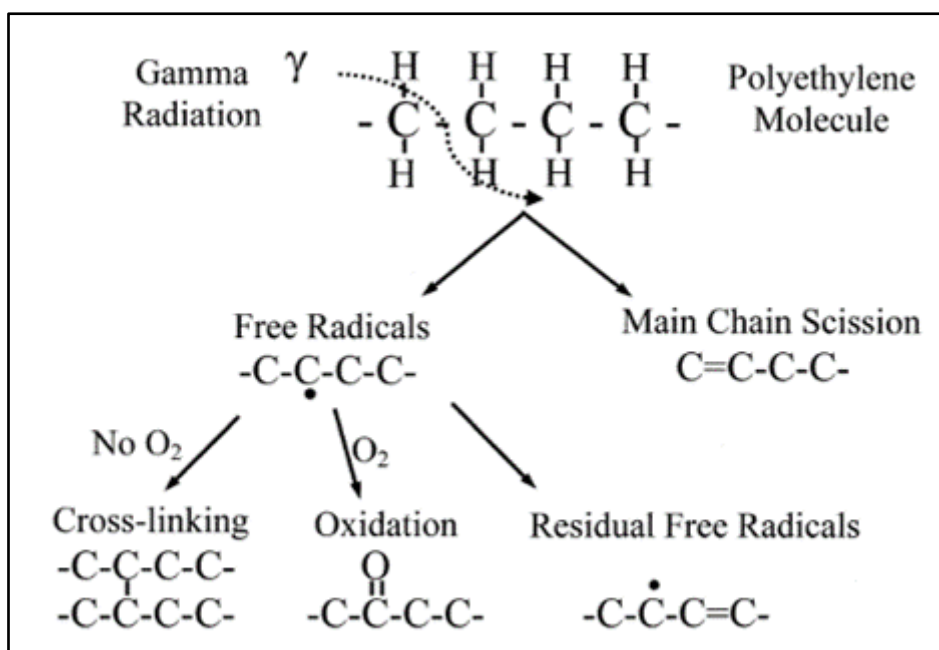


Figure 26 Gamma (γ) or electron beam (Eb) radiation of UHMWPE. Image from Campbell et al. (2004)¹⁴¹.

2.3.5 Potential causes of failure of primary THR and revision THR

The failure of a THR leads to the need for revision surgery. The most recent National Institute for Health and Care Excellence (NICE) guidance recommended that THR and HR prostheses should have revision rates 5% or less at ten years¹⁴². Potential causes of failure of the primary THR can be summarised into three groups, which are shown in Table 5.

Table 5 Potential causes of failure of primary THR¹⁴³.

Group	Associated conditions
Patient-related factors	Poor bone quality, sickle cell anaemia, high body mass index
Implant-related factors	Aseptic loosening, osteolysis, metallosis, periprosthetic fractures, delamination of the porous coating
Failures related to inadequate surgical technique	Malpositioning of components

Since the introduction of the NJR, aseptic loosening, dislocation (instability), adverse soft tissue reaction to particulate debris, pain and periprosthetic fracture are common indications

for revision surgery⁵. Aseptic loosening means the loosening of the prosthesis that may result from wear debris or inadequate fixation during the surgery. In 2017/18, aseptic loosening was recorded as the most common reason in 41% of revision surgeries⁵, see Figure 27. The initial response to particulate debris comprises a subtle inflammatory response that becomes more prominent as osteolysis progresses¹⁴⁴. The inflammatory environment triggers a cellular response characterised by elevated levels of tumour necrosis factor (TNF), receptor activator of nuclear factor- κ B (RANK)/RANK ligand (RANKL), Interleukin (IL) -6, IL-1, and IL-11. Most of these cytokines directly affect the differentiation and activity of osteoclasts leading to enhanced osteolysis¹⁴⁴.

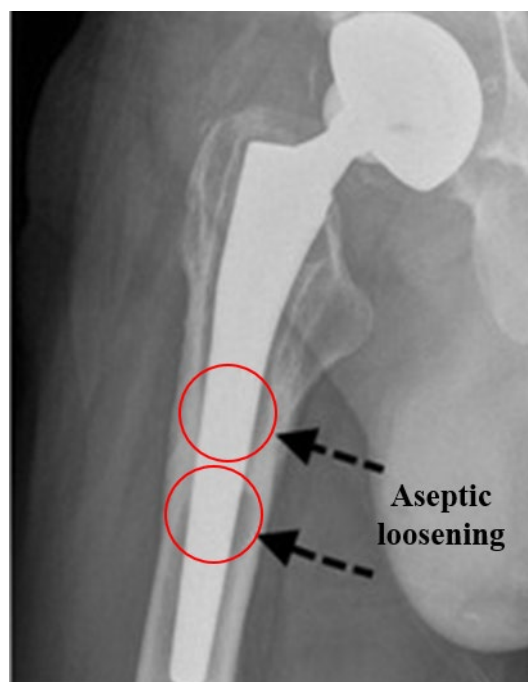


Figure 27 Aseptic loosening at the femoral stem indicated by black arrows. Image from Vanrusselt et al. (2015)¹⁴⁵.

Non-cross-linked UHMWPE has been used in the majority of THRs for over five decades^{7,8}. However, the articulation of the softer polymeric acetabular component against the harder metallic femoral bearing surfaces leads to the production of numerous submicron-sized polyethylene wear particles which can lead to osteolysis⁹⁻¹¹. As these submicron-sized polyethylene wear particles are produced and released into the periprosthetic tissues, the body's immune system attacks these particles by initiating a foreign body response. As a result of a foreign body response, macrophages attempt to break down polyethylene particles. However, polyethylene particles are inert, and they cannot be broken down. Therefore, a

complex biological cascade sequence is initiated where osteoclasts, i.e. bone-resorbing cells, are activated at the bone-implant interface leading to loosening of the implant.

The improvement of polyethylene wear resistance by cross-linking, and the alternative bearing materials such as hard-on-hard bearings including MoM and CoC with lower wear rates were introduced to solve problems associated with polyethylene wear particle-induced osteolysis and therefore hopefully increase implant longevity.

Clinical problems associated with higher than expected failure rates of MoM prostheses were collectively defined by the term, ‘Adverse reactions to metal debris (ARMD)’. In 2010, Langton *et al.* introduced, ARMD, as an umbrella term to illustrate the painful failure of large-diameter MoM THR and HR prostheses with one or more of the following features: large sterile effusion of the hip, macroscopic tissue necrosis, aseptic lymphocyte dominated vasculitis associated lesion (ALVAL) and metallosis including pseudotumor^{21,126}. In 2008, Pandit *et al.* introduced the term ‘pseudotumor’ to describe a cystic, solid, or mixed mass communicating with MoM HR prostheses¹⁴⁶. The NJR used the ALVAL term to describe *“the generality of adverse responses to metal debris, but in its strict sense refers to the delayed type-IV hypersensitivity response”*⁵. Initially, ARMD related failure were reported for MoM bearing surfaces^{126,147}; however, subsequently, it has been shown that this type of failure could also arise from the taper trunnion junction of MoM THRs^{19,20}. Recently, many studies have been reported ARMD associated with modular THRs without MoM bearing surfaces^{42-45,148,149}.

In 2008, the NJR introduced the term ‘adverse soft tissue reaction to particulate debris’ for an indication of the revision surgery⁵. Furthermore, the NJR reported adverse soft tissue reaction to particulate debris responsible for 11% of revision surgeries in 2017/18⁵. Additionally, researchers, particularly in the US, used the term ‘adverse local tissue reaction’ (ALTR) rather than ARMD to describe problems associated with the failure of MoM hip prostheses^{150,151}. Furthermore, in the same term, ALTR has been used more commonly to describe similar clinical problems associated with conventional MoP hip prostheses^{148,152-154}.

Figure 28 shows the overall risks of revision for cemented and uncemented hip prostheses at 14 years⁵. Metal-on-metal prostheses (both THR and HR) showed a high overall risk of

revision, and the NJR reported minimal current usage of these prostheses⁵. In cemented prostheses, cement mixing time and pressure required for the setting of the cement require skills and precision^{155,156}. In uncemented prostheses, the cement is not used; instead, the surface is coated with the hydroxyapatite for bone ingrowth. The uncemented prostheses are expensive than the cemented for bone ingrowth¹⁵⁶. Hence, it would be cost-effective for the NHS (public healthcare provider) to utilise cemented rather than uncemented prostheses.

The optimal method of fixation for primary THR, especially cemented or uncemented fixation, is still debatable^{155,157}. It has been hypothesized that the generation of wear debris either from bone cement or PE particle, may have a common route in the damage of periprosthetic bone^{155,158}. Common causes of revision in cemented and uncemented THRs included aseptic loosening, pain, periprosthetic fracture, implant wear, infection, dislocation, lysis, malalignment or adverse reaction to particulate debris⁵. In a randomised control trial, Abdulkarim et al. reported no significant difference between cemented and uncemented fixation group in terms of implant survival as measured by mortality, revision rates or the complication rate¹⁵⁵. Thien et al. investigated the prevalence of periprosthetic fracture around the femoral component in cemented and uncemented THRs¹⁵⁹. They reported a rate of 0.47% for uncemented stems and 0.07% for cemented stems. However, the risk of revision was very low. Moreover, Nayak et al. compared the incidence of acetabular osteolysis and reported found no significant difference in the cemented and uncemented THRs¹⁵⁸. The risk of revision in CoP bearing surfaces remained particularly low, see Figure 28 and therefore, the NJR reported increased use of CoP with time⁵.

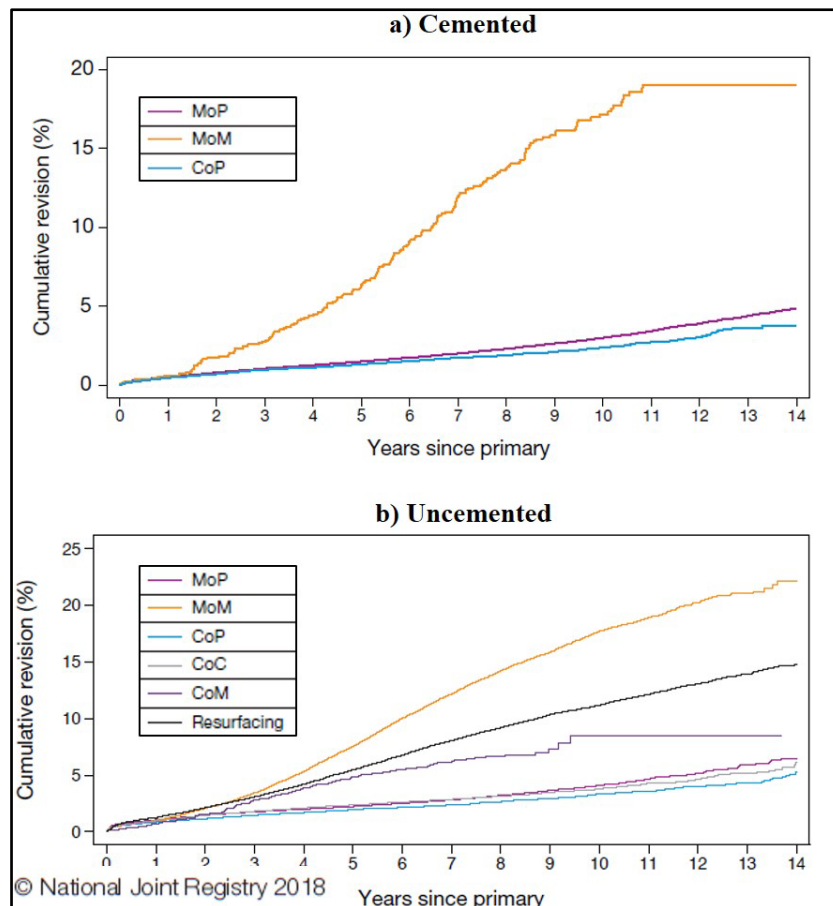


Figure 28 Risk of revision in a) cemented and b) uncemented prostheses by bearing surface as recorded by the NJR. Images from the NJR's 15th Annual Report 2017/18⁵.

2.4 Biotribology and *in vitro* wear testing of THRs

This section describes the biotribology, i.e. friction, lubrication and wear of THRs. Then, laboratory hip simulator wear testing methods and review of *in vitro* hip simulator wear testing of CoC and MoP bearing surfaces as well as retrieval studies are summarised. Additionally, an overview of the wettability of the biomaterials used for THR is provided.

“God made the bulk; surfaces were invented by the devil” is one of the famous quotes from Nobel laureate Wolfgang Ernst Pauli¹⁶⁰. Even at the atomic level, the elimination of an electron from the surface of an atom (i.e. ionisation) alters the fundamental structure of its surface layer. In THR, bearing surfaces successfully articulating against each other is one of the essential factors of the long-term success of a prosthesis due to the wear generated by this articulation. Therefore, it is necessary to investigate friction, wear and lubrication phenomena, i.e. biotribology of hip prostheses. The word “tribology” (Greek: ‘tribos’ means

to rub and ‘ology’ means the study of) was coined by Dr Peter Jost in 1966 and is defined as “*the science and technology of interacting surfaces in relative motion*” and includes the study of friction, wear, and lubrication¹⁶¹. In 1970, Dowson introduced the term ‘biotribology’ as “*those aspects of tribology concerned with biological systems*”¹⁶².

2.4.1 Wear

The international standard, ASTM G40-17 defined ‘wear’ as “*alteration of a solid surface by progressive loss or progressive displacement of material due to relative motion between that surface and a contacting substance or substances*”¹⁶³. The most common wear mechanisms in artificial joints are abrasive wear, adhesive wear, fatigue wear and third-body wear suggested by Burwell and Strang¹⁶⁴. The definitions of common wear mechanisms as per the international standards are given in Table 6.

Table 6 Wear mechanisms and their definitions as per the international standard ASTM G40-17¹⁶³.

Type of wear	Definition
Abrasive wear	<i>“wear due to hard particles or hard protuberances forced against and moving along a solid surface”.</i>
Adhesive wear	<i>“wear due to localized bonding between contacting solid surfaces leading to material transfer between the two surfaces or loss from either surface”</i>
Corrosive wear	<i>“wear in which chemical or electrochemical reaction with the environment is significant”</i>
Fatigue wear	<i>“wear of a solid surface caused by fracture arising from material fatigue”</i>

The significance of wear is not only linked to the reduced function and replacement expense of a THR component but also the adverse reactions of wear particles^{165,166}. Such as, wear particles generated from hip prostheses have been shown to produce adverse local tissue reactions, osteolysis and loosening of the implant^{106,167}. Furthermore, the wear mechanisms from Table 6 may occur in sequence or simultaneously, e.g. wear particles generated as a result of adhesive wear, can cause abrasive wear by acting as a third body between contacting

surfaces. ‘Three-body abrasive wear’ is defined as “*a form of abrasive wear in which wear is produced by loose particles introduced or generated between the contacting surfaces*” and the loose particles are considered as a “third body”¹⁶³. There are many sources of third bodies in hip arthroplasty, and they are: assembly/impaction chipping, bone cement, bone particles, burnishing from loose stems, cutting guide abrasion, fixation screw fretting, hydroxyapatite particles, instrument scratching, locking mechanism breakage, matte/precoat stem abrasion, microseparation impact, modular connection fretting, neck impingement, porous coating particles, radiopacifier particles, trochanteric reattachment wires¹⁶⁸.

Archard proposed the theory of sliding wear¹⁶⁹. Sliding wear can be defined as “wear due to the relative motion in the tangential plane of contact between two solid bodies”¹⁶³. The Archard’s wear equation is defined below, see Equation I¹⁷⁰:

$$Q = \frac{KW}{H}$$

Equation I

Where Q is the volumetric wear per unit sliding distance, W is the normal load, H is the hardness of the softer surface and K is the wear coefficient or coefficient of wear. It is important to note that K is dimensionless and always less than 1. In engineering applications, the quantity K/H is usually incorporated together and given the symbol, k , the dimensional wear coefficient (mm^3/Nm)¹⁷⁰. The resulting wear equation is defined below, see Equation II¹⁷¹:

$$V = kLx$$

Equation II

Where V is the volumetric wear, k is the dimensional wear coefficient, L is the applied load and x is the sliding distance. This equation is called the Lancaster wear equation¹⁷¹. The dimensional wear coefficient, k , represents the volume of material removed by wear (in mm^3) per unit sliding distance (in metres), per unit normal load (in newtons) and is often referred to as the wear factor.

The wear factor has been calculated in laboratory studies involving pin-on-plate or pin-on-disc wear testing rigs. Jin et al. reported the use of wear rates rather than wear factors for

comparison between different bearing surfaces because the wear factors determined from pin-on-plate rigs may be quite different from those measured in the hip joint simulators¹⁶⁵. In hip simulator tests, the determination of the wear rate plays a significant role in the assessment of THR designs¹⁷². It allows direct comparison of bearing surface material combination to be used in THR prostheses. As specified in the international standard, ISO 14242-2, Implant for surgery- Wear of total hip-joint prostheses Part 2: Methods of measurement, the wear behaviour is acquired after fitting a line by least square method throughout the cumulative mass loss data, as a function of the number of test cycles¹⁷³. The wear rate (in mm^3/Mc) is simply calculated as the slope of the linear regression line by plotting the average volumetric loss (mm^3) against the number of cycles (Mc). Therefore, the wear factor using Equation II has not been calculated in this study. However, the wear rates as per the ISO 14242-2 have been obtained throughout this study and the results were compared with the literature.

Various types of wear tests are conducted in the laboratory to measure wear and to study the tribological processes in THR prostheses. In the 1960s, the American Society for Lubrication Engineers recorded over 200 types of wear tests and laboratory equipment in use¹⁷⁴. Later, multi-axis wear simulation devices were employed in order to assess the wear of biomaterials, in clinically relevant testing conditions and motions^{41,175,176}. In the late 1970s, Wright and Scales highlighted:

“Although it is not yet mandatory, it is inexcusable to use total hip prostheses in man that have not been adequately tested in the laboratory”¹⁷⁷.

2.4.2 Wear screening devices

Biomaterials are initially tested in relatively uncomplicated and inexpensive wear screening devices such as pin-on-plate or pin-on-disk machines, see Figure 29. These test rigs offer information exclusively on the intrinsic characteristics of the biomaterial under investigation. Wear screening tests are relatively inexpensive and require simplified specimen geometry. However, the actual hip prostheses are not involved in the wear screening tests.

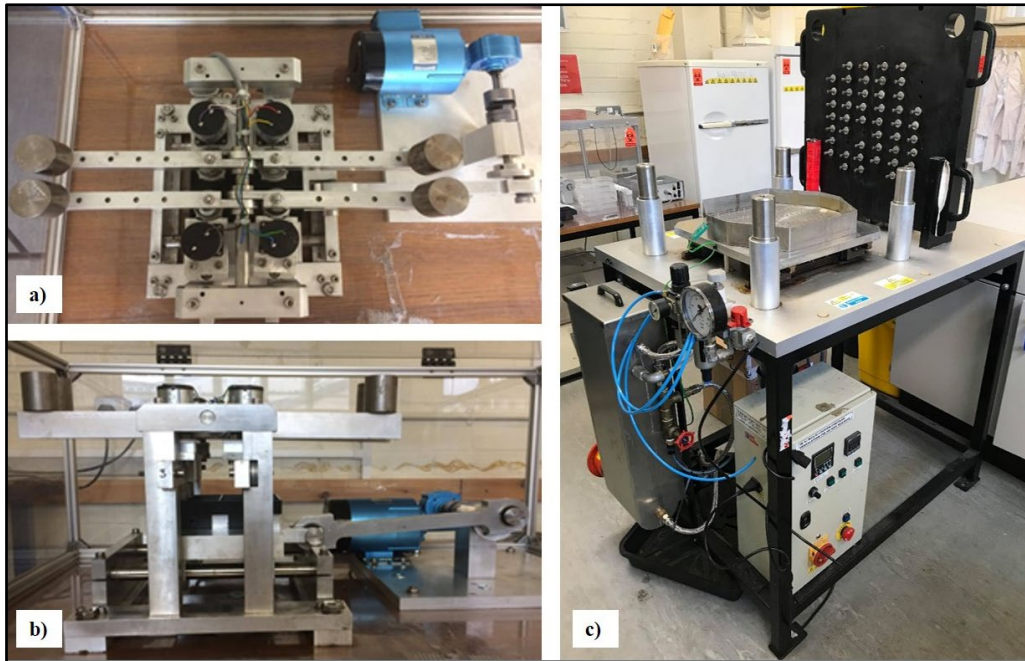


Figure 29 a) and b) shows top and side views of pin-on-plate wear testing rig respectively and c) shows pin-on-disk rig from the Biotribology lab, Newcastle University.

Wear screening is an essential preliminary step in assessing biomaterials for THRs.

Following wear screening tests, further testing is necessary to evaluate the performance of the actual hip prostheses in simulated physiological conditions. This is accomplished through the use of sophisticated machines called hip simulators, which test actual hip prostheses with clinically relevant loading and motion to predict some features of clinical performance of the prostheses under investigation^{166,175}.

2.4.3 The human gait cycle and hip joint wear simulators

In the 1960s, the first hip simulators were developed as a consequence of Sir John Charnley's work¹⁷⁸⁻¹⁸⁰. In 1970, Dowson et al. described 'a joint simulating machine for load-bearing joints' with a single station¹⁸¹. However, in the early 1980s, Clarke described a multi-station and computer-controlled hip joint simulator¹⁸². Clarke reported an overview of hip simulators to that date and also reported the benefit of having multiple stations over a single station in a single hip simulator test¹⁸². Since then, hip simulator wear testing has been continuously upgrading to simulate actual prostheses in as close as clinically relevant conditions⁴¹.

Commercial hip simulators have been available since the 1990s. Nowadays, the laboratories of almost every one of the major orthopaedic companies and several universities worldwide possess hip joint simulators¹⁶⁶. Figure 34 shows the commercially available hip simulators.

A hip simulator can be defined as:

*“Any device which, under appropriate test conditions, causes a prosthesis to wear in a manner substantially equivalent to that which it would experience in typical clinical use in a patient. In order to accomplish this, a hip joint wear simulator will typically apply a set of motions and loads and a lubricant that, in combination, create tribological conditions comparable, but not necessarily identical, to those occurring in vivo”*¹⁶⁶.

To understand hip joint wear simulator motion, it is first important to consider human gait cycle as explained in the following section.

2.4.3.1 Gait cycle

The systemic study of human walking is known as gait analysis. Michael W. Whittle defined walking as *“A method of locomotion involving the use of the two legs, alternately, to provide both support and propulsion”*¹⁸³. In order to differentiate walking from running, Whittle added: *“at least one foot being in contact with the ground at all times”*¹⁸³. Also, Whittle defined the gait cycle as *“the time interval between two successive occurrences of one of the repetitive events of walking”*¹⁸³.

The gait cycle encompasses all the events that occur between two leg movements in the cycle. Many researchers use the initial contact of the right foot (leading leg), i.e. the moment at which right foot touches the ground, for gait analysis. Each gait cycle consists of seven distinct events initial contact (heel strike), opposite toe-off, heel-rise, opposite initial contact, toe-off, feet adjustment and tibia vertical, see Figure 30. The seven events of the gait cycle are subdivided into seven distinct periods: heel strike, loading response, mid-stance, terminal swing, pre-swing, initial and mid-swing and terminal swing, see Figure 30.

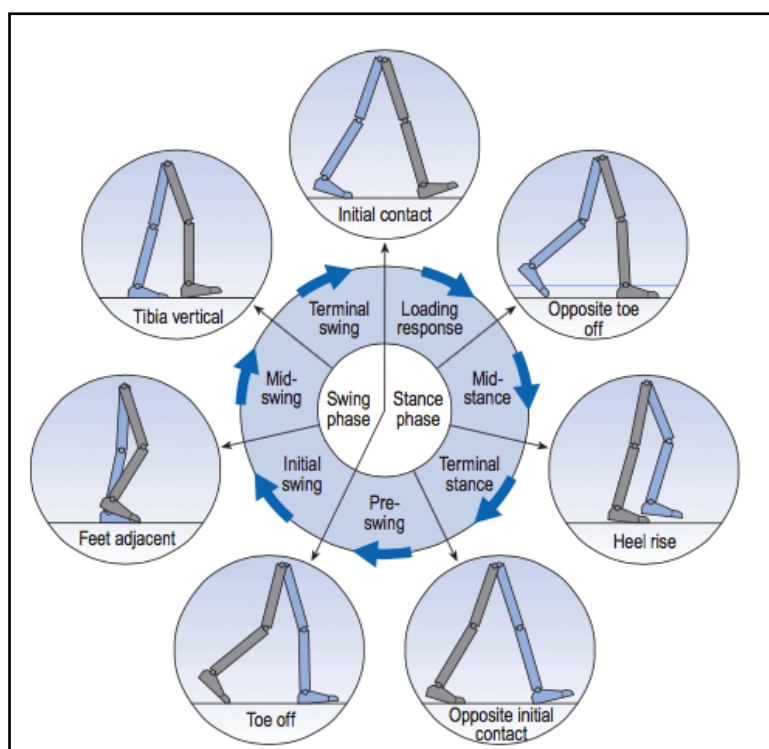


Figure 30 Seven events in a Gait cycle. Image from Whittle (2014)¹⁸³.

The gait cycle is divided into two main phases: stance phase and swing phase¹⁸³. The stance phase begins at the moment the heel of one leg touches the ground (heel strike) and terminates at the instant that the toes of the same leg leave the ground (toe-off). The time required to accomplish all the events of the stance phase contributes approximately 60% of the total gait cycle time. The swing phase begins as soon as the toe of one leg leaves the ground and terminates at the instant that heel of the same leg strikes the ground. The time required to accomplish all the events of the swing phase contributes approximately 40% of the total gait cycle time¹⁸³.

If the gait cycle of the right foot begins (right initial contact) then at the same time the gait cycle of left foot ends (left toe-off) and at this point of time both feet come in contact with the ground, and this is known as double support¹⁸³. During the swing phase of one leg, only the opposite leg is on the ground, and entire body weight is supported by this leg and is known as single support. Thus, each gait cycle consists of two periods of double support and two periods of single support¹⁸³. The human gait cycle is summarised in Figure 31¹⁸⁴.

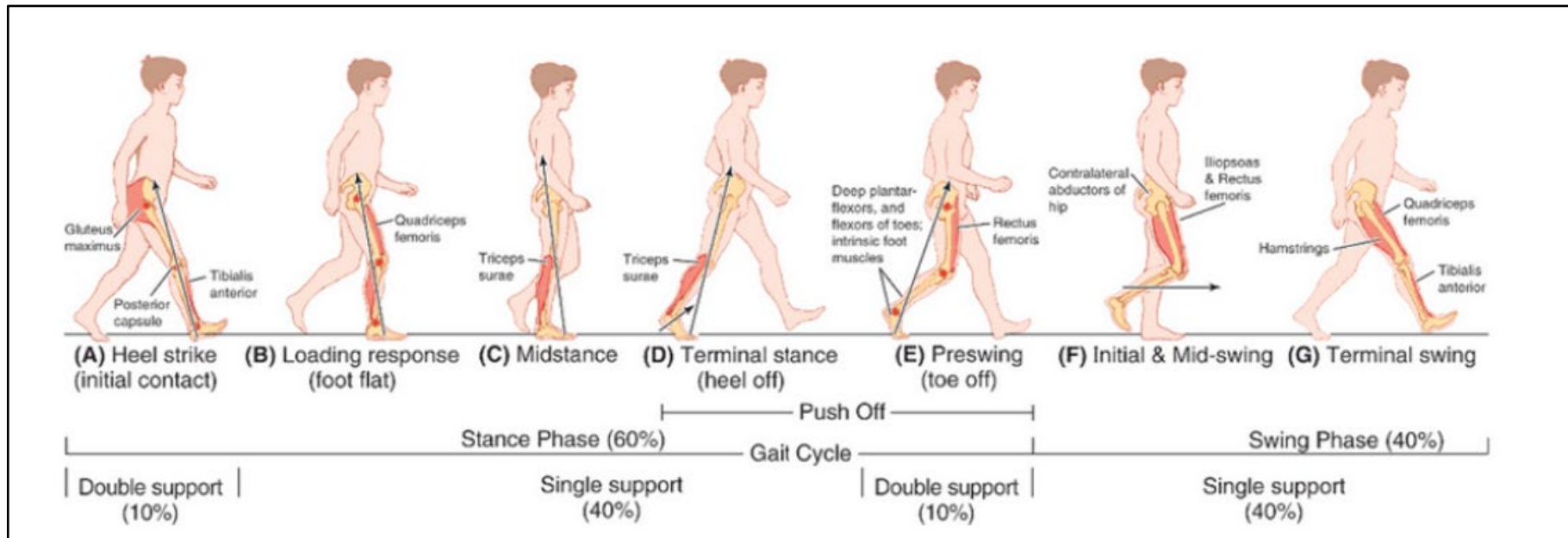


Figure 31 Normal gait cycle. Image from Rajtůková et al. (2014)¹⁸⁴.

2.4.3.2 Load acting on the natural hip joint

The hip joint is continuously loaded during day-to-day activities of a healthy human being. While standing upright on both legs, the weight of the upper body is equally distributed across both legs via both hip joints. In 1966, Paul established a double peak loading profile during normal gait¹⁸⁵. Paul measured the muscle activity during standard walking from 16 healthy volunteers using body markers to measure movement with cinematic recording, and a force plate on the floor. Paul reported a peak force value of 3.9 times body weight at the hip joint and low force (1.24 times bodyweight) during the swing phase.

The load acting on the hip joint during different activities such as walking, running, and climbing stairs is significantly different from each other. The forces acting on the hip joint *in vivo* are summarised in Table 7. It is essential to notice that all these measurements were carried out using instrumented femoral prostheses (i.e. an implant with a transducer in the femoral stem) on the patient who had undergone total hip replacement surgery⁵⁰. Instrumented femoral prostheses were intended for research focused on *in vivo* examining the biomechanics of the THRs¹⁸⁶. They have been designed to collect data, optimise the mechanical design, track the healing process and improve the rehabilitation processes after THR surgery¹⁸⁶. Furthermore, up to 9 years of *in vivo* data were obtained from instrumented femoral prostheses without reporting any side effects¹⁸⁶.

Table 7 Force acting on the hip joint measured using instrumented prostheses. Adapted from Byrne et al. (2010)⁵⁰.

Activity	Force acting on the hip joint × Body Weight (N)
Slow walking	1.6 to 4.1
Normal walking	2.1 to 3.3
Fast walking	1.8 to 4.3
Ascending stairs	1.5 to 5.5
Descending stairs	1.6-5.1
Jogging, running	4.3 to 5.0
Standing up	1.8 to 2.2
Sitting down	1.5 to 2.0
Stumbling	7.2-8.7

2.4.3.3 Hip joint simulators

Hip joint simulators have been built to simulate the biomechanics of the natural hip joint and replicate wear rates, wear patterns and wear debris observed clinically, in controlled laboratory conditions using actual hip prostheses^{40,41}. The international standard ISO 14242, ‘Implants for surgery - Wear of total hip-joint prostheses’ have been established for wear testing¹⁸⁷ and wear measurement¹⁷³ of THRs. Testing condition as per the ISO 14242-1 (*“Implants for surgery -Wear of total hip-joint prostheses Part 1: Loading and displacement parameters for wear-testing machines and corresponding environmental conditions for test”*) are shown in Table 8.

Table 8 Testing conditions as per the ISO 14242-1¹⁸⁷.

Dynamic loading	Minimum 0.3 kN and maximum 3.0 kN
Applied motion	Flexion/extension (FE), abduction/adduction (AA) and internal/external rotation (IER)
Frequency	1 Hz \pm 0.1 Hz
Test duration	5 million cycles
Test fluid	Calf serum diluted with deionised water (a protein 30 g/L \pm 2 g/L)
Test fluid volume	Capable of maintaining the contact surfaces immersed in the fluid test medium (at 37 °C \pm 2 °C)

As per the ISO 14242-1, the hip simulator test must be conducted until one of the following three things occurs: completion of 5 million cycles, break-up or delamination of the bearing surfaces, failure of the hip simulator to maintain applied loading and displacement parameters¹⁸⁷.

As a day-to-day activity for evaluating performance after THR, reference is generally made to the gait cycle or normal walking cycle. A comparison of the normal gait cycle (see Figure 31) to ISO standard is shown in Figure 32.

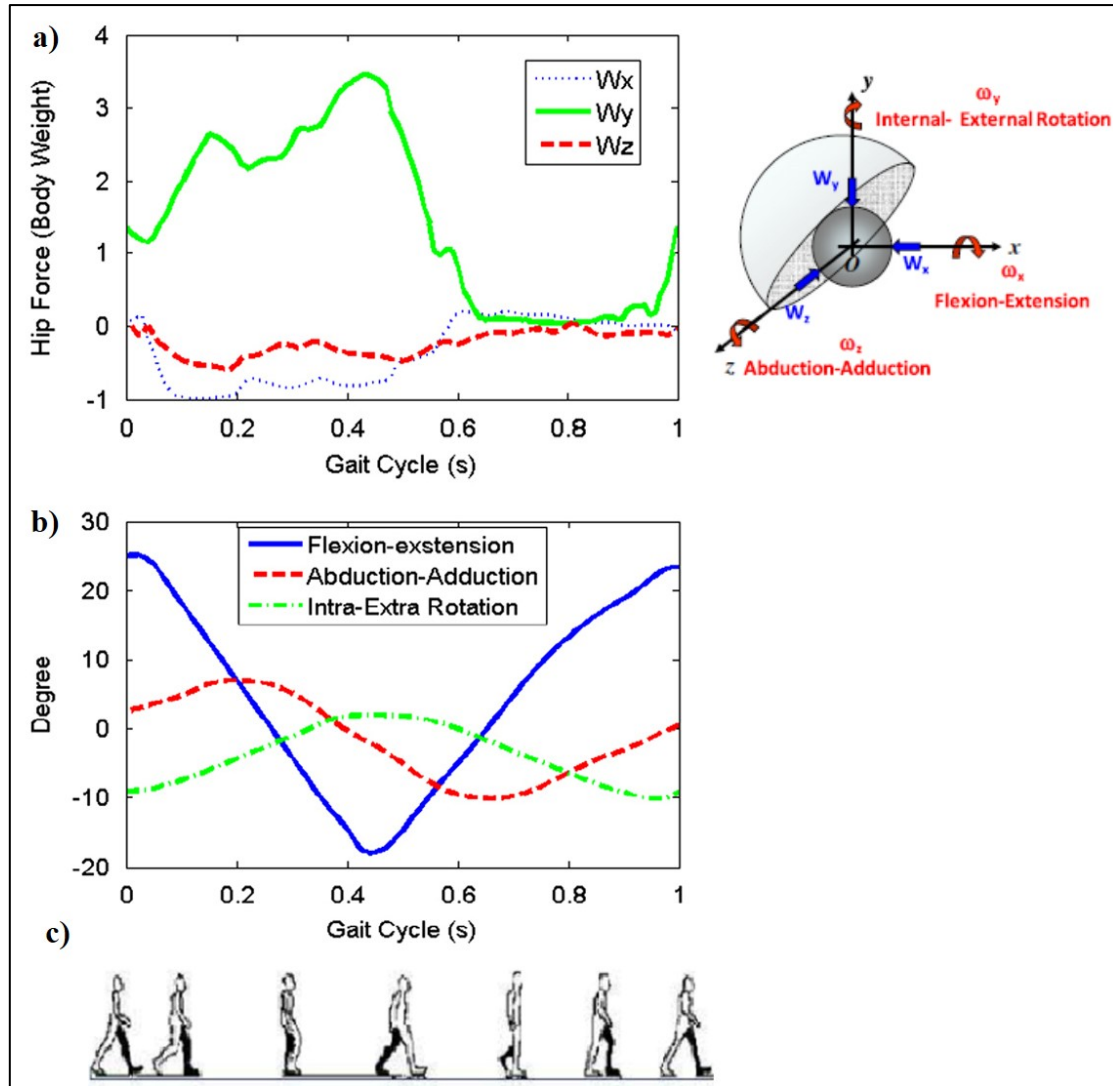


Figure 32 Comparison of the normal gait cycle with the hip simulator motion and forces: a) the three components of the hip force (W_x , W_y and W_z), scaled with respect to the body weight (BW) and corresponding hip angles taken from the ISO 14242-1 and c) normal gait cycle. Image from Mattei et al. (2011)⁸¹.

In most hip simulators only the vertical load [W_y , see Figure 32 a)] component and FE motion of the standard walking cycle are considered, see Figure 33. The variation of vertical loading and FE motion along with either AA or IR or both motions could be added in the hip simulator depending upon the manufacturer. The applied motion and dynamic loading in the hip simulators usually represent a standard gait cycle also called steady walking conditions or continuous level walking with double peak loading. Figure 34 and Table 10 shows pictures and description of currently used hip simulators, respectively. Hip simulators used in various laboratories for testing of the bearing surfaces of hip prostheses differ from each other in many parameters such as applied dynamic loading, applied motions, the position of the hip prostheses (anatomical/non-anatomical).

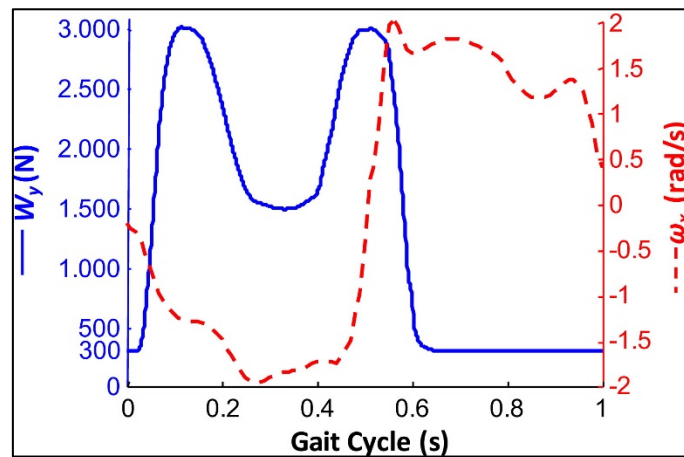


Figure 33 Vertical load (W_y) and FE angular velocity (ω_x) for BW= 750N according to ISO 14242-1. Image from Mattei et al. (2011)⁸¹.

Furthermore, type of lubricant and additives such as antibacterial agents, the temperature of the lubricant bath varies across the laboratories, which are summarised later in Table 11 for CoC and Table 12 for MoP hip simulator tests.

The natural lubricant in the human body is synovial fluid. Therefore, it may seem appropriate that synovial fluid should be employed for *in vitro* wear testing of hip prostheses.

Nevertheless, there are many concerns with this concept⁵⁵. Firstly, there may be ethical issues with taking synovial fluid from humans as these individuals need the natural lubricant to allow their joints to function. Secondly, in the natural hip joint, the volume of synovial fluid is in the range of 0.2-0.4 mL^{54,55}. It would not be possible to obtain the required volume of synovial fluid to carry out a hip simulator test for minimum of five million cycles. Thirdly, the characteristics such as pH and protein concentration of natural synovial fluid differ between humans and are influenced by disease^{54,59,188}.

Therefore, a variety of alternative lubricants have been used for laboratory testing of biomaterials in the literature, examples of commonly used lubricants are water, ringer's, solution, dilute bovine serum, gelatine-based protein solutions⁵⁵. The effectiveness of these alternative lubricants has been investigated based on comparison of the wear debris and wear rates with that seen *in vivo*⁵⁵. Harsha and Joyce summarised the advantages and disadvantages of alternative lubricant⁵⁵ and the results are shown in Table 9. Therefore, diluted bovine serum with the protein concentration within the physiological range of the joint fluid is used for hip simulator wear testing¹⁸⁷.

Table 9 Advantages and disadvantages of commonly used lubricants in *in vitro* studies⁵⁵.

Lubricant	Advantages	Disadvantages
Water	Inexpensive and safe, minimal degradation or contamination by bacteria	Wear rates are inconsistent due to transfer film. Wear debris size and shape are not representative of clinical wear debris
Ringer's solution	Inexpensive and safe, minimal degradation or contamination by bacteria	Wear rates are inconsistent due to transfer film. Wear debris size and shape are not representative of clinical wear debris
Dilute bovine serum	Wear rates generally of the same order of magnitude as those seen clinically	Relatively expensive, degrades fairly quickly and may be contaminated by bacteria
Gelatin-based protein solution (Gelofusine)	Wear rates are similar to bovine serum	Expensive and may be contaminated by bacteria. Wear debris size is similar to that produced when water is the lubricant
Gelatin-based protein solution (Plasmion)	Synthetic serum with protein content of 30 g/l	Expensive, wear rates are similar to that observed when water is used as the lubricant. Wear debris produced is not representative of clinical wear debris



a)  **PHOENIX
TRIBOLOGY**

b)  **ENDOLAB**
MECHANICAL ENGINEERING
GMBH



c)  **MTS**®

d)  **AMTI**
FORCE AND MOTION



e)  **ProSim**
www.prosim.co.uk

Figure 34 Commercially available hip simulators. Images from manufacturers websites, respectively.

Table 10 Description of the modern hip simulators.

Hip Simulator's Name	Applied dynamic loading data					Applied motions			Number of test stations (A:Anatomical, N:Non-anatomical)
	Type	Max(kN)	Min(kN)	Profile	f (Hz)	FE	AA	IER	
HUT-4 ¹⁸⁹ (Figure 34 a)	Pneumatic	2.000	0.400	Double-peak	1.0	±23°	±6°	-	12 or 6 (A)
Endolab ¹⁹⁰ (Figure 34 b)	Hydraulic	3.000	0.300	Paul	1.0	+25° to -18°	+7° to -4°	+2° to -11°	6 (N)
MTS ¹⁹¹ (Figure 34 c)	Hydraulic	2.450	0.050	Physiologic	1.0	Bi-axial rocking motion ±22.5°			12 (A)
AMTI ¹⁹² (Figure 34 d)	Hydraulic	2.870	NG	Paul	NG	±23°	±8.5°	±10°	12 (N)
ProSim ¹⁹³⁻¹⁹⁵ (Figure 34 e)	Pneumatic	3.000	0.100	Double-peak	1.0	+30° to -15°	-	±10°	10 (A)
Durham Mark II ¹⁹⁶ (Figure NA)	Pneumatic	2.500	0.100	Square wave	1.0	+30° to -15°	-	±10° or ±5°	5 (A)
Leeds Mark II ¹⁹⁷ (Figure NA)	Pneumatic	3.000	0.050	Double-peak	1.0	+30° to -15°	-	±10°	6 (A)
Shore Western ^{198,199} (Figure NA)	Hydraulic	2.000	0.200	Sinusoidal	1.1	Bi-axial rocking motion ±22.5°			12 (N)

Max: Maximum, Min: Minimum, F: Frequency, FE: Flexion-Extension, AA: Abduction-Adduction, IER: Internal External Rotation, NG: Not given, NA: Not available

2.4.4 Ceramic-on-ceramic (CoC) THR

Ceramic-on-ceramic (CoC) bearing surfaces exhibit extremely low wear rates in hip simulator tests in the range of 0.05 – 0.1 mm³/million cycles (Mc) ^{196,200-202}. Various hip simulator wear tests (under standard gait cycle) of CoC bearing surfaces are shown in Table 11. This compares with MoP hips which have wear rates of 10 – 51 mm³/Mc for conventional PE and less than 20 mm³/Mc for crosslinked PE ²⁰³⁻²⁰⁵. Despite over 100-fold differences in wear rates between CoC and conventional PE hips, revision rates at 13 years for uncemented CoC (5.69%) and uncemented MoP (5.90%) procedures are currently very similar ⁵. The fact that ceramic wear particles may be fewer in number but more reactive than polyethylene cannot be an explanation, as ‘ceramic wear debris has shown to be less biologically active’²⁰⁶. Furthermore, wear rates for retrieved third-generation ceramic bearings reported in the literature range from 0.3 – 1.9 mm³/year ^{207,208}, so they show relatively good agreement with hip simulator studies.

Table 11 Laboratory wear rates found for different CoC hip joints under standard testing conditions.

Authors (year)	CoC materials	Hip Joint Simulator	Femoral head diameter size (in mm)	Test Lubricant (protein concentration)	Test Duration (million cycles)	Wear rate (mm³/Mc) (Mean ± SD)
Smith et al¹⁹⁶ (2001)	BIOLOX [®] <i>forte</i>	Durham Mark II	28	25% NBCS + 0.1% SA (not given)	5.0	0.097 ± 0.039
Nevelos et al²⁰⁰ (2001)	BIOLOX [®] <i>forte</i>	Leeds	28	25% bovine serum (not given)	2.0	~ 0.05
Nevelos et al²⁰⁹ (2001)	BIOLOX [®] <i>forte</i>	Leeds PA2	28	25% NBCS + 0.1% SA	5.0	0.09 ± 0.04
Tipper et al²¹⁰ (2001)	BIOLOX [®] <i>forte</i>	Leeds	28	25% NBCS + 0.1% SA (not given)	5.0	0.05 ± 0.02
Richardson et al¹⁹⁹ (2005)	Alumina-on-Alumina	Shore Western	28	90% bovine serum+ 0.1% SA + 20 mmol EDTA	14.4	< 0.01
Essner et al²⁰¹ (2005)	Alumina-on-Alumina	MTS	32	50% diluted alpha calf serum	5.0	< 0.1
Spinelli et al²⁰² (2009)	BIOLOX [®] <i>forte</i>	Shore Western	36	25% diluted bovine calf serum (not given)	2.0	< 0.02
Al-Hajjar et al¹⁹⁷ (2010)	BIOLOX [®] <i>delta</i>	Leeds Mark II	36	25% NBCS + 0.03% SA	2.0	0.05

NBCS: new-born-calf serum, SA: sodium azide (antibacterial agent), EDTA: Ethylenediaminetetraacetic acid

2.4.5 Metal-on-polyethylene (MoP) THR

Following laboratory wear testing, in 1962 the late Sir John Charnley replaced PTFE with high-molecular-weight polyethylene as acetabular bearing material⁹⁴. This material combination, MoP is still the most commonly implanted bearing surface combination with the majority consisting of a CoCrMo alloy femoral head articulating against a polyethylene (PE), either cross-linked polyethylene (XLPE) or non-XLPE, acetabular liner⁵.

The wear rates of MoXLPE bearing surfaces are typically less than 11 mm³/million cycles (Mc)^{191-193,195,198,205,211,212} compared to metal-on-non-XLPE, which have reported wear rates ranging from 10 – 51 mm³/Mc²⁰³⁻²⁰⁵. Various hip simulator wear tests (under standard gait cycle) of MoXLPE bearing surfaces are shown in Table 12. Clinical trials and mid- to long-term follow-up studies of XLPE have shown significantly reduced wear, less osteolysis and a lower risk of revision than conventional non-XLPE²¹³⁻²¹⁶. A further point to note is that the revision rates for MoXLPE appear to vary according to the size of the femoral head^{5,6}, with 32mm femoral heads showing the lowest wear for MoXLPE in the AOANJRR⁵.

Table 12 Laboratory wear rates found for different MoXLPE hip joints under standard testing conditions

Authors (year)	XLPE liner manufacturer γ or Eb in kGy	Hip Joint Simulator	Femoral head diameter size (in mm)	Test Lubricant (protein concentration)	Test Duration (million cycles)	Wear rate (mm ³ /Mc) (Mean \pm SD)
D'Lima et al¹⁹² (2003)	Durasul™, Sulzer Orthopaedics (Eb95) Crossfire™, Howmedica Osteonics (γ 75)	AMTI	28	90% bovine serum + 2% SA +20-mmol EDTA (not given)	5	-1.5 \pm 1.6 1.6 \pm 1.3
Affatato et al²¹¹ (2005)	Longevity®, Zimmer, Inc (Eb95)	Shore Western	28	bovine calf serum (not given)	3	1
Dumbleton et al¹⁹¹ (2006)	Trident®, Stryker Orthopaedics (γ 90)	MTS	36	50% Fetal substitute alpha-calf serum + 20-mmol EDTA serum (20 g/L)	10	3 \pm 1.3
Fisher et al¹⁹⁴ (2006)	Not given (Eb100)	Leeds Prosim	28 and 36	25% NBCS (15 g/L)	5	~ 5 (28mm) 10.6 \pm 11.4 (36mm)
Fisher et al²¹² (2006)	Durasul® Alpha, Zimmer	Leeds Prosim	36	25% NBCS + 0.1% SA (15.45 g/L)	7	9.5
Galvin et al¹⁹⁵ (2010)	Durasul® Alpha, Zimmer (-)	Leeds Prosim	36	25% NBCS + 0.1% SA (15.46 g/L)	10	10.4 \pm 1.6
Affatato et al¹⁹⁸ (2016)	Not given [γ 75(\pm 10%)]	IORSynthe, Bologna, Italy	32	25% NBCS + 0.2% SA + 20-mmol EDTA	2	3.29
Partridge et al¹⁹³(2017)	Marathon® DePuy Synthes (γ 50)	Prosim	36	25% NBCS + 0.03% SA (15.46 g/L)	5	8.7

γ : Gamma irradiation, Eb: electron beam irradiation, NBCS: new-born-calf serum, SA: sodium azide (an antibacterial agent), EDTA: Ethylenediaminetetraacetic acid

2.4.6 Friction

The frictional force is defined as the resistance encountered to the motion of one body moving tangentially over another (with no or constant lubrication)²¹⁷. It is defined by $F = \mu N$, where F is the frictional force, N is the normal load and μ is the coefficient of the friction. For the bearing surfaces of THR, the friction factor (f) is similar to the coefficient of friction and is defined using Equation III:

$$f = \frac{T}{rL}$$

Equation III

Where T is the frictional torque, r is the femoral head radius, and L is the applied load²¹⁸. Typical friction factor values for different bearing surfaces used for THR are shown in Table 13¹⁶⁵.

Table 13 Typical friction factor values for different bearing surfaces used for THR in the presence of diluted bovine serum¹⁶⁵.

Bearing surfaces	Friction Factor (f)
MoP	0.06–0.08
CoP	0.06–0.08
MoM	0.22–0.27
CoC	0.002–0.07
CoM	0.002–0.07

2.4.7 Lubrication

A lubricant is defined as “*any material interposed between two surfaces that reduces the friction or wear between them*”¹⁶³. Lubrication is the addition of a lubricant to the surfaces under relative motion usually to reduce friction and wear. The type of lubrication between two surfaces under relative motion can be divided into three distinct regimes: boundary lubrication, mixed lubrication and fluid film lubrication, see Figure 35.

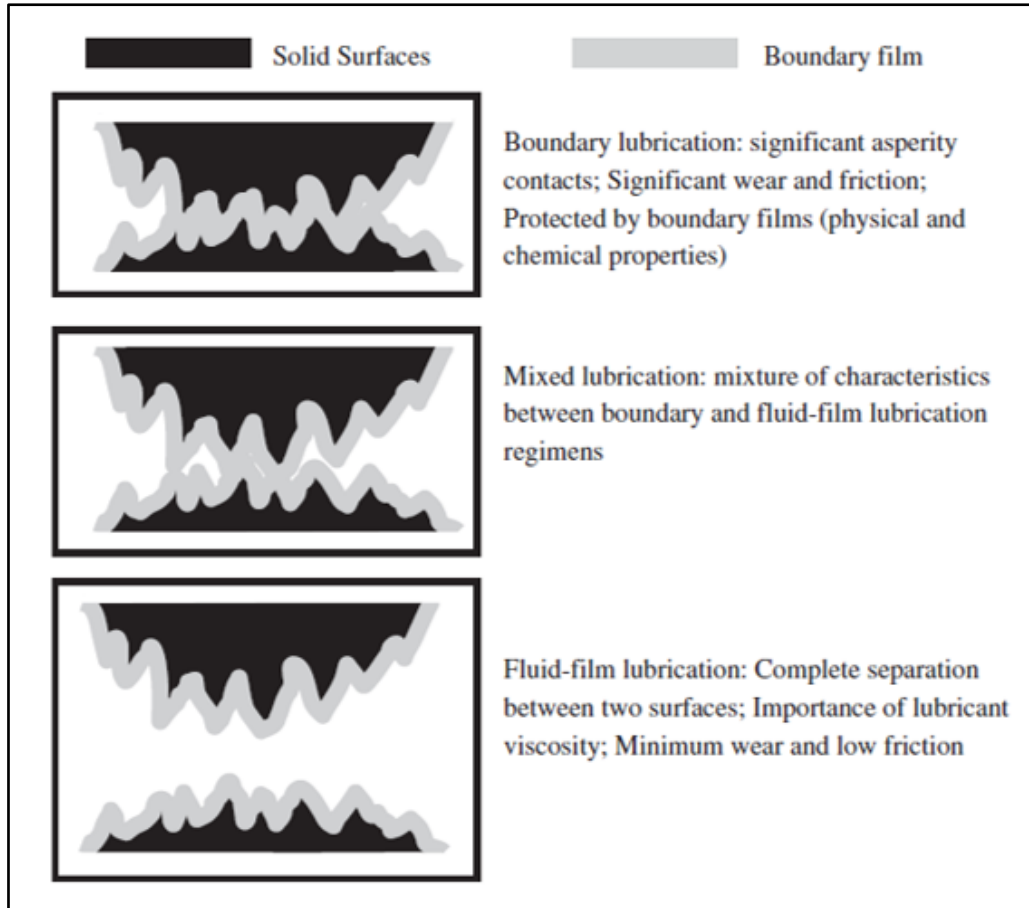


Figure 35 Different lubrication regimes. Image from Jin et al. 2006¹⁶⁵.

The trend of the Stribeck curve shows different lubricant regimes, see Figure 36. The friction factor (f or coefficient of friction) is plotted against the Sommerfeld number (z), defined in Equation IV

$$z = \frac{\eta u r}{L}$$

Equation IV

where η is the viscosity of the lubricant, u is the entraining velocity of the bearing surfaces, r is the femoral head radius, and L is the applied load²¹⁸.

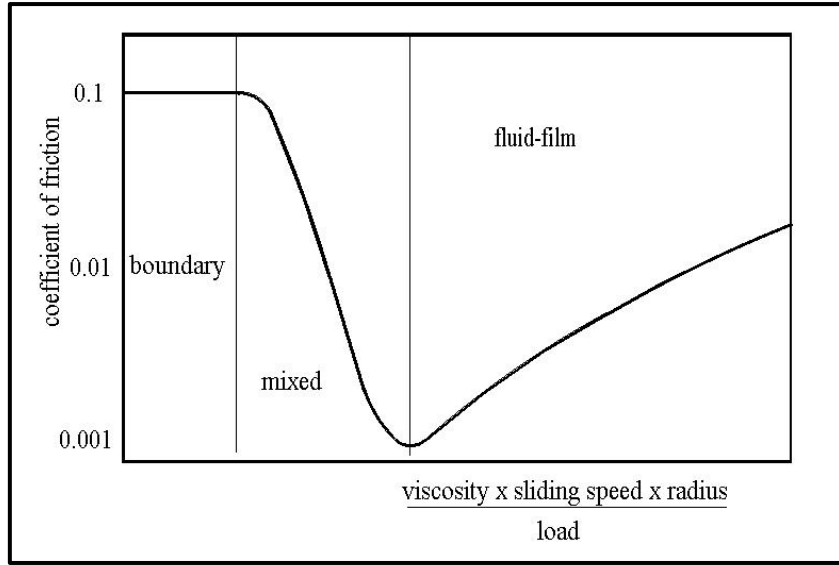


Figure 36 An Idealised Stribeck curve showing different lubrication regimes. Image from Smith and Joyce (2017)⁴¹.

The trend of the Stribeck curve illustrates different lubricant regimes. The initial flat line of the Stribeck curve, where the coefficient of friction is at its maximum, indicates the boundary lubrication regime. In a boundary lubrication regime, the load over the joint supported by the asperity contact between the joint surfaces and wear will, therefore, lean towards a maximum. The decreasing trend in the Stribeck curve, where the coefficient of friction is reducing indicates a mixed lubrication regime. In a mixed lubrication regime, the load over the joint is supported partially by the asperity contact between the joint surfaces and partially by the lubricant fluid. Finally, the increasing trend in the Stribeck curve indicates the fluid film lubrication regime. In a fluid film lubrication regime, the load over the joint entirely supported by the lubricant fluid, and the asperity contact between the joint surfaces is absent. Therefore, wear will be at a minimum between the joint surfaces. Additionally, the friction is produced by shear of the lubricant fluid in a fluid film lubrication regime.

The dimensionless parameter λ gives the likely prevalent lubrication regime in an artificial hip joint and is calculated using Equation V ²¹⁹:

$$\lambda = \frac{h_{min}}{[(Sq_1)^2 + (Sq_2)^2]^{0.5}}$$

Equation V

Where Sq_1 and Sq_2 are the root mean squared (r.m.s) surface roughness values of the femoral head and acetabular liner respectively, and h_{min} is the minimum film thickness of the

lubricant. After evaluation of the λ ratio, lubrication regimes are classified as boundary lubrication when $\lambda < 1$, mixed lubrication when $1 \leq \lambda \leq 3$ and fluid film lubrication when $\lambda > 3$ ²¹⁹.

For MoP, CoP, MoM, CoC and CoM bearing surfaces of artificial hip joints, the minimum film thickness (h_{min}) is calculated using Hamrock-Dowson equation, see Equation IV²²⁰:

$$\frac{h_{min}}{R_x} = 2.798 \left(\frac{\eta u}{E' R_x} \right)^{0.65} \left(\frac{L}{E' R_x^2} \right)^{-0.21}$$

Equation VI

Where R_x is the equivalent radius, η is the viscosity of the lubricant (Pa s), u is the entraining velocity (m/s), E' is the equivalent elastic modulus (Pa) and L is the load (N). If $R_{femoral\ head}$ is the radius of the femoral head and $R_{acetabular\ liner}$ is the radius of the acetabular liner, then the equivalent radius R_x is calculated using Equation VII,

$$\frac{1}{R_x} = \frac{1}{R_{femoral\ head}} - \frac{1}{R_{acetabular\ liner}}$$

Equation VII

Using this equation, MoP bearing surfaces operates in a mixed or boundary regime whereas MoM and CoC bearing surfaces can operate in a fluid film lubrication regime²²¹. CoC bearing surfaces are very hard and can be polished to an extremely fine surface finish ($\sim 4\text{nm}$ Sa) when compared to PE. The enhanced manufacturing tolerances of CoC bearing surfaces result in a reduced radial clearance ($R_{acetabular\ liner} - R_{femoral\ head}$). This reduced radial clearance of the CoC bearings when combined with extremely low surface roughness leads to predicted fluid film lubrication regime during walking⁶¹, see Figure 36. In MoP bearing surfaces, the lubrication regime is mainly boundary¹⁶⁵, Figure 36. In MoP bearing surfaces, due to relatively high surface roughness of PE acetabular liner than the finely polished metal femoral head, the radial clearance and head diameter do not improve the lubrication significantly¹⁶⁵. The load and the speed on the hip joint fluctuate significantly during walking²²². In the literature, it has been shown that the predicted minimum film thickness (h_{min}) in the natural hip joint remains relatively constant during walking despite large fluctuations in both load and the speed²²³. This is predominantly because of the combined effect of squeeze-film and entraining actions. During the stance phase, see Figure 31, when

the load is high and the speed is low, squeeze-film action conserves the lubricating film thickness produced by entraining action during the swing phase when the load is low and speed is high²²².

2.4.8 Wettability and THR

In the 16th century, Galileo identified the wettability phenomenon, and approximately two hundred years later, Thomas Young established scientific research related to this phenomenon²²⁴. The surface wettability influences the tribological properties of the hip prosthesis biomaterials²²⁵. However, a very modest amount of literature is available on the topic of wettability of the bearing surfaces of THRs.

Similar to biotribology, wetting is also a surface characteristic of the material. The term ‘wettability’ refers to the ability of the fluid to spread over the solid surface and is quantified by measuring the contact angle (CA). The Young equation establishes the balance between three interfacial forces acting on the wettability of the solid surface and the angle formed at the point of intersection of these forces see Equation VIII

$$Y_{sv} = Y_{sl} + Y_{lv} \cos \theta_y$$

Equation VIII

These three interfacial forces are: Y_{sv} [surface free energy (SFE) of the solid], Y_{lv} (surface tension of the liquid) and Y_{sl} (interfacial tension between solid and liquid interface) whereas θ_y is Young’s contact angle, see Figure 37.

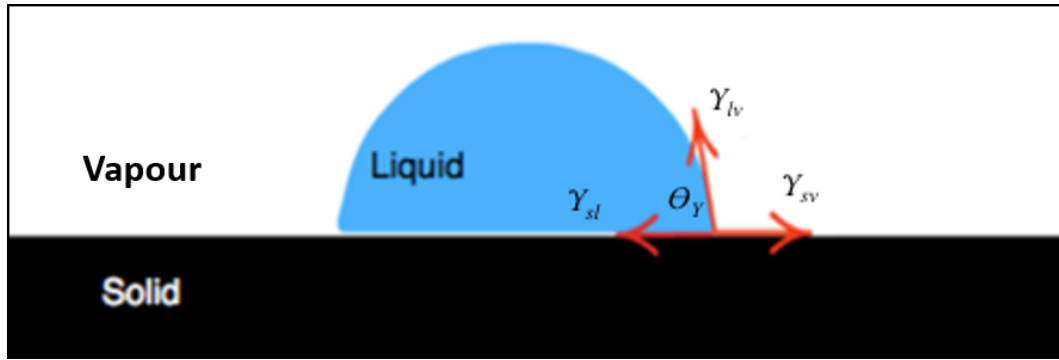


Figure 37 The Young's contact angle (θ_Y), formed at the intersection of three interfacial forces: γ_{sv} : surface free energy of the solid, γ_{lv} : surface tension of the liquid and γ_{sl} : interfacial tension between solid and liquid interface.

It is important to emphasise that θ_Y is an ideal CA because Young pioneered this equation for an ideal solid surface that is chemically homogeneous, smooth, non-reactive, rigid and insoluble. Geometrically, θ_Y is the angle formed by the liquid at the intersection of solid, liquid and vapour phases. It is essential to take into account that θ_Y is independent of gravity and only dependent on the chemistry of three phases.

If the CA is in the range of 150° - 180° then the liquid form beads and does not wet the surface even partially and the surface is known as superhydrophobic, see Figure 38 a). If the CA is greater than 90° when the liquid does not wet the surface, and the solid surface is termed as hydrophobic, see Figure 38 b). If the CA is lower than 90° then the liquid quickly spreads over the surface, and the solid surface is known as hydrophilic, see Figure 38 c). At CA less than 5° , the liquid thoroughly wets the solid surface, and the surface is known as superhydrophilic see Figure 38 d).

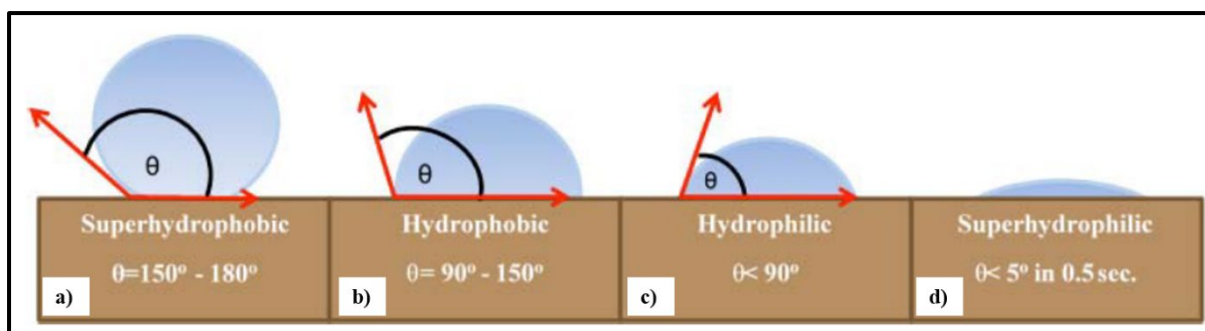


Figure 38 Schematic views of a) superhydrophobic, b) hydrophobic, c) hydrophilic and d) superhydrophilic surfaces. Image from Asmatulu (2016)²²⁶.

Contact angle goniometry (from the Greek: gōnia = angle and metron = measure) is the study of the shape of the drop of liquid placed on the test material and the instrument used for CA measurement is called a contact angle goniometer. Dr William Zisman²²⁷ designed the first contact angle goniometer and was later manufactured by ‘ramé-Hart Surface Science Instruments’. The basic goniometer instrument consists of a light source, sample stage, an image capturing device and data analysis system, see Figure 39.

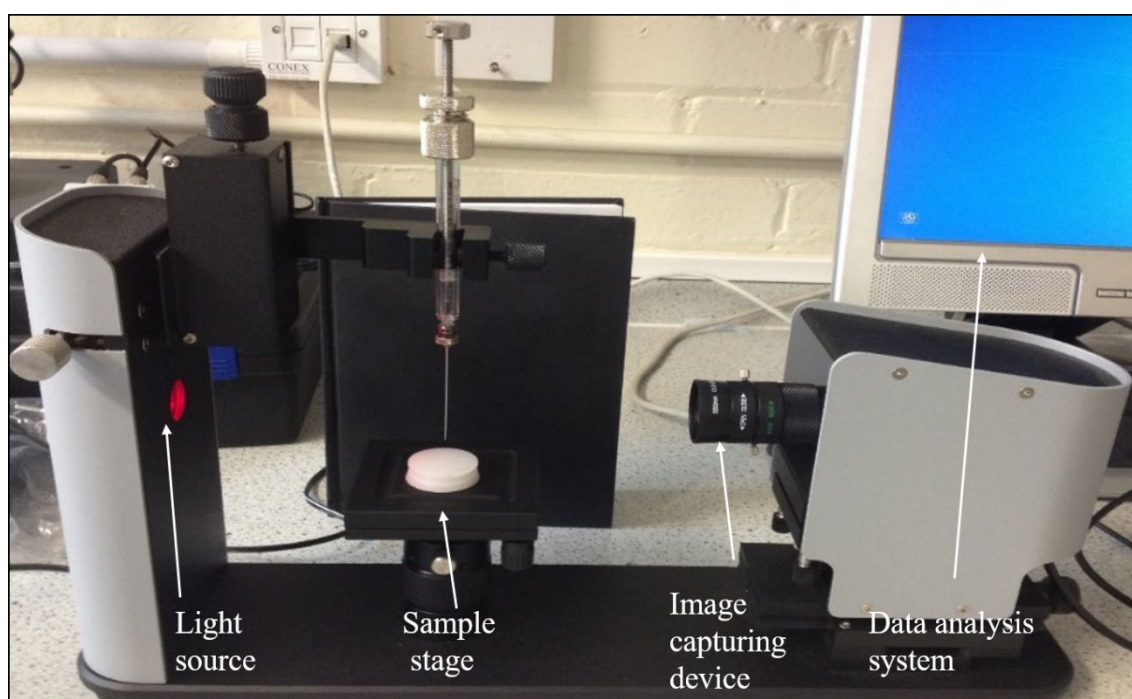


Figure 39 The basic goniometer/ contact angle measurement instrument.

The sessile drop method is an extensively used technique in which a drop of test liquid is placed on the surface using a syringe and the angle formed at liquid-solid interface CA is measured using a goniometer, see Figure 39. Two major drawbacks of this method are evaporation of the test liquid and dehydration of the test surface; however; they could be resolved using a

vapour tight chamber. Nowadays, computer software is used for the drop shape analysis to generate consistent CA data. It is essential to mention the technique used for CA measurements because the above-mentioned methods may give different CA for the same test liquid.

The predominant lubrication mechanism in the natural hip joint is fluid-film lubrication under physiological walking conditions²²². Therefore, artificial hip joints are designed so that they could operate under full or partial fluid-film lubrication regime^{222,228}. If these prostheses could generate fluid-film lubrication, then the pressurised fluid film could separate the bearing surfaces, which will then reduce friction and wear, thus giving long life to respective implants *in-vivo*. According to the fluid-film lubrication theory, the lubricant attaches to the bearing surfaces and travels with identical velocity as the surfaces²²². In an artificial hip joint, the lubricant is drawn into the surface area and generates a fluid film to carry the load. However, if the bearing surfaces are hydrophobic, then it is difficult for this film to cover the surfaces. Therefore, it is necessary to determine the wettability of the bearing surfaces for excellent lubrication and low wear. In 2005, Borruto et al. carried out wear screening tests using different biomaterials with different/same wettability and later published a patent describing the importance of wettability for hip prosthesis biomaterials²²⁸, which states the following:

“Biocompatible materials, which will form the cotile and the femoral head can no longer be selected only taking low wear and low friction coefficients, geometry of the coupling and the mechanical characteristics into consideration. It is also necessary to use the wettability difference between the two materials in the coupling as the main consideration.” Furthermore, Borruto et al. also concluded, *“The higher is the wettability difference ($\Delta\theta$) between coupling materials, the more efficient is the lubricant condition, i.e. a stable supporting meatus is formed (meatus: film of water between hydrophobic and hydrophilic surfaces).”* Table 14 summaries wettability measurements of different biomaterials reported in the literature.

Table 14 Wettability measurements of different biomaterials reported in the literature

Authors	Wettability measurement technique	Test liquid	Contact Angle (in °)		
			Metals	Ceramics	Polymers
Kubiak et al²²⁵	PG-X goniometer	Distilled water	SS-65 Ti-68	20-40	-
Salehi et al²²⁹	Sessile drop method	50% bovine serum in water	CoCrMo-57 SS-63	OxZr-44.3 Zirconia-39 Alumina-48	-
Bourruto et al²²⁸	Photographic method	Water	CoCrMo-47 SS-57	-	UHMWPE-65
Gispert et al²³⁰	Sessile drop method	Water	CoCrMo-61 SS-64	-	UHMWPE-86

2.5 Head-neck modularity for total hip replacement: taper-trunnion junction

This section illustrates the head-neck modularity, i.e. the taper-trunnion junction of modular THRs in terms of different materials, designs and geometry. Later, retrieval studies reporting the material loss at the taper-trunnion junctions are described.

2.5.1 *The taper-trunnion junction of the modular hip prostheses*

As described in 2.3.4, ceramics or CoCrMo alloys are used to manufacture femoral heads owing to their biocompatibility, wear and corrosion resistance and high hardness. Therefore, the femoral tapers (internal tapers of the femoral heads) are commonly fabricated from Alumina ceramics or CoCrMo alloys. The femoral heads of modular THRs are paired with CoCrMo, Ti alloys or 316L stainless steel (an alloy of Iron, Chromium and generally Nickel¹⁰⁵) trunnions of the femoral stems.

Based on the metallic material combination used for manufacturing the femoral taper and trunnion, the taper-trunnion junction can be divided into two categories: mixed metal interface: CoCrMo/Ti alloy, CoCrMo/SS, Ti alloy/CoCrMo and similar metal interface: CoCrMo/CoCrMo, SS/SS. By convention, the femoral taper material is listed first, and the

trunnion material is second. For example, mixed metal combination CoCrMo/Ti alloy represents a CoCrMo femoral head mounted on a Ti alloy trunnion.

Femoral taper sizes are described corresponding to the proximal and distal diameters (approximately) in mm and taper angle. Various available femoral taper sizes are 9/11, 10/12, 11/14 and 14/16. Additionally, there is a range of femoral taper designs from different manufacturers such as C-taper (Stryker), V-40 (Stryker), Type-I, PCA (Stryker). Figure 40 shows a schematic of different dimensions of the femoral tapers and Table 15 shows a summary of different femoral taper designs.

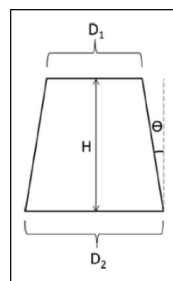


Figure 40 Schematic showing dimensions used for describing femoral tapers: D1= proximal diameter, D2= distal diameter, Θ = femoral taper angle Image from Triantafyllopoulos et al. (2015) ²³¹.

Table 15 Dimensions used for describing various femoral tapers. Adapted from Triantafyllopoulos et al. (2015).

Taper design	Proximal diameter (D1) in mm	Distal diameter (D2) in mm	Taper angle (Θ) in degrees	Contact length (H) in mm
11/13	11.2 ± 0.1	13.5 ± 0.1	9.74 ± 1.9	9.74 ± 1.9
V40	11.3 ± 0.1	13.3 ± 0.6	8.63 ± 0.31	8.63 ± 0.31
Type I	11.7 ± 0.9	12.7 ± 0.9	5.27 ± 0.24	10.3 ± 0.68
PCA	12.3 ± 0.7	13.3 ± 0.5	3.65 ± 0.8	16.5 ± 1.0
C-taper	12.4 ± 0.4	13.8 ± 0.7	7.07 ± 2.6	11.9 ± 2.6
12/14	12.4 ± 0.4	13.7 ± 0.7	6.07 ± 1.4	11.3 ± 1.4

The taper-trunnion angular mismatch, also known as taper clearance, is defined as the difference between the femoral taper and trunnion angle²³². The mating of femoral taper and trunnion at a junction can result in positive, zero or negative mismatch. The level of angular mismatch controls the contact area and the position of contact between the femoral taper and trunnion. Thus, a positive angular mismatch also called as “Tip locked”, represents a femoral taper angle greater than the trunnion angle and creates a connection at the proximal end, see Figure 41 a). The perfectly matched interfaces have the same femoral taper and trunnion angles, see Figure 41 b). In contrast, a negative angular mismatch also called as “Base locked”, represents a femoral taper angle smaller than the trunnion angle and creates a connection at the distal end, see Figure 41 c).

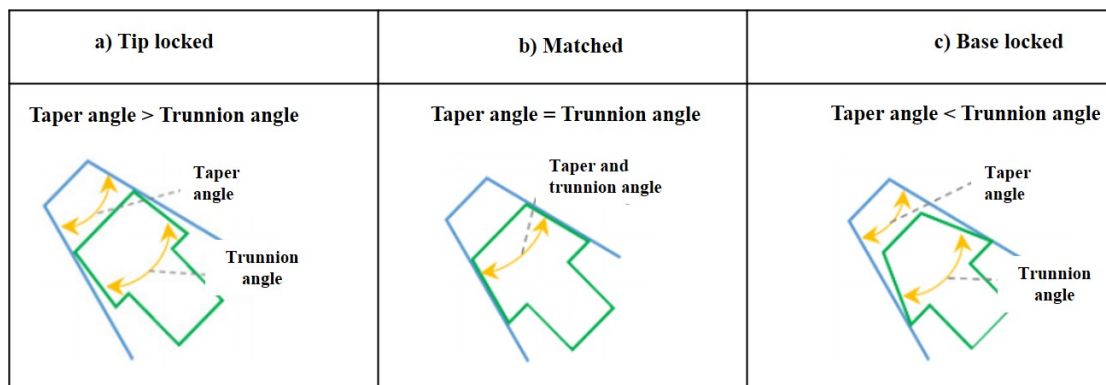


Figure 41 Femoral taper and trunnion cone angles and associated mismatches: a) Tip locked, b) Matched and c) Base locked. Image adapted from Ashkanfar et al. (2017)²³³.

Modern designs of femoral tapers feature shorter length along with smaller proximal and distal diameters to reduce the chance of impingement of the femoral neck against the acetabular device and improve the range of motion²³⁴. Therefore, trunnion contact lengths have been shortened from 20 mm to ≤ 10 mm and, 12/14 and V40 tapers are more commonly used instead of 14/16 femoral tapers²³⁵. Although, all 12/14 tapers are not uniform²³⁶. The taper geometry (proximal and distal diameter, contact length, taper angle), as well as surface topography (smooth and rough) of 12/14 tapers, varies across the manufacturers^{236,237}. Based on the surface roughness (R_a), trunnions are divided into two types: smooth and rough, see Figure 42. A smooth trunnion has a polished surface whereas rough trunnions have micro-grooved surface.

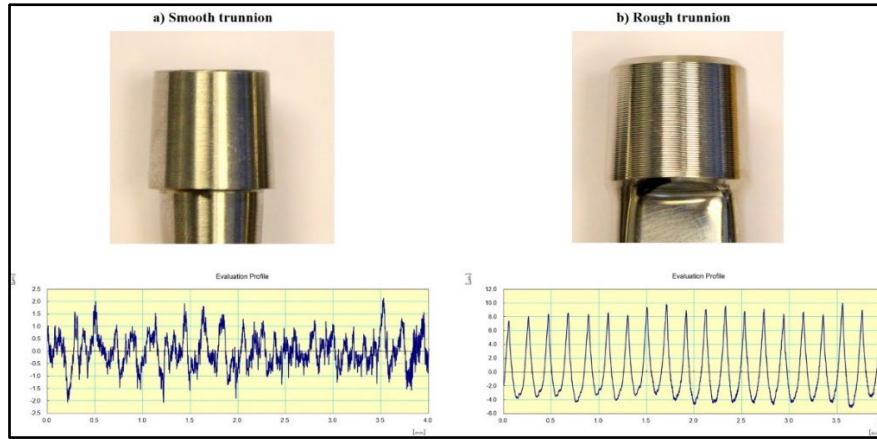


Figure 42 Smooth and rough trunnion with evaluation profile obtained using two-dimensional contacting profilometer, respectively. a) Smooth trunnion ($R_a = 0.520 \mu\text{m}$) and b) Rough trunnion ($R_a = 3.281 \mu\text{m}$).

2.5.2 Contact mechanics

The femoral tapers are employed to transfer the loads applied at the femoral head, along the taper-trunnion axis to the femoral stem. Figure 43 shows forces acting on a THR prosthesis: torsional forces, compressive forces, and bending moments²³⁸. Bishop et al. reported that compressive radial stress originates from the impaction force, the radial component of the joint force and press-fit stresses¹⁸. The torsional moment is arisen at the taper-trunnion junction due to friction at the bearing surfaces. If the torsional moment aligned about the taper axis, then it can act as a removal torque where increased friction at the bearing surfaces induces rotational micromotion about the femoral neck axis²³⁹. Additionally, the off-axis anatomy of the natural hip will induce a bending moment which will be experienced by the taper-trunnion junction. The bending moments at the taper-trunnion junction are a product of the transverse component of the joint force and axial distance from the femoral head centre to the point of taper support. Although, the bending moments may also originate from the friction at the bearing surfaces²³⁸.

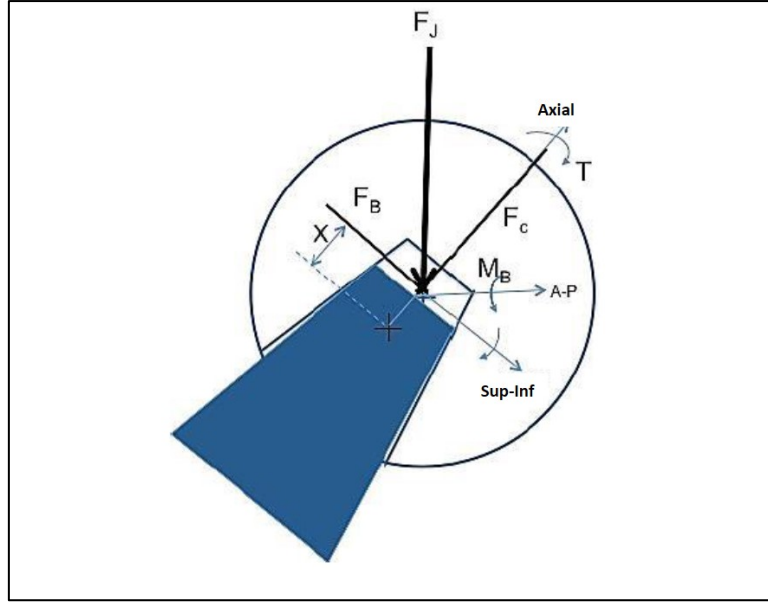


Figure 43 Loading mechanics for the taper-trunnion junctions. M_B = bending moment due to friction at the bearing surfaces, F_J = joint force, F_C = axial compressive joint force along taper axis, F_B = bending component of the joint force, T = torsional moment due to friction at the bearing surfaces, x = axial distance from the femoral head center to the point of taper support. Taper axes are: A-P: anterior-posterior, and Sup-Inf: superior-inferior. Image adapted from Gilbert et al. (2015)²³⁸

Retrieval studies reported a correlation between the flexural rigidity of the trunnion and taper design with the material loss at the taper trunnion junction^{44,240}. Short and small diameter trunnions are more flexible and may have a higher prevalence of material loss at the taper-trunnion junction due to micromotions. The flexural rigidity of the trunnion is dependent on the material and geometry of the trunnion and is defined below²⁴¹, see Equation IX

$$\text{Flexural rigidity} = E \times I = E \times \left(\frac{\pi}{4} r_t^2 \right)$$

Equation IX

Where E is the elastic modulus, and I is the second moment of inertia and r_t is the radius of the trunnion at the distal end where the trunnion exists the femoral taper. Various materials can be used with different trunnion geometries by manufacturers due to unavailability of the international standard describing the taper-trunnion junction specifications. Therefore, there is significant variety in r_t and E dimensions and thus, large variability in the flexural rigidity of the trunnion across the literature. Material properties of CoCrMo, Ti6Al4V, Ti6Al7Nb, TMZF and ceramics are summarized in Table 16.

Table 16 Material properties of various materials used for the taper-trunnion junction.
Adapted from Lundberg et al. (2015)²⁴²

Material	Young's modulus (GPa)	Yield Stress (MPa)	Poisson's Ratio
CoCrMo	230	450	0.33
Ti6Al4V	115	795	0.33
Ti6Al7Nb	105	800	0.33
TMZF	80	1030	0.33
Ceramic	350	NA	0.23

2.5.3 Material loss from the taper-taper trunnion junction of modular hip prostheses

The truest test of any implant is its performance *in vivo*, i.e. in the body. Therefore, the truest evaluation of the material loss will come from prostheses explanted or retrieved from the body. Based on retrieval studies, the importance of metal debris from the taper-trunnion junction in MoM hip prostheses has been widely recognized^{19,20,23,27,49,126}.

A recent retrospective observational study by Matharu *et al.* compared ARMD revision risk in different commonly implanted MoM and non-MoM (MoP, CoC and CoP) bearing surfaces using data from the NJR²⁴. Interestingly, increasing the risk of ARMD revision surgery in non-MoM THRs was highlighted. Intriguingly, Matharu *et al.* additionally showed that CoC bearings were revised for ARMD 2.35 times more when compared to other non-MoM bearings. Furthermore, Matharu *et al.* reported a higher risk of revision in 36 mm MoP THRs compared to ≤ 36 mm MoP THRs. Persson et al. reported a 0.5% prevalence of revision surgery for ARMD after a mean follow-up of 7 years in a single-centre observational cohort study of MoP THRs with the same Ti6Al4V femoral stems¹⁴⁹. Retrieval studies reported ARMD due to wear debris produced from the taper-trunnion junction of modular MoP THRs⁴²⁻⁴⁵. Furthermore, several case studies reported metal release due to fretting, corrosion or both and associated pseudotumour formation after MoP THR^{42,45,148}.

In CoC hips, the only sources of metal (usually Ti) would be the trunnion of the femoral stem and the acetabular shell. Additionally, the potential sources of metal debris in MoP hips would be the bearing surface of the metallic femoral head (usually CoCrMo), the taper-trunnion junction, and the acetabular shell. Out of these three sources, the head-liner bearing

surfaces and the acetabular shell and backside of the liner have metal against softer polymer contact whereas the taper-trunnion junction has a metal-on-metal contact.

2.6 Mechanism responsible for the material loss released from the taper-taper trunnion junction of modular hip prostheses

This section reports various theories for the material loss at the taper-trunnion junction followed by factors affecting this material loss. Furthermore, retrieval studies reporting the quantification of the material loss at the taper-trunnion junction are presented.

2.6.1 Various theories for the material loss from the metallic taper-trunnion junction reported in the literature

Various theories for this material loss have been put forward, essentially from largely a wear process to largely a corrosion process, with synergistic mechanisms suggested too. Additionally, retrieval studies have shown that the material loss is predominantly from the metallic femoral tapers rather than trunnions¹⁸⁻²⁰. Despite this, the term ‘trunnionosis’ has been used to describe material loss at the femoral taper^{26,86,154,243,244}. Material loss from the taper-trunnion junction of artificial hip joints is the key issue in contemporary orthopaedics.

There are various theories for the material loss from the metallic taper-trunnion junction. A number of historical explant studies reported ‘corrosion’ at the taper-trunnion junction of modular THRs^{16,17,245-248}. In the early 1990s, Gilbert et al. examined 148 explanted modular THRs of mixed (CoCrMo/Ti) and similar (CoCrMo/CoCrMo) alloys combination and reported ‘corrosion’¹⁷. Gilbert et al. scanned 148 femoral tapers using an optical microscope for visible evidence of corrosion and established a ‘subjective corrosion-score ranking system’ to identify the severity of the corrosion¹⁷. Scanning electron microscopy and energy dispersive x-ray (EDX) analysis were performed on the CoCrMo femoral tapers to identify several forms of corrosive attacks such as etching, pitting, fretting, the selective leaching of cobalt, intergranular attack in similar alloy combination only and the formation of interfacial layer in mixed alloy combination only¹⁷. Gilbert et al. hypothesised that “*the progression of*

events which result in corrosive attack is a minor modification of the classic crevice corrosion mechanism”¹⁷.

Based on this hypothesis, the restricted crevice environment coupled with high cyclic loading that causes the repeated breakdown of the passive oxide layers, leading to an unstable electrochemical environment inside the crevice for CoCrMo and Ti alloy passive films. The passivity of these alloys subsequently vanishes leading to active corrosion attack at the taper-trunnion junction. Furthermore, the repeated breakdown of the passive films would result in to the formation of corrosion products. This corrosion and the accumulation of particulate corrosion products could cause loss of mechanical integrity of the modular THR *in vivo*, leading to particle release in the surrounding tissue and eventually third-body wear due to these particles¹⁷. In this manner, based on microscopic and EDX analysis, the idea of ‘mechanically assisted crevice corrosion’ (MACC) was introduced in the same study and Figure 44, explaining MACC was developed¹⁷. Interestingly no other chemical analysis [such as X-ray Photoelectron Spectroscopy (XPS)] was performed on the retrieved samples to establish the chemical equation. Moreover, out of 106 mixed alloys retrieved components only eight components were utilised for SEM and EDX analysis. The process of MACC is described in detail as follows:

In the MACC process, see Figure 44, micromotion between the taper-trunnion junction surfaces due to cyclic loading causes the breakdown of the surface oxide layer followed by oxidation of the underlying bulk metal alloy (repassivation)^{17,249}. As the cyclic loading and micromotion persist, oxide film breakdown/repassivation process continues, causing reduction of dissolved oxygen in the fluid present in the crevice. This leads to the generation of excessive metal ions in the fluid and as a result, the accelerated migration of chloride ions into the crevice to maintain charge neutrality¹⁷. The consequent electrochemical reactions lead to an increase in hydrogen and chloride ion concentration forming hydrochloric acid and leading to a drop in the pH of the crevice fluid²⁴⁹. Continuation of the oxide film breakdown/repassivation process further lowers the pH of the crevice fluid and auto-catalyses the corrosion process until the stability of the oxide film reduces and therefore accelerated corrosion attack of the bulk metal occurs²⁴⁹. In a 2003 study including two of the Gilbert et al. authors, Goldberg et al. suggested that the MACC process was responsible for corrosion at the taper-trunnion junction in a retrieval study of 231 modular THRs³⁰.

In vivo environment at the taper-trunnion junction of the modular THR is same as the rest of the prostheses which is surrounded by pseudo-synovial fluid⁵⁵. The fluid environment contains inorganic as well as organic components at a pH of 7.2 to 7.4¹⁸⁸. However, as a result of infection and inflammation, the pH could become more alkaline or acidic respectively²⁵⁰. The crevice-like geometrise which may be present at the taper-trunnion junction and micromotions between the taper-trunnion junction of modular THRs are the potential sites for fluid ingress^{17,249,251}. As explained in the model of MACC process (see Figure 44), fluid ingress at the taper-trunnion junction begins to alter the chemistry of the crevice solution including drop in the pH and increase in chloride concentration leading to acidic environment^{17,249,251}. Furthermore, the passive metal oxide layer on the surface is less stable and thinner to reset attack eventually resulting into localised corrosion. When the crevices formed at the passive oxide layer are large enough at the taper-trunnion junction, the fluid exchange can easily occur with the outside environment and if the oxygen ingress into the crevice is greater than the rate of ionic dissolution then the crevice corrosion will be restricted²⁴⁸.

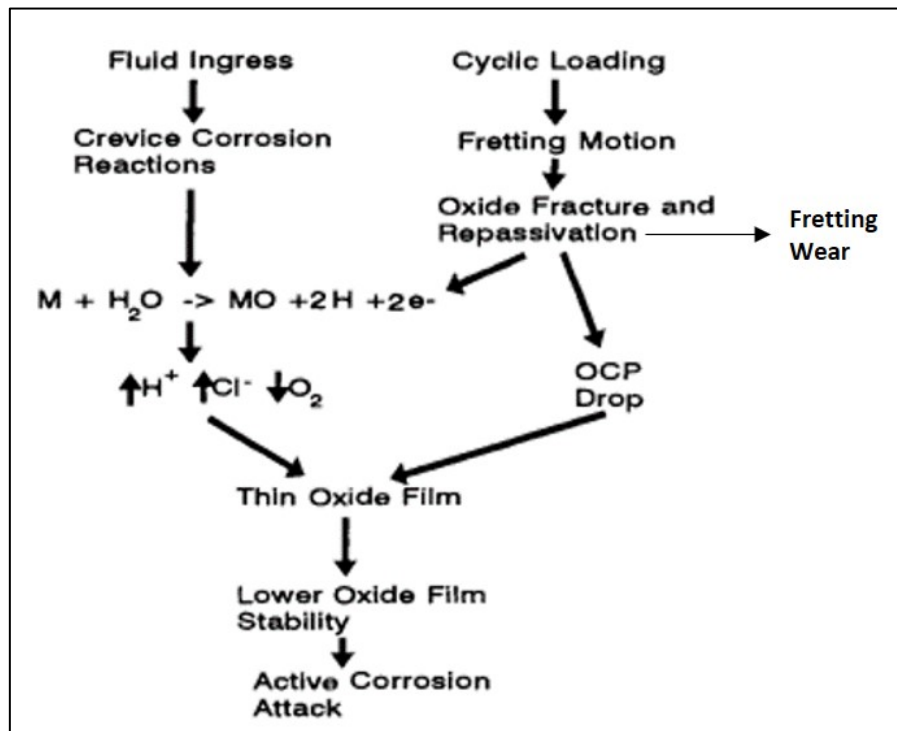


Figure 44 Mechanically Assisted Crevice Corrosion (MACC). Image adapted from Gilbert and Jacobs (1997)²⁴⁹.

In 1995, Brown et al. investigated 79 retrieved modular THRs using stereo and scanning electron microscopic analysis and reported that ‘fretting corrosion’ accelerates ‘crevice

corrosion’ using semi-quantitative scoring method²⁵². Many studies have been published evidence of ‘fretting corrosion’ at the taper-trunnion junction interfaces of explanted modular THRs^{35,36,245,252-257}. Out of these studies, few used an actual hip prosthesis for *in vitro* electrochemical analysis under dynamic loading without applying physiologically relevant walking motion^{35,36}. Moreover, a real hip prosthesis was not used in other electrochemical studies for investigation of fretting corrosion^{253,255,256}. Additionally, retrieval studies did not perform any electrochemical analysis; only semi-quantitative scoring was presented for the examination of fretting corrosion^{254,257}.

In contrast to studies which reported mainly corrosion and associated processes responsible for the material loss, in a 1993 study, Cook et al. noted ‘wear’ and ‘corrosion’ at the taper-trunnion junction interfaces in a retrieval study of 108 modular THRs based on semi-quantitative scoring method²⁵⁸. In 2012, Langton et al. quantified the material loss from 126 explanted metallic femoral tapers and suggested that mechanical ‘wear’ was the primary mechanism responsible for the damage at the taper-trunnion junction¹⁹. In a follow-up study, Moharrami et al. offered evidence of ‘corrosion assisted wear’ as responsible for the material loss from CoCrMo-Ti alloy taper-trunnion junctions³². Separately, Bishop et al. quantified material loss and analysed ‘wear’ patterns microscopically from explanted metallic femoral tapers and also quantified taper ‘wear’¹⁸.

In a 2013 study of MoM hips, Matthies et al. suggested that ‘galvanic corrosion’ was a more significant mechanism responsible for material loss than ‘fretting corrosion’, based on semi-quantitative scoring and quantified material loss of 110 retrieved femoral tapers²⁰.

Moreover, in a 2014 study with the same two senior authors, Hothi et al²⁵⁹ supported the theory by Matthies et al²⁰ and proposed that ‘corrosion’ was a more significant mechanism than mechanical ‘wear’ after examination of 150 explanted metallic femoral tapers using the semi-quantitative scoring and quantification of material loss²⁶⁰. Most recently, in a 2018 study, Hall et al. examined 364 explants with the scanning electron microscope (SEM) coupled with energy dispersive X-ray (EDX) analysis³⁴. They reported that the taper-trunnion junction of modular THRs undergoes single or overlapping damage modes driven by mechanical or electrochemical processes or combination of both³⁴. Since 2011, the synergistic (i.e. greater than the sum of the parts) mechanism resulting from wear and corrosion at the taper-trunnion junction has been termed ‘tribocorrosion’^{33,45,261-264}. *In vitro*

studies performed electrochemical analysis using tribometers for the investigation of ‘tribocorrosion’, however, actual prosthesis was not included in these studies^{33,261}.

It has been reported that deterioration of the passive oxide layer due to fretting wear could leave the underlying bulk metal exposed to the physiological fluids that may lead to corrosion^{245,252,253}. Intriguingly, Hutchings noted that *“the importance of oxidation in fretting wear, and the fact that the debris after the initial stages is predominantly oxide, has led to the use of the term fretting corrosion as a synonym for fretting wear, although the earliest stages of fretting wear do not involve appreciable chemical attack. It is preferable to use the more general term fretting wear to denote all types of wear due to fretting motion, and to restrict the term fretting corrosion to cases where the debris is predominantly the product of a chemical reaction”*¹⁷⁰. Yet, many scientific papers report ‘fretting corrosion’, as the reason for the material loss from the taper-trunnion junction^{16,35,36,38,245,252-257}. Furthermore, ‘fretting corrosion’ on the femoral taper can be inappropriately shortened to ‘taper corrosion’ or ‘corrosion’^{31,37,42,152,259,263-265}. Moreover, ‘corrosion’ has been assessed using a visual scoring method (Goldberg Scoring³⁰) on explanted THR components. In this visual scoring assessment method, a discoloured surface or black debris on the surfaces of the taper-trunnion junction was considered to be implications of ‘corrosion’³⁰. Langton et al. found extensive black debris on explanted CoCrMo femoral tapers²⁶⁶. As per the Goldberg scoring criteria the presence of extensive black debris would contribute to increased Goldberg score. However, Langton et al. reported that this black debris did not represent corrosion rather deposition of debris²⁶⁶.

As can be seen, there is no consensus in the literature regarding the mechanisms behind the material loss at the taper-trunnion junction. Researchers need to utilise standardised terminologies to describe the damage mechanism at the taper-trunnion junction. For a clear understanding, terminologies used in the literature to describe damage relating to corrosion, wear and a combination of both, for the material loss at the taper-trunnion junction of modular hip prostheses, as defined in international standards, are given in Table 17. This thesis subsequently uses the terminologies relating to wear and corrosion as described in Table 17.

Table 17 Standard terminology relating to wear and corrosion described in American Society for Testing and Materials (ASTM) international standards (in alphabetical order) ^{38,163,267}

Terminology	Definition
Abrasion	<i>“The process by which relative motion between a surface and hard particles or protuberances on an opposing surface produces abrasive wear of that surface”¹⁶³</i>
Abrasive wear	<i>“Wear due to hard particles or hard protuberances forced against and moving along a solid surface”¹⁶³</i>
Corrosion	<i>“The deterioration of a material, usually a metal, that results from a chemical or electrochemical reaction with its environment”²⁶⁷</i>
Crevice corrosion	<i>“Localized corrosion of a metal or alloy surface at, or immediately adjacent to, an area that is shielded from full exposure to the environment because of close proximity of the metal or alloy to the surface of another material or an adjacent surface of the same metal or alloy”²⁶⁷</i>
Fretting	<i>“Small amplitude oscillatory motion, usually tangential, between two solid surfaces in contact”¹⁶³ (amplitude range 1 to 100 μm)¹⁷⁰</i>
Fretting corrosion	<i>“A form of fretting wear in which corrosion plays a significant role”¹⁶³. “The deterioration at the interface between contacting surfaces as the result of corrosion and slight oscillatory slip between the two surfaces”³⁸</i>
Fretting wear	<i>“Wear arising as a result of fretting”¹⁶³</i>
Galvanic corrosion	<i>“Accelerated corrosion of a metal because of an electrical contact with a more noble metal or non-metallic conductor in a corrosive electrolyte”²⁶⁷</i>
Sliding wear	<i>“Wear due to the relative motion in the tangential plane of contact between two solid bodies”¹⁶³</i>
Tribocorrosion (wear-corrosion synergism)	<i>“Form of solid surface alteration that involves the joint action of relatively moving mechanical contact with chemical reaction in which the result may be different in effect than either process acting separately”¹⁶³</i>
Wear	<i>“Alteration of a solid surface by progressive loss or progressive displacement of material due to relative motion between that surface and a contacting substance or substances”¹⁶³</i>

2.6.2 Factors affecting the material loss from the taper- trunnion junction of modular hip prostheses

The exact mechanisms accountable for the material from the taper-trunnion junction are not entirely determined. Furthermore, it is widely accepted that these mechanisms are multifactorial, and this could be implant factors, surgical factors or patient factors^{240,268}. Factors affecting the material loss from the taper-trunnion junction or neck-stem junction of modular hip prostheses are summarised in Figure 45.

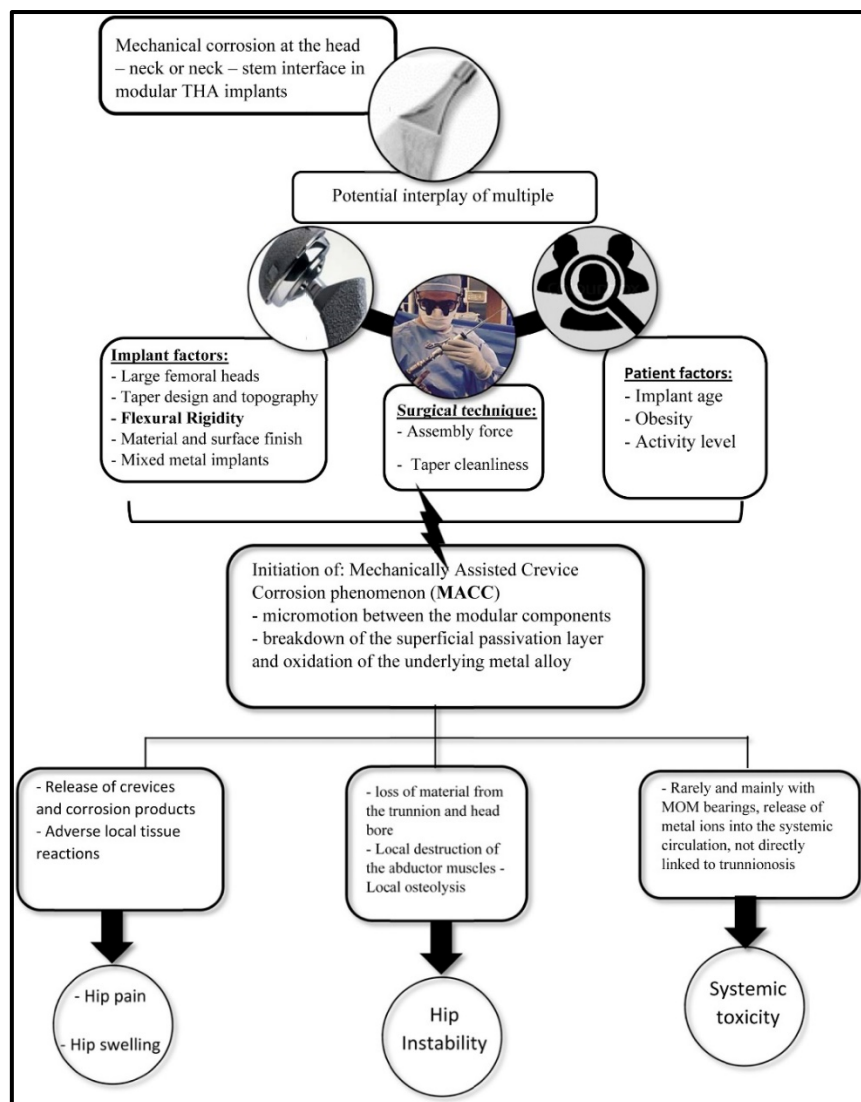


Figure 45 Summary of Factors affecting the material loss from the taper-trunnion junction or neck-stem junction of modular hip prostheses. Image from Sultan et al. (2018)²⁶⁹.

The most common design of modular THR has a single head-neck interface, i.e. the taper-trunnion junction^{27,86}. Therefore, factors affecting the material loss from the taper-trunnion junction of the modular hip prostheses are described in this section.

2.6.2.1 Implant factors

When a femoral head of 36mm diameter or greater, i.e. large-diameter is used as a bearing surface, it is expected that it results in fewer dislocations by allowing an increased range of motion and stability for the patient^{270,271}. Figure 46 shows an increase in the range of motion as the femoral head diameter size increases. From Equation III, the frictional torque (T) is directly proportional to the femoral head radius (r) for given applied load (L) and the bearing surfaces combination. Therefore, the increased femoral head diameter will generate higher frictional torque. The increased torque at the bearing surfaces consecutively can transfer larger shear forces to the taper-trunnion junction surfaces leading to material loss^{272,273}. Furthermore, retrieval studies reported an increased material loss in large-diameter MoM THRs^{18-20,23,126}. Also, the NJR shows higher revision rates for MoP hips ≥ 36 mm head diameter⁵.

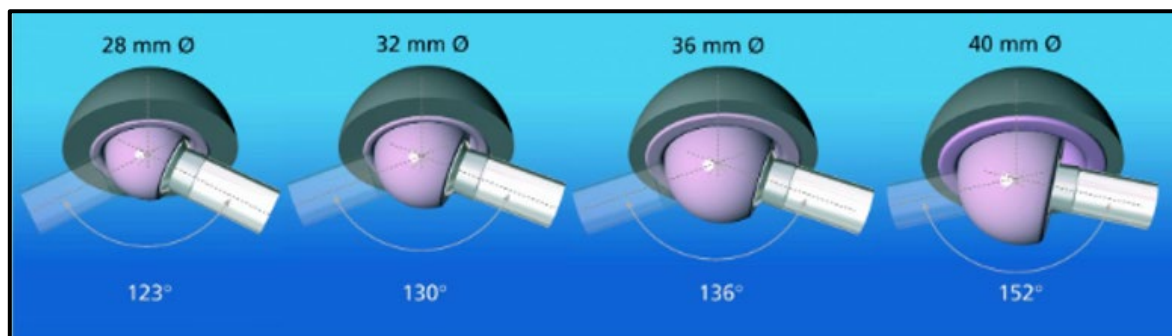


Figure 46 From left to right: range of motion (in degrees) increases as the femoral head diameter (Ø) size (in mm) increases. Image from Altimed JSC²⁷⁴.

Arnholt et al.²⁵⁴ reported no correlation between trunnion surface finish and the material loss or fretting corrosion damage at the taper-trunnion junction of retrieved MoP THRs. However, Ashkanfar et al.²⁷⁵ investigated the effect of the surface roughness of the trunnions (smooth and threaded/micro-grooved/rough) on the volumetric material loss at the taper-trunnion junction in a computational study using 3D finite element models of THRs with CoCrMo femoral heads. The study suggested the use of trunnions with a smoother rather than micro-grooved surface finish to reduce the material loss at the taper trunnion junction. Furthermore,

Brock et al.²⁷⁶ found significantly higher material loss at the CoCrMo femoral tapers mated with 12/14 threaded trunnions than 11/13 smooth trunnions of retrieved large-diameter MoM THRs from a single manufacturer. Therefore, rougher trunnions are associated with an increased rate of material loss at the taper-trunnion junction.

Additionally, modularity allows mixing and matching of different materials used for taper-trunnion junction either mixed-metal interface (CoCrMo alloy femoral taper and Ti alloy trunnion) or similar-metal interface (CoCrMo alloy femoral taper and CoCrMo alloy trunnion) as described in 2.5.1. Goldberg et al.³⁰ reported more corrosion in the mixed-metal interface (with a 42% incidence of corrosion) than the similar-metal interface (with a 28% incidence of corrosion) in 231 retrieved modular hip prostheses. Also, Goldberg et al.³⁰ reported higher fretting and corrosion scores for the femoral tapers than the trunnions and identified evidence of a MACC process responsible for *in vivo* corrosion of prostheses. Furthermore, Gilbert et al.¹⁷ also reported evidence of MACC on the taper-trunnion junction of the mixed-metal interface as well as the similar-metal interface of the retrieved modular hip prostheses. However, Kocagoz et al.²⁴¹, in a retrieval study of 50 MoP hips, found no correlation between the volumetric material loss and material combination used (mixed or similar metal interface) for the taper-trunnion junction. Moreover, Langton et al. in a retrieval study of LD MoM hips reported a more significant material loss in similar-metal interface than mixed-metal-interface²⁶⁶.

The radial clearance and lubricant film thickness may affect the wear at the taper-trunnion junction. The Hamrock-Dowson equation²²⁰, see Equation VI, showing the relationship of the variables affecting lubricant fluid entrainment at the bearing surfaces. The minimum film thickness (h_{min}) generated is directly proportional to the equivalent radius (R_x) of the bearing surfaces. From Equation VII, the equivalent radius (R_x) is calculated as the product of the radius of the two surfaces ($R_{acetabular\ liner} \times R_{femoral\ head}$) in contact divided by their difference ($R_{acetabular\ liner} - R_{femoral\ head}$). This difference between the radius of bearing surfaces ($R_{acetabular\ liner} - R_{femoral\ head}$), is called as the radial clearance. Therefore, with reduced radial clearance (i.e. more sophisticated manufacturing tolerances) the R_x increases leading to an increase in the h_{min} and eventually reduced wear at the bearing surfaces⁶¹. In this manner, the radial clearance plays a vital role in the tribological performance of the THR.

2.6.2.2 Surgical factors

Many studies have reported the correlation between impaction technique force and cleanliness of the taper-trunnion junction surfaces with the performance of the modular THRs^{27,277-279}. Each surgeon uses a unique surgical impaction technique for fixing the femoral head on the trunnion of the femoral stem during the surgery²⁸⁰. A minimum impaction force of 4 kN has been recommended on a clean taper-trunnion junction surfaces for locking modular THRs²⁸¹. Grosso et al. evaluated wear patterns after impaction and removal of the taper-trunnion junction of ceramic femoral heads mounted on Ti6Al4V trunnions at different impaction forces (2 kN, 4kN or 6kN)²⁸². The femoral taper and trunnions surfaces were inspected using a CMM to calculate taper angle and surface deviation for assessment of the damage. Additionally, surface roughness, Ra was measured on the taper-trunnion surfaces. Grosso et al. concluded that the impaction and removal procedure had no significant damage to Ti6Al4V trunnions or ceramic femoral tapers²⁸².

2.6.2.3 Patient factors

Various patient-related factors such as patient weight^{257,283}, prostheses age^{30,86,257,283} and activity level²⁵⁷ have been identified, mainly from retrieval studies. Interestingly, Higgs et al²⁸³ in a retrieval study of 252 CoCrMo femoral tapers estimated that an increase of approximately 450 g in patient weight results in a 1% increase in propensity for the damage at the femoral taper.

2.6.3 Quantification and evaluation of the material loss from the taper-trunnion junction.

Historically, MACC and fretting corrosion have been assessed using a visual scoring method on explanted THR components³⁰. In 1993, Gilbert et al. established a qualitative system for classification of corrosion at the retrieved taper-trunnion junction and categorised the damage into four groups: no visible corrosion, mild corrosion, moderate corrosion and severe corrosion¹⁷. In 2002, Goldberg et al. allocated numbers along with criteria to the categories

and developed the ‘Goldberg score’ system³⁰, see Table 18. Figure 47 shows an example of the ‘Goldberg score’ system²⁵⁷.

Table 18 The Goldberg scoring system³⁰.

Severity of corrosion and fretting	Score	criteria
None	1	No visible corrosion observed No visible signs of fretting observed
Mild	2	<30% of taper surface discoloured or dull Single-band or bands of fretting scars involving 3 or fewer machine lines on
Moderate	3	>30% of taper surface discoloured or dull, or <10% of taper surface containing black debris, pits, or etch marks Several bands of fretting scars or single band involving more than 3 machine lines
Severe	4	>10% of taper surface containing black debris, pits, or etch marks Several bands of fretting scars involving several adjacent machine lines, or flattened areas with nearby fretting scars

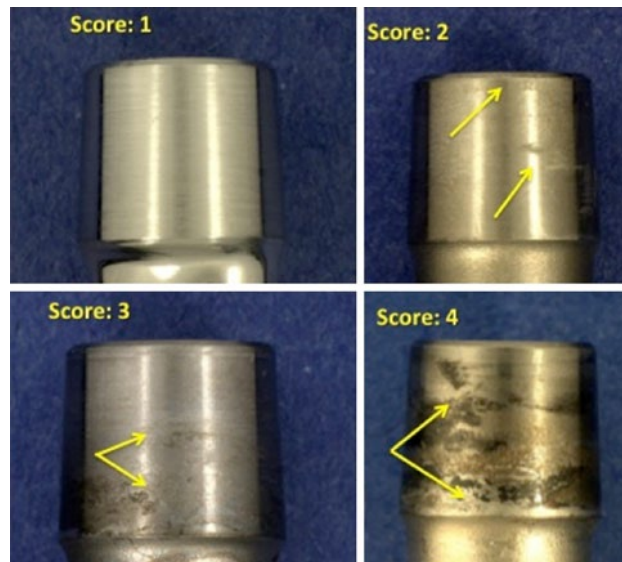


Figure 47 A sample image of ‘Goldberg score’ criteria. Examples of fretting and corrosion scores for metallic trunnions mounted on CoCrMo femoral heads. Image from Kurtz et al. (2013)²⁵⁷.

The ‘Goldberg score’ system affected by the material combination. Concerns have been raised regarding the use of mixed-metal interface taper-trunnion junctions due to the apparent elevated risk of corrosion¹⁶. The reported incidence of corrosion at the taper-trunnion junction in THRs ranges from 0% to 28% for similar-metal interface (CoCrMo alloy femoral taper and CoCrMo alloy trunnion) and up to 50% for mixed metal CoCrMo alloy femoral taper and Ti alloy trunnion)²⁶⁶. Goldberg et al.³⁰ reported more corrosion in the mixed-metal interface (with a 42% incidence of corrosion) than the similar-metal interface (with a 28% incidence of corrosion) in 231 retrieved modular hip prostheses. Furthermore, Gilbert et al.¹⁷ also reported evidence of MACC on the taper-trunnion junction of the mixed-metal interface as well as the similar-metal interface of the retrieved modular hip prostheses.

It is important to note that this semi-quantitative grading system is based on visual assessment of one or multiple observers and no quantitative results. Furthermore, Kocagoz et al. (in MoP) and Hothi et al. (in MoM) found a positive correlation between the volumetric material loss and visual scoring analysis^{241,259}. However, Nassif et al. (in large-diameter MoM) reported no correlation between corrosion score and volumetric wear. Furthermore, Langton et al. demonstrated that the use of visual scoring analysis would have resulted in a different conclusion in the explant study of the taper-trunnion junction of large-diameter MoM²⁶⁶. Moreover, Langton et al. noted an apparent ceiling effect to scoring scale and suggested that the visual scoring analysis can be useful for identification of the damage²⁶⁶.

Only a few explant studies have quantified material loss volumetrically at the taper-trunnion junction^{19,241,244}, see Table 19. In part, this is because the measurement equipment to achieve this has only recently become available.

Table 19 Explant studies involving the quantification of material loss from the taper-trunnion junction of modular hip prostheses.

Authors (year)	Explant type	Femoral Taper / Trunnion	Volumetric material loss	
			Femoral taper mm ³ /year	Trunnion mm ³ /year
Langton et al¹⁹ (2012)	MoM	• Articuleze (CoCrMo/ Ti6Al4V)	0.13 (0.01 – 3.15) mean(range)	No measurable wear
	(n=124)	• ASR XL (CoCrMo/ Ti6Al4V)	0.44 (0.02 – 8.34) mean(range)	
Matthies et al²⁰ (2013)	MoM	CoCrMo/ Ti6Al4V, CoCrMo/ CoCrMo	0.54 (0.00 – 4.29) mean(range)	0.08 (0.00–0.36) mean(range)
Bishop et al¹⁸ (2013)	MoM	CoCrMo/ Ti6Al4V	2.04 (0.6 – 4.9) mean(range)	Measured for only two stems (0.006 and 0.005 mm ³ /year)
Nassif et al²³ (2014)	MoM	CoCrMo/ Ti6Al4V, CoCrMo/ CoCrMo, Ti6Al4V / CoCrMo, Ti6Al4V / Ti6Al4V	< 4	Not measured
Hothi et al²⁵⁹ (2014)	MoM	CoCrMo/ not mentioned	*1.52 mm ³ (0.13–25.89) median material loss (range)	Not measured
Brock et al²⁷⁶ (2015)	MoM	• CoCrMo/ Ti6Al4V: S-ROM	0.37 (-) median(range)	*0.19 mm ³ (0.07–0.27) (median total volume loss)
		• CoCrMo/ Ti6Al4V: Corail	0.48 (-) median(range)	
Hothi et al²⁸⁴ (2015)	MoM	• CoCrMo/ Ti6Al4V: S-ROM	0.13 (0.01–0.52) median (range)	Not measured
		• CoCrMo/ Ti6Al4V: Corail	0.24 (0.00–2.18) median (range)	
Kocagoz et al²⁴¹ (2016)	MoP,	• CoCrMo cohort (CoCrMo/ CoCrMo and	0.02 (0 – 8.67) median(range)	0.00 (0 – 0.32) median(range)
	CoC and CoP	CoCrMo/ Ti alloy) • Ceramic cohort (Ceramic/ CoCrMo and Ceramic/Ti alloy)	0.00 (0 – 0.04) median(range)	0.00 (0–0.37) median(range)
Langton et al²⁶⁶ (2017)	MoM	• CoCrMo/ Ti6Al4V	0.10 (0.01 to 2.16) mean(range)	0.04 (0.01 to 0.12) mean(range)
		• CoCrMo/ CoCrMo	0.41 (0.01 to 1.65) mean(range)	0.30 (0.03 to 0.53) mean(range)

Authors (year)	Explant type	Femoral Taper / Trunnion	Volumetric material loss	
			Femoral taper mm ³ /year	Trunnion mm ³ /year
Hothi et al²⁴⁴ (2017)	MoP	• CoCrMo/ CoCrMo	0.08 (0 to 0.24) median(range)	Not measured
Langton et al²⁸⁵ (2018)	MoM and	• CoCrMo/ Ti6Al4V (MoM)	0.25 (0.01 to 8.34) mean(range)	Not measured
	MoP	• CoCrMo/ CoCrMo (MoM)	0.29 (0.01 to 3.15) mean(range)	
		• SS/SS (MoP)	0.05 (0 to 3.84) mean(range)	
Hothi et al²⁸⁶ (2018)	MoM and	• CoCrMo/ Ti6Al4V (MoM)	0.81 (0.01-3.45) median(range)	Not measured
	MoP	• CoCrMo/ Ti6Al4V (MoP)	0.03 (0-1.07) median(range)	

*Volume wear rate not given

2.7 What can *in vitro* studies tell us about what happens *in vivo*?

This section gives an overview of current *in vitro* methodologies that have been used for the evaluation of the material loss at the taper-trunnion junction of modular hip prostheses.

Various theories have been reported in the literature including mechanical, electrochemical or a combination of both for metal debris formation at the taper-trunnion junction of the modular THR^{16-19,30-34}. Much of the data for these theories has, appropriately and sensibly, come from explant studies, as these are based on the truest test of all, that in the human body. However, explants come from individuals, each with unique attributes, including loading, motion, activity, etc. Relatively few *in-vitro* studies have assessed MACC or fretting corrosion from the taper-trunnion junction of modular THR³⁵⁻³⁷. The purpose of these *in vitro* studies includes mainly an assessment of electrochemical characteristics and metallurgy of the implant materials used for the taper-trunnion junction. These tests comprise of triboelectrochemical testing of different material combinations, i.e. similar metal, mixed metal or ceramic-metal, under sliding contact using pin-on-plate, ball-on-flat or pin-on-disc configuration under well-defined loading and displacement conditions^{251,253,287,288}. The most commonly used electrochemical measurement comprises of following methods²⁵³:

1. Acquiring information on the rate of electrochemical reaction at the interface of the material combinations under investigation by monitoring corrosion currents at a fixed potential, and/ or
2. Acquiring qualitative information on the tribocorrosion performance of material combinations under investigation by monitoring the open circuit potential

Furthermore, the material loss due to wear and corrosion can be estimated by including wear volume characterisation in some *in vitro* tests²⁸⁹⁻²⁹¹. However, these testing methodologies do not use actual hip prostheses for laboratory testing. In terms of standards, ASTM F1875 “Standard practice for fretting corrosion testing of modular implant interfaces: hip femoral head-bore and cone taper interface” mentions only uniaxial dynamic loading for fretting wear and corrosion testing of modular THR^{38,39}, which utilises realistic femoral head and trunnion modular of THR. This standard highlights two types of testing methods, long-term testing and short-term testing^{38,292}. These two methods differ in their purpose, frequency, test duration, measurement techniques; however, mechanical loading and test fluid conditions are the same. Testing conditions reported in ASTM F1875 are summarised in Table 20.

Table 20 Testing conditions as per the ASTM F1875³⁸.

ASTM 1875	Long-term testing	Short-term testing
Frequency	5 Hz	1 Hz
Test duration	10 million cycles	1 million cycles
Specimen Mounting	Anatomical	Inverted
Measurement	Chemical analysis of the testing liquid and of the particulate debris	Semi-quantitative measurement of corrosion rates
Purpose	To determine the amount of damage (quantitative measure of total elemental level)	To evaluate differences in design during device development
Dynamic loading	Minimum 0.3 kN and maximum 3.3 kN	
Test fluid	Electrolyte Solutions [0.9 % sodium chloride (NaCl) in distilled water] or Proteinaceous Solutions (10 % solution of calf serum in 0.9 % NaCl in distilled water)	
Test fluid volume	5 to 100 mL	

Furthermore, ‘anatomical’ and ‘inverted’ testing methods were provided in the ASTM F1875. These two sample orientation methods differ from one another in terms of lubricant ingress, lubricant pressure and retention of wear debris at the taper-trunnion junction and may affect the subsequent wear and corrosion process³⁶. Physiologically relevant testing frequency of 1 Hz was mentioned in the short-term testing; however, the specimen mounting was ‘inverted’ which is non-anatomical. Bingley et al. compared ‘anatomical’ and ‘inverted’ testing methods mentioned in the ASTM F1875 and reported a higher material loss from the femoral tapers used in the inverted than the anatomical orientation³⁶. In contrast, the long-term testing method utilises ‘anatomical’ specimen mounting position, although the testing frequency was five times higher than the frequency of standard physiological walking conditions. Moreover, diluted bovine serum with the protein concentration within the physiological range of the joint fluid is a better lubricant for *in vitro* testing of hip prostheses¹⁸⁷. However, both testing methods employ either electrolyte solution (with no

proteins) or proteinaceous solutions (with 10% calf serum), which is again not physiologically relevant.

Note that employment of physiological walking motion is not included in the ASTM F1875³⁸. Interestingly, analysis of retrieved modular THR^s demonstrated toggling of the femoral head on the trunnion^{18,19,34,45,293}. The toggling is not just superoinferior but appears to involve anteroposterior/posteroanterior direction too. Therefore, the taper-trunnion junction of modular hips should be examined rigorously under clinically relevant test conditions prior to implantation into patients^{27,36,265,294,295}.

2.8 Summary

ARMD released from the taper-trunnion junction of modular THR^s is an issue of contemporary concern in CoC and MoP THR^s^{24,43,45}. In CoC hips, the only sources of metal (usually titanium) would be the trunnion of the femoral stem and the acetabular shell. The potential sources of this metal debris in MoP hips would be the bearing surface of the metallic femoral head (usually CoCrMo), the taper-trunnion junction, and the acetabular shell. Out of these three sources, the head-liner bearing surfaces and the acetabular shell and backside of the liner have a metal against softer polymer contact, whereas the taper-trunnion junction has an MoM contact. Of these two sources, the importance of metal debris from the taper-trunnion junction in MoM hip prostheses has been widely recognized¹⁸⁻²⁰. Historically, MACC or fretting corrosion has been evaluated using visual examination method and comparatively recent retrieval studies quantified material loss at this modular junction^{251,259}. However, very few *in vitro* studies evaluated MACC or fretting corrosion from modular junctions²⁸⁹⁻²⁹¹. The ASTM F1875, standard for fretting corrosion testing of modular THR^s employs only uniaxial dynamic loading³⁸. Interestingly, analysis of retrieved modular THR^s demonstrated toggling of the femoral head on the trunnion^{18,19,45}.

Following research questions not been answered in the literature:

- In CoC articulating components, comprised of ceramic material, where is the metal debris originating from?
- Dynamic loading & articulating motion vs dynamic only loading, does the material loss at the taper-trunnion junction change?

- In MoP articulating components, comprised of metal and softer polymer contact, where is the metal debris originating from?
- What are the mechanisms responsible for the material loss from the taper-trunnion junction of modular MoP THRs, when CoCrMo/Ti alloy combinations are used for the taper-trunnion junction?

To the authors' best knowledge, no other hip simulator tests have investigated material loss from the taper-trunnion junction of a modular CoC and MoP THR. Therefore, the aim of this thesis is to quantify the material loss, if any, at the taper-trunnion junction of modular CoC and MoP THRs under standard physiological walking cycle. In order to achieve this aim and to find answers to the research questions, multi-station hip simulator testing of modular hips mounted on titanium (Ti) alloy trunnions was undertaken under standard physiological walking cycle, replicating the clinical scenario as closely as possible.

Chapter 3: Materials and Methods

In this chapter, materials, machines and instruments used for *in vitro* testing of hip prostheses are briefly described. New hip prostheses were wear tested as per the international standard ISO 14242¹⁸⁷ in the hip joint simulator; this includes loading and motion conditions.

3.1 Hip simulator wear testing of the taper-trunnion junction and bearing surfaces of modular CoC hip prostheses

This section illustrates the materials and the test summary of the hip simulator wear testing of the latest 4th generation ceramic-on-ceramic (CoC) hip prostheses focusing on material loss at the taper-trunnion junction and bearing surfaces.

3.1.1 Materials

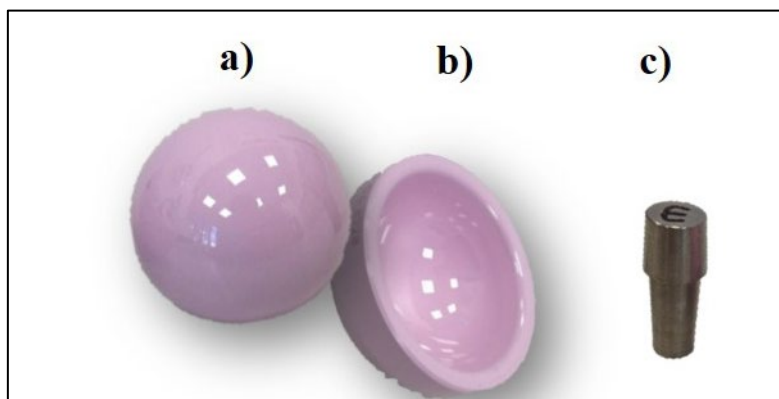


Figure 48 a) Ceramic femoral head (BIOLOX®delta), b) ceramic acetabular liner (BIOLOX®delta) and c) 12/14 Ti6Al4V trunnions.

For the CoC hip simulator wear test, three 36mm BIOLOX®delta, Pinnacle® (DePuy Synthes, UK), CoC hip replacement bearings were used. Newcastle University provided all implants. Each ceramic femoral head had +5.0 associated neck length (REF 1365-320, manufacturer's code), see Figure 48 a). Each ceramic acetabular liner had REF 1218-81-754, manufacturer's code, see Figure 48 b). The 12/14 Ti trunnions with a neck length of 34.5 mm, see Figure 48 c) were manufactured by Phoenix Tribology Limited, UK based on the Corail® (DePuy Synthes, UK) stem, see Figure 49 which, when employed with 36mm ceramic heads, gives the most commonly implanted CoC hip in the UK². Table 21 summarises dimensions of all components used in MoXLPE hip simulator wear test.

Table 21 Summary of CoC components used in CoC hip simulator wear test.
Dimensions of the bearing surfaces of CoC joints

36mm CoC joints	Number of samples	Radius (mm) (Mean \pm SD)	Radial clearance (mm)
Femoral head	3	17.9993 \pm 0.0053	0.037 \pm 0.073
Acetabular liner	3	18.0360 \pm 0.0067	
Dimensions of the measured taper-trunnions			
12/14 tapers	Proximal radius (mm)	Distal radius (mm)	Cone angle (°)
Femoral taper	6.9379 \pm 0.0033	6.4373 \pm 0.0054	5.7901 \pm 0.0137
Trunnions	6.9013 \pm 0.0280	6.4424 \pm 0.0188	5.6713 \pm 0.0042

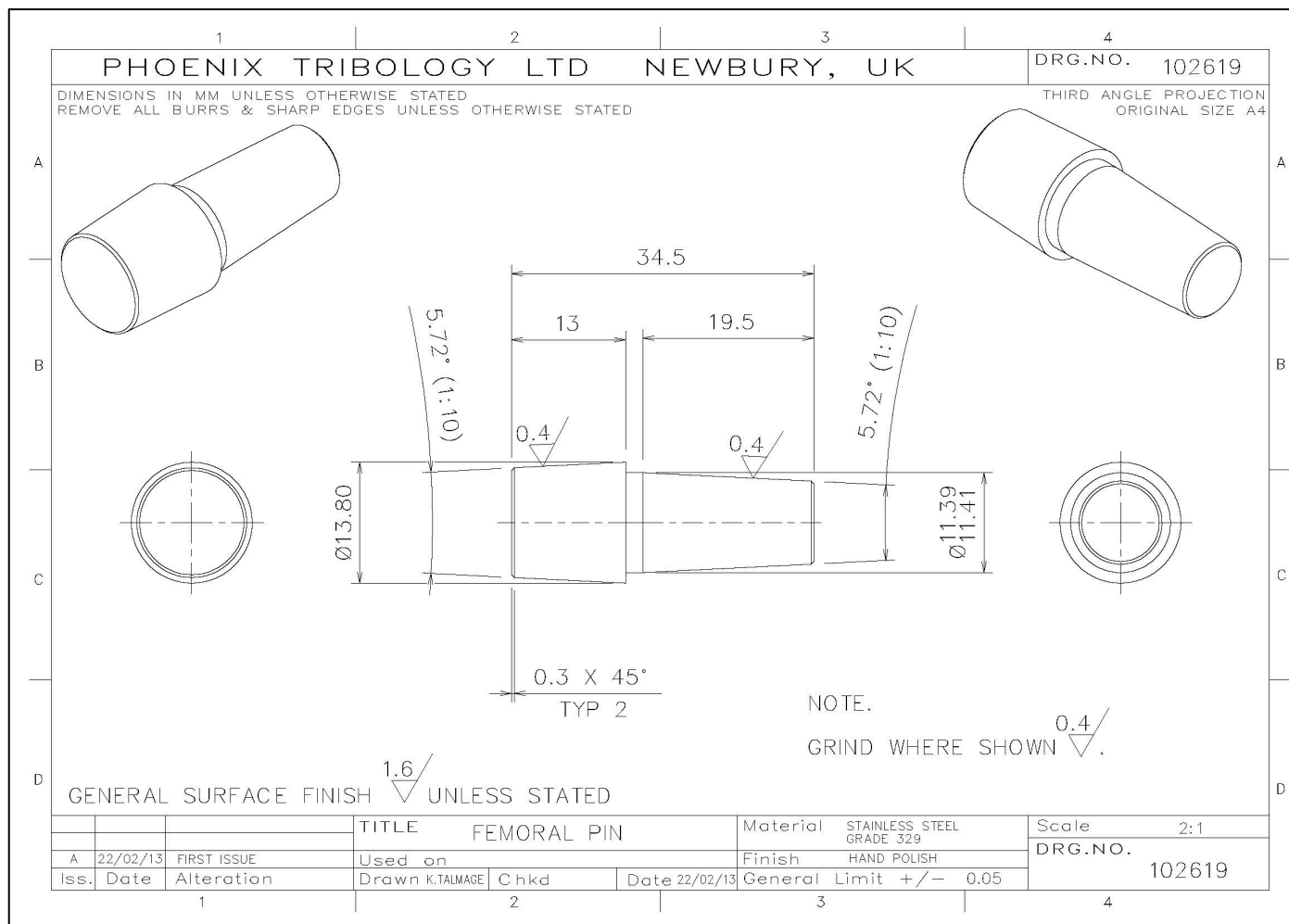


Figure 49 Engineering drawing of the trunnion used in tests involving CoC THR.

3.1.2 Hip simulator wear test

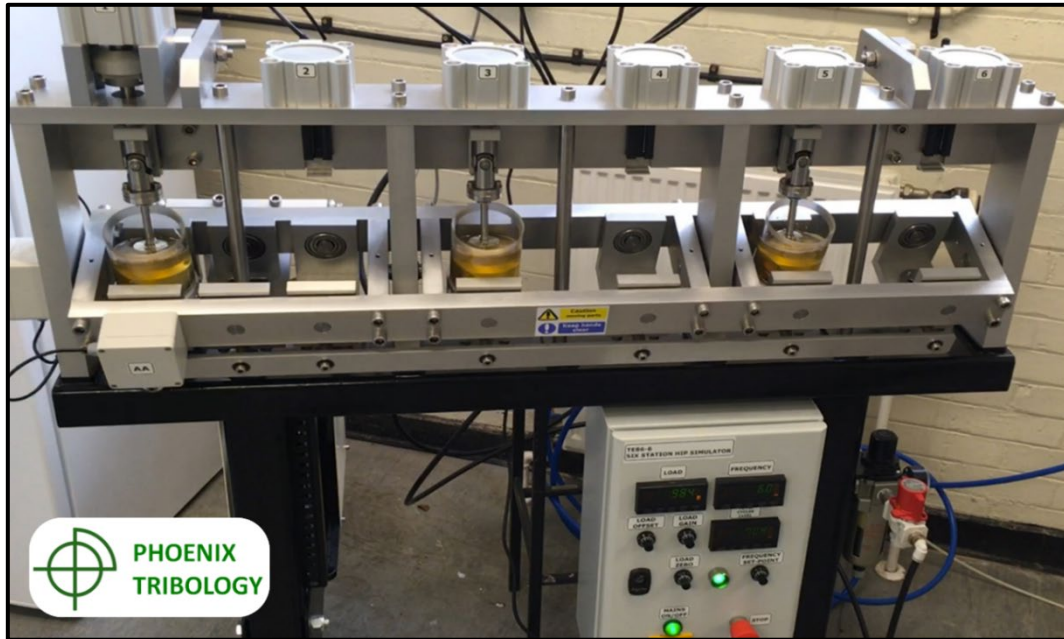


Figure 50 The six-station anatomical hip joint simulator showing three CoC test components immersed in diluted new-born-calf serum²⁹⁵.

Ceramic-on-ceramic (CoC) hip replacement bearings were tested in the 6-station anatomical hip joint simulator shown in Figure 50¹⁸⁹. The kinematics used in the MoXLPE hip simulator test was based on Saikko (2005)¹⁸⁹. The walking cycle applied in the simulator combines sinusoidal flexion-extension and abduction-adduction motions with the excursion of 46° and 12° respectively, resulting in an elliptical wear path¹⁸⁹. The test ran for 5 million cycles. A double-peak load was applied to the three articulating samples with a minimum value of 400 N and a maximum value 2000 N¹⁸⁹. Although the hip simulator had six test stations, only three were used in the CoC hip simulator wear test. Two further samples were required for the Dynamic loading (DL) but no articulating motion test, see section 3.2, and the impaction test, see section 3.3, both of which were fundamental to this investigation. As these samples were all the latest fourth generation of ceramic BIOLOX®*delta*, obtaining such samples for independent testing was both challenging and expensive as this project was unfunded.

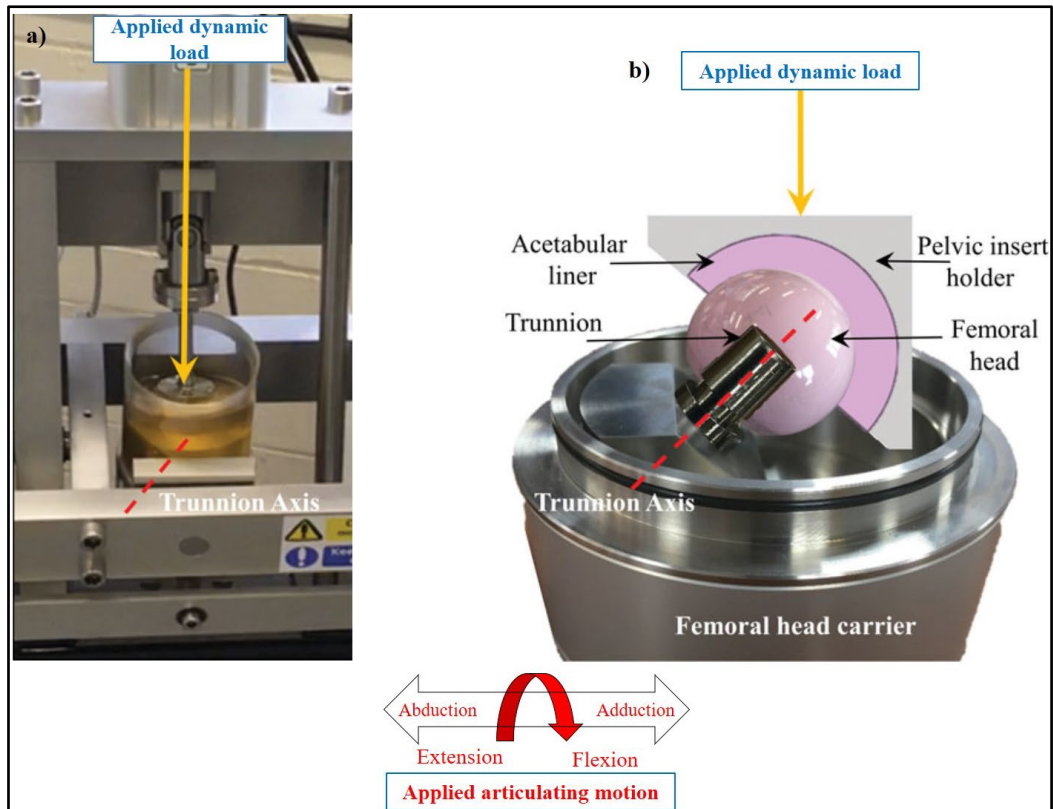


Figure 51 a) A test station from the hip simulator and b) schematic of the ceramic femoral head, ceramic acetabular liner, and Ti trunnion in the hip simulator wear test set up. All prostheses were subject to dynamic loading and articulating motion.

Each ceramic femoral head was mounted using a plastic femoral head impactor, replicating that used in surgery, onto a 12/14 Ti trunnion (Ti6Al4V). When impacting, at least two firm, axially aligned blows to impact the femoral head onto the trunnion were employed⁸⁷. In turn, each trunnion was located into a femoral head carrier [See Figure 51 a) and b)]. All trunnions and femoral head carriers were marked prior to testing to enable correct repositioning following cleaning and measurement intervals. Each ceramic acetabular liner was held in an aluminium 3105 alloy pelvic insert holder with 45° cup abduction angle and 15° anteversion angle of the simulator¹⁸⁹. This is different to the clinical situation where a Ti shell would serve to connect the liner to the acetabulum, but it is common not to use a shell in hip simulators where the historical focus has been on wear testing the bearing surfaces^{189,196,296}.

New-born-calf serum (Gibco™, Life Technologies), diluted with de-ionised water to give a protein concentration of 21g/L, was used as the lubricant. The lubricant was changed every 500,000 cycles when the components were cleaned and weighed following the relevant international standard, ISO 14242-2¹⁷³. In addition to this, Sidol cleaner was used to remove any visual marking seen at the internal taper of the femoral heads and the backside of the

liners, see Figure 52, following disassembly²⁹⁷. In a hip simulator study, Saikko and Pfaff detected metal transfer on the femoral taper and backside of the liner after the disassembly and found to cause slight weight gain on the components²⁹⁷. Therefore, they removed the metal transfer using Sidol cleaner which contained clay as an abrasive. Hence, visual markings were removed using Sidol cleaner to minimise the effect of metal transfer that would affect the gravimetric measurements.

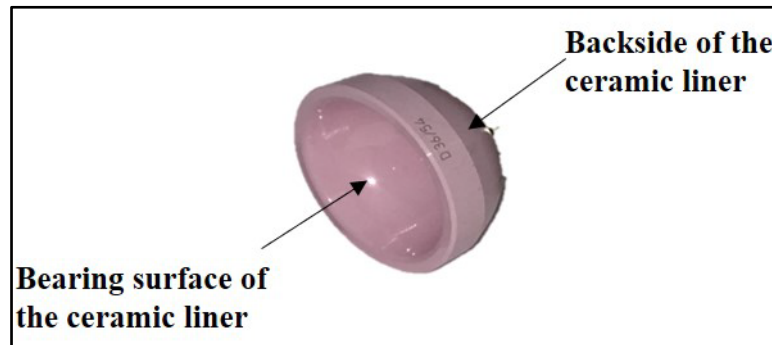


Figure 52 Surfaces of the BIOLOX®delta ceramic liner.

Table 22 summarises all the experimental variables that have been tested in CoC hip simulator test.

Table 22 Summary of all the experimental variables for CoC hip simulator test

<i>Motion</i>	Standard physiological walking cycles
<i>Loading</i>	Double-peak load (min 400 N and max 2000 N at 1 Hz)
<i>Components</i>	Three 36 mm BIOLOX®delta femoral heads Three 36 mm BIOLOX®delta acetabular liners Three 12/14 Ti6Al4V trunnions
<i>Test duration</i>	5 million cycles (Mc)
<i>Lubricant</i>	Diluted new-born-calf serum (protein concentration 21g/L)
<i>Wear measurement</i>	As per the ISO 14242-2 ¹⁷³

3.1.3 Quantification of the material loss from the taper-trunnion junction and bearing surfaces

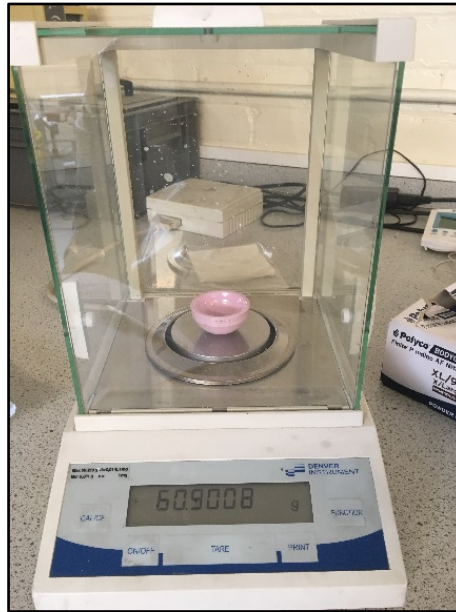


Figure 53 Gravimetric measurement of a ceramic acetabular liner using an analytical balance.

The material loss was measured gravimetrically using an analytical balance (TB – 215D; Denver Instruments, Germany) see Figure 53, with a 0.1mg sensitivity, for ceramic femoral heads, acetabular liners and Ti trunnions after every million cycles, with measurements taken in triplicate to ensure repeatability. Although the lubricant was changed every 0.5 Mc, femoral heads and trunnions could not be able to disassemble by the author at the 0.5 Mc and 1.5 Mc. Therefore, gravimetric measurements were performed at 1Mc, 2 Mc, 2.5Mc, 3Mc, 3.5Mc, 4Mc, 4.5Mc and 5Mc. Taking the density of the BIOLOX[®]*delta* as 0.00437 g/mm³¹³¹ and Ti6Al4V as 0.00443 g/mm³²⁹⁸, gravimetric wear in mg was converted to volumetric wear in mm³. The average volumetric loss for heads, liners, CoC joints (heads + liners) and trunnions was plotted against the number of cycles and the slope of the linear regression line taken as the wear rate in mm³/Mc, see Figure 54.

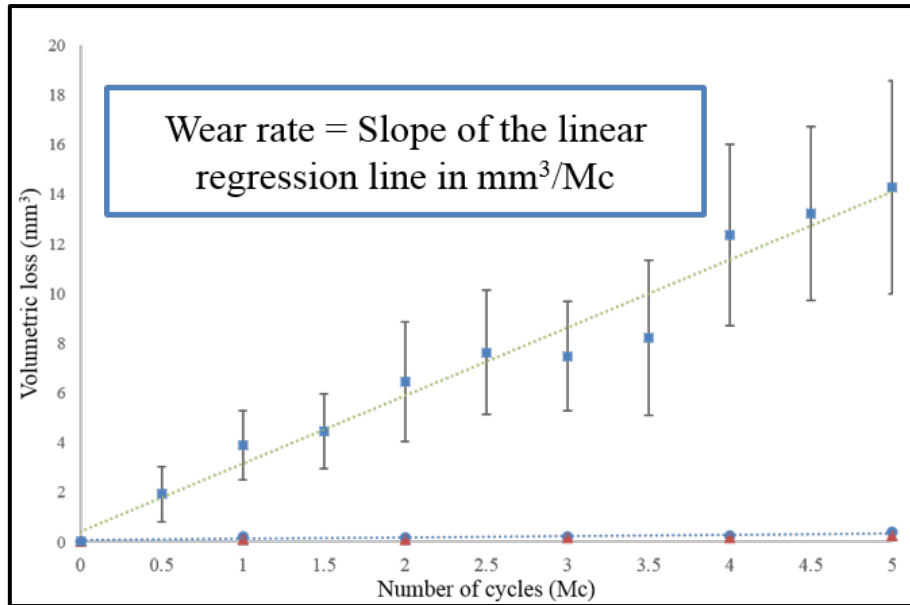


Figure 54 An example of a wear plot used for the wear rate calculations.

Additionally, after 5 million cycles, the material loss from the ceramic femoral tapers and Ti trunnions was measured geometrically using a coordinate measuring machine (CMM) (Legex CMM; Mitutoyo, Tokyo, Japan) as described in section 3.9. All taper wear measurements were carried out using previously published methodology with an accuracy of approximately 0.2 mm^3 ¹⁹. The volumetric wear rates of the tapers were calculated by dividing the average volume loss obtained from the geometric measurement by the total number of cycles.

3.1.4 Visual and microscopic analysis of Ti trunnions

At the end of the hip simulator wear test, images of trunnion surfaces were obtained using a Vision Measuring System Quick scope QS-L (Mitutoyo, UK). The majority of the damaged area was found to be localised at the proximal-superior aspect of the trunnion. Therefore, the trunnion surface was divided into two distinct areas; unworn and worn. Scanning electron microscopy was performed on the trunnions from the hip simulator wear test using a TM3030 SEM (Hitachi, Japan) to give high-resolution images (spatial resolution $< 100 \text{ nm}$ and depth resolution $> 10 \text{ nm}$). Prior to the SEM analysis, the trunnions were cleaned with isopropanol.

3.1.5 Surface roughness measurement

A two-dimensional (2D) contacting profilometer was used for the surface roughness (Ra) analysis of the tapers and trunnions, pre and post-test as described in section 3.10.1²⁹⁹.

Pre-and post-wear test three-dimensional (3D) surface roughness (Sa) measurements for ceramic femoral heads and acetabular liners were performed using the same non-contacting profilometer Zygo NewView 5000 with 0.1 nm vertical resolution, as described in section 3.10.2

Furthermore, in order to get a better understanding of the trunnion topography, the same non-contacting profilometer was used in these regions to obtain 3D surface roughness (Sa). Prior to these measurements, the trunnion surface was divided into two distinct areas; unworn and worn. A total of 20 measurements (10 on the unworn area and 10 on worn area) on each trunnion were acquired.

3.2 Dynamic loading (DL) but no articulating motion testing of CoC hip prosthesis

This section gives the summary of the dynamic loading (DL) but no articulating motion testing of the CoC prosthesis hip prostheses focusing on the material loss generated from the taper-trunnion junction and bearing surfaces.

3.2.1 Materials

A fourth 36mm BIOLOX[®]*delta*, Pinnacle[®](DePuy Synthes, UK), CoC hip replacement bearing was employed in a separate dynamically loaded (DL) station, with no articulating motion, to investigate the material loss, if any, at the bearing surfaces and the taper-trunnion junction.

3.2.2 Test summary

The fourth CoC sample was subject to the same dynamic loading as the hip simulator wear test, with a minimum value 400 N and a maximum value 2000 N ²³, but no articulating motion referred to henceforth as the DL test station. All other testing conditions such as assembly-disassembly procedures, the same lubricant etc. were used as mentioned previously for the CoC hip simulator wear test. It is important to note that the trunnion in the DL station was not loaded along its axis, but in the same way as the test samples, such that loading of the head was offset relative to the trunnion, replicating that seen when an artificial hip is implanted [(see Figure 55 a) and b)].

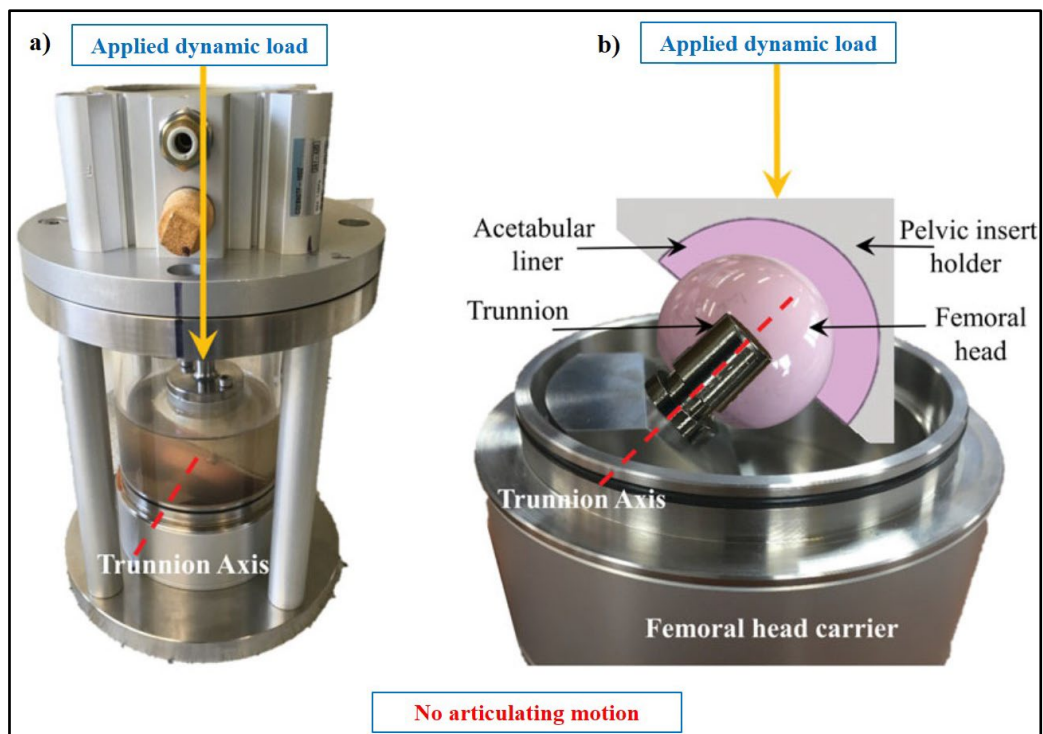


Figure 55 a) A DL station and b) schematic of the ceramic femoral head, ceramic acetabular liner, and Ti trunnion in the DL test set up

The following measurements on the DL test components were performed using the methodology described previously for the CoC hip simulator wear test:

- Gravimetric wear analysis for ceramic femoral head, acetabular liner and Ti trunnion
- Geometric wear analysis for ceramic femoral taper and Ti trunnion
- Two-dimensional (2D) surface roughness (Ra) of ceramic femoral taper and Ti trunnion
- Three-dimensional (3D) surface roughness (Sa) of the CoC bearing surfaces

3.3 Impactation test of CoC hip prosthesis

This section describes the summary of the impactation test performed on the CoC prosthesis.

3.3.1 Materials

It was appreciated that both the assembly and disassembly of the femoral head from the trunnion could produce wear at the taper-trunnion junction. Therefore, this important concern was investigated using a fifth CoC hip replacement bearing sample of 36mm BIOLOX®*delta*, Pinnacle®(DePuy Synthes, UK).

3.3.2 Test summary

In order to study the potential effect of material loss due to assembling and disassembling the femoral heads on the trunnions, a separate impactation test was conducted. A ceramic femoral head and Ti trunnion were assembled and disassembled eight times in an identical manner to that of the method used throughout the hip simulator test. After each disassembly procedure, the cleaning and weighing procedures, detailed previously, were carried out. Two-dimensional (2D) surface roughness (Ra) measurements of the taper and trunnion were also repeated after each disassembly following the methodology described in section 3.10.1.

3.4 Hip simulator wear testing of the taper-trunnion junction and bearing surfaces of modular metal-on-cross-linked polyethylene hip prostheses

This section illustrates the materials and the test summary of the hip simulator wear testing of the metal-on-cross-linked-polyethylene (MoXLPE) hip prostheses focusing on the material loss at the taper-trunnion junction and bearing surfaces. Explant studies showed that the material loss arises mainly from the CoCrMo alloy femoral tapers rather than the Ti alloy trunnions when CoCrMo/Ti alloy combinations are used for the taper-trunnion junction^{18,20}. Therefore, this test was focused on the assessment and quantification of the material loss from CoCrMo femoral tapers.

3.4.1 Materials

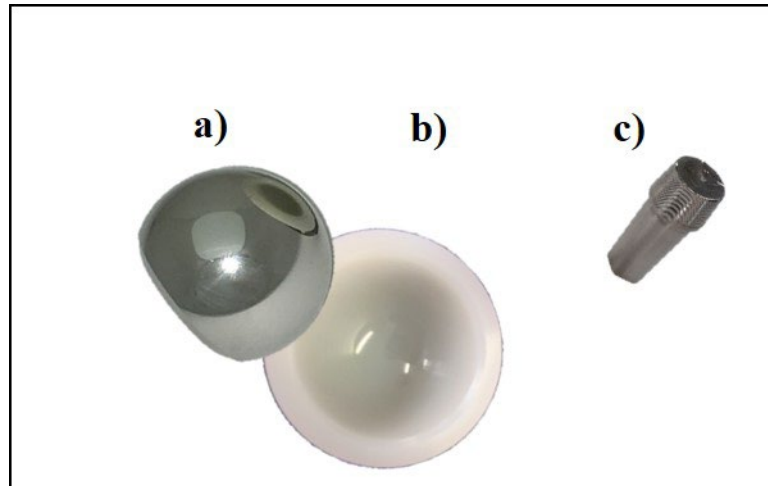


Figure 56 a) CoCrMo femoral head b) XLPE acetabular liner and c) 12/14 Ti6Al4V trunnion.

For the MoXLPE hip simulator wear test, five 32mm JRI Orthopaedics Limited, UK, MoXLPE hip replacement bearings were tested in the hip joint simulator. All specimens were commercially available MoXLPE joints composed of CoCrMo femoral heads articulating against XLPE acetabular liners (75kGy). Newcastle University provided all implants. Each CoCrMo femoral head had +4.0 associated neck length (REF 47-32-30, manufacturer's code), see Figure 56 a). Each XLPE acetabular liner had REF 150-52-32, manufacturer's code, see Figure 56 b). The 12/14 Ti trunnions (Ti6Al4V) with a neck length 30.6 mm [see Figure 56 c)] were manufactured, see Figure 57, based on the Corail® (DePuy Synthes, UK) femoral stem which has been implanted in 1.6 million surgeries worldwide³⁵. Table 23 summarises dimensions of all components used in MoXLPE hip simulator wear test. The ISO 14242-1 states, “*A control specimen, if polymers are the object of investigation, is subjected to the same time-varying force to determine the creep of the test specimen and/or the amount of mass change due to fluid transfer*”¹⁸⁷. Therefore, a sixth MoXLPE joint was used as a loaded soak non-articulating control specimen.

Table 23 Summary of MoXLPE components used in MoXLPE hip simulator wear test.
Dimensions of the bearing surfaces of MoXLPE joints

32mm MoXLPE joints	Number of samples	Radius (mm) (Mean \pm SD)	Radial clearance (mm)
Femoral head	5	15.9753 \pm 0.0053	0.2987 \pm 0.065
Acetabular liner	5	16.2737 \pm 0.0510	
Dimensions of the measured taper-trunnions components			
12/14 tapers	Proximal radius (mm)	Distal radius in (mm)	Cone angle (°)
Femoral taper	6.8116 \pm 0.0086	6.2734 \pm 0.0054	5.6807 \pm 0.0313
Trunnions	6.7690 \pm 0.0120	5.6950 \pm 0.0201	5.7213 \pm 0.0032

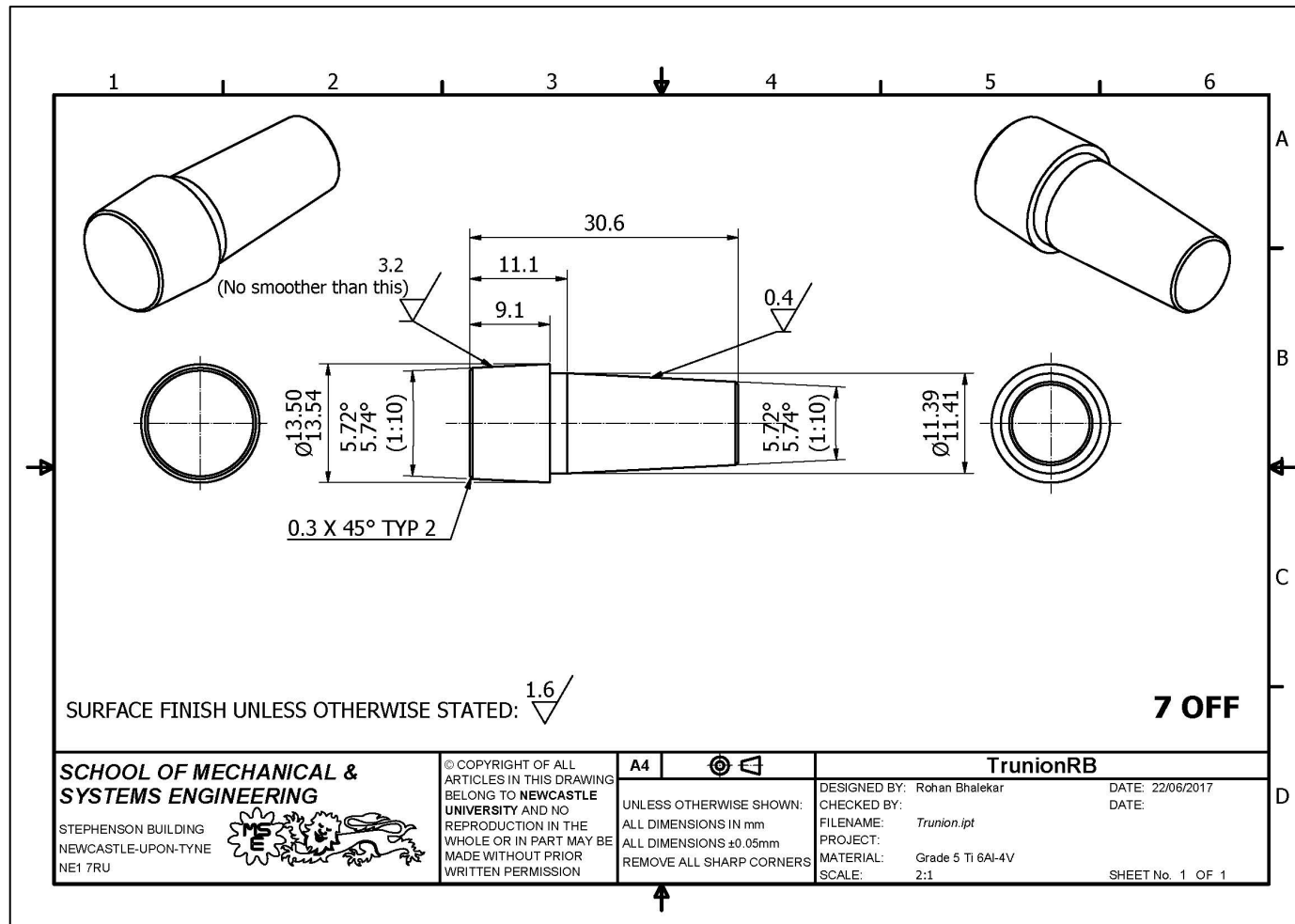


Figure 57 Engineering drawing of the trunnion used in tests involving MoXLPE THR.s.

3.4.2 Hip simulator wear test



Figure 58 The six-station anatomical hip joint simulator showing five MoXLPE test components immersed in diluted new-born-calf serum³⁰⁰.

The 6-station anatomical hip joint was used for *in vitro* wear testing of five MoXLPE joints mounted on Ti trunnions for 5 Mc, see Figure 58¹⁸⁹. Although the hip simulator had six test stations, only five were used in this wear test. The kinematics used in the MoXLPE hip simulator test was based on Saikko (2005)¹⁸⁹. All test specimens were subject to time-varying double-peak load with a minimum load value 400 N and a maximum load value 2000 N and relative articulating motion, generating an elliptical wear path^{189,295}. The articulating motion of the simulator comprised of sinusoidal flexion-extension and abduction-adduction with an excursion of 46° and 12° respectively¹⁸⁹. Although the hip simulator had six test stations, only five were used in the MoXLPE hip simulator wear test. A sixth MoXLPE joint used as a dynamically loaded soak control specimen was subject to the same time-varying loading but no articulating motion as per the international standard for wear testing of total hip prostheses ISO 14242-1¹⁸⁷.

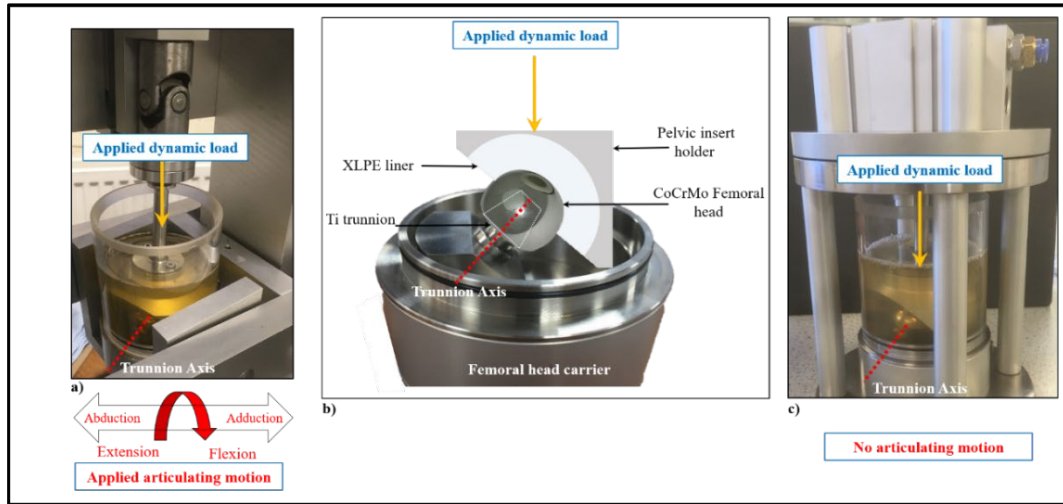


Figure 59 a) A test station, b) schematic of CoCrMo femoral head, XLPE acetabular liner, and Ti trunnion in test and control station setup, and c) the control station.

In the hip joint simulator, all prostheses were mounted anatomically. The cup abduction angle and anteversion angles were 45° and 15° respectively¹⁸⁹. Each acetabular liner was held in an aluminium 3105 alloy pelvic insert holder rather than a Ti shell which is used in the clinical situation. However, the pelvic insert holder was designed to reproduce the clinically relevant support system¹⁸⁷. Furthermore, it is common not to use a shell in hip simulators as these are wear-screening devices used for characterising wear from the bearing surfaces of artificial hip joints^{189,205,211,301}. Each Ti trunnion was inserted into the femoral head holder with 45° neck axis angle, and then the CoCrMo femoral head was mounted on the trunnion with a polymeric femoral head impactor. Fixation of the femoral head onto the trunnion was carried out by impacting a minimum of two firm blows in an axial direction⁸⁷ in dry conditions, replicating surgical scenarios. All impactions were carried out using a previously published methodology²⁹⁵. The estimated impaction force was 4-5kN, based on separate measurements undertaken on CeramTec equipment. All test and the control trunnions were loaded anatomically such that loading of the femoral head was offset relative to the trunnion, see Figure 59 a), b) and c). The lubricant was new-born-calf serum (Gibco™ life-technologies) diluted with de-ionized water to give 21 g/L protein content. The lubricant was replaced after every 0.5 Mc, all specimens were cleaned, and gravimetric measurements were performed in accordance with ISO 14242-2¹⁷³. Table 24 summarises all of the experimental variables that have been tested in MoXLPE hip simulator test.

Table 24 Summary of all the experimental variables for MoXLPE hip simulator test

<i>Motion</i>	Standard physiological walking cycles
<i>Loading</i>	Double-peak load (min 400 N and max 2000 N at 1 Hz)
<i>Components</i>	Five 32 mm CoCrMo femoral heads Five 32 mm XLPE acetabular liners Five 12/14 Ti6Al4V trunnions Sixth MoXLPE sample as load soak control
<i>Test duration</i>	5 million cycles (Mc)
<i>Lubricant</i>	Diluted new-born-calf serum (protein concentration 21g/L)
<i>Wear measurement</i>	As per the ISO 14242-2 ¹⁷³

3.4.3 Quantification of the material loss from the taper-trunnion junction and bearing surfaces

The gravimetric wear of heads, liners and trunnions were measured using an analytical balance (TB-215D; Denver Instruments, Germany) with a 0.1mg sensitivity. Each specimen was weighed for a minimum of three times for repeatability. The weight loss in mg was subsequently converted into volume loss in mm³ using the density of CoCrMo as 0.00833 g/mm³³⁰², XLPE as 0.0009355 g/mm³ (supplier's data) and Ti6Al4V as 0.00443 g/mm³²⁹⁸. The amount of lubricant absorption was accounted for by using the dynamically loaded control XLPE liner. The wear rates in mm³/Mc were calculated from the slopes of the linear regression lines in the volumetric loss versus a number of cycles plot for heads, liners and trunnions, as described previously in the CoC hip simulator wear test, see Figure 54.

Additionally, after 5 million cycles, the material loss from the CoCrMo femoral tapers was measured geometrically using a CMM as described in section 3.9. Again, the volumetric wear rates of the CoCrMo femoral tapers were calculated by dividing the average volume loss obtained from the geometric measurement by the total number of cycles.

3.4.4 Visual and microscopic analysis of CoCrMo femoral tapers

The material loss arises mainly from the CoCrMo alloy femoral tapers rather than the Ti alloy trunnion, when CoCrMo/Ti alloy combinations are used for the taper-trunnion junction^{18-20,32}. Therefore, visual and microscopic analysis was performed on the CoCrMo femoral tapers. At the end of the wear test, the femoral heads were cut in half using a cut-off wheel (Rapier abrasive cut-off wheel Type FEM; MetPrep, UK). Microscopic images of these tapers were obtained using a Vision Measuring System Quickscope QS-L (Mitutoyo, UK). The area where the femoral taper made contact with the base of the trunnion was considered as the worn area. Distal to this worn area (in anatomical terms), the non-contacting area of the femoral taper was considered as the unworn area. In addition, high-resolution images of these areas on the CoCrMo femoral tapers were obtained using the same TM3030 SEM (Hitachi, Japan). Scanning electron microscopic analysis of the CoCrMo femoral tapers was conducted using a similar methodology, as explained in section 3.1.4.

Additionally, the distal end of the femoral taper from the cut femoral heads was subject to energy-dispersive X-ray spectroscopy (EDX) for quantification and identification of elemental composition. Energy-dispersive X-ray spectroscopy measurements were performed using the same SEM at an accelerating voltage of 15 kV. To investigate and compare elemental composition of the femoral head alloy with the damaged area, if any, the surface of a cut test CoCrMo femoral head was polished and an EDX measurement was taken on the polished surface, see Figure 60.

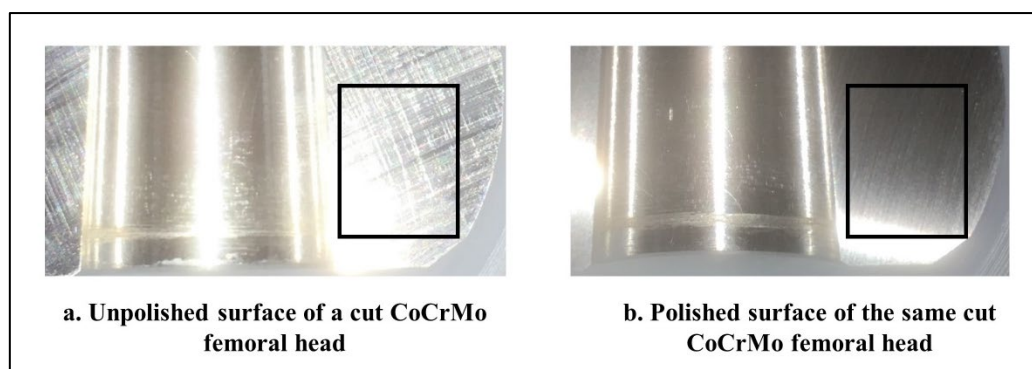


Figure 60 A cut CoCrMo femoral head showing a) before polishing and b) after polishing the surface.

3.4.5 Surface roughness measurement

A 2D contacting profilometer was used for the surface roughness (Ra) analysis of the CoCrMo femoral tapers, pre and post-test, as described in section 3.10.1²⁹⁹. For consistency with the bearing surface parameter, mainly Ra were used to represent pre and post-test taper-trunnion junction surfaces. Moreover, Rq and Rz results for the taper-trunnion surfaces are also presented in this thesis.

Furthermore, in order to get a better understanding of the CoCrMo femoral taper topography, the non-contacting profilometer, Zygo NewView 5000 was used in these regions to obtain 3D surface roughness (Sa). On the CoCrMo femoral taper surface of each half of the cut femoral head, a total of 20 Sa measurements (10 on the unworn area and 10 on worn area) were acquired at the end of the test.

Pre-and post-wear test 3D surface roughness (Sa) measurements for femoral heads and acetabular liners were performed using a non-contacting Zygo NewView 5000 as described in 3.10.2

3.4.6 Microscopic inspection of the backside of the XLPE liner

The backside surface of the XLPE liners was inspected using the Quickscope (QS-L Mitutoyo, UK).

3.5 Metal debris analysis

This section describes the methodology used for the metal debris analysis after CoC and MoXLPE hip simulator tests.

Metal debris analysis after the CoC hip simulator test was performed in collaboration with the University of Surrey. The lubricant samples were digested using enzymes, then centrifuged. The pellet was then deposited onto a substrate and left to dry prior to SEM coupled with EDX analysis.

Inductively Coupled Plasma Mass Spectrometry (ICPMS) is an extremely sensitive category of mass spectrometry³⁰³. ICPMS can detect metals concentration lower than one part in 10^{12} ^{303,304}. The specimen to be examined is positioned in a chamber of the ICPMS and pumped into the nebuliser containing argon gas to form an aerosol. Only very fine aerosol droplets then pass through oxygen plasma at high temperature (8000-1000 °C) where most elements are dissociated, atomised and ionised. The plasma ions are accelerated in the direction of electrostatic discs by a differential vacuum system that extracts the positively charged ions. The positively charged ions are transported to the mass filter which selects the ions according to their charge and mass³⁰³. Metal debris analysis after the MoXLPE hip simulator test was performed in collaboration with the London Metallomics Facility, Kings College London, UK. Initially, the sample preparation was carried out, followed by ICPMS analysis for quantification of metal ions in the lubricant. Lubricant sample digestion was carried out by adding concentrated HNO₃ (400 µL, 67-69%) to a 100 µL of the lubricant samples and digesting at 60°C overnight. After cooling, the samples were diluted to 14 mL with MilliQ water (18Ω). Samples were analysed using an ICP-MS (PerkinElmer NexION 350D, Massachusetts, USA). The ICP-MS settings were: gas flow 1 L/min; auxiliary gas flow 1.2 L/min; plasma flow 18 L/min; RF power 1600 Watts; collision cell gas flow: He 4.2 mL/min. Calibration was performed by injecting the elemental standards (Co, Cr and Ti), dissolved in a solution of 2% HNO₃, into the ICP-MS and detected as Co⁵⁹, Cr⁵², and Ti⁴⁸ isotopes. Five replicates of each sample were performed.

3.6 Lubricant pH measurement

This section gives pH measurement method for the lubricant used for testing of CoC and MoXLPE hip prostheses.

The pH of the lubricant was measured using a pH tester (HI98103, Hanna Instruments, UK), with a pH range of 0.0 to 14.0 and accuracy ± 0.2 pH. The pH measurement was carried out on unused lubricant and after every 0.5 million cycles, at least three times to ensure repeatability of results for the CoC and MoXLPE hip simulator wear tests. Before measurement, the pH meter was calibrated using a reference pH 7.01 buffer solution (supplied with the pH meter). The electrode of the pH meter was cleaned with deionised water.

3.7 Wettability measurement

This section provides a contact angle measurement method for the determination of the wettability of the femoral heads of the modular hip prostheses.

The wettability of the 36mm BIOLOX[®]*delta* and 32mm CoCrMo femoral was examined using Theta Lite Optical Tensiometer (TL100, Biolin Scientific, Espoo, Finland), see Figure 61. The same lubricant fluid, i.e. diluted new-born-calf serum (Gibco[™], Life Technologies) with a protein concentration 21 g/L, was used for analysing the wettability of the femoral heads. The contact angle measurements were performed pre- and post-hip simulator wear tests. Before measurement and whenever the camera optics had adjusted, the TL 100 was calibrated using a 4 mm calibration ball provided by the supplier.

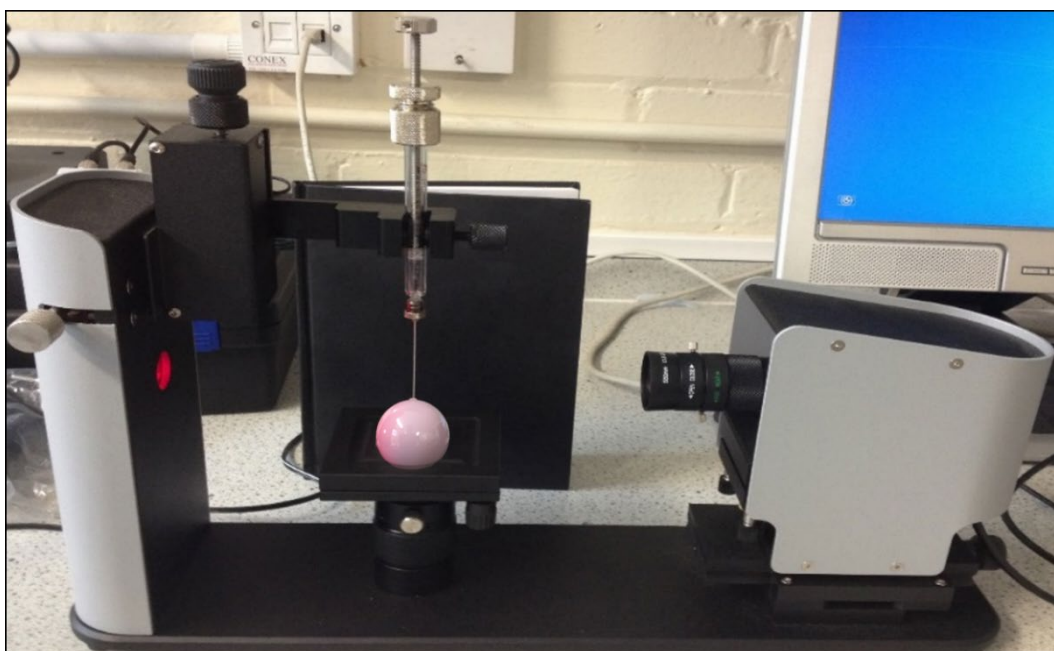


Figure 61 Contact angle measurement of BIOLOX[®]*delta* femoral head using Theta Lite Optical Tensiometer

The TL 100 utilises a USB2 digital camera (160 frames per seconds maximum) to record the contact angle. The TL 100 was operated with the OneAttension[™] software (Version 2.8), see. The sessile drop experiment from the software was used for the contact angle measurement. Before each measurement, the femoral head was cleaned with isopropanol, and lint-free cloth followed by a jet of inert gas. The one-touch dispenser was used to place the droplet (approximately 10 μ l) of the lubricant on the femoral head. The image recording was started manually at the instant the droplet touched the femoral head for 20 seconds.

Then the OneAttension software calculated the mean contact angle, see Figure 62. For each femoral head, three measurements were taken followed by the previously mentioned cleaning procedure. Additionally, as the femoral head surfaces were curved ‘Use circular baseline’ option was enabled in the software for the baseline correction, and all results were analysed using the circular baseline option.

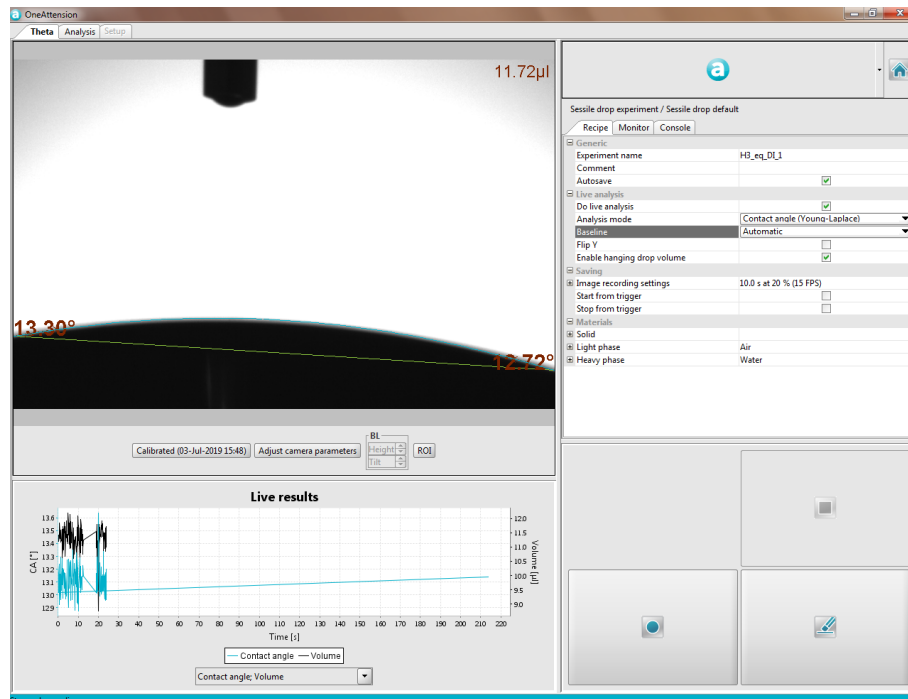


Figure 62 Screenshot of the OneAttension™ software window.

3.8 The six-station anatomical hip simulator

This section briefly illustrates the working mechanism of the hip simulator, including hip prostheses mounting, applied loading and motions along with the procedure used for assembly-disassembly of the components.

The TE-86 (PLINT, Phoenix Tribology Limited, UK) hip simulator was used for *in vitro* wear testing of the modular hip prostheses. The TE 86 design is based on Helsinki University of Technology (HUT)-4 simulator designed by Saikko¹⁸⁹. The hip simulator contains an electromechanical drive system and servo pneumatic loading system. Figure 50 and Figure 58 shows the TE-86 hip joint simulator.

3.8.1 Installation of the hip prostheses on the hip simulator

In the hip joint simulator, all prostheses were mounted anatomically. The femoral head is mounted on the femoral head holder. Different assembly components used for carrying hip prosthesis are shown in Figure 63.

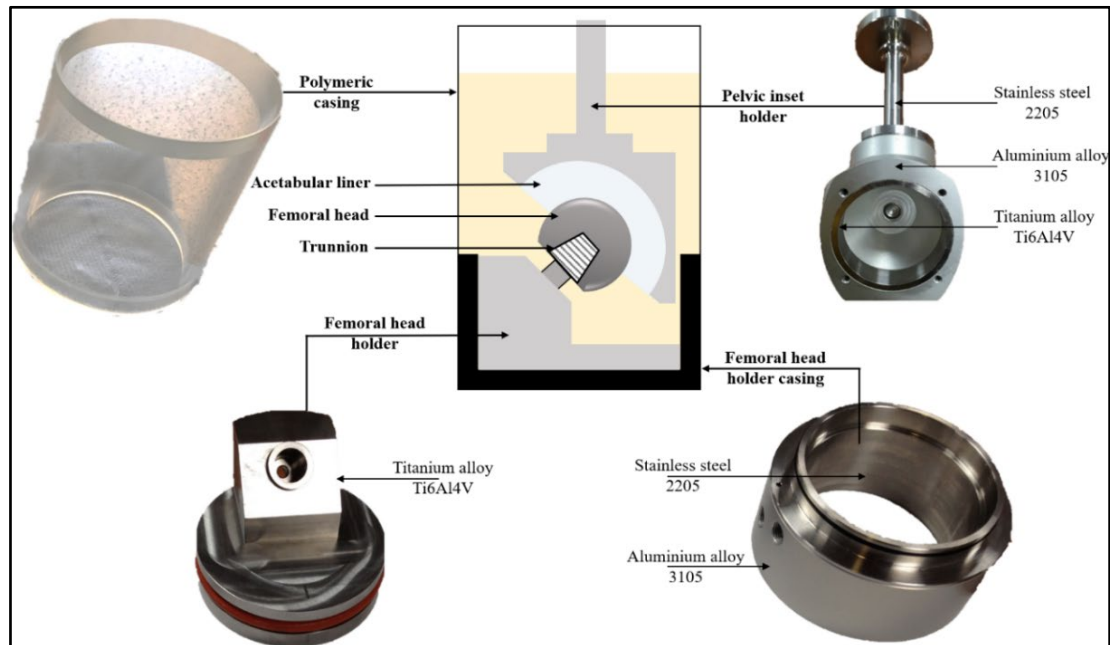


Figure 63 Various components used for carrying a hip prosthesis.

The femoral head holder was press-fitted into a femoral head holder casing. The head holder is fixed on the positioning disc with the help of a single screw so that it remains in the same position, see Figure 64 a) and b). Saikko tested the positioning by assembling and disassembling the femoral head holder multiple times and reported that the centre of the femoral head remained at the intersection of the FE and AA axes with an accuracy of 0.01 mm¹⁸⁹. Additionally, the femoral head holder casing and the baseplate were marked [see Figure 64 c)] so that they could be relocated at the same location after multiple assembly and disassembly procedures.

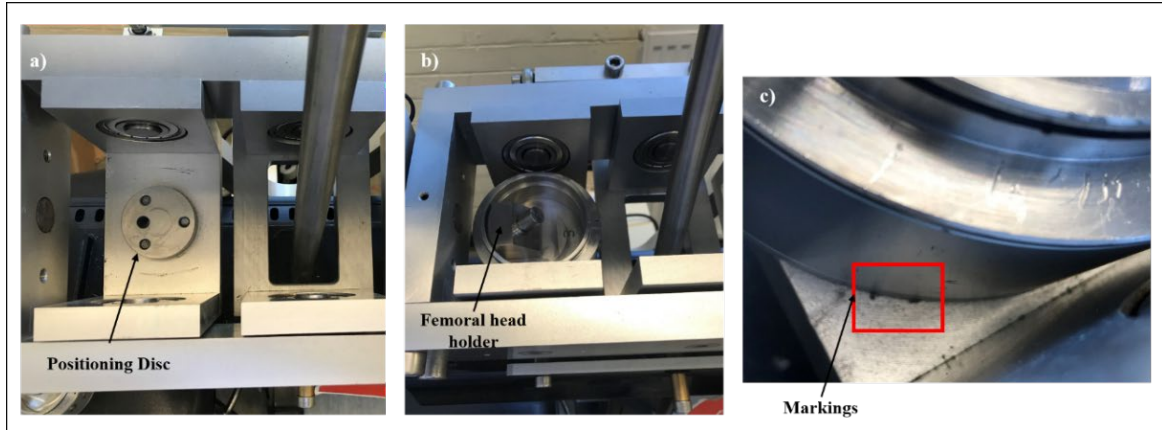


Figure 64 a) A positioning disc, b) a femoral head holder fixed on the positioning discs, and c) markings on the femoral head carrier casing and the base plate for the exact location after disassembly.

Each femoral head was mounted using a plastic femoral head impactor, replicating that used in surgery, onto a 12/14 Ti6Al4V trunnion. Fixation of the femoral head onto the trunnion was carried out by impacting a minimum of two firm blows in an axial direction⁸⁷ in dry conditions, replicating surgical scenarios. The estimated impaction force was 4-5kN, based on separate measurements undertaken on CeramTec equipment. In turn, each trunnion was located into a femoral head holder with a neck inclination angle of 45°, see Figure 65 a). All trunnions and femoral head carriers were marked before the test to enable correct repositioning following cleaning/measurement intervals, see Figure 65 b).

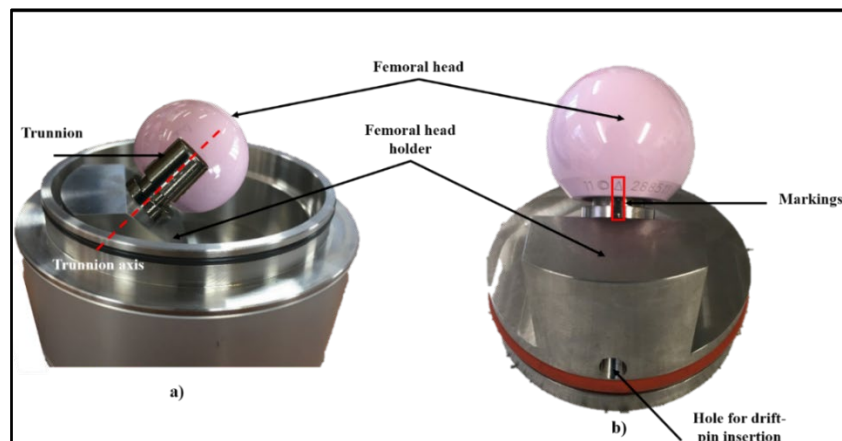


Figure 65 a) Femoral head and trunnion assembly on the femoral head carrier of the hip simulator and b) Markings were made on the trunnion and the femoral head holder for exact repositioning after cleaning/measurement intervals.

Each acetabular liner was stationery and press-fitted into the pelvic insert holder. Additionally, all acetabular liners were secured inside the pelvic insert holders by polymeric

rings and screws. According to the ISO 14242-1, the cup abduction angle should be 30° ¹⁸⁷, which is less than the typical clinical value of 45° ¹⁸⁹. Furthermore, the majority of the hip prostheses manufacturers suggested that the acetabular liner should be placed at 45° ³⁰⁵. Therefore, the acetabular liner abduction and anteversion angles were 45° and 15° respectively¹⁸⁹. A universal joint and a loading bar of the hip simulator provided dynamic and vertical loading via a pneumatic cylinder (bore diameter 80mm) which made the acetabular liner self-centring on the femoral head in such a way that any misalignment of the femoral head ($>0.01\text{mm}$) would not have affected the hip simulator wear test results¹⁸⁹.

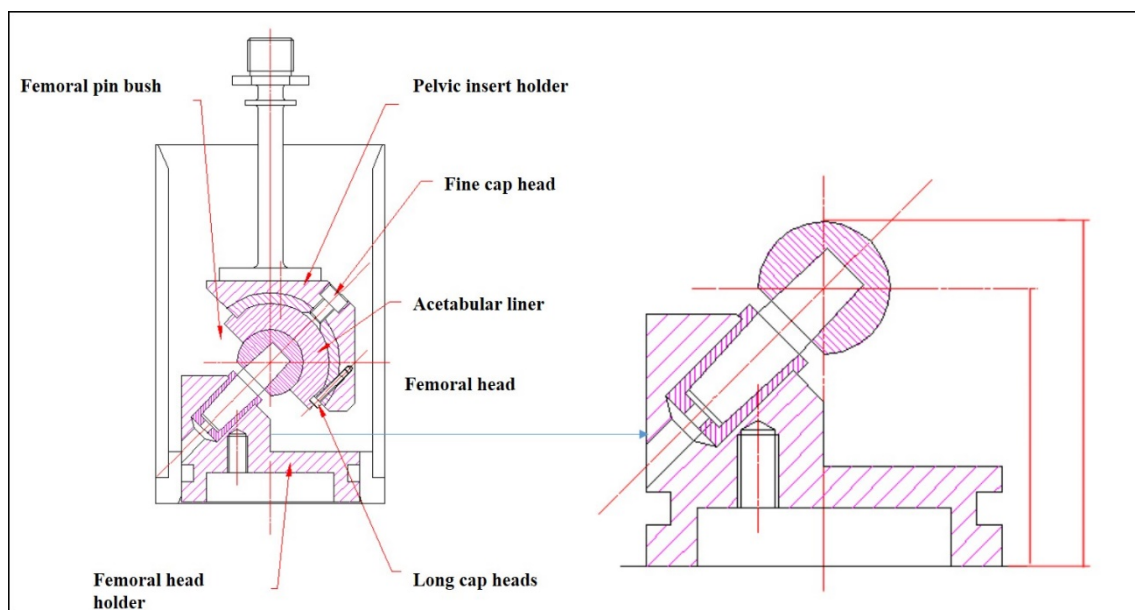


Figure 66 Schematic diagram showing the self-centring alignment of the components.

3.8.2 Description of the hip simulator loading and motions

The TE-86 is a 6-station anatomical hip joint simulator and simulates two-axis motion which consists of flexion-extension (FE) and abduction-adduction (AA) but no internal-external rotation (IER). According to the international standard ISO14242-1, the hip simulator must simulate AA, FE and IER motions. However, in the TE-86 design, IER is not included. The FE and AA motions are made by the outer cradle and the inner cradle respectively. The FE and AA movement angles are in accordance with biomechanical studies of walking, 46° and 12° respectively^{189,306,307}. These electromechanical motions are applied with a specially developed crank mechanism driven by a variable speed gear motor. The phase difference of

$\pi/2$ is present between the applied motions, see Figure 67, to produce an elliptical force track to represent the human gait cycle^{189,308}.

The cycle frequency was set at 1 Hz, and one million cycles of the hip simulator were taken to be equivalent to 1 year in the body³⁰⁹. The double-peak load was applied in accordance with the biomechanical studies of walking, with a maximum load of 2.0 kN and a minimum load of 0.4 kN¹⁸⁹. It has been previously shown that the ISO 14242-1 recommended peak load of 3.0 kN resulted in a protuberance on the bearing surface of polymeric acetabular liners³¹⁰. Furthermore, the protuberance formation were not seen in the retrieved polymeric liners. However, they were common in the wear testing as per the international standard¹⁹⁰. Therefore, for clinically relevant testing, the peak load was reduced from 3.0 kN to 2.0 kN to eliminate the protuberance formation¹⁸⁹.

As shown in Figure 67, at maximum flexion, the load begins to rise, the temporal distance between the two load peaks is one-third of the cycle time. The force track on the femoral head created by the applied load and articulating motion is elliptical with an aspect ratio of 3.8¹⁸⁹. With applied load and articulating motion, the force track is defined as ‘the theoretical track of the resultant force vector on the femoral head¹⁸⁹.

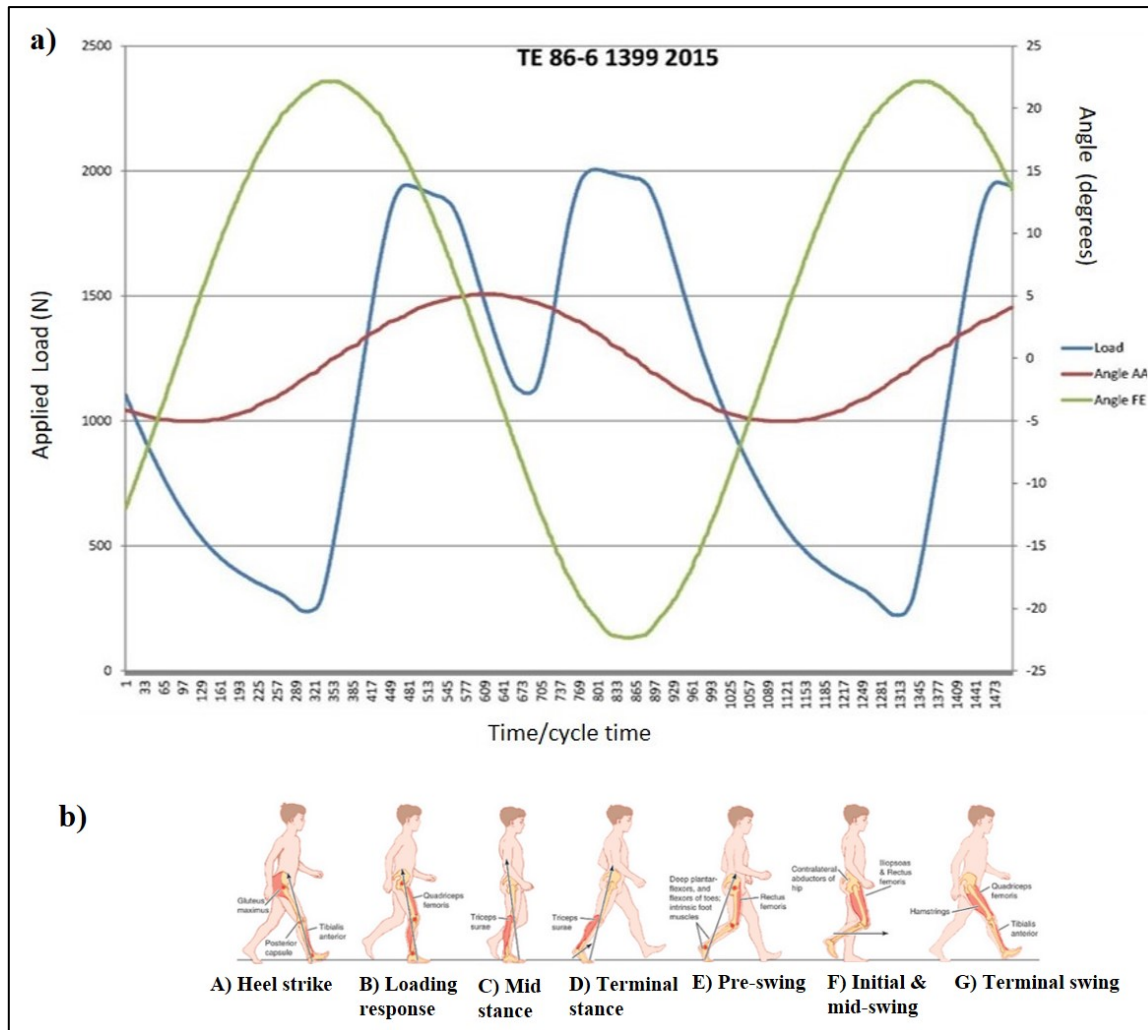


Figure 67 a) Variation with time of flexion-extension (FE) and abduction-adduction (AA) angles, and load (L) measured in the TE-86 hip joint simulator and b) Normal gait cycle [Image adapted from Rajčúřková et al. (2014)¹⁸⁴]

Each station of the hip simulator is loaded with a pneumatic cylinder. A universal joint and a loading bar provided dynamic and vertical loading via a pneumatic cylinder (bore diameter 80mm) which made the acetabular liner self-centring on the femoral head in such a way that any misalignment of the femoral head ($>0.01\text{mm}$) would not have affected the hip simulator wear test results¹⁸⁹. The slider of a vertical linear guide, which is driven downwards by the cylinder, was attached to the universal joint, which resulted in a vertical load applied fixed relative to the pelvic insert holder, see Figure 68. The pneumatic cylinders are connected to a common manifold. The output pressure from the proportional pressure regulator (SMC ITV3050-31F4BL3 Electro-Pneumatic Regulator) is amplified pneumatically, and equal pressure is provided to the pneumatic cylinder in each of the six stations.

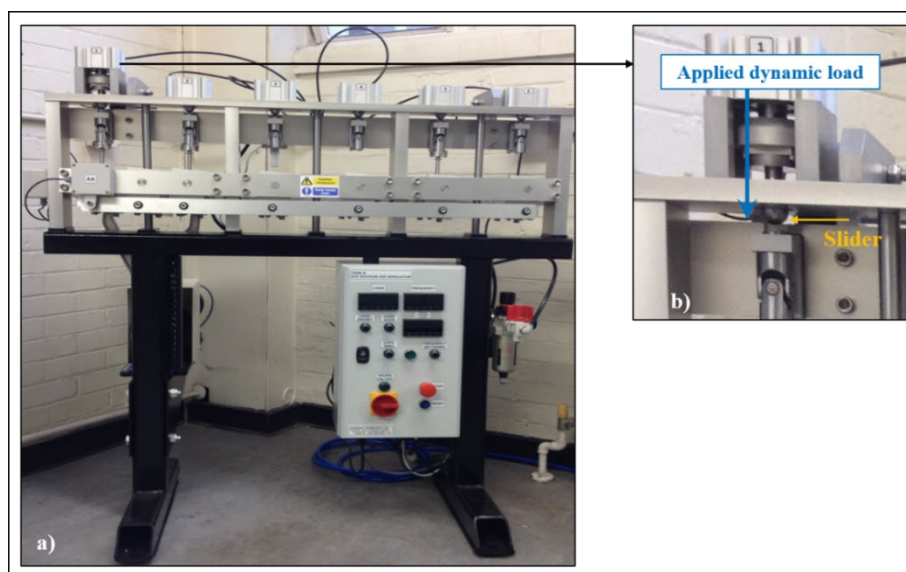


Figure 68 a) TE-86 hip simulator and b) Zoomed-in image of the station no. 1 showing the slider of a vertical linear guide.

Additionally, a separate control station containing the same hip prosthesis mounting and loading profile as described in 3.8.2 was used, however, no articulating motion was applied for the DL test of the CoC prosthesis and as a soak control for the MoXLPE hip simulator test.

3.8.3 Assembly and disassembly procedures

The femoral heads and trunnions were assembled on the femoral head carriers, and the polymeric casing was fitted on each carrier. All assembled femoral head carriers were then fixed on the hip simulator. After that, all sample fluid tubes were filled with a minimum of 250 mL of lubricant. The lubricant used throughout this project was new-born-calf serum (Gibco™, Life Technologies), diluted with de-ionised water to give a protein concentration of 21g/L.

According to the ISO 14242-1, for the prevention of lubricant evaporation, the lubricant should be encapsulated. However, lubricant removes heat generated from the friction of the articulation of the bearings and lowers the risk of overheating of the lubricant and the components as well as clears the debris¹⁸⁹. Therefore, lubricant chambers are left open in the TE-86 hip simulator. Additionally, as per ISO 14242-1, the temperature of the lubricant should be maintained at $37^{\circ} \pm 2^{\circ} \text{C}$ and addition of an antimicrobial reagent. However,

Saikko performed wear testing at the lower temperature (20°C) than the ISO standard temperature of 37°C and reported clinically relevant wear results³¹¹. Furthermore, at the lower temperature, the microbial growth was reduced so that the addition of toxic antimicrobial reagent was avoided^{189,311}. Moreover, problems associated with the formation of the anti-wear protein precipitate layer (not seen *in vivo*) were avoided as at the lower temperature, the rate of protein degradation process was reduced³¹². Therefore, all testing was carried out at an ambient temperature and without any additives.

Finally, the pelvic insert holder fitted with the acetabular liners were immersed on the respective femoral head and the hip simulator wear testing was initiated. All test and a control station lubricant chambers were topped up with deionised water to compensate for any evaporation. The hip simulator wear test was stopped at every 500,000 cycles. The lubricant was changed every 500,000 cycles when the components were cleaned and weighed following the relevant international standard, ISO 14242-2¹⁷³. The used lubricant was stored in the freezer for future analysis. A protocol for the cleaning and weighing procedures used throughout this project is presented in Appendix A.

3.9 Quantification of the material loss from the taper-trunnion junction of hip prostheses using geometric wear measurement

This section describes the geometrical wear measurement method used for quantification of the material loss from the internal taper of the femoral heads (femoral tapers) and trunnions.

3.9.1 Materials

Geometric wear measurements are mostly used to determine volumetric wear of the explanted hip prostheses^{19,313}. However, it can also be used to determine volumetric wear of the hip components subject to *in vitro* hip simulator testing³¹⁴. The geometric wear measurement methods for the femoral taper, trunnions and bearing surface have previously been validated and published by our group^{19,313,315}. A coordinate measuring machine (CMM, Legex 322, Mitutoyo, UK) in combination with a custom-designed MATLAB program (MathWorks) were used for geometric wear analysis of the taper-trunnion junction. A 0.5mm ruby probe was used throughout the project. The resolution of the CMM is 0.8µm

and its accuracy for taper-trunnion surfaces is reported as 0.2mm^3 ¹⁹. Besides the quantification of the material loss in mm^3 , the geometric wear analysis also produces a visual representation of the surface by generating a wear map.

The geometric measurements performed throughout this project are shown in Table 19. Figure 63 a), b) and c) shows the post-test CMM measurement set-up for a BIOLOX[®] *delta* femoral taper used in the CoC hip simulator wear test, CoCrMo femoral taper used in the MoXLPE hip simulator wear test and Ti trunnion used in the CoC hip simulator wear test respectively. A protocol for the geometric wear measurement used throughout this project is presented in Appendix B.

Tests→ Hip prosthesis component↓	CoC Hip simulator wear test (section 3.2)	DL test of the CoC hip prosthesis (section 3.3)	Impaction test of the CoC hip prosthesis (section 3.4)	MoXLPE Hip simulator wear test (section 3.5)
Femoral taper	Post-test	Post-test	No	Post-test
Trunnion	Post-test	Post-test	No	No

Table 25 Geometric wear measurements on the various components.

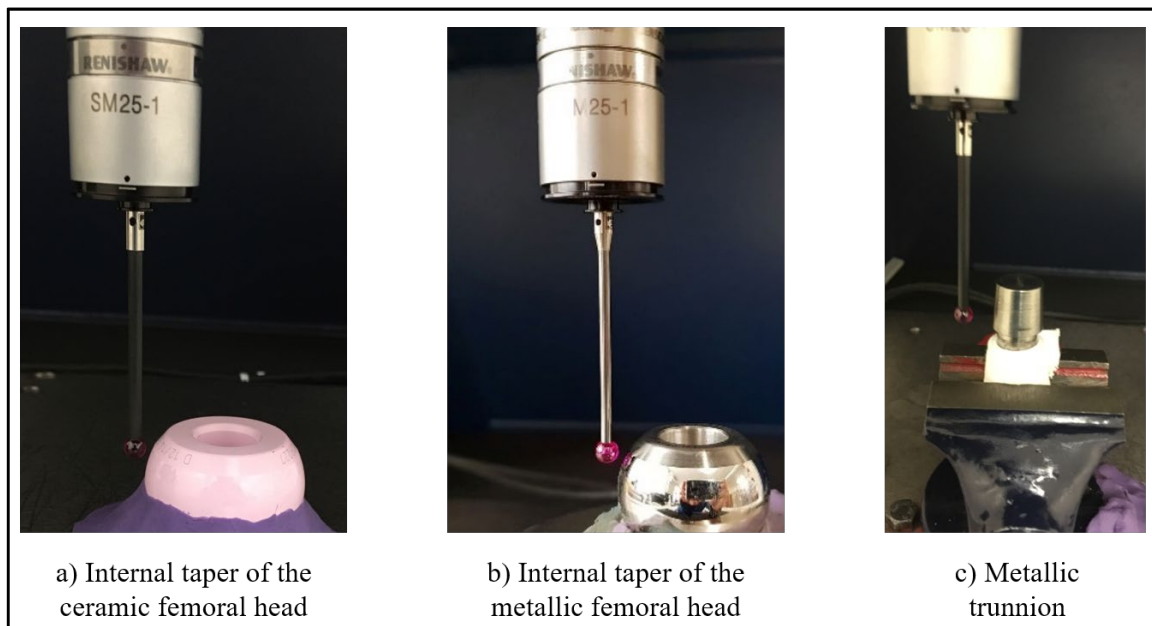


Figure 69 CMM measurement set up of a) ceramic femoral taper, b) metallic femoral taper and b) metallic trunnion.

3.9.2 *Methods*

The CMM uses MCOSMOS, (Mitutoyo) software for scanning of the femoral tapers and trunnions, with the help of customised “2016 taper scan” and “trunnions” program respectively. Both programs work in the following three stages:

Stage 1: Identification of the first coordinate system.

Stage 2: Generation of a perfect theoretical cone representing the original perfect unworn surface (either femoral taper or trunnion)

Stage 3: Measurement of the entire surface and comparison the data points with the perfect cone to determine any deviations, which represent volumetric wear.

a. Femoral taper scan

- Secure the femoral head using the plasticine on the CMM platform, as shown in Figure 70. Use the spirit-level to determine the horizontal level.

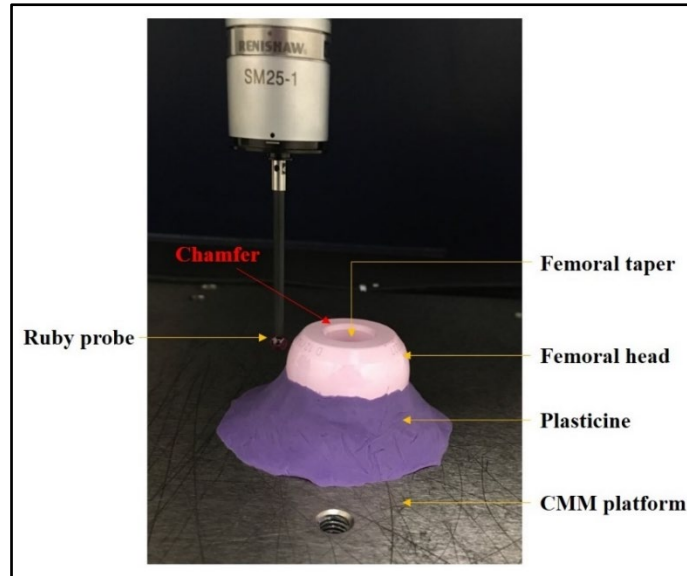


Figure 70 Mounting of the femoral head on the CMM platform

- Before starting the femoral taper scanning using customised “2016 Taper Scan” program, open “Taper Height” program. The “Taper Height” program is used to identify the testing area and to obtain the following values for the “2016 Taper Scan” program:
 - The centre of rotation (COR) to rim value: to determine the start point to begin the scan by avoiding the chamfer on the rim see Figure 71
 - Depth of the taper value (scan depth): to finish the contour, see Figure 71 (The linear traces carried by the ruby probe of the CMM to collect points are known as contours.)

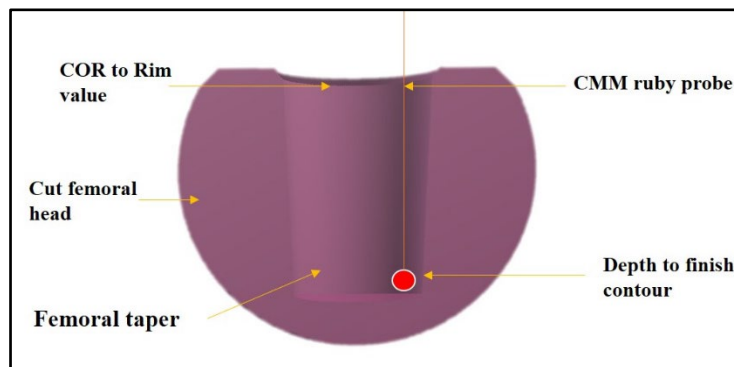


Figure 71 Cross-section of an internal femoral taper showing COR to rim value and Depth to finish contour value.

Steps involved in “Taper Height” MCOSMOS program are shown below.

Step1: Start the “Taper Height” program

Step2: The CMM will give COR Rim value and Depth value.

Step3: “Input COR to Rim value” = COR value is given by “Taper Height” – (Height of the chamfer at the rim + radius of the ruby probe)

Step4: “Input depth to finish contour” = Depth value given by “Taper Height” – (Height of the chamfer at the rim + radius of the ruby probe + 0.5)

- Steps involved in “2016 Taper Scan” MCOSMOS program are given below:

Step1: “Input file name” = FILE_Taper (user-defined name for each scan)

Step2: “Input COR to Rim value” = obtained from “Taper Height”

Step3: “Input highest “z” for the perfect cone = 0

Step4: “Input lowest “z” for the perfect cone = -6

Step5: “Input Scan depth” = obtained from “Taper Height”

Step6: “Input point pitch” = 0.1 [Point pitch: the distance (in mm) between each point in the contour]

After completion of the “2016 Taper Scan” MCOSMOS program, the cone angle will be shown on the screen. Note down the CMM generated cone angle.

- Steps involved in customised “WearVol”, MATLAB program for quantification of the volumetric wear from the femoral tapers.

Step1: open the “WearVol” program

Step2: input filename “FILE_Taper.asc”, select “taper” in the dialogue box and number of contours = 30

Step3: “Please enter the highest point for angle calculation” = 0

Step4: “Please enter the lowest point for angle calculation” = -6

Step5: “Please enter taper angle” = Enter the CMM generated cone angle from “2016 Taper Scan.”

b. Trunnions

Secure the trunnion using the clamp on the CMM platform, as shown in Figure 72. Use the spirit-level to determine the horizontal level.

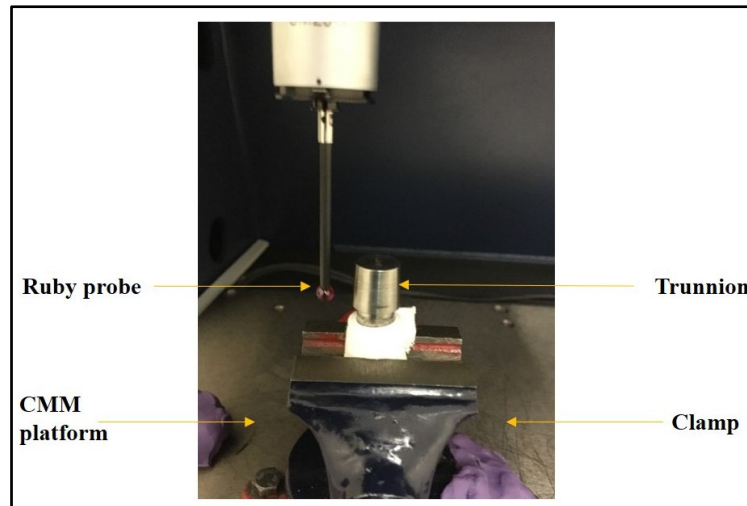


Figure 72 Mounting of the trunnion on the CMM platform

- Steps involved in “Trunnion” MCOSMOS program are given below:

Step1: “Input file name” = FILE_Trunnion” (user-defined name for each scan)

Step2: “Input lowest “z” for the perfect cone = -6

Step3: “Input highest “z” for the perfect cone = -2

Step4: “Input the lowest value for a final scan “= -10

Step5: “Input point pitch” = 0.150

Step6: “Input number of contours” = 30

After completion of “Trunnion” MCOSMOS program, the cone angle will be shown on the screen. Note down the CMM generated cone angle.

- Steps involved in customised “WearVol”, MATLAB program for quantification of the volumetric wear from the trunnions.

Step1: open the “WearVol” program

Step2: input filename “FILE_Trunnion.asc”, select “trunnion” in the dialogue box and number of contours = 30

Step3: “Please enter the highest point for angle calculation” = -2

Step4: “Please enter the lowest point for angle calculation” = -6

Step5: “Please enter cone angle” = Enter the negative value of the CMM generated cone angle from “Trunnion” program.

3.10 Surface roughness analyses

This section gives the procedures used for two-and-three-dimensional (2D and 3D) surface roughness measurements. In the literature, previous hip simulator studies represented the surface roughness of the bearing surfaces with the mean surface roughness (Ra/Sa)^{195,211,212}. Therefore, for comparing the results obtained for the bearing surfaces during this research work with previous hip simulator studies, only Ra/Sa has been utilised in this thesis. No other hip simulator study investigated the author's best knowledge; no other hip simulator studies reported the surface roughness of the taper-trunnion junction surfaces. Therefore, for consistency with the bearing surface parameter, mainly Ra/Sa were used to represent pre and post-test taper-trunnion junction surfaces. Moreover, Rq and Rz results for the taper-trunnion surfaces are also presented in this thesis.

Mean surface roughness (Ra/Sa)

The mean surface roughness is defined as the arithmetic mean deviation of the surface height from the mean line through the profile. To describe 2D surface roughness of a liner profile the symbol Ra is used, see Equation X³¹⁶ and to describe 3D surface roughness of an areal profile the symbol Sa is used, see Equation XI³¹⁷.

$$R_a = \frac{1}{L} \int_0^L |y(x)| dx$$

Equation X

$$S_a = \frac{1}{A} \iint_A |z(x, y)| dx dy$$

Equation XI

3.10.1 Two-dimensional (2D) surface roughness (Ra) measurements

Two-dimensional (2D) surface roughness (Ra) measurements were performed using a contacting profilometer SurfTest (SJ-210, Mitutoyo Hampshire, UK), see Figure 73 a). In all tests, ten linear scans for each femoral taper and trunnion were performed with a cut off length of 0.8mm, giving each scan a total roughness evaluation trace length of 4.0mm³¹⁸.

Although, for the CoC hip simulator test only six linear scan measurements each from the pre and post-test measurements were used for, mean Ra calculation and statistical analysis. This was due to the output excel files from SurfTest software were corrupted and did not open (showed an error message). Additionally, 2D surface roughness (Ra) of the trunnion was not measured in the MoXLPE hip simulator wear test as we were guided by previous retrieval studies, which show that the material loss arises mainly from the CoCrMo alloy femoral tapers rather than the Ti alloy trunnion, when CoCrMo/Ti alloy combinations are used for the taper-trunnion junction.

Additional roughness parameters such as Rq and Rz, pre and post-test were measured on following: a) ceramic femoral tapers and trunnions used in the CoC hip simulator test, and b) metallic femoral taper used in the MoXLPE hip simulator test.

Root Mean Square Surface Roughness (Rq)

The root mean square (r.m.s.) roughness is defined as the root mean square deviation of the profile from the mean line. To describe 2D r.m.s. roughness of a liner profile the symbol Rq is used, see Equation XI ³¹⁶.

$$R_q^2 = \frac{1}{L} \int_0^L |y(x)|^2 dx$$

Equation XII

Peak to valley height (Rz)

The peak to valley height is defined as the sum of the highest peak and deepest valley of the profile. To describe 2D r.m.s. roughness of a liner profile the symbol Rz is used.

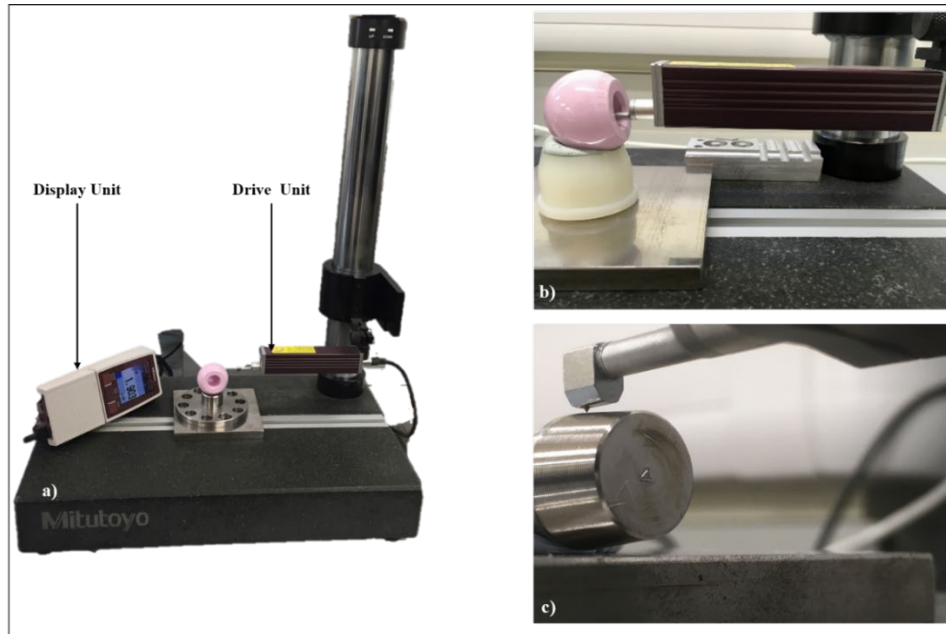


Figure 73 a) Two-dimensional (2D) surface roughness (R_a) measurements using the Surftest SJ-210 profilometer on, b) femoral taper and c) trunnion.

3.10.2 Three-dimensional (3D) surface roughness (S_a) measurements

A non-contacting profilometer has been used throughout this project not only to look at the bearing surfaces of modular hip prostheses from all tests but also to assess the change on the damaged areas of the trunnions from the CoC hip simulator test and CoCrMo femoral tapers from the MoXLPE hip simulator test. Three-dimensional (3D) surface roughness (S_a) measurements were performed using a non-contacting Zygo NewView 5000 white light interferometer³¹⁹ with 0.1 nm vertical resolution. For all measurements, a 10x objective lens and 2.0x manual zoom were used to give an area of view 317 x 238 μm . For S_a measurements of all bearing surfaces, a “remove sphere” form filter was used. For S_a measurements of all taper-trunnion surfaces, a “remove cylinder” form filter was used. All other settings on the MetroPro[®] software were kept unchanged for pre and post-test surface roughness measurements of the components.

In the literature^{13,195,196,200,202,211}, most hip simulator studies reported the surface topographical information of the bearing surfaces of the hip prostheses in terms of mean surface roughness (R_a or S_a). Therefore, pre and post-test hip simulator tests surface roughness measurements were acquired for all bearing surfaces. A total of 10 measurements on each bearing sample were acquired on the pole and at 45°, see Figure 74. For setting up

the components for Zygo measurement, two holders were used. The first holder for getting point on the pole of the femoral heads and acetabular liners [see Figure 74 b) and c)] and the second holder was manufactured to get the points at 45°.

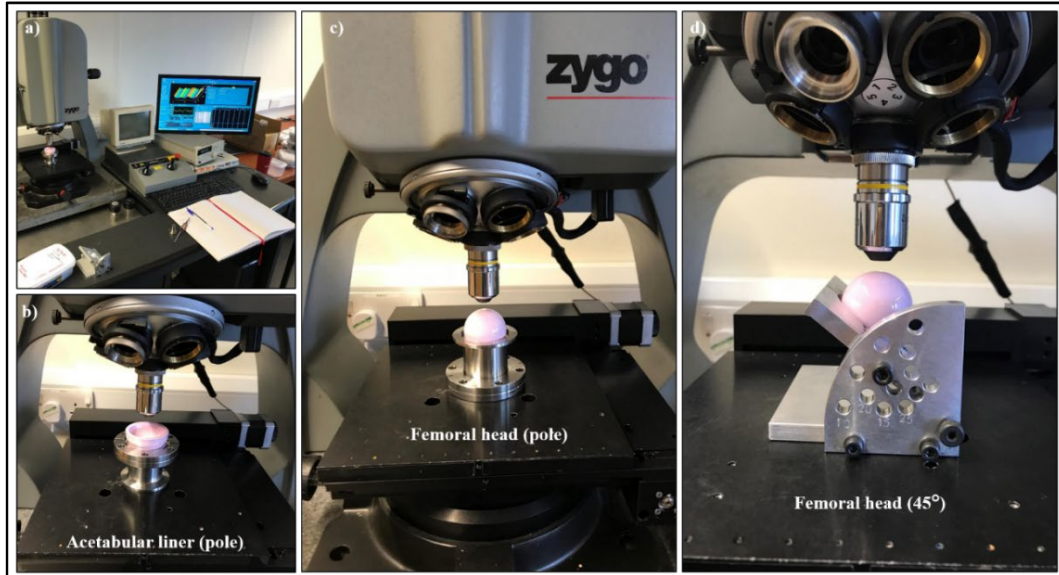


Figure 74 a) Three-dimensional (3D) surface roughness (Sa) measurements using Zygo NewView 5000 on b) an acetabular liner at the pole, c) a femoral head at the pole and d) femoral head at 45° tilt.

3.11 Statistical methods

Statistical analyses were performed using Minitab® 17.1.0 statistical software. Pre-and post-test surface roughness measurements for femoral heads and acetabular liners were analysed using a paired t-test with a significance level of 0.05 in all tests after confirming the normality of the data. The volumetric wear rates of CoC joints and Ti trunnions were analysed using a 2-Sample t-test with a significance level of 0.05 in the CoC hip wear test. In the MoXLPE hip simulator wear test, for statistical comparisons of the following: gravimetrically measured mean wear rates of the femoral heads and trunnions; gravimetrically measured mean wear rates of the femoral heads and the wear rates of the femoral tapers obtained using the CMM; and the surface roughness measurements of the femoral tapers on unworn and worn areas; all were compared using a 2-Sample t-test with a significance level of 0.05. Additionally, box plots were plotted of volumetric measurement using multiple comparison one-way ANOVA (analysis of variance) test with the Bonferroni post-hoc test with 95% confidence interval using GraphPad Prism 8 software for components used in CoC and MoXLPE hip simulator test.

Chapter 4: Results

This chapter presents the experimental results obtained during the *in vitro* studies.

4.1 Hip simulator wear testing of the taper-trunnion junction and bearing surfaces of modular CoC hip prostheses

This section gives the results from the hip simulator study testing 36mm CoC THRs mounted on Ti alloy trunnions. To the authors' best knowledge, no *in vitro* tests have quantified material loss from the taper-trunnion junction of a modular CoC THRs. Therefore, in this section, quantification of material loss obtained gravimetrically and geometrically from the taper-trunnion junction of CoC THRs will first be offered. Then the 2D surface roughness (Ra) measurements on the surface of the tapers and the trunnions used in the CoC hip wear test are presented. Next, 3D surface roughness measurements (Sa) on the unworn and worn areas of the wear test trunnions are presented. Visual and microscopic images taken on the taper-trunnion junction post-test are also displayed. Additionally, wear of the ceramic components obtained gravimetrically will be offered as it is the most common way that results have been presented in the scientific literature. Following the wear data, results of Sa measurements on the bearing surfaces of CoC components are given.

4.1.1 Quantification of the material loss from the taper-trunnion junction

4.1.1.1 Gravimetric analysis of Ti trunnions

After 5 million cycles, the volumetric wear rate (mean \pm standard deviation) for the Ti trunnions was $0.061 \pm 0.015 \text{ mm}^3/\text{Mc}$, with a range of 0.045–0.075 mm^3/Mc . The mean volumetric wear rates for all Ti trunnions from the hip simulator wear test, measured gravimetrically, are shown in Figure 75. The total average volumetric wear over 5 million cycles was 0.29 mm^3 for the Ti trunnions. Additionally, there was no statistically significant difference in the volume loss of Ti Trunnion 1 and Ti trunnion 2 (with adjusted p value > 0.0599), Ti Trunnion 2 and Ti trunnion 3 (with adjusted p value > 0.1888), see Figure 76.

However, there was statistically significant difference in the volume loss of Ti Trunnion 1 and Ti trunnion 3 (with adjusted p value < 0.001) as shown in Figure 76.

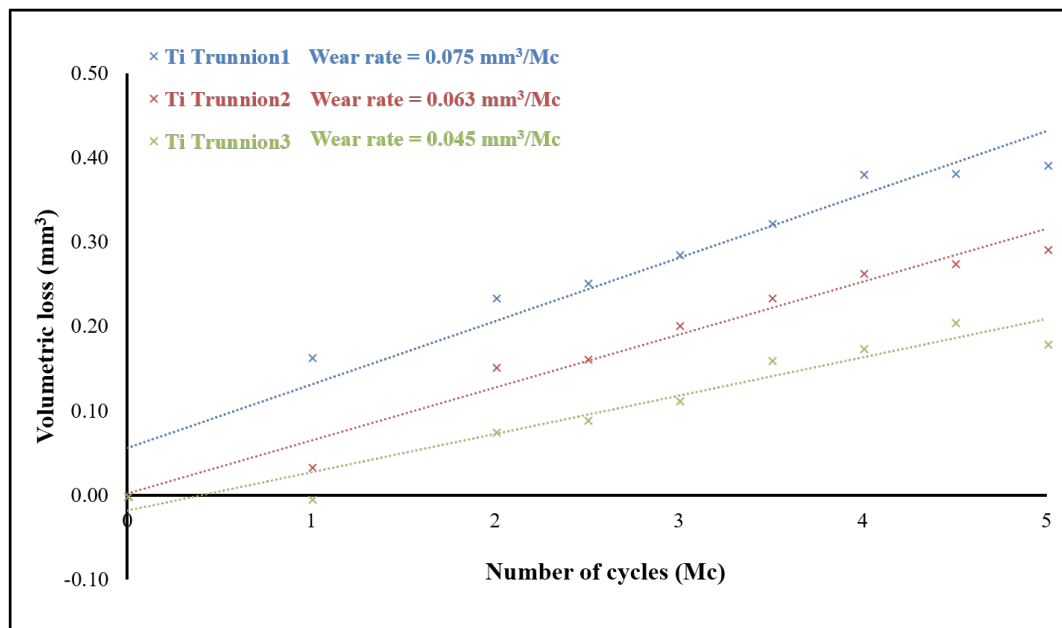


Figure 75 Mean volumetric measurements of all titanium (Ti) trunnions from CoC hip simulator wear test (measured gravimetrically).

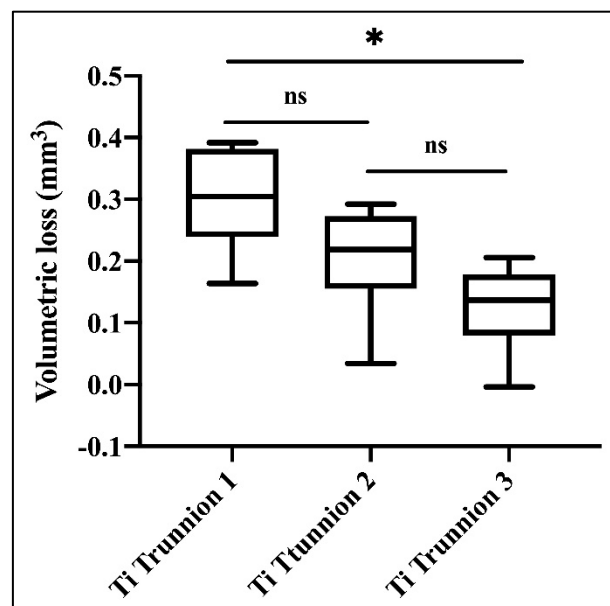


Figure 76 Box-plot of volumetric measurement of all titanium (Ti) trunnions from CoC hip simulator wear test (measured gravimetrically). ns: no significant difference with adjusted p-value > 0.999 and *: adjusted p-value < 0.001.

4.1.1.2 Geometric analysis of the ceramic femoral tapers

After 5 million cycles, the volumetric wear rate (mean \pm standard deviation) of the ceramic femoral tapers was $0.024 \pm 0.040 \text{ mm}^3/\text{Mc}$. The total volumetric wear over 5 million cycles was 0.12 mm^3 for the ceramic femoral tapers. The CMM generated wear maps showed a minimal material loss from the ceramic femoral tapers, see Figure 77. As can be seen from Figure 77, minimum wear was observed (greenish-yellow colour) on the femoral taper supporting the volumetric wear measurement. The CMM measurement on the ceramic femoral taper was taken on the trunnion engagement length. The proximal end of the trunnion engages at the bottom part of this wear map, whereas the distal end of the trunnion engages at the top part of this wear map.

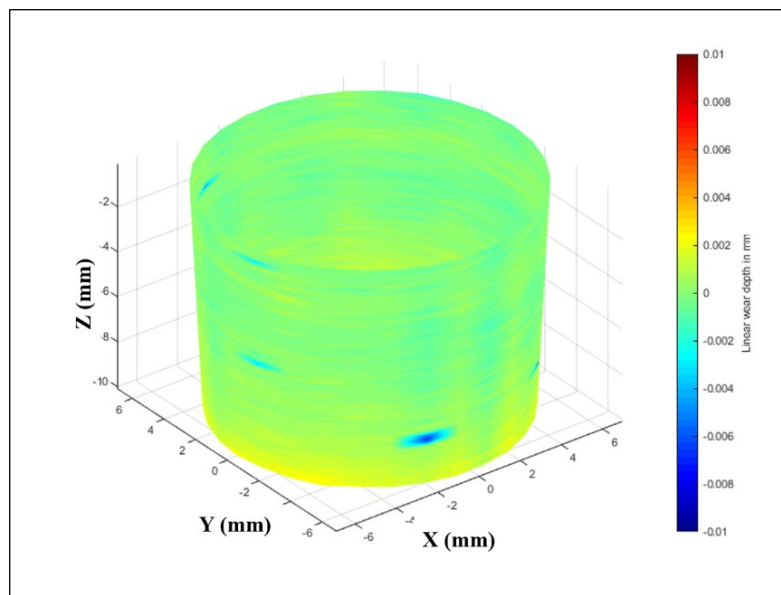


Figure 77 A CMM wear map of the internal taper of a test ceramic head.

After 5 million cycles, the volumetric wear rate (mean \pm standard deviation) obtained geometrically of Ti trunnions was $0.050 \pm 0.012 \text{ mm}^3/\text{Mc}$. The total volumetric wear over 5 million cycles was 0.25 mm^3 for the Ti trunnions. Furthermore, the mean volumetric wear rate of the Ti trunnions obtained geometrically ($0.050 \pm 0.012 \text{ mm}^3/\text{Mc}$) was not statistically different ($p = 0.398$) to the mean volumetric wear rate obtained gravimetrically ($0.061 \pm 0.015 \text{ mm}^3/\text{Mc}$).

4.1.2 Visual and microscopic inspection of the taper-trunnion junction

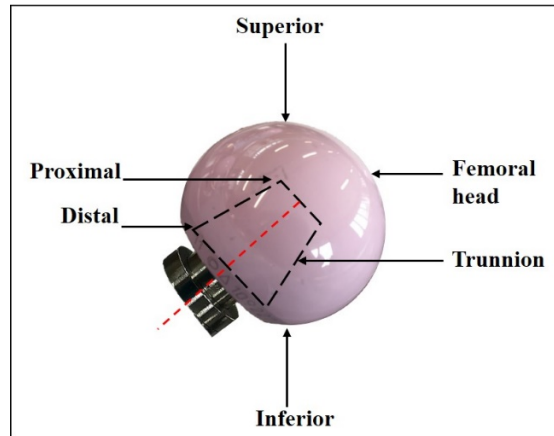


Figure 78 A femoral head and trunnion assembly showing terminologies used to describe the location of the material loss.

The femoral head and trunnion assembly are shown in Figure 78. On the trunnions, material loss (as indicated by a reduction in mass and decrease in roughness) was seen visually at the proximal-superior end and the distal-inferior end, as shown in Figure 79.

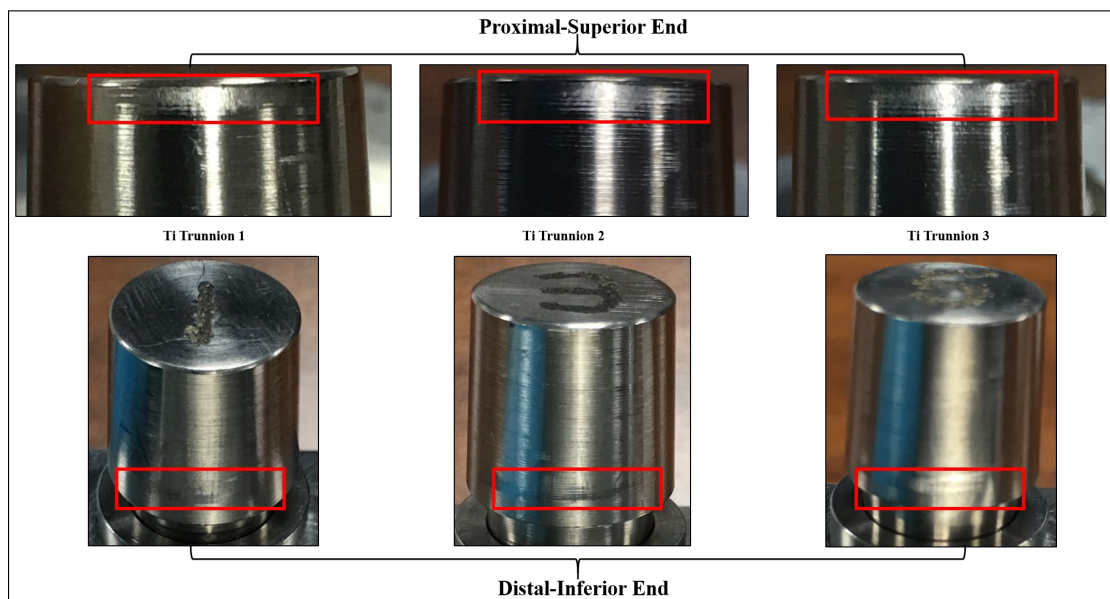


Figure 79 Hip simulator wear test trunnions showing wear from the proximal-superior end and distal-inferior end respectively.

Optical micrographs taken with $0.65\times$ magnification at the proximal-superior end and the distal-inferior end are shown in Figure 80 d) and e), respectively. Unworn and worn areas are clearly visible, with the original circumferential machining marks evident in the unworn areas.

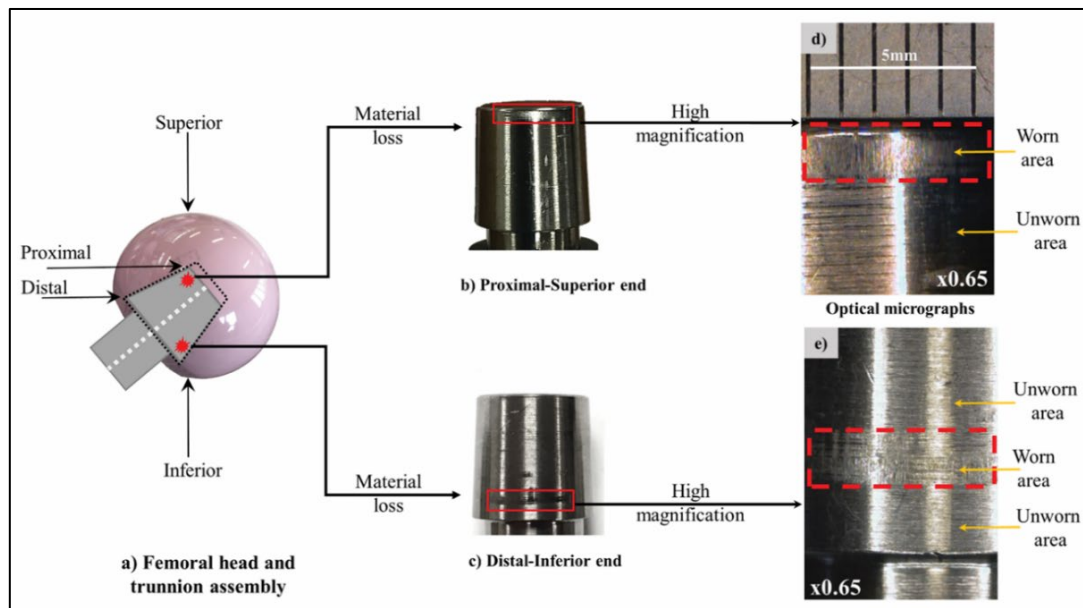


Figure 80 a) A femoral head and trunnion assembly showing the different anatomical planes, b) and c) a test trunnion showing wear from the proximal-superior end and distal-inferior end respectively, d) and e) optical microscopic images of a test trunnion captured at 0.65 \times magnification showing worn and unworn areas of the proximal-superior end and distal-inferior ends, respectively.

The proximal-superior end of a test trunnion can be seen at 2.5 \times magnification using an optical microscope in Figure 81 a), and at 500 \times magnification with an SEM in Figure 81 b). Again, two distinct areas are shown in the SEM image; a worn area and an unworn area with the original machining marks.

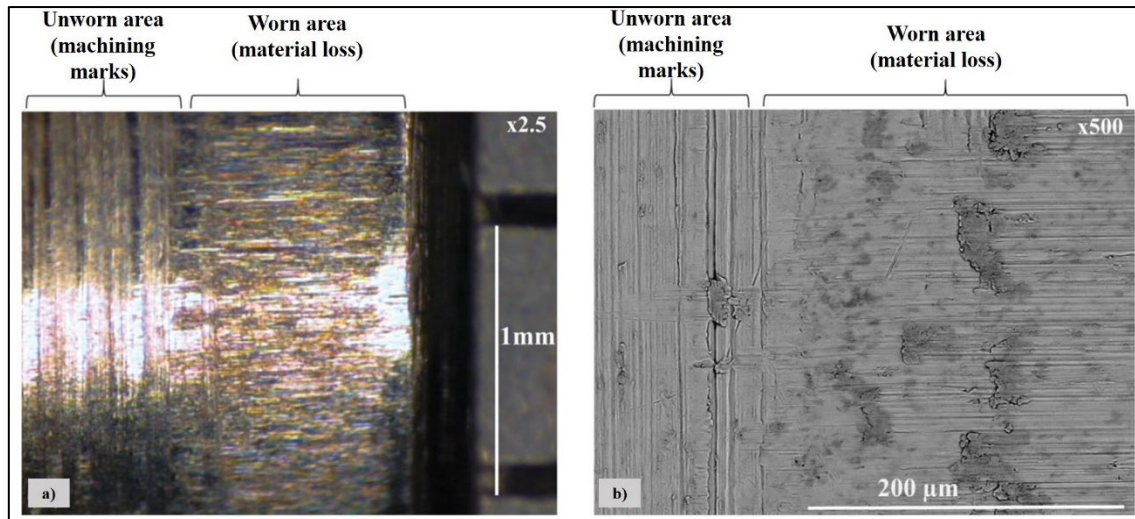


Figure 81 a) An optical microscopic image at 2.5× magnification and b) scanning electron microscopy (SEM) image of the test trunnion at 500× magnification showing worn and unworn areas.

As can be seen in Figure 82 b), at disassembly, a visual inspection of the internal taper of the femoral head revealed a grey coloured ring at the proximal end of all the femoral tapers. The majority of the grey-coloured area was observed at the superior half of the femoral taper. After cleaning with Sidol, these grey coloured areas were removed.

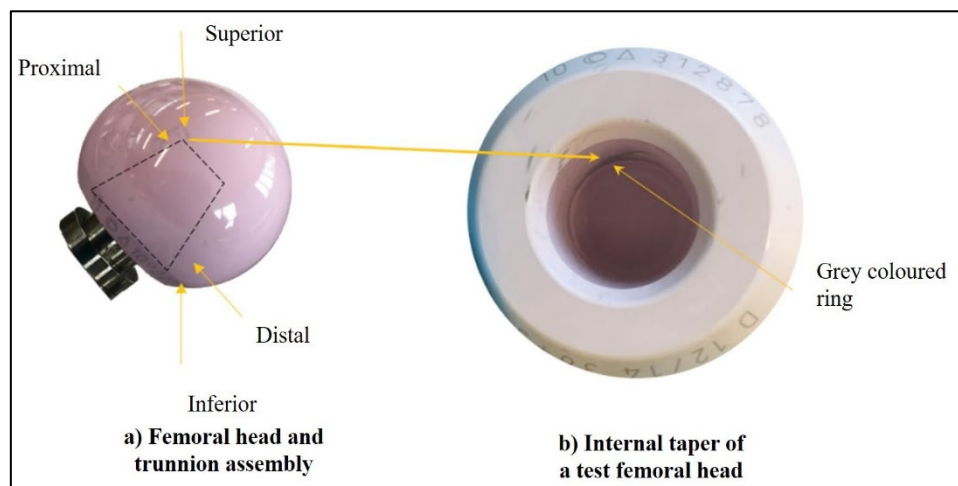


Figure 82 a) A femoral head and trunnion assembly showing the different terminologies used to describe the location of the material loss, and b) An internal taper of a test femoral head showing grey coloured ring. Image from Bhalekar et al. (2018)²⁹⁵.

The visual and microscopic inspection of the Ti trunnions is summarised in Figure 83.

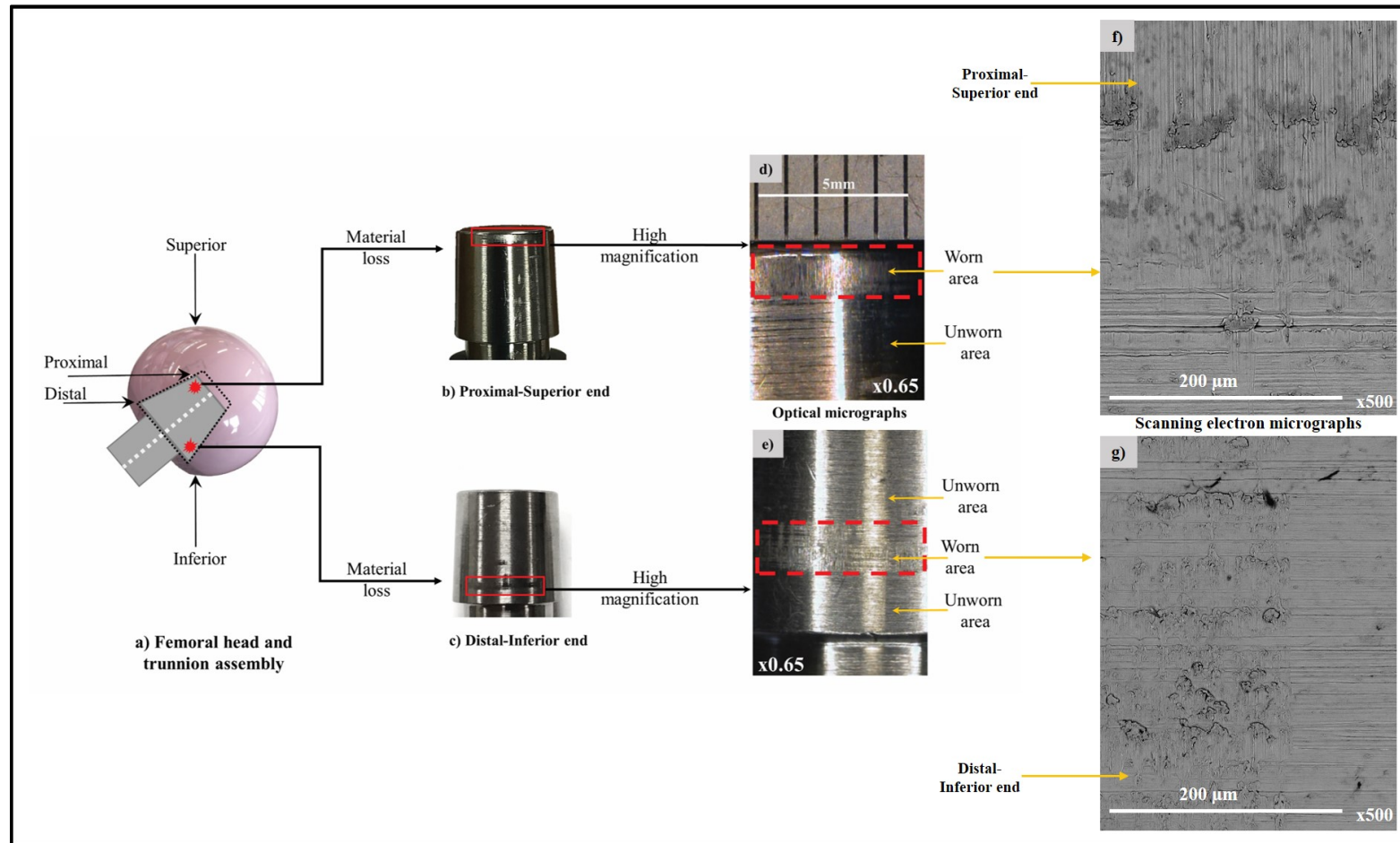


Figure 83 a) A femoral head and trunnion assembly showing the different anatomical planes, b) and c) a test trunnion showing wear from the proximal-superior end and distal-inferior end respectively, d) and e) optical microscopic images of a test trunnion captured at 0.65 \times magnification showing worn and unworn areas of the proximal-superior end and distal-inferior ends, respectively. In the SEM image f) shows, a worn area and an unworn area with the original machining marks at the proximal-superior end and g) shows, worn area at distal-inferior end of the trunnion.

4.1.3 Two-dimensional (2D) surface roughness (Ra) of ceramic femoral tapers and Ti trunnions

There was no statistical difference ($p = 0.210$), pre and post-test, for the femoral taper surfaces with Ra (mean \pm standard deviation) values of 0.351 ± 0.142 and $0.302 \pm 0.071 \mu\text{m}$ respectively, See Figure 84.

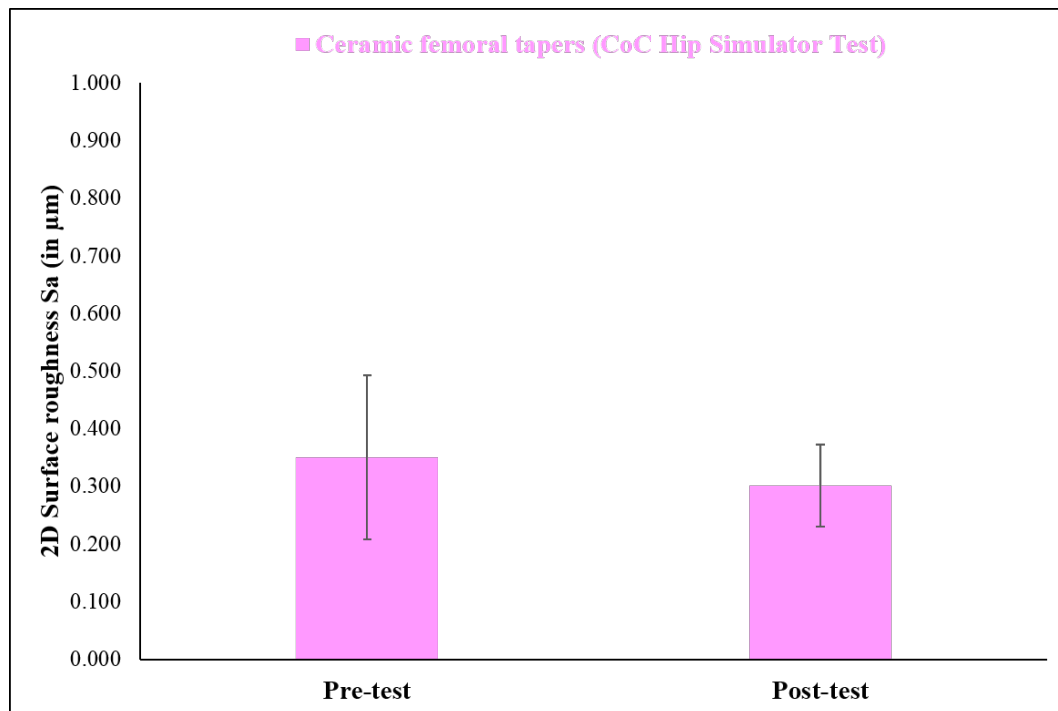


Figure 84 Mean 2D surface roughness Ra (in μm), of ceramic femoral tapers measured pre and post-CoC hip simulator wear test. Error bars represent \pm standard deviation.

Furthermore, there was no statistical difference ($p = 0.110$), pre and post-test, for the femoral taper surfaces with Rz (mean \pm standard deviation) values of 2.683 ± 1.122 and $2.185 \pm 0.425 \mu\text{m}$ respectively. Additionally, there was no statistical difference ($p = 0.755$), pre and post-test, for the femoral taper surfaces with Rq (mean \pm standard deviation) values of 0.415 ± 0.162 and $0.403 \pm 0.082 \mu\text{m}$ respectively.

However, Ra of the trunnions showed a statistically significant decrease ($p < 0.001$) from 0.612 ± 0.070 to $0.527 \pm 0.090 \mu\text{m}$ in pre and post-test measurements, respectively, see Figure 85. Figure 86 shows an evaluation profile trace obtained over the distal-inferior end of a test trunnion displaying the worn area.

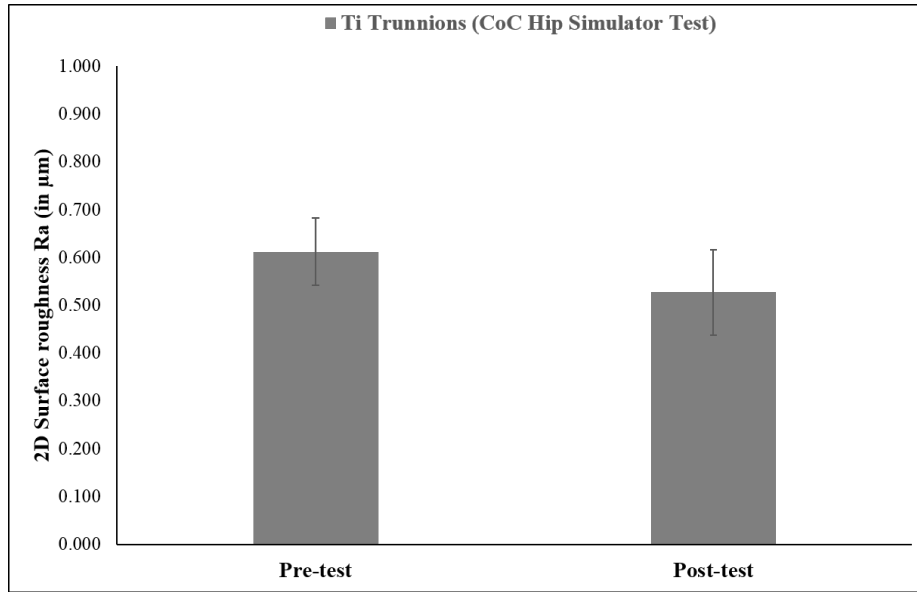


Figure 85 Mean 2D surface roughness Ra (in µm), of titanium (Ti) trunnions measured pre and post-CoC hip simulator wear test. Error bars represent \pm standard deviation.

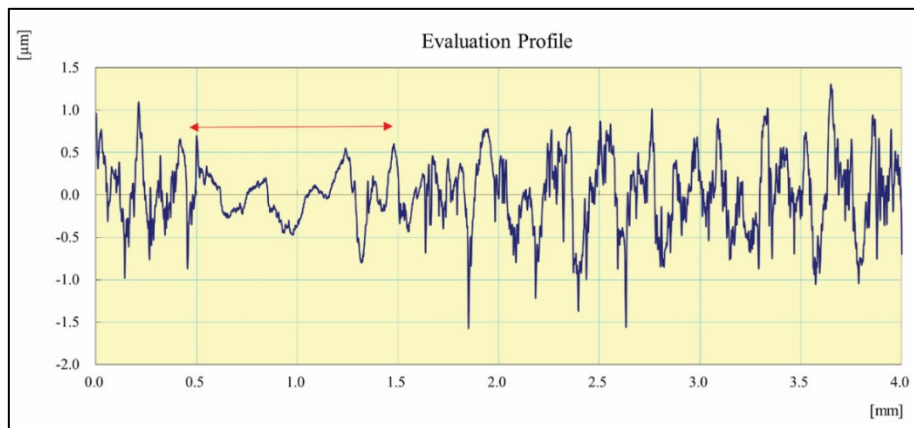


Figure 86 An evaluation profile obtained over the distal-inferior end of a test trunnion ($R_a = 0.321 \mu\text{m}$). The red arrow indicates the worn area. Image from Bhalekar et al. (2018)²⁹⁵.

Similarly, R_q of the trunnions showed a statistically significant decrease ($p < 0.001$) from 0.756 ± 0.082 to $0.646 \pm 0.108 \mu\text{m}$ in pre and post-test measurements, respectively.

Moreover, R_z of the trunnions showed a statistically significant decrease ($p < 0.001$) from 3.903 ± 0.412 to $3.158 \pm 0.512 \mu\text{m}$ in pre and post-test measurements, respectively.

4.1.4 Three-dimensional (3D) surface roughness (S_a) of Ti trunnions

Figure 87 a) and b) show images acquired by the non-contacting profilometer (Zygo) on the a) unworn and b) worn areas at the proximal-superior end of a test trunnion respectively. On

the unworn area, the original machining marks could be seen. However, they were not observed on the worn area. The Sa of the trunnions on the unworn and worn areas showed a statistically significant decrease from 0.558 ± 0.060 to 0.312 ± 0.028 μm , respectively ($p < 0.001$), see Figure 88.

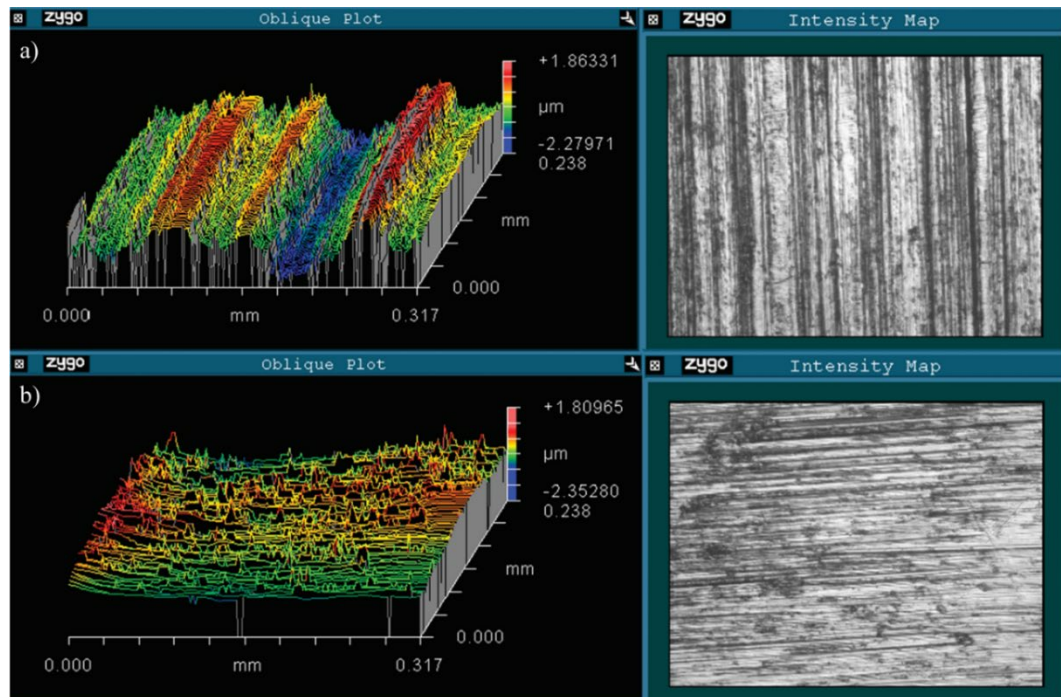


Figure 87 Surface topography images of a titanium trunnion a) unworn with machining marks visible ($S_a = 0.565$ μm) and b) worn ($S_a = 0.284$ μm). Image from Bhalekar et al. (2018)²⁹⁵.

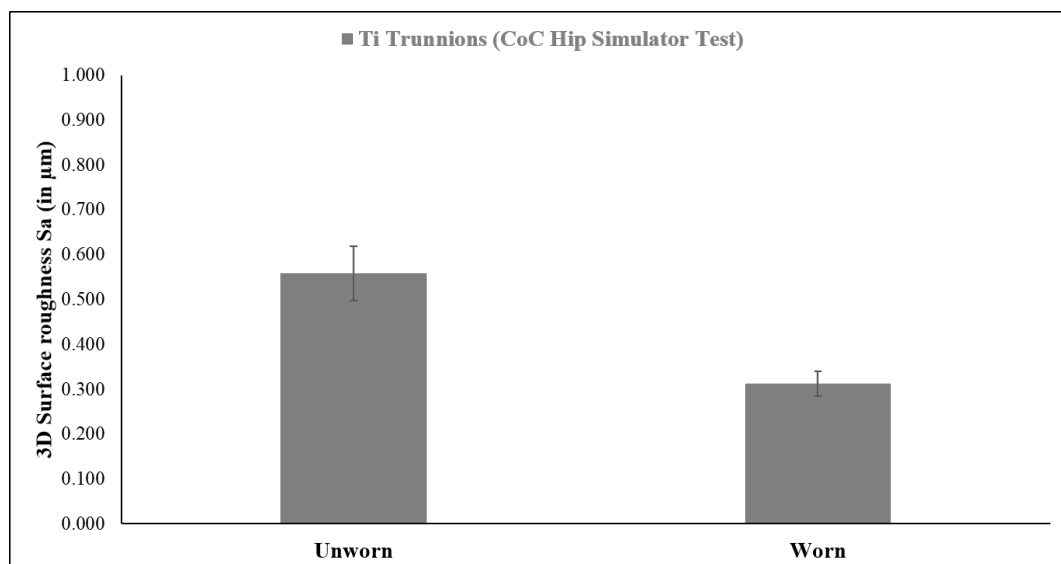


Figure 88 Mean 3D surface roughness S_a (in μm), of titanium (Ti) trunnions measured on unworn and worn areas after CoC hip simulator wear test. Error bars represent \pm standard deviation.

4.1.5 Quantification of the material loss from the bearing surfaces

4.1.5.1 Gravimetric analysis of the material loss from the bearing surfaces

After 5 million cycles, the volumetric wear rate (mean \pm standard deviation) for the ceramic femoral heads was $0.036 \pm 0.005 \text{ mm}^3/\text{Mc}$, and for the ceramic acetabular liners, it was $0.031 \pm 0.002 \text{ mm}^3/\text{Mc}$. For the CoC joints, the mean volumetric wear rate was, therefore $0.067 \pm 0.003 \text{ mm}^3/\text{Mc}$. The mean volumetric wear rates for all-ceramic femoral heads, acetabular liners and CoC joints from the hip simulator wear test, measured gravimetrically are shown in Figure 89, Figure 91 and Figure 93, respectively. The total average volumetric wear over 5 million cycles was 0.25 mm^3 for the three CoC hip joints. Additionally, there was no statistically significant difference in the volume loss of all ceramic femoral heads (with adjusted p value > 0.999), ceramic liners (with adjusted p value > 0.999), and CoC joints (with adjusted p value > 0.999) as shown in Figure 90, Figure 92 and Figure 94 respectively.

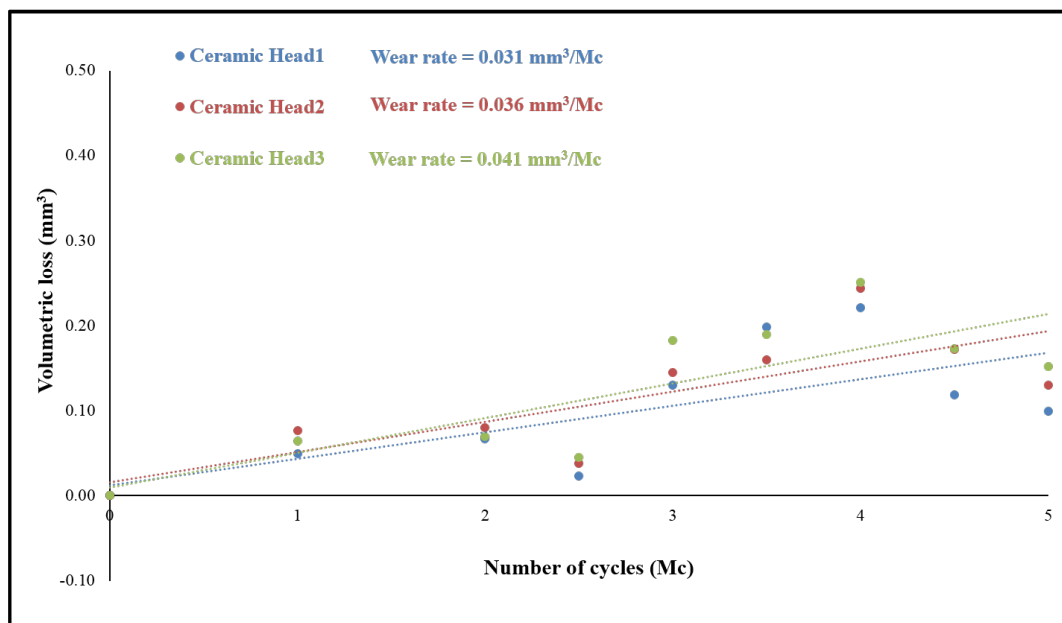


Figure 89 Mean volumetric measurements of all ceramic femoral heads from CoC hip simulator wear test (measured gravimetrically).

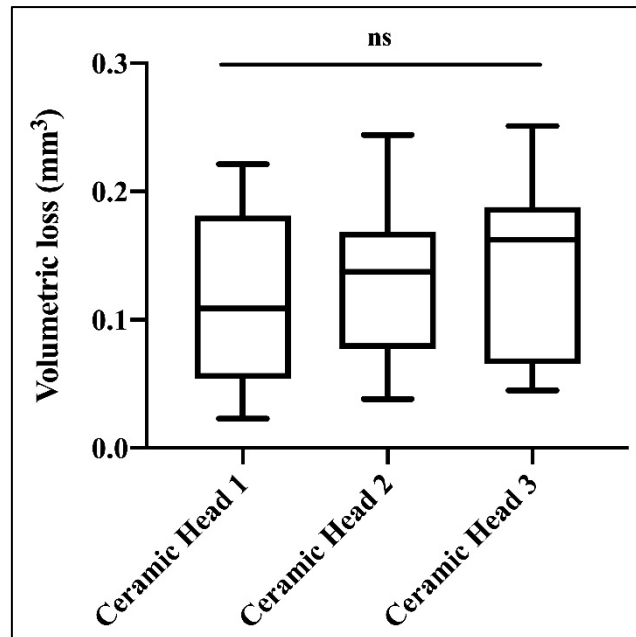


Figure 90 Box-plot of volumetric measurement of all ceramic heads from CoC hip simulator wear test (measured gravimetrically). ns: no significant difference with adjusted p-value >0.999.

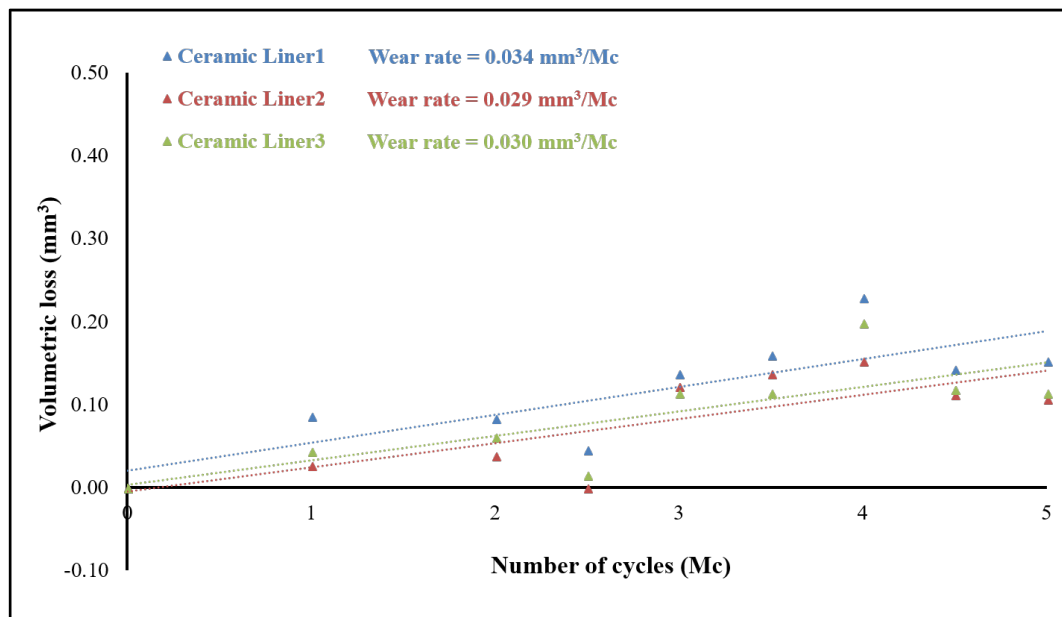


Figure 91 Mean volumetric measurements of all ceramic acetabular liners from CoC hip simulator wear test (measured gravimetrically).

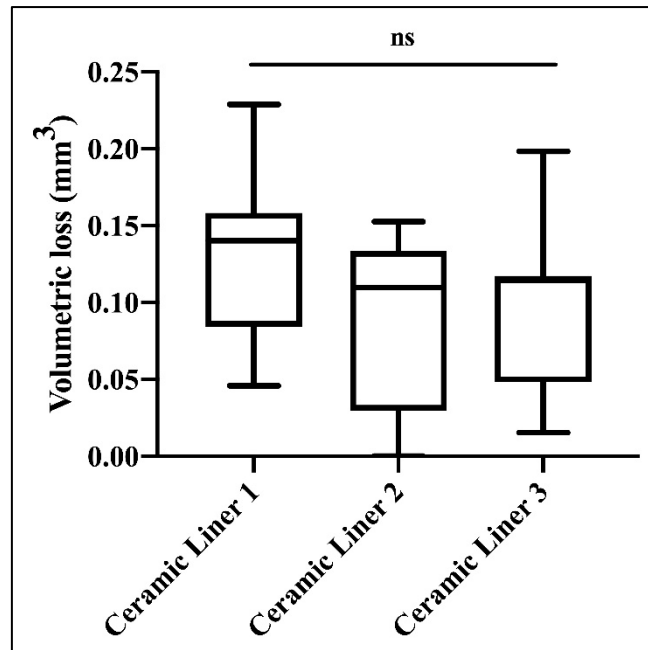


Figure 92 Box-plot of volumetric measurement of all ceramic liners from CoC hip simulator wear test (measured gravimetrically). ns: no significant difference with adjusted p-value >0.999.

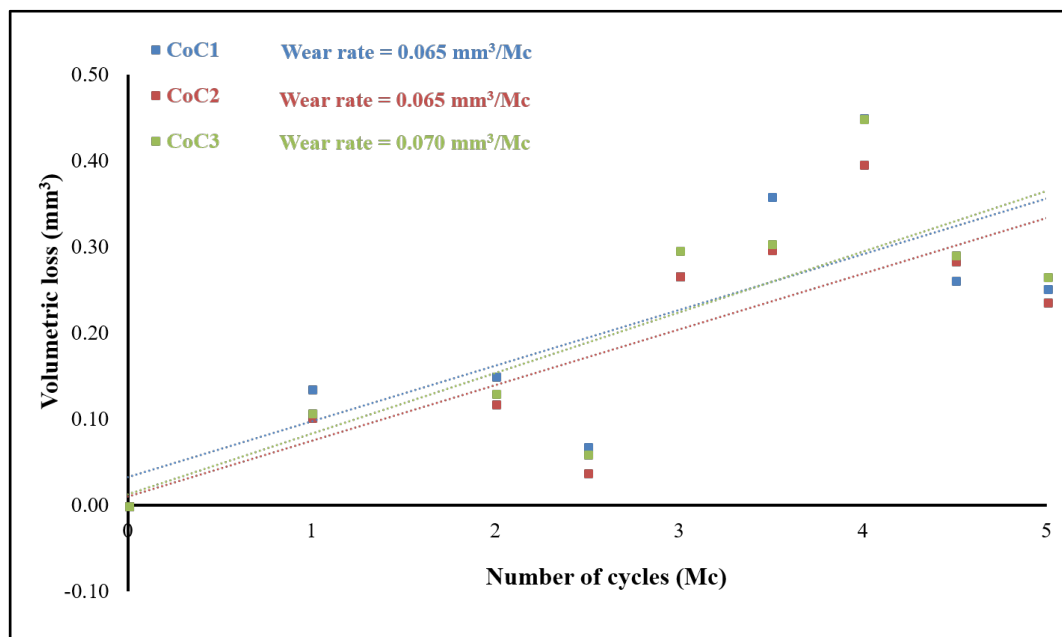


Figure 93 Mean volumetric measurements of all CoC joints from CoC hip simulator wear test (measured gravimetrically).

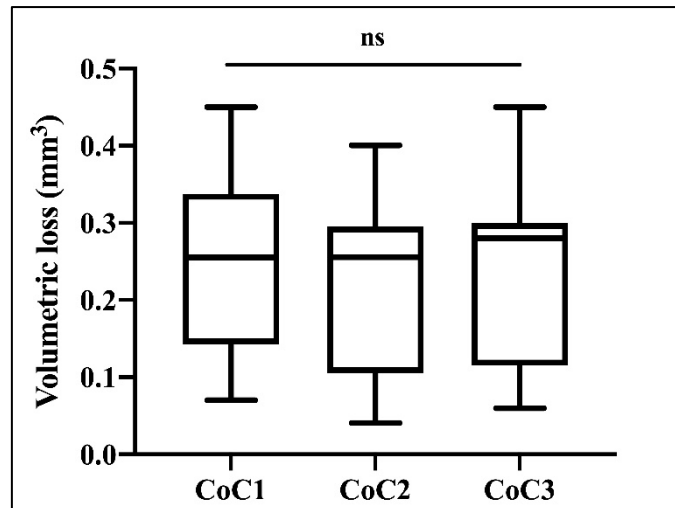


Figure 94 Box-plot of volumetric measurement of all CoC joints from CoC hip simulator wear test (measured gravimetrically). ns: no significant difference with adjusted p-value >0.999.

The volumetric wear rate of the CoC joints and Ti trunnions measured gravimetrically were not significantly different ($p = 0.592$). These results are presented in Figure 95.

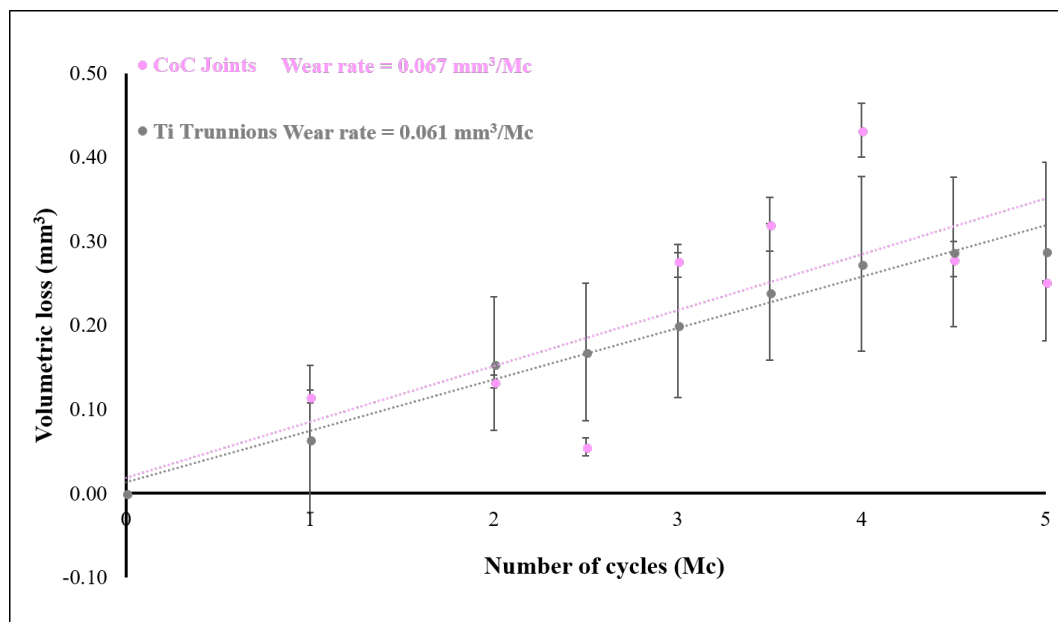


Figure 95 Mean volumetric measurements of CoC joints and titanium (Ti) trunnions from CoC hip simulator wear test (measured gravimetrically). Error bars represent \pm standard deviation ²⁹⁵.

4.1.6 Three-dimensional (3D) surface roughness (S_a) of the bearing surfaces

Figure 96 shows the mean 3D surface roughness (S_a), pre and post-test, for the bearing surfaces used in the CoC hip simulator wear test. There was no statistically significant

difference in the Sa values pre and post-test for the ceramic femoral heads ($p = 0.184$), with Sa values, pre-test 0.003 ± 0.002 and post-test $0.004 \pm 0.001 \mu\text{m}$. Similarly, there was no statistically significant difference in the Sa values pre and post-test for the ceramic acetabular liners ($p = 0.184$), with Sa values, pre-test test 0.005 ± 0.001 and post-test $0.005 \pm 0.001 \mu\text{m}$. Indicative surface topography images of the bearing surfaces of the ceramic femoral heads and acetabular liners obtained using the Zygo, non-contacting profilometer pre and post CoC hip simulator wear test, are shown in Figure 97 and Figure 98, respectively.

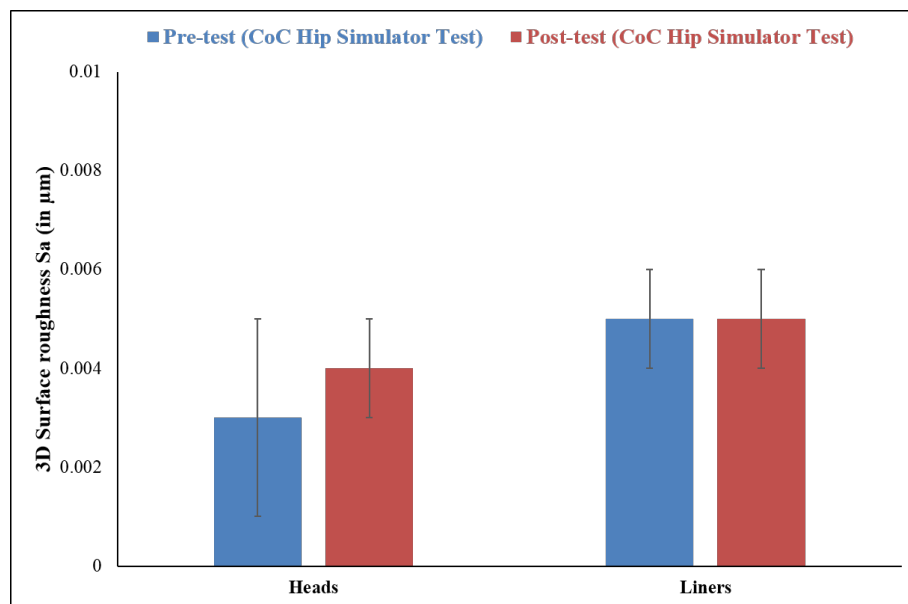


Figure 96 Mean 3D surface roughness Sa (in μm), of the ceramic femoral head and acetabular liners measured pre and post-CoC hip simulator wear test. Error bars represent \pm standard deviation.

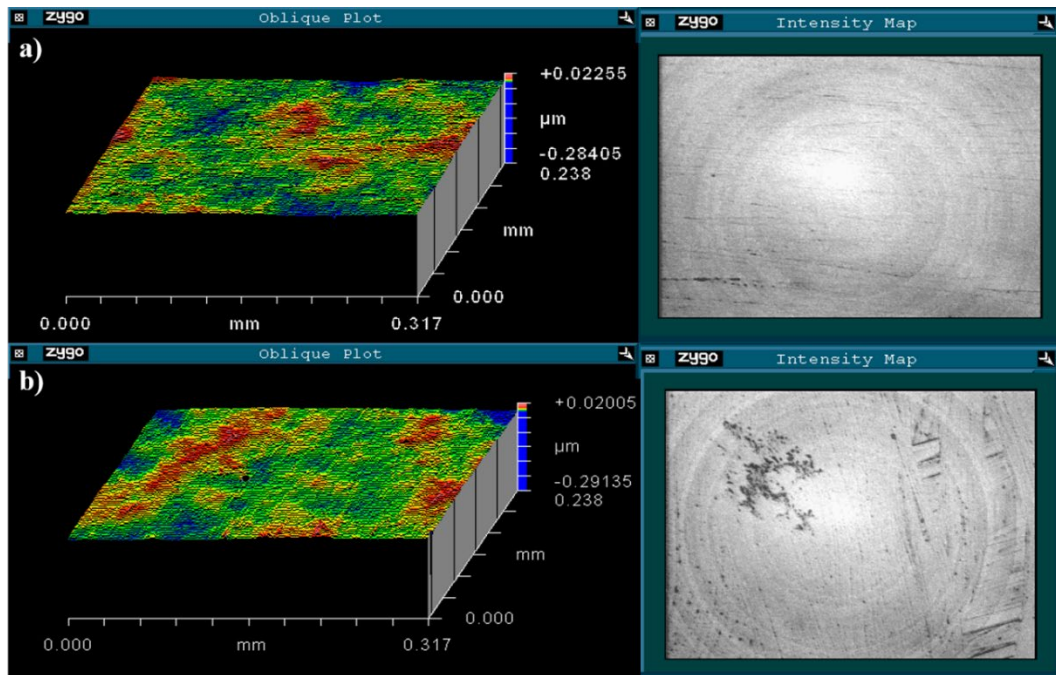


Figure 97 Surface topography images of a ceramic femoral head a) pre-test ($S_a = 0.003 \mu\text{m}$) and b) post-test ($S_a = 0.003 \mu\text{m}$).

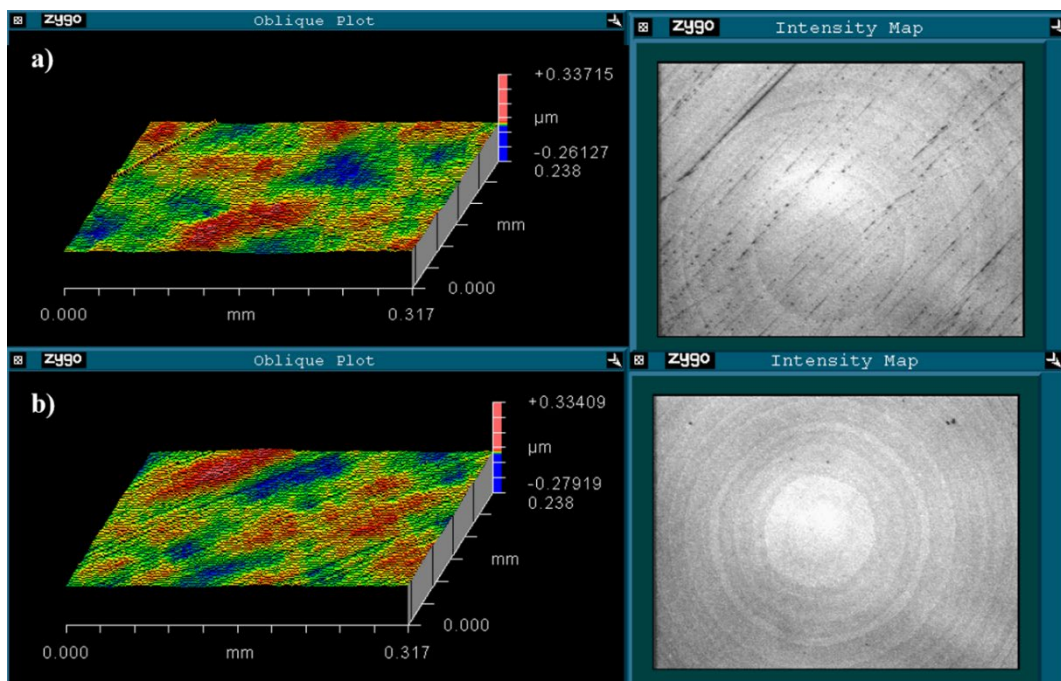


Figure 98 Surface topography images of a ceramic acetabular liner a) pre-test ($S_a = 0.006 \mu\text{m}$) and b) post-test ($S_a = 0.005 \mu\text{m}$).

4.2 Dynamic loading (DL) but no articulating motion testing of ceramic-on-ceramic (CoC) hip prosthesis

This section gives the wear of the ceramic components, and the Ti trunnions used in the DL test. The 2D surface roughness (Ra) measurements on the surface of the taper and the trunnion used in the DL test are then presented. Next, the results of 3D surface roughness (Sa) measurements on the bearing surfaces of the ceramic component are given. Finally, the wear data of Ti trunnions from the CoC hip simulator test and the DL test are compared.

4.2.1 Quantification of the material loss from ceramic femoral head, acetabular liner and Ti trunnion

4.2.1.1 Gravimetric analysis

After 5 million cycles of dynamic loading (DL) but no articulating motion, the mean volumetric wear rates were $0.033 \text{ mm}^3/\text{Mc}$ for the femoral head and $0.032 \text{ mm}^3/\text{Mc}$ for the acetabular liner, see Figure 99. The mean volumetric wear rates for the CoC joint and Ti trunnion were $0.065 \text{ mm}^3/\text{Mc}$ and $0.012 \text{ mm}^3/\text{Mc}$ respectively. The total volumetric wear over 5 million cycles was 0.23 mm^3 for the CoC joint and 0.05 mm^3 for the Ti trunnion.

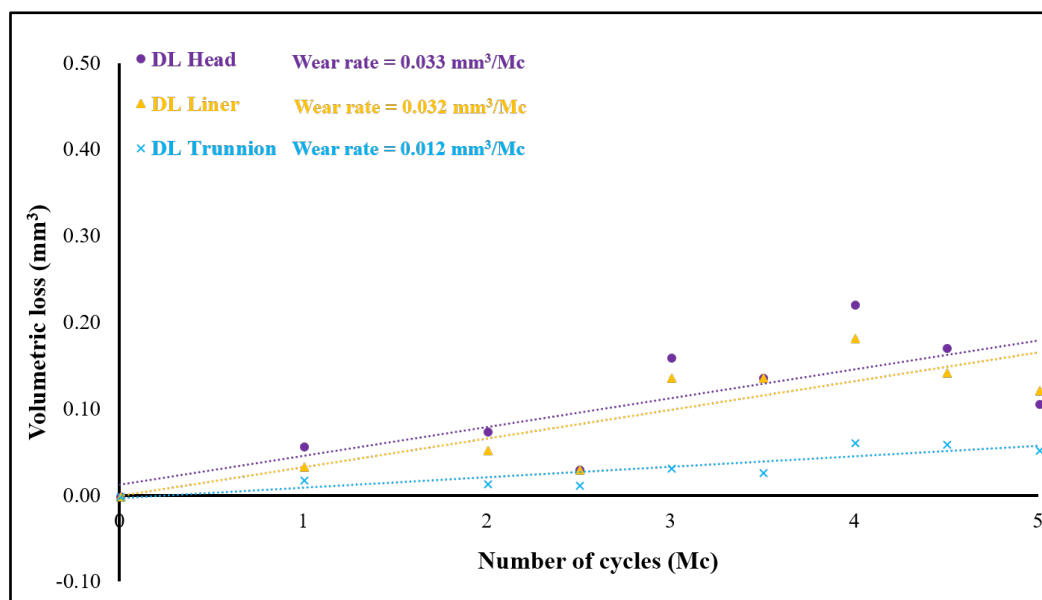


Figure 99 Mean volumetric measurements of the ceramic femoral head, ceramic acetabular liner and titanium (Ti) trunnion used in the DL test (measured gravimetrically).

4.2.1.2 Geometric analysis of the ceramic femoral taper used in the DL test

After 5 million cycles of dynamic loading but no articulating motion, the mean volumetric wear rates were $0.009 \text{ mm}^3/\text{Mc}$ for the ceramic femoral taper and $0.018 \text{ mm}^3/\text{Mc}$ for the Ti trunnion. The total volumetric wear over 5 million cycles was 0.04 mm^3 for the ceramic femoral taper and 0.09 mm^3 for the Ti trunnion.

4.2.2 Two-dimensional (2D) surface roughness (Ra) of ceramic femoral taper and Ti trunnion

There was no statistical difference ($p = 0.862$), pre and post-test, for the femoral taper surfaces with Ra (mean \pm standard deviation) values of 0.365 ± 0.093 and $0.355 \pm 0.055 \text{ }\mu\text{m}$ respectively, see Figure 100.

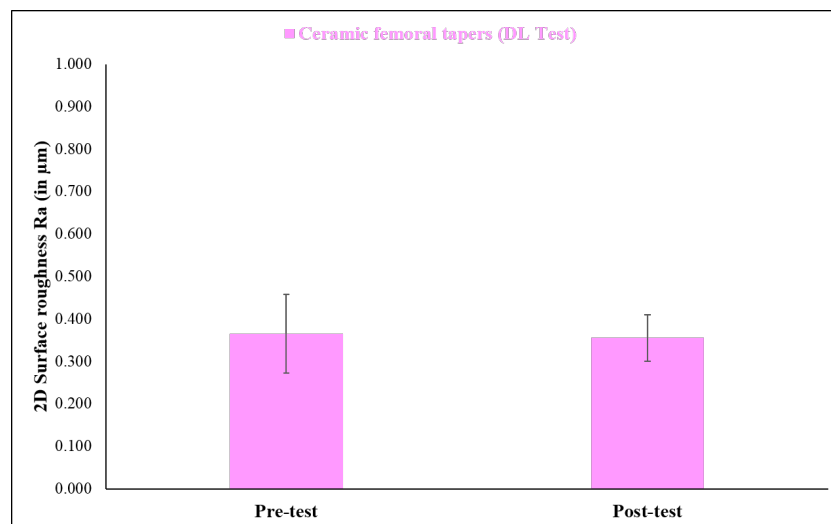


Figure 100 Mean 2D surface roughness Ra (in μm), of ceramic femoral taper measured pre and post-DL test. Error bars represent \pm standard deviation.

Similarly, the Ra of the trunnion did not show any statistically significant difference ($p = 0.146$) with Ra values of 0.541 ± 0.040 and $0.520 \pm 0.045 \text{ }\mu\text{m}$ pre and post-test, respectively see Figure 101.

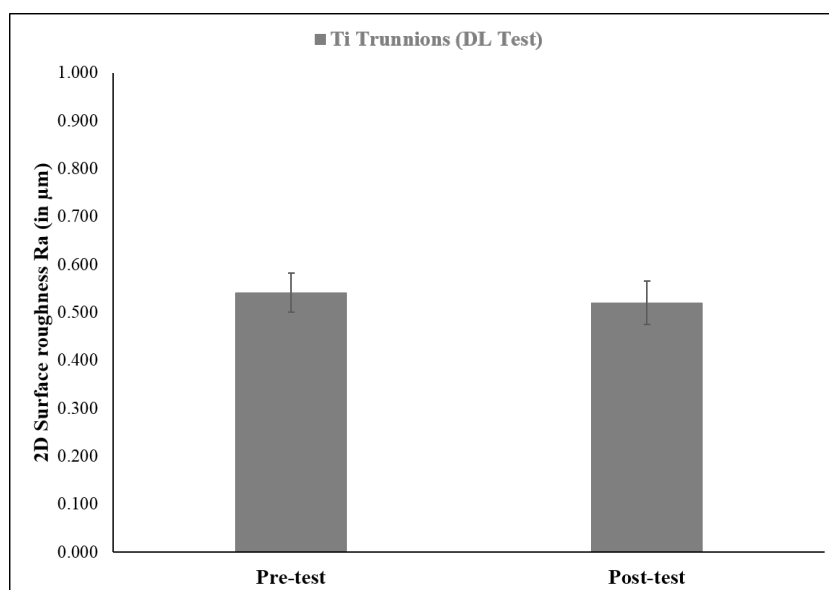


Figure 101 Mean 2D surface roughness Ra (in μm), of titanium (Ti) trunnions measured pre and post-DL test. Error bars represent \pm standard deviation.

4.2.3 Three-dimensional (3D) surface roughness (Sa) of the CoC bearing surfaces

Figure 102 shows the mean 3D surface roughness (Sa), pre and post-test, for the bearing surfaces used in the DL test. There was no statistically significant difference in the Sa values pre and post-test for the ceramic femoral head ($p = 0.111$) used in the DL test, with Sa values, pre-test 0.005 ± 0.001 and post-test $0.006 \pm 0.001 \mu\text{m}$. Similarly, there was no statistically significant difference in the Sa values pre and post-test for the ceramic acetabular liners ($p = 0.139$) used in the DL test, with Sa values, pre-test test 0.005 ± 0.001 and post-test $0.004 \pm 0.001 \mu\text{m}$.

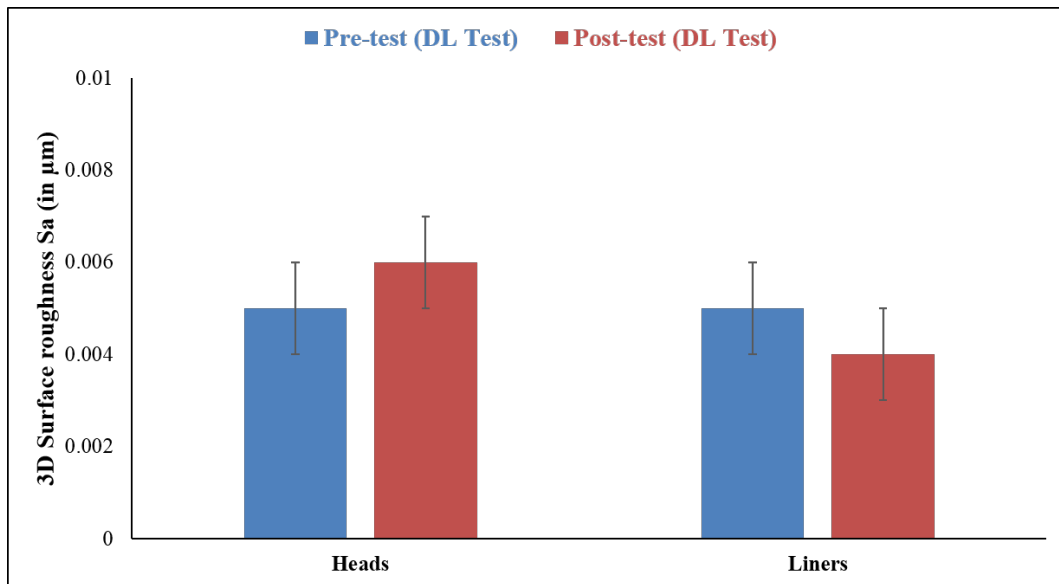


Figure 102 Mean 3D surface roughness Sa (in µm), of the ceramic femoral head and acetabular liner measured pre (blue) and post (red)-DL test. Error bars represent \pm standard deviation.

4.2.4 Comparison of the material loss from Ti trunnions used in CoC hip simulator wear test and DL test.

After 5 million cycles, the mean volumetric wear rate of the DL test trunnion ($0.012 \text{ mm}^3/\text{Mc}$) was lower than the hip simulator trunnions ($0.061 \text{ mm}^3/\text{Mc}$) as shown in Figure 103. Therefore, based on this measurement, the metallic material loss from the hip simulator wear test (i.e. dynamic loading and articulating motion) was much larger than from the DL test (i.e. dynamic loading but no articulating motion).

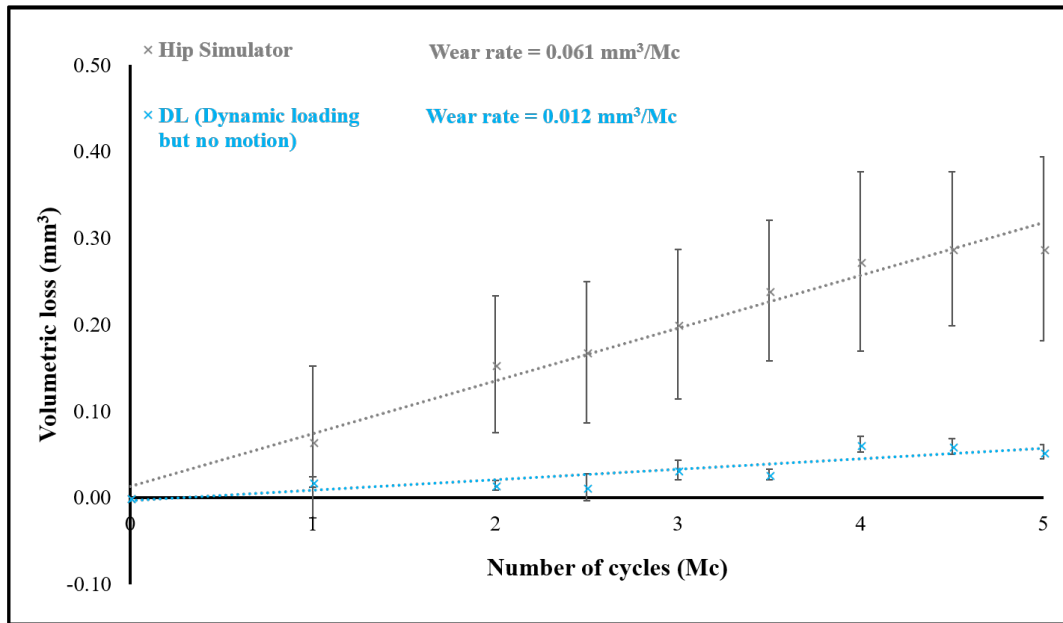


Figure 103 The mean volumetric measurements of titanium trunnions used in CoC hip simulator wear test and the DL test (measured gravimetrically). Error bars represent \pm standard deviation²⁹⁵.

4.3 Impact test

This section gives the results of the impact test of CoC hip prosthesis, and its influence on the wear and surface roughness of the taper-trunnion junction.

The effect of assembly and disassembly on the wear of the taper-trunnion junction was minimal. Figure 104 shows a graph of weight loss against a number of impactations. If there were any weight changes in the trunnion due to assembly and disassembly, they were minimal.

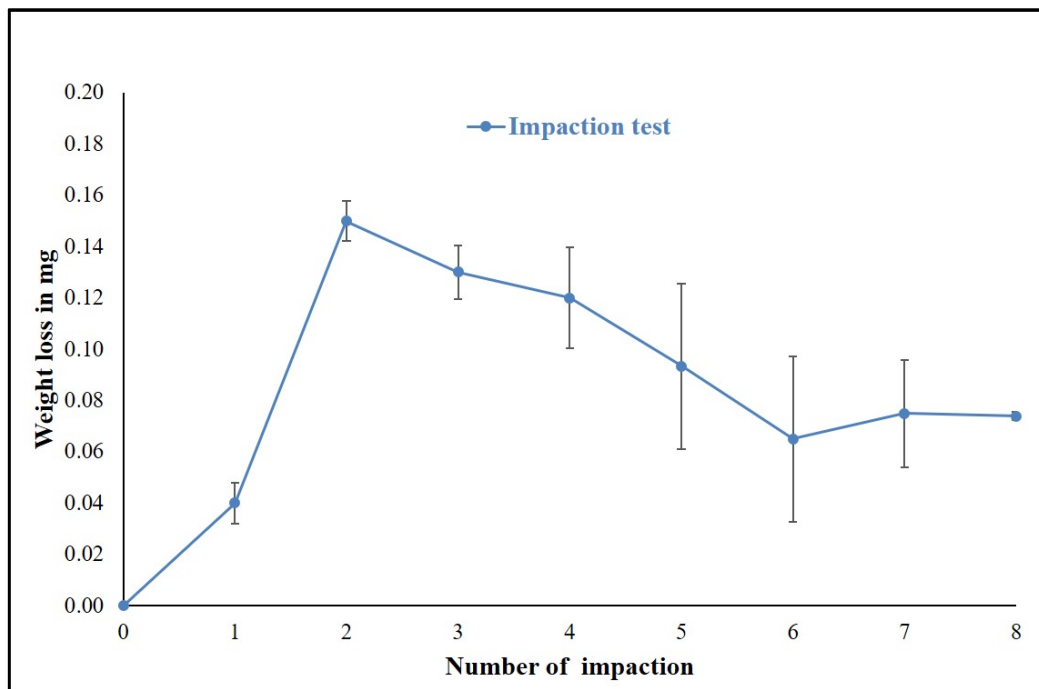


Figure 104 Gravimetric measurement of impaction test trunnions. Error bars represent \pm standard deviation.

Moreover, there was no statistically significant difference in the Ra values pre and post-test, for either the trunnion ($p=0.187$) or the femoral taper ($p=0.193$). Table 26 shows the mean surface roughness (Ra) pre and post impaction test for the femoral taper and the trunnion. Therefore, based on gravimetric and surface roughness measurements the impaction showed negligible damage.

Table 26 Mean surface roughness of femoral taper and trunnion used for an impaction test.

Ra (in μm)	Before test (Mean \pm SD)	After test (Mean \pm SD)	p value
Femoral taper	0.324 \pm 0.084	0.254 \pm 0.054	0.187
Trunnion	0.602 \pm 0.068	0.598 \pm 0.042	0.193

Additionally, a light grey discolouration was observed on the internal taper of the femoral head during this test; as shown in Figure 105; however, it was removed during the cleaning procedure.

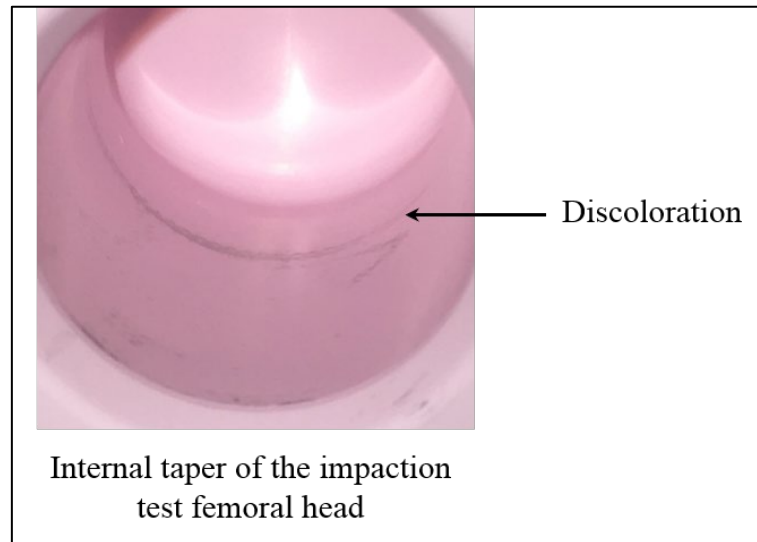


Figure 105 An internal taper of an impaction test femoral head showing discolouration prior to cleaning²⁹⁵.

The impaction test showed a minimal material loss from the titanium trunnions (0.09 mm^3) compared with the trunnions (0.25 mm^3) used in the hip simulator test. Pre-and post-test, Ra values did not show statistically significant change on trunnion surface ($p= 0.187$).

Moreover, visual analysis of the impaction test trunnions showed very minimal damage at the proximal-superior end; however, no visible damage at the distal-inferior end. Therefore, the impaction had minimal effect on the material loss of the titanium trunnions used in the CoC hip simulator test.

4.4 Hip simulator wear testing of the taper-trunnion junction and bearing surfaces of modular metal-on-cross-linked polyethylene (MoXLPE) hip prostheses

This section gives the results from the hip simulator study testing 32mm MoXLPE THRs mounted on Ti alloy trunnions. To the authors' best knowledge, no hip simulator tests have quantified metal release from the taper-trunnion junction of contemporary MoP THRs.

Therefore, in this section, quantification of metallic loss from the taper-trunnion junction of MoXLPE THRs obtained gravimetrically and geometrically is first offered. Then the 2D surface roughness (Ra) measurements on the surface of the CoCrMo femoral tapers are

presented. Furthermore, 3D surface roughness measurements (Sa) on the unworn and worn areas of the CoCrMo femoral tapers are presented. Visual and microscopic images taken on the CoCrMo femoral tapers post-test and energy dispersive X-ray spectroscopy (EDX) analysis are also displayed. Additionally, wear of the CoCrMo femoral head, and XLPE acetabular lines from the hip simulator wear test obtained gravimetrically are offered. Following the wear data, results of Sa measurements on the bearing surfaces of MoXLPE components are given.

4.4.1 Quantification of the material loss from the taper-trunnion junction

4.4.1.1 Gravimetric analysis

After 5 million cycles, the volumetric wear rate (mean \pm standard deviation) for the titanium (Ti) trunnions was $0.044 \pm 0.003 \text{ mm}^3/\text{Mc}$, with a range of $0.039\text{--}0.047 \text{ mm}^3/\text{Mc}$. The mean volumetric wear rates for all Ti trunnions from the hip simulator wear test, measured gravimetrically, are shown in Figure 106. There was no statistically significant difference in the volume loss of all test trunnions with adjusted p value > 0.999 , see Figure 107. The total average volumetric wear over 5 million cycles was 0.24 mm^3 for the Ti trunnions.

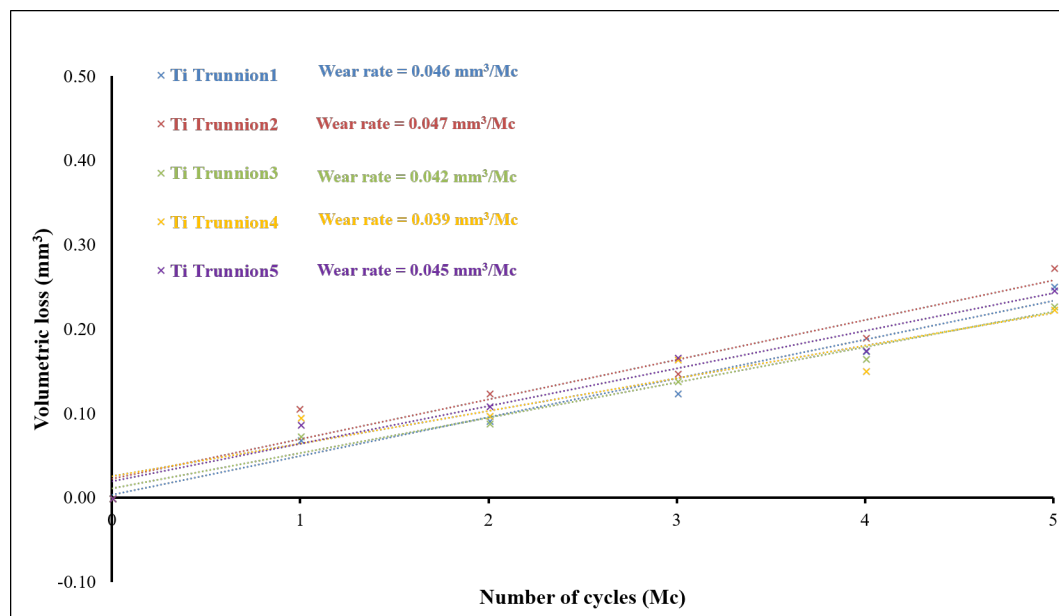


Figure 106 Mean volumetric measurements of all titanium (Ti) trunnions from MoXLPE hip simulator wear test (measured gravimetrically).

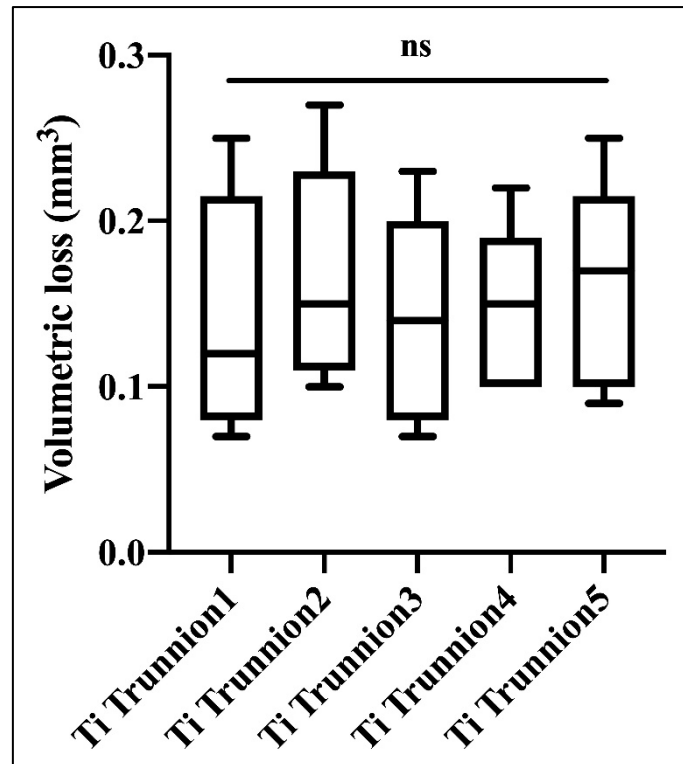


Figure 107 Box-plot of volumetric measurement of all titanium (Ti) trunnions from MoXLPE hip simulator wear test (measured gravimetrically). ns: no significant difference with adjusted p-value >0.999.

4.4.1.2 Geometric wear measurement of the CoCrMo femoral tapers obtained using the CMM

After 5 million cycles, the volumetric wear rate (mean \pm standard deviation) of the ceramic femoral tapers was $0.045 \pm 0.024 \text{ mm}^3/\text{Mc}$. The total volumetric wear over 5 million cycles was 0.22 mm^3 for the CoCrMo femoral tapers. The CMM generated wear maps showed a circumferential wear band at the distal end of the femoral taper, as shown in Figure 108, where the distal end of the trunnion made contact with the CoCrMo femoral taper. However, the wear band was not present at the proximal end of the CoCrMo femoral taper. Thus indicating, the CoCrMo femoral taper and titanium trunnion had base-locked condition at the taper-trunnion junction.

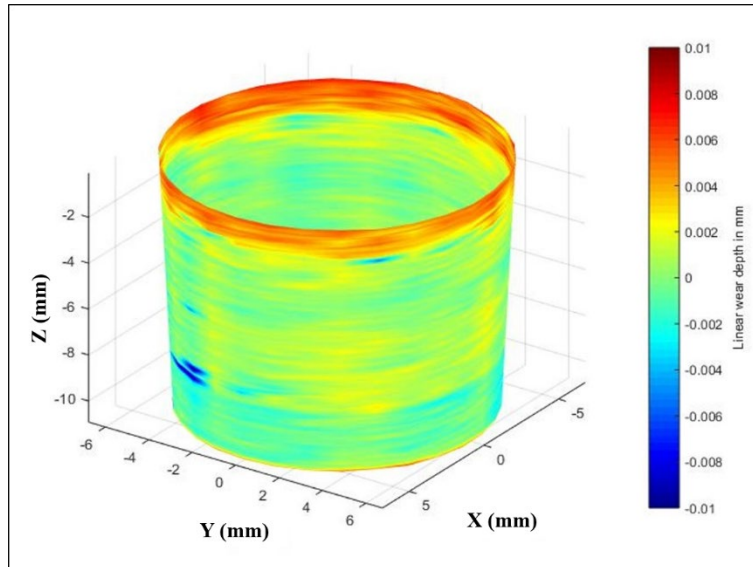


Figure 108 A CMM wear map showing the wear pattern of the internal taper of a test CoCrMo head. The circumferential red band at the distal end indicates the worn area.

4.4.2 Two-dimensional (2D) surface roughness (R_a) of the CoCrMo femoral tapers

There was no statistical difference ($p = 0.711$), pre and post-test, for the CoCrMo femoral taper surfaces with R_a (mean \pm standard deviation) values of 0.428 ± 0.078 and 0.424 ± 0.077 μm respectively, see Figure 109.

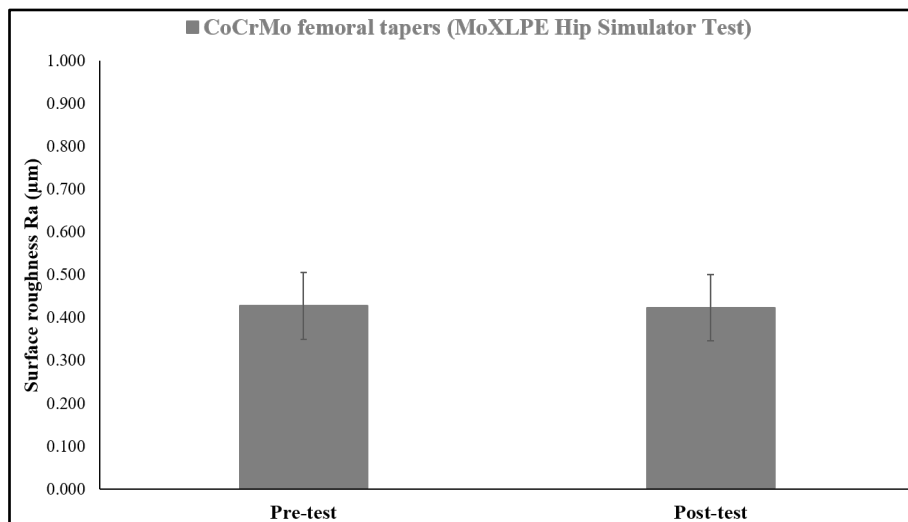


Figure 109 Mean 2D surface roughness, R_a (in μm), of CoCrMo femoral tapers measured pre and post-MoXLPE hip simulator wear test. Error bars represent \pm standard deviation.

Furthermore, there was no statistical difference ($p = 0.724$), pre and post-test, for the femoral taper surfaces with R_q (mean \pm standard deviation) values of 0.531 ± 0.097 and 0.526 ± 0.100 μm respectively. Additionally, there was no statistical difference ($p = 0.755$), pre and

post-test, for the femoral taper surfaces with R_q (mean \pm standard deviation) values of 2.412 ± 0.683 and $2.408 \pm 0.703 \mu\text{m}$ respectively.

4.4.3 Three-dimensional (3D) surface roughness (S_a) of the CoCrMo femoral tapers

The surface topography images obtained using the non-contacting profilometer on the a) unworn and b) worn areas of the femoral tapers post-test are shown in Figure 110 a) and b) respectively. The original machining marks could be seen on the unworn area, but not on the worn area. The surface roughness of the femoral tapers on the worn area showed a statistically significant increase ($p < 0.001$) compared with unworn, with S_a values of $0.510 \pm 0.068 \mu\text{m}$ and $0.867 \pm 0.233 \mu\text{m}$ for unworn and worn respectively. The S_a results were contradicting to R_a results which did not show statistically significant difference ($p = 0.711$), pre and post-test, as shown in section 4.4.2. As can be seen from the CMM wear map (see Figure 108), the majority of the material loss occurred at the distal end of the femoral taper. The R_a was 2D surface roughness of a linear profile (length=4mm) taken on the femoral taper whereas S_a measurement was an areal profile (area = $0.317 \times 0.238\text{mm}$) measured on the worn area. Hence, there was a discrepancy between S_a and R_a measurement.

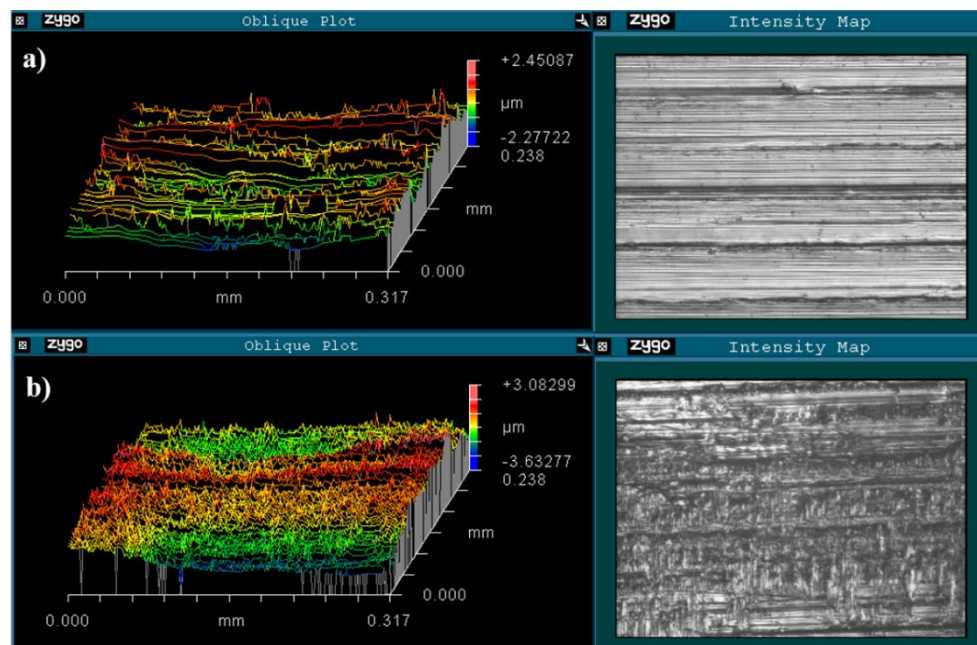


Figure 110 Surface topography images of the internal taper of CoCr femoral heads a) unworn with machining marks visible ($S_a = 0.482 \mu\text{m}$) and b) worn ($S_a = 0.699 \mu\text{m}$).

4.4.4 Visual and microscopic inspection of the CoCrMo femoral tapers

Figure 111 shows the internal taper of a test CoCrMo head. At the distal end, a localised worn area (as indicated by the CMM wear map) could be seen which corresponded to contact with the trunnion base. Above this, there was the original unworn surface and below this, an imprint caused by the microgrooves of the trunnion surface. Additionally, the distal end of a CoCrMo femoral taper can be seen at 0.65× magnification using an optical microscope in Figure 111 c), and at 150× magnification with an SEM in Figure 111 d).

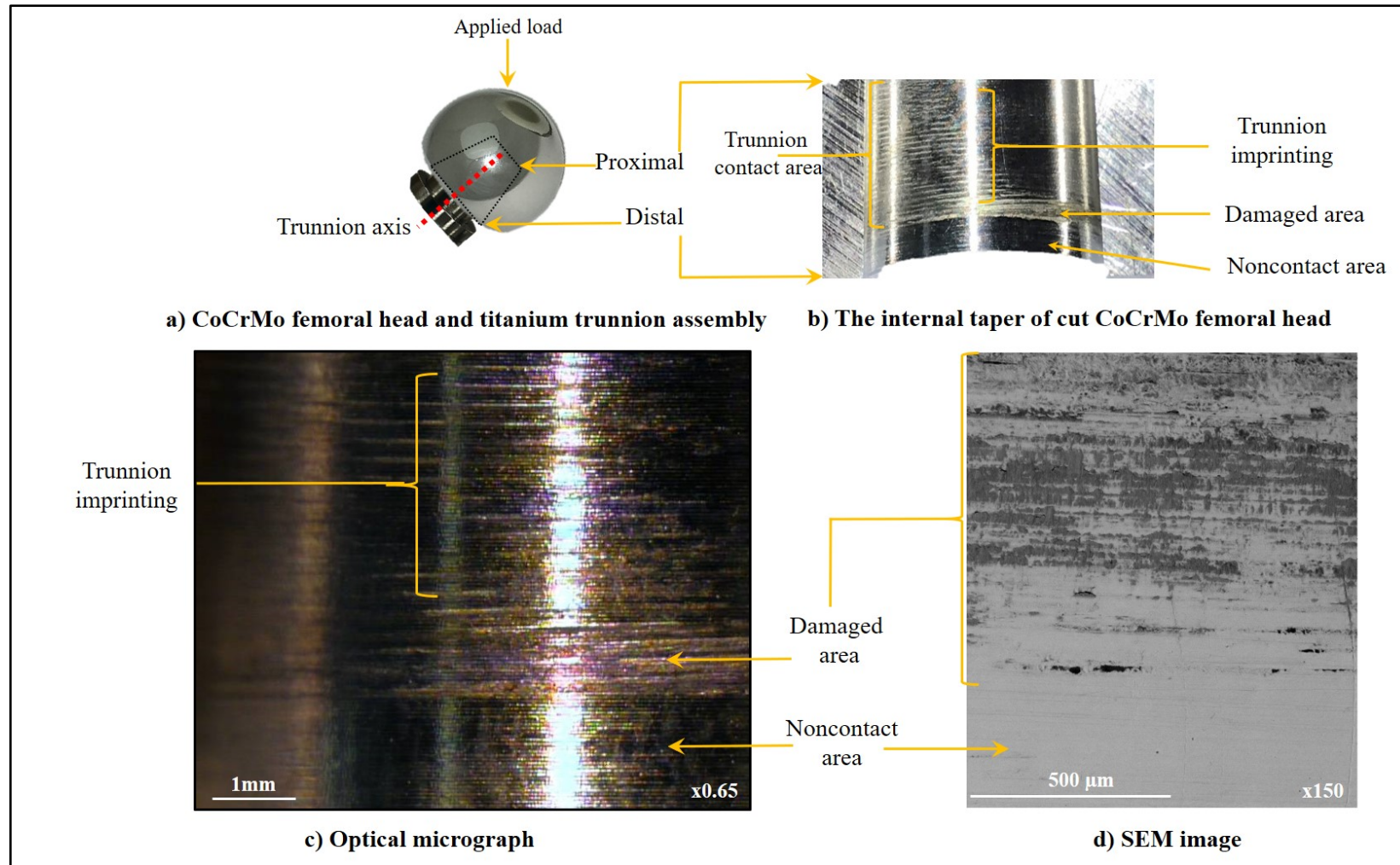


Figure 111 a) A test CoCrMo femoral head and titanium trunnion assembly, b) the internal taper of cut CoCrMo femoral head showing unworn area at distal end, worn area, and trunnion imprinting, and c) an optical microscopic image of a test femoral taper captured at $0.65\times$ magnification showing unworn area, worn area, and trunnion imprinting.

4.4.5 Energy-dispersive X-ray spectroscopy (EDX) analysis of the CoCrMo femoral tapers

The orientation of the cut CoCrMo head taper for SEM coupled with EDX analysis is shown in Figure 112 a) while Figure 112 b) shows the SEM image of the CoCrMo taper at this orientation. The position of spot EDX analysis on undamaged area 1 (U1), damaged area 1 (D1) and damaged area 2 (D2) are shown in Figure 112 c), d) and e), respectively.). The majority of the damage was perpendicular to machining lines on the femoral taper. The EDX spectra on the cut CoCrMo femoral tapers taken on three different spots are shown in Figure 113 undamaged area (U1), Figure 114 damaged area 1 (D1), and Figure 115 damaged area 2 (D2). The chromium (Cr), cobalt (Co), molybdenum (Mo) and Ti peaks were comparable on D1 and U1. However, D1 showed a strong presence of oxygen (O) peak and a weak presence of Co peak compared to the undamaged area, indicating the presence of a mixed oxide rich area. The Co, Cr and Mo peaks on D2 were reduced compared to the undamaged area. However, D2 showed a strong presence of Ti, aluminium (Al) and vanadium (V) peaks compared to the undamaged area. Indicating adhesion of Ti6Al4V from the trunnion.

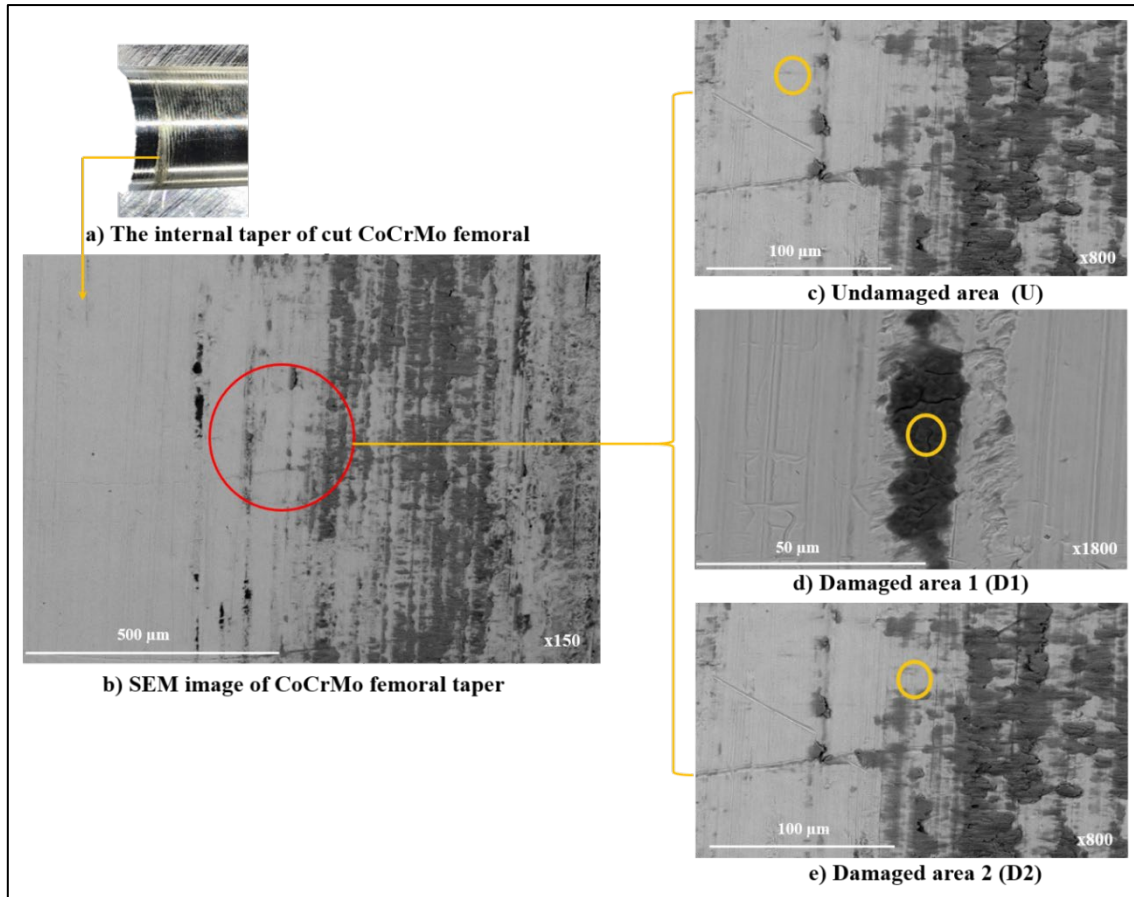


Figure 112 a) The position of the internal taper of a cut CoCrMo femoral head in the SEM, b) SEM image of the same femoral taper showing the area (red circle) where spot EDX analysis were taken, c), d) and e) SEM images of the undamaged area (U1), damaged area 1 (D1) and damaged area 2 (D2), respectively. The yellow circle on each SEM image represent the spot used for EDX analysis.

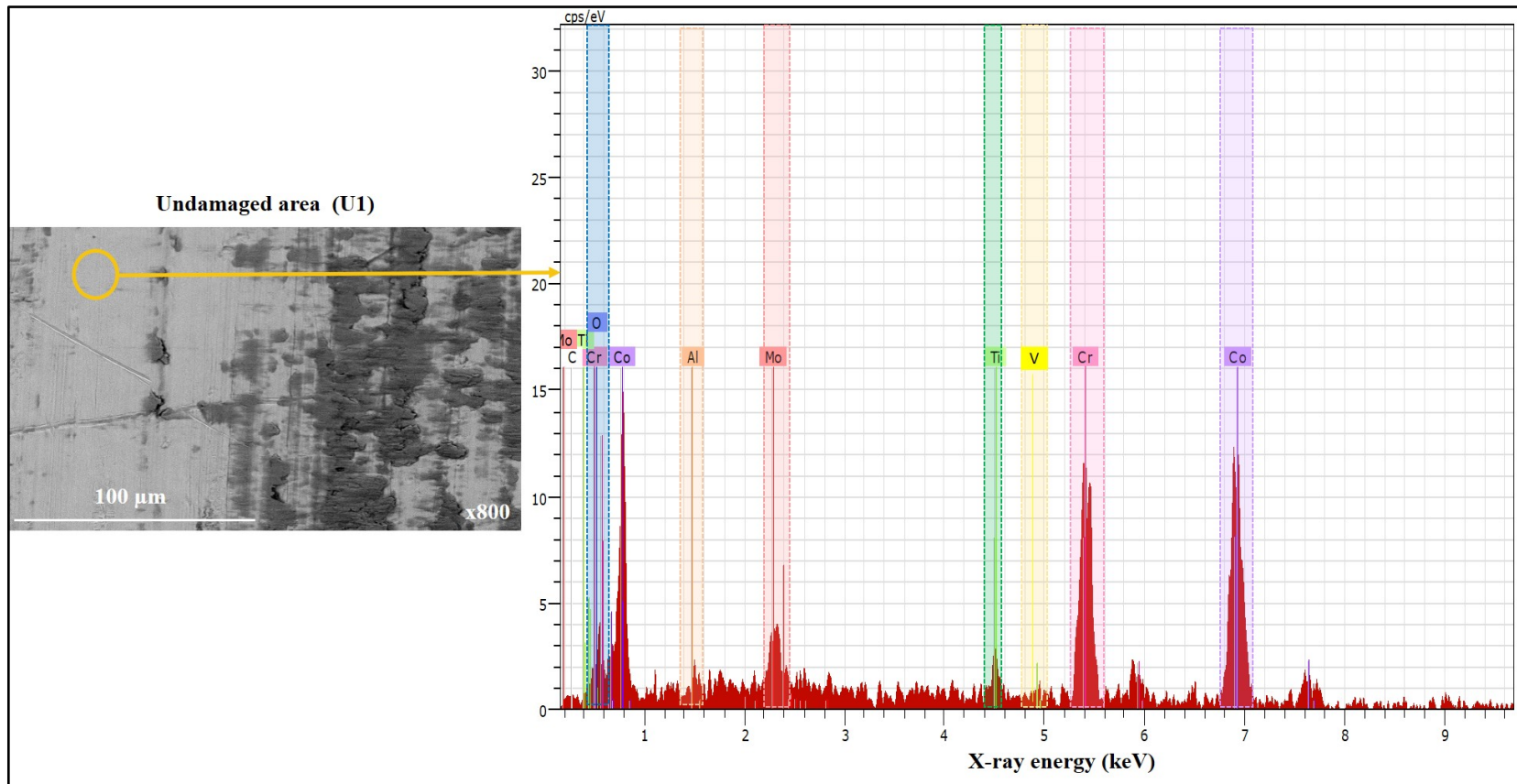


Figure 113 SEM image of the same femoral taper showing the area (yellow circle) where spot EDX analysis was taken and Spot EDX spectrum showing undamaged area (U1).

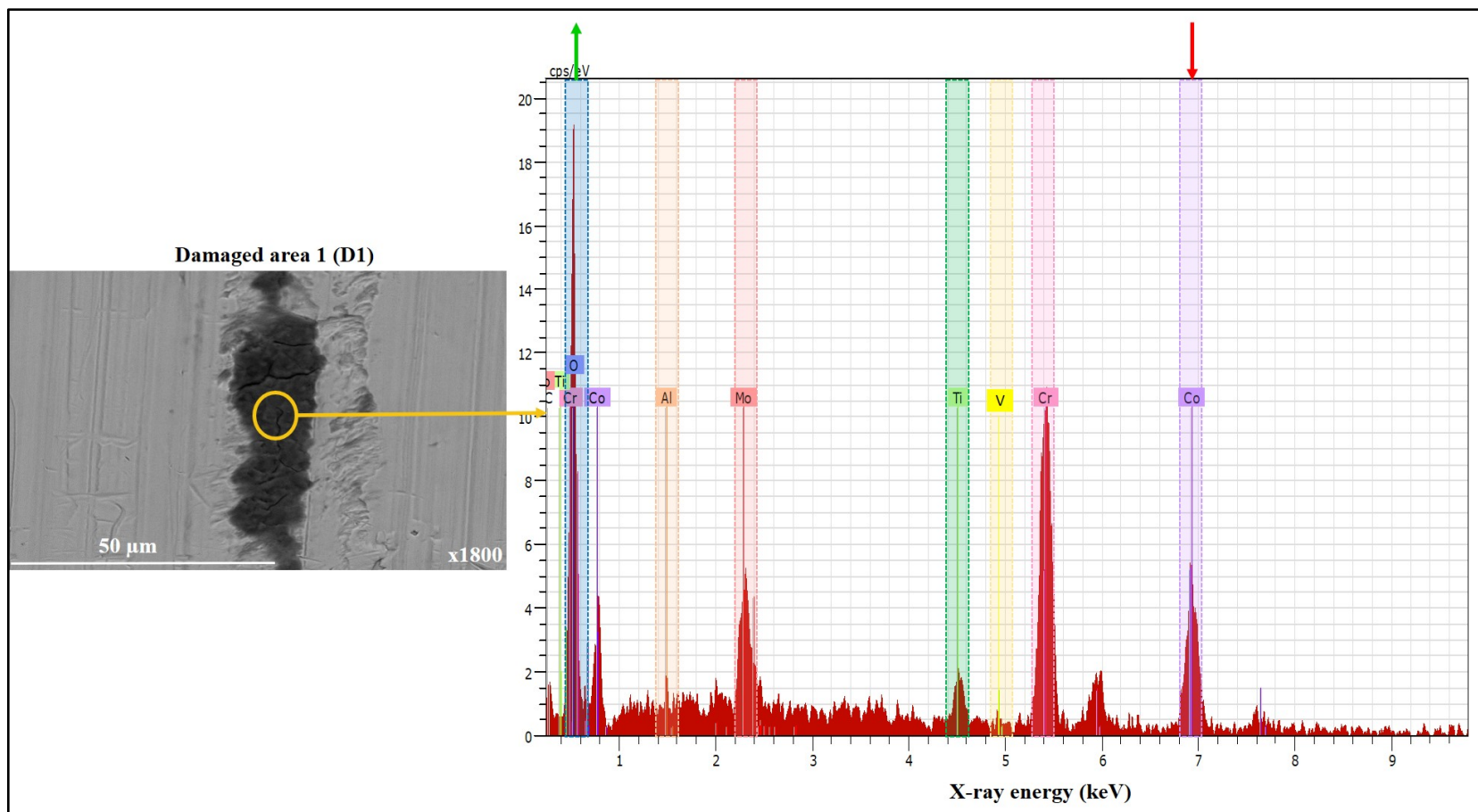


Figure 114 SEM image of the same femoral taper showing the area (yellow circle) where spot EDX analysis were taken and Spot EDX spectrum showing damaged area (D1). The green arrow indicates an increase in Oxygen, whereas the red arrow indicates a decrease in Cobalt.

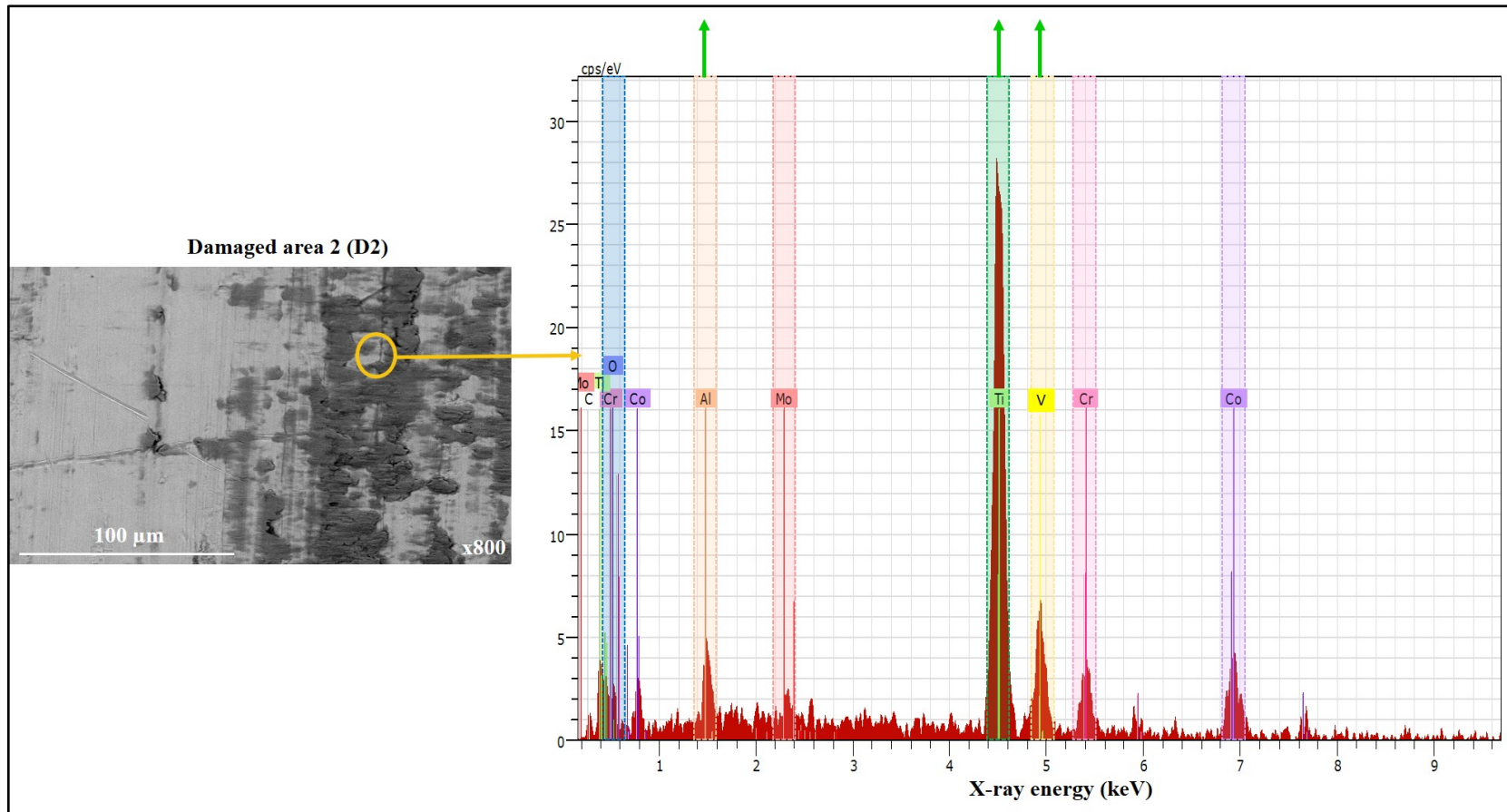


Figure 115 SEM image of the same femoral taper showing the area (yellow circle) where spot EDX analysis were taken and Spot EDX spectrum showing damaged area 2 (D2). Green arrows indicate an increase in the alloying elements of titanium alloy (Ti6Al4V).

Table 27 shows the spot EDX results for the CoCrMo femoral head taken on the polished surface, U1, D1, and D2 areas. The Cr/Co ratio on the polished surface, U1, D1, and D2 was 0.39, 0.41, 1.09 and 0.42, respectively. Area D1 showed a strong presence of O as indicated by EDX spectrum on D1 [see Figure 113 d)]. Furthermore, D1 showed presence of Ti but minimal, or no, presence of Al and V. Area D2 showed a strong presence of Ti, Al and V [as indicated by EDX spectrum on D2, see Figure 113 e)] compared to the polished area and U. Oxygen was present on U1, D1, and D2 except for the polished area suggestive of considerable oxidation took place on the femoral taper. The appearance of carbon was similar in all areas.

Table 27 The spot EDX results showing norm. C [Wt. %] of polished CoCrMo surface and CoCrMo femoral taper used in the hip simulator wear test.

Elements	Polished	CoCrMo femoral taper		
	CoCrMo surface	Undamaged area (U1)	Damaged area 1 (D1)	Damaged area 2 (D2)
	Wt.%	Wt.%	Wt.%	Wt.%
Co K	67.4	62.5	28.5	31.1
Cr K	26.6	25.9	31.2	13.2
Mo L	04.8	04.3	06.7	02.4
C K	01.6	02.7	03.8	02.9
O K	0	01.2	26.5	06.8
Ti K	0	03.0	02.9	39.4
Al K	0	00.2	00.1	03.0
V K	0	00.2	0	01.3

Figure 116 shows the corresponding elemental X-ray map taken on the D1 area. In the red dotted rectangle, Co was absent, and the strong presence of O compared to the outside areas was observed. Additionally, Cr, Mo, C and Ti showed an even distribution on D1 suggestive of the occurrence of mixed oxide inside the red dotted rectangle (as indicated by the spot

EDX results shown in Table 27). Furthermore, the oxidation of the lubricant used in this test may contribute to the presence of O in this area.

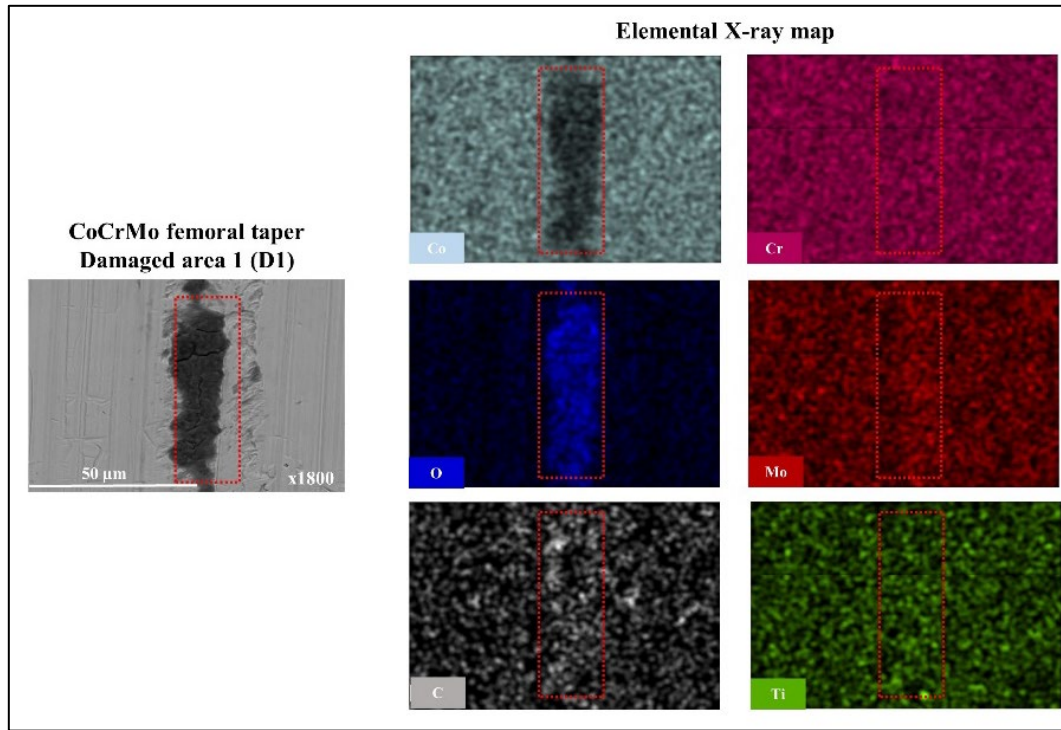


Figure 116 The elemental X-ray map taken on the damaged area 1 of a CoCrMo femoral taper subject to hip simulator wear test. The red dotted rectangle shows the presence of mixed oxides.

The elemental X-ray map acquired on the D2 area showed a strong presence of Ti, Al and V whereas Co, Cr and Mo showed a weak presence inside the area enclosed by a yellow dotted rectangle, see Figure 117. Therefore, suggesting adhesion of the alloying elements of Ti6Al4V trunnions on CoCrMo femoral tapers. On the left side of the dotted rectangle in f, the core elements of CoCrMo femoral tapers Co, Cr and Mo are clearly seen on the elemental X-ray map. However, an absence of Ti and a very weak presence of Al and V was observed, representing comparatively undamaged CoCrMo surface.

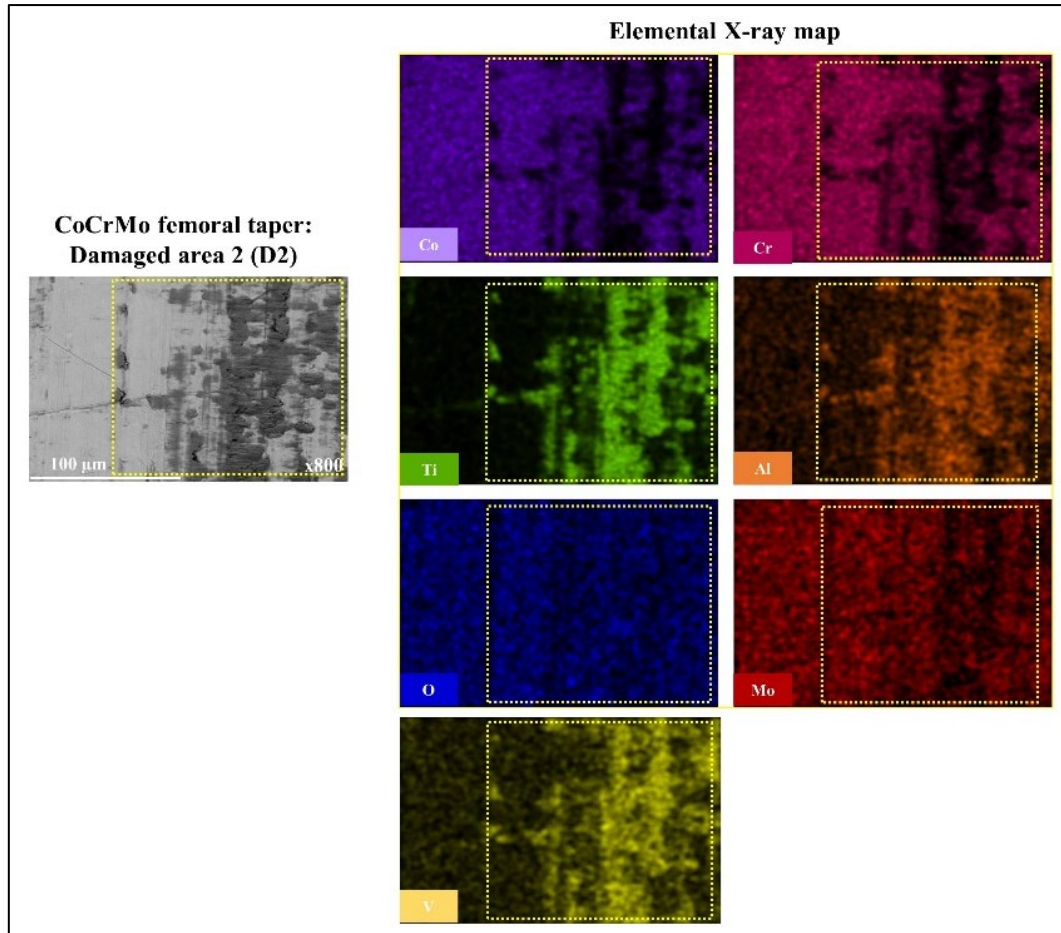


Figure 117 The elemental X-ray map taken on the damaged area 2 of a CoCrMo femoral taper subject to hip simulator wear test. The yellow dotted rectangle showing a strong presence of alloying components of Ti6Al4V trunnion.

4.4.6 Quantification of the material loss from the bearing surfaces

4.4.6.1 Gravimetric analysis of the bearing surfaces

After 5 million cycles, the volumetric wear rate (mean \pm standard deviation) for the CoCrMo femoral heads was 0.057 ± 0.020 mm³/Mc, and for the XLPE acetabular liners it was 2.74 ± 0.74 mm³/Mc. The mean volumetric wear rates for all CoCrMo femoral heads and XLPE acetabular liners from the hip simulator wear test, measured gravimetrically are shown in Figure 118 and Figure 120, respectively. The total volumetric wear over 5 million cycles was 0.38 mm³ for the CoCrMo femoral heads and 14.28 mm³ for the XLPE acetabular liners. Additionally, there was no statistically significant difference in the volume loss of CoCrMo Head 1, CoCrMo Head 2, CoCrMo Head 3 and CoCrMo Head 5 with adjusted p-value >0.999 , see Figure 119. However, the volume loss of CoCrMo Head 5 was statistically

significant when compared to all other heads with adjusted p-value < 0.001. Moreover, there was no statistically significant difference in the volume loss of all test XLPE liners with adjusted p value > 0.999, see Figure 121.

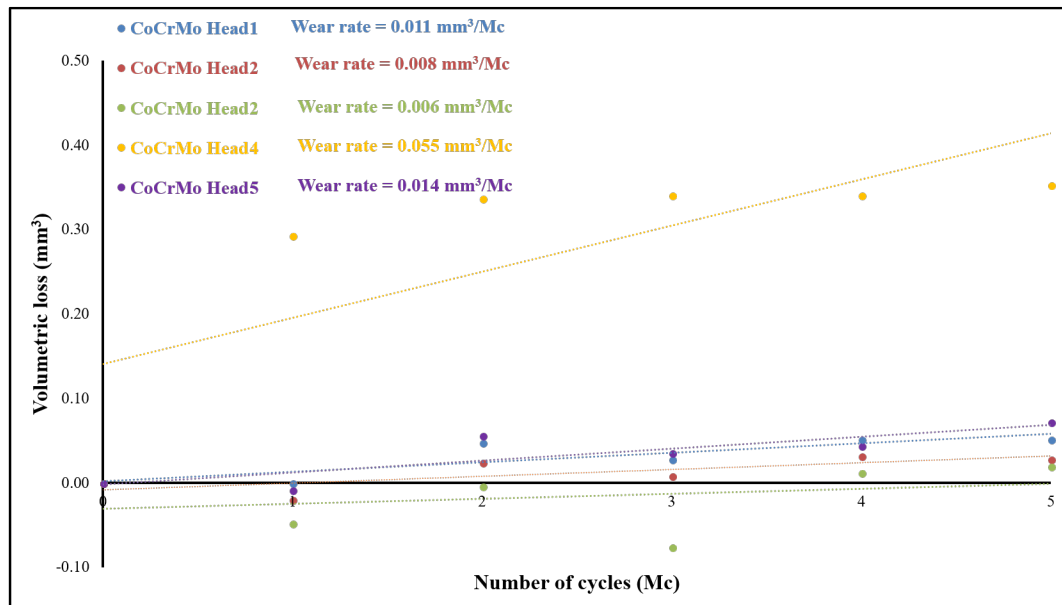


Figure 118 Mean volumetric measurements of all CoCrMo femoral heads from MoXLPE hip simulator wear test (measured gravimetrically).

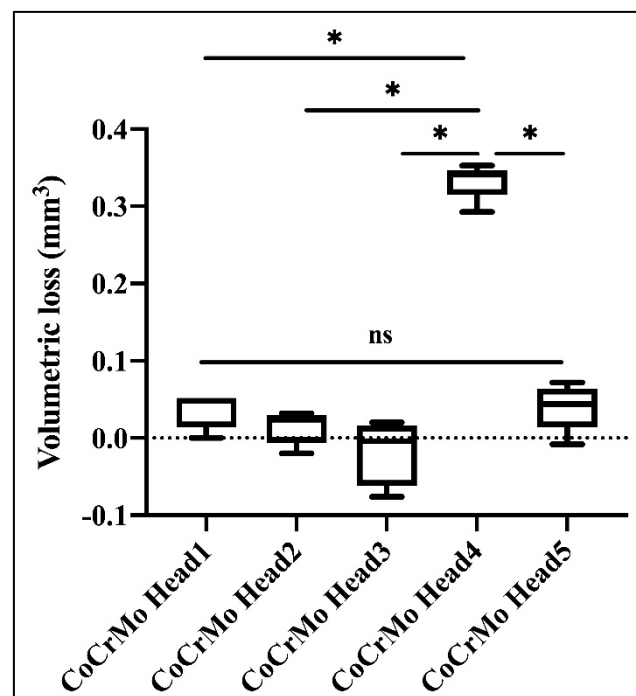


Figure 119 Box-plot of volumetric measurement of all CoCrMo heads from MoXLPE hip simulator wear test (measured gravimetrically). ns: no significant difference with adjusted p-value >0.999 and *: p<0.001.

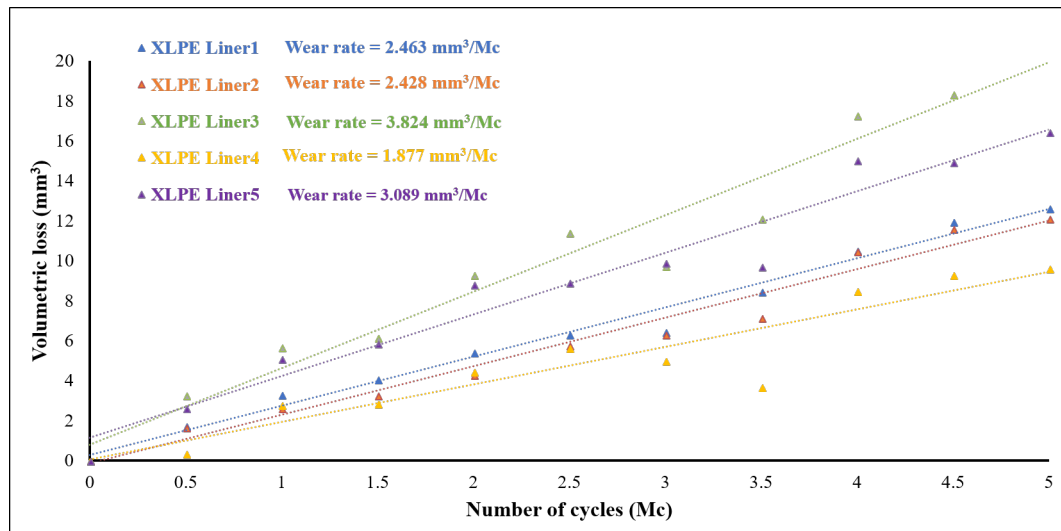


Figure 120 Mean volumetric measurements of all XLPE acetabular liners from MoXLPE hip simulator wear test (measured gravimetrically).

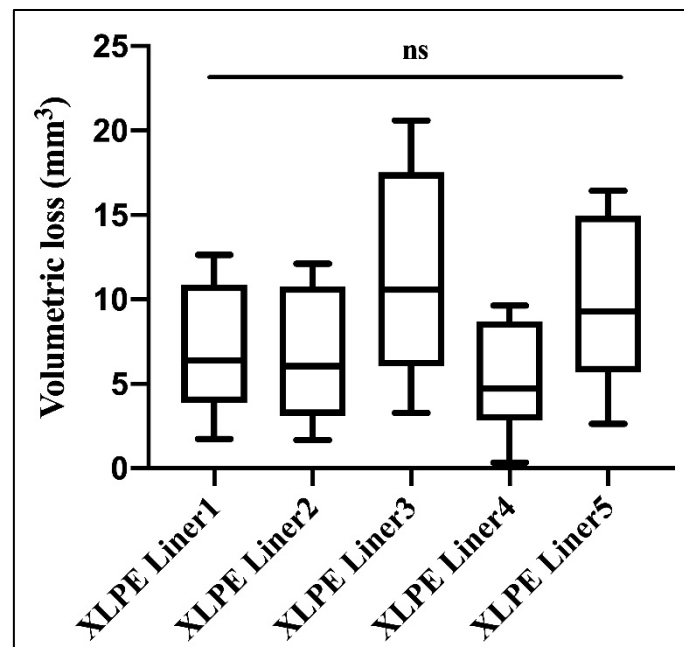


Figure 121 Box-plot of volumetric measurement of all XLPE liners from MoXLPE hip simulator wear test (measured gravimetrically). ns: no significant difference with adjusted p-value >0.999.

The mean volumetric wear rate of the femoral tapers obtained geometrically using the CMM ($0.045 \pm 0.024 \text{ mm}^3/\text{Mc}$) was not statistically different ($p = 0.416$) to the mean volumetric wear rate obtained gravimetrically for the femoral heads ($0.057 \pm 0.020 \text{ mm}^3/\text{Mc}$).

Therefore, based on these measurements, most of the metallic material loss came from the taper and not from the bearing surface. Figure 122 shows the mean volumetric wear rates of CoCrMo femoral heads and Ti trunnions. The volumetric wear rate of the CoCrMo heads was not significantly different from the Ti trunnions ($p = 0.592$).

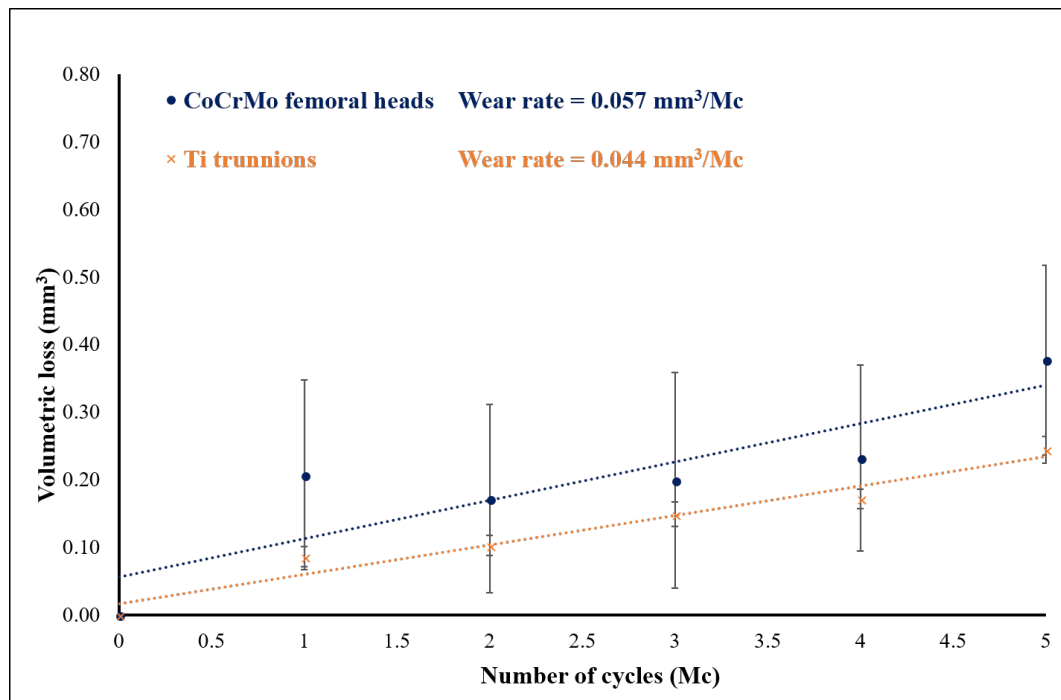


Figure 122 Mean volumetric wear of CoCrMo femoral heads and titanium trunnions (measured gravimetrically). Error bars represent \pm standard deviation.

4.4.7 Three-dimensional (3D) surface roughness (S_a) of the bearing surfaces

Figure 123 and Figure 124 shows the mean 3D surface roughness (S_a), pre and post-test, for the CoCrMo femoral heads and XLPE acetabular liners used in the MoXLPE hip simulator wear test, respectively. There was no statistically significant difference in the S_a values pre and post-test for the CoCrMo femoral heads ($p = 0.338$), with S_a values, pre-test 0.007 ± 0.003 and post-test 0.008 ± 0.003 μm . However, the XLPE acetabular liners showed a statistically significant decrease ($p < 0.001$) in roughness with an associated removal of the original machining marks, with S_a values, pre-test 1.192 ± 0.217 and post-test 0.041 ± 0.016 μm . Indicative surface topography images of the bearing surfaces of the CoCrMo femoral heads and XLPE acetabular liners obtained using the Zygo non-contacting profilometer, pre and post MoXLPE hip simulator wear test, are shown in Figure 125 and Figure 126, respectively.

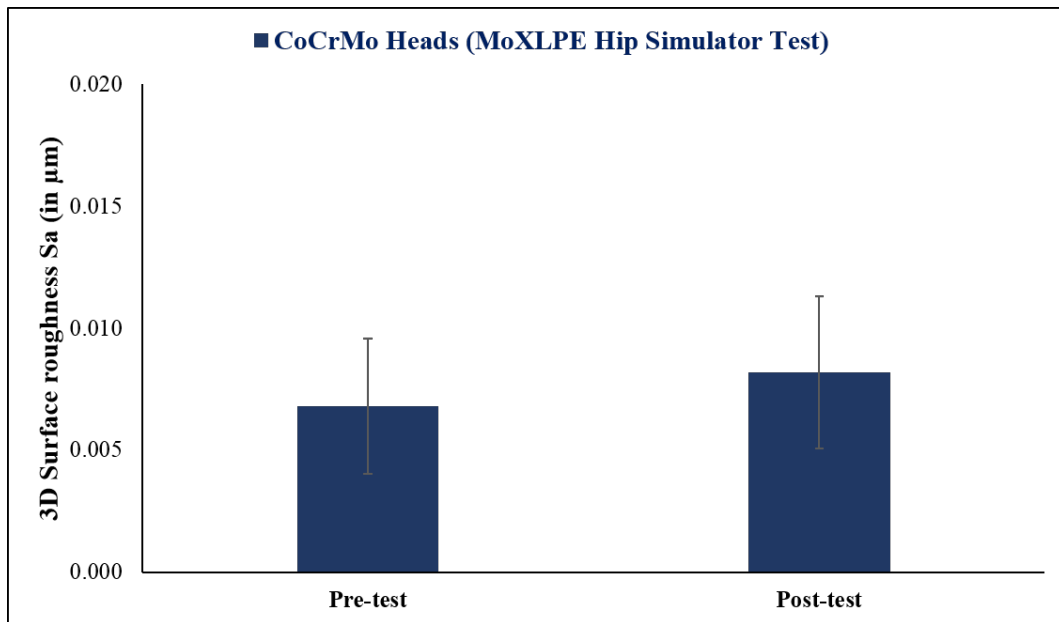


Figure 123 Mean 3D surface roughness Sa (in μm), of CoCrMo femoral heads measured pre and post-MoXLPE hip simulator wear test. Error bars represent \pm standard deviation.

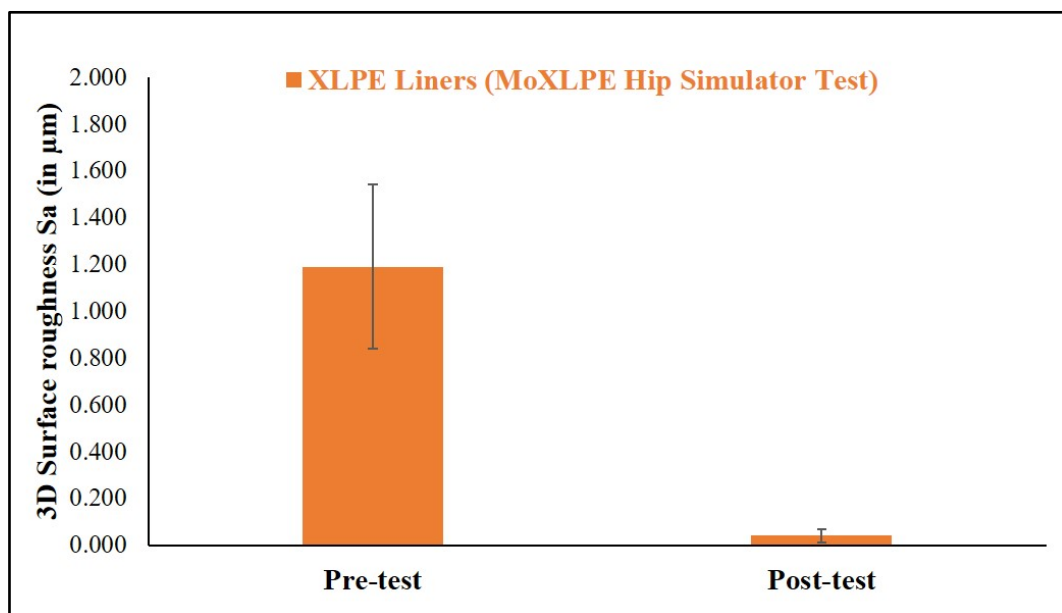


Figure 124 Mean 3D surface roughness Sa (in μm), of XLPE liners, measured pre and post-MoXLPE hip simulator wear test. Error bars represent \pm standard deviation.

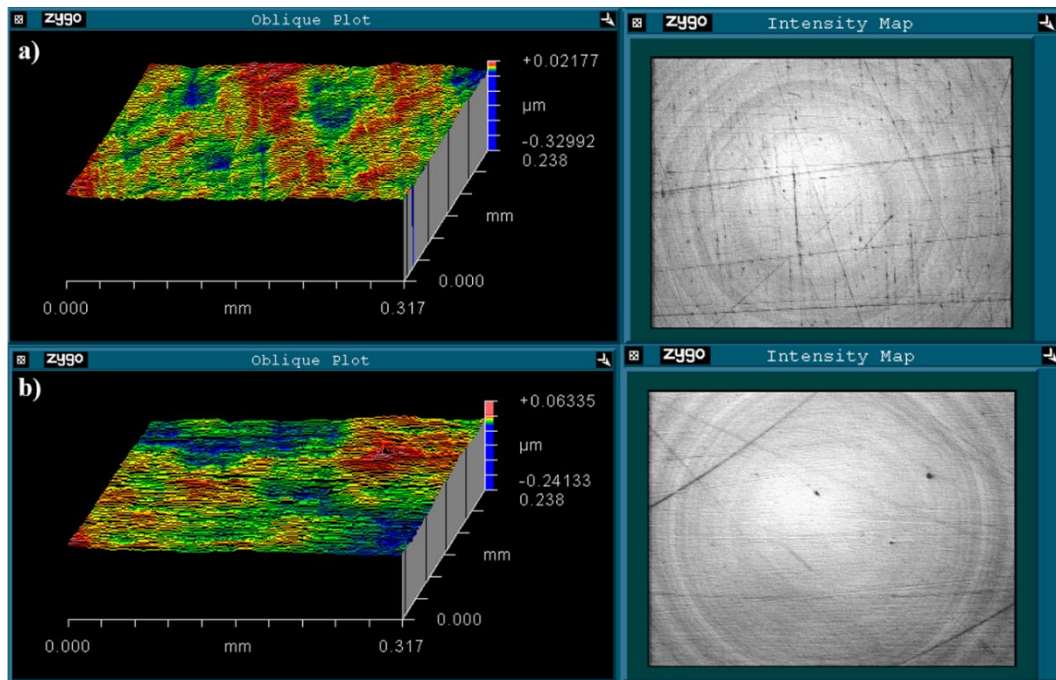


Figure 125 Surface topography images of a CoCrMo femoral head a) pre-test ($S_a = 0.005 \mu\text{m}$) and b) post-test ($S_a = 0.006 \mu\text{m}$).

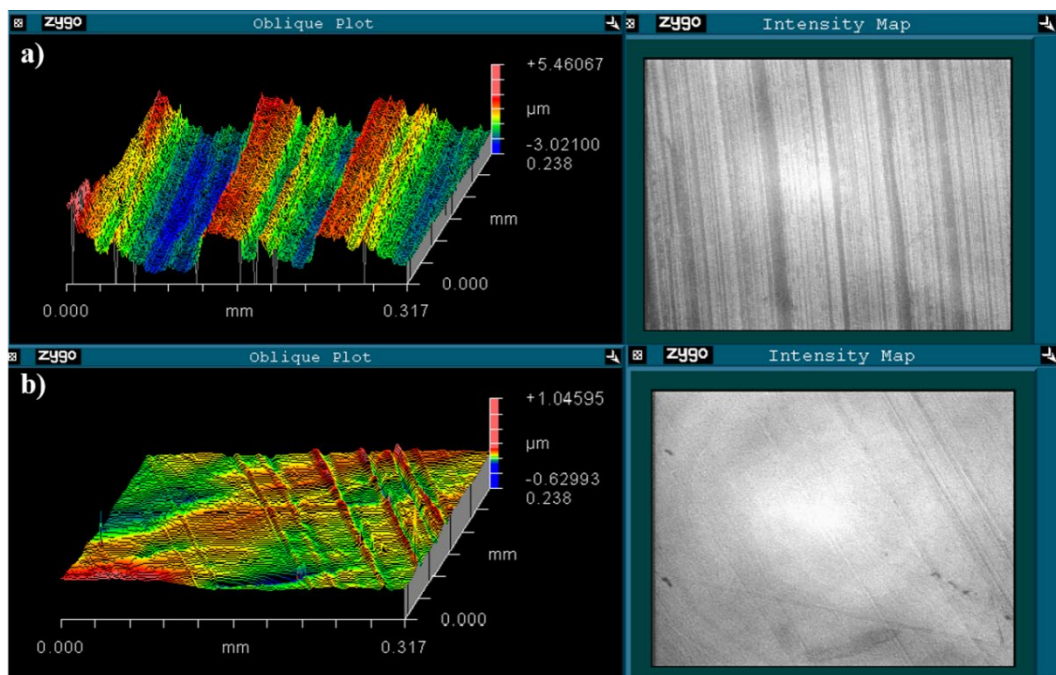


Figure 126. Surface topography images of an XLPE acetabular liner a) pre-test ($S_a = 1.080 \mu\text{m}$) and b) post-test ($S_a = 0.042 \mu\text{m}$).

4.4.8 Microscopic inspection of the backside of the XLPE liner

An optical micrograph taken with $3.5\times$ magnification at the backside of XLPE liner is shown in Figure 127. This shows minimal damage and the original machining marks, and therefore an absence of wear.

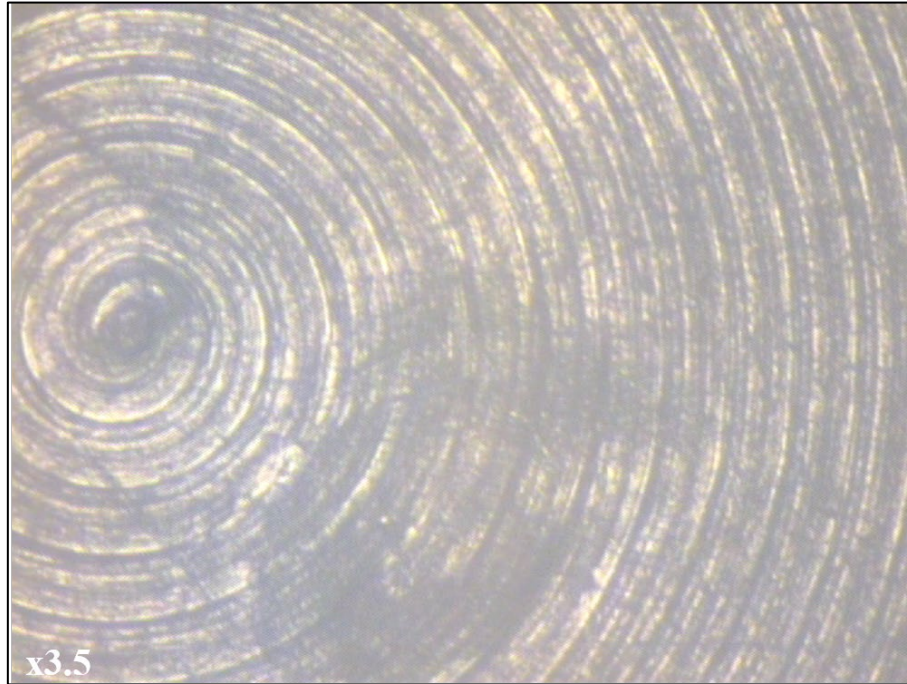


Figure 127 An optical microscopic image at a $3.2\times$ magnification of the backside of XLPE liner taken at the end of hip simulator testing, showing original machining marks, and thus an absence of wear.

4.5 Metal debris analysis

This section gives the results obtained from the SEM coupled with EDX analysis of the metallic wear debris after CoC hip simulator test. Then, the ICP-MS analysis on the lubricant samples of MoXLPE hip simulator wear test are presented.

4.5.1 Ceramic-on-ceramic (CoC) hip simulator wear test

Figure 128 shows SEM coupled with EDX analysis of the lubricant samples after the CoC hip simulator test. As can be seen from Figure 128, EDX analysis confirmed the presence of Ti within the lubricant. Thus, supporting material loss from Ti trunnion wear as indicated by reduction in mass and decrease in roughness.

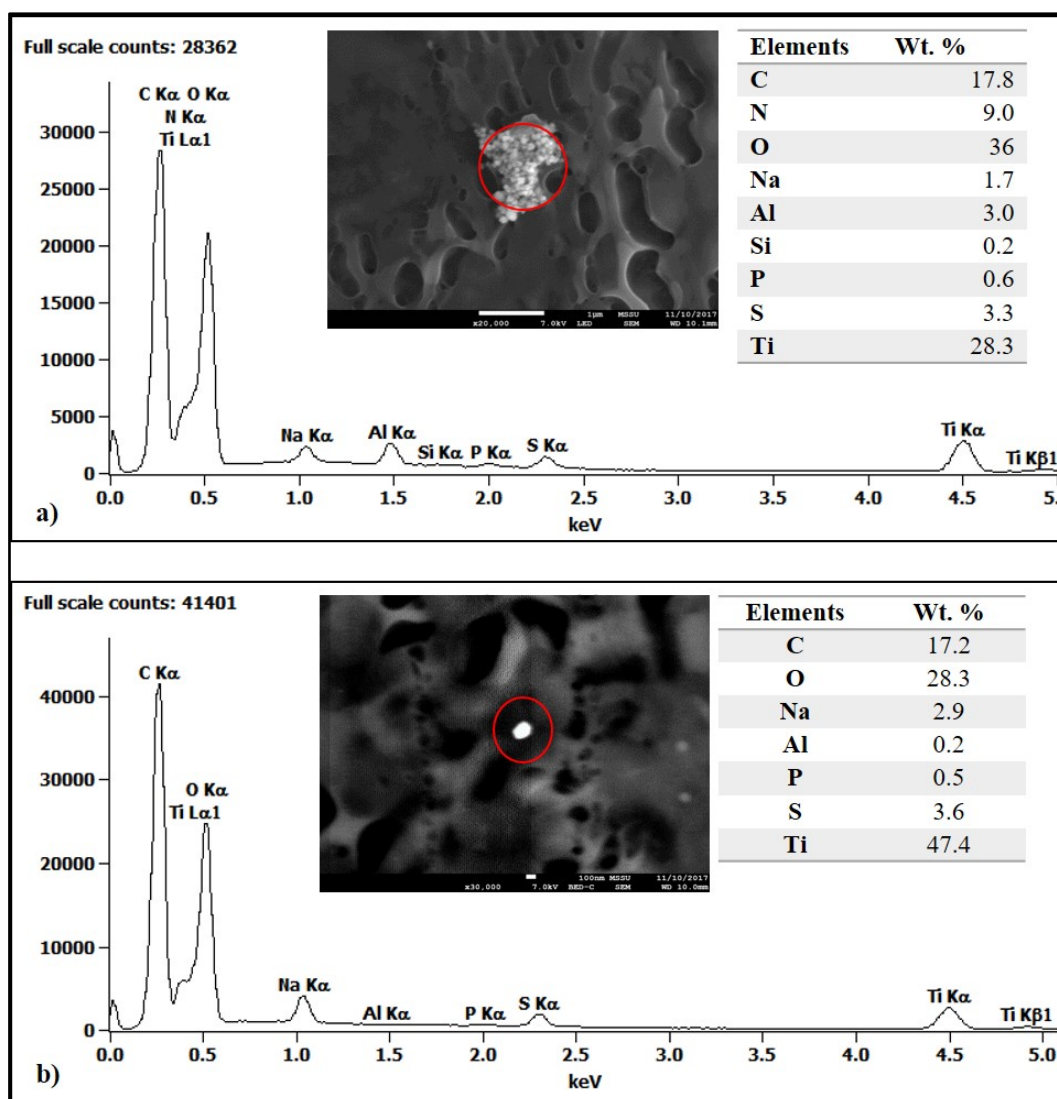


Figure 128 a) and b) SEM coupled with EDX analysis of the lubricant samples showing the presence of titanium. Red circles on SEM images represents a spot of EDX analysis. Tables in a) and b) represent spot EDX analysis on the points respectively.

4.5.2 Metal-on-cross-linked polyethylene (MoXLPE) hip simulator wear test

Figure 129 shows Co, Cr and Ti ion concentration [in $\mu\text{g/L}$ or parts per billion (ppb)] of the lubricant samples at different intervals of the MoXLPE hip simulator test and the unused lubricant sample. As can be seen from Figure 129, Co, Cr and Ti ions from MoXLPE hip simulator test lubricant were elevated more than in the unused lubricant sample. Thus, supporting material loss from CoCrMo femoral tapers and Ti trunnions as indicated by other experimental data.

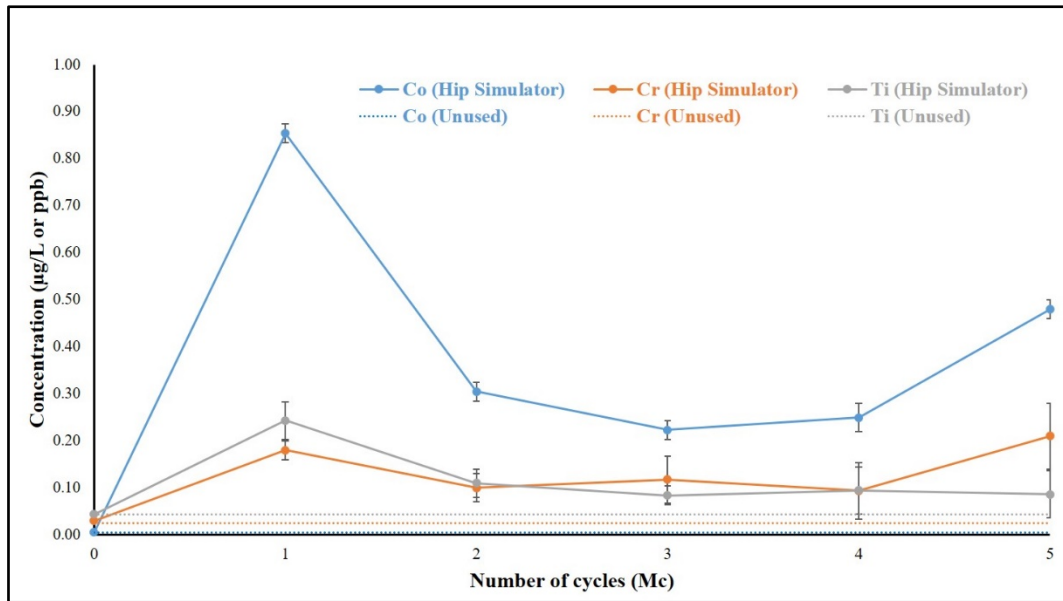


Figure 129 Lubricant cobalt (Co), chromium (Cr) and titanium (Ti) ion concentration at different intervals of the MoXLPE hip simulator wear test. Dotted lines indicate Co, Cr and Ti ions measured from the unused lubricant. Error bar represents \pm standard deviation.

4.6 Lubricant pH measurement

This section gives the results from lubricant pH measurement every 500,000 cycles of CoC and MoXLPE hip simulator wear tests. The pH of the lubricant showed an increase with a range of 7.18-7.77 after every 0.5 Mc of CoC hip simulator wear test compared to pre-test lubricant ($\text{pH} = 7.06 \pm 0.02$), see Figure 130.

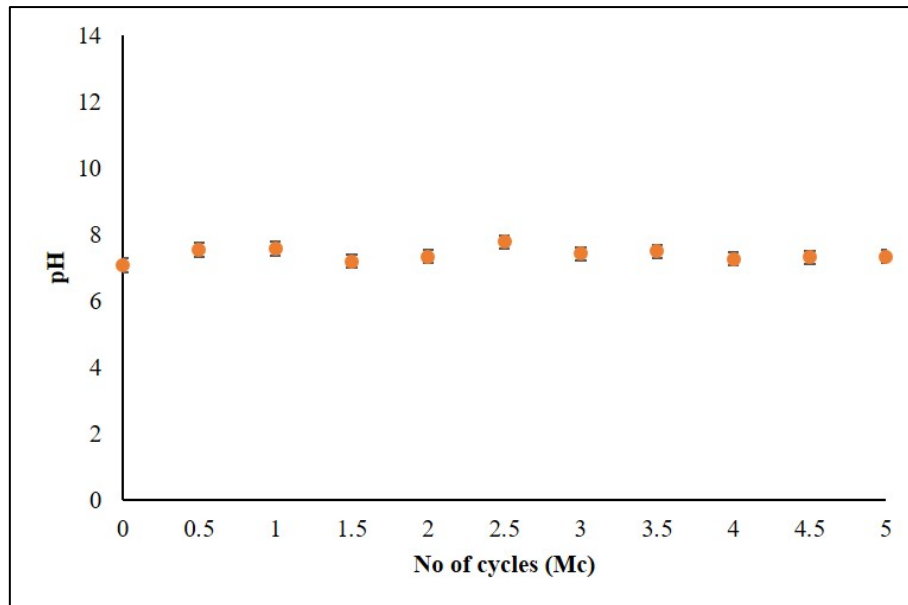


Figure 130 pH of the lubricant measured over every 0.5Mc of the CoC hip simulator test. Error bars represent \pm standard deviation.

In MoXLPE hip simulator test, the pH of the lubricant showed an increase with a range of 7.49-8.15 after every 0.5 Mc compared to pre-test lubricant ($\text{pH} = 7.13 \pm 0.02$), see Figure 128.

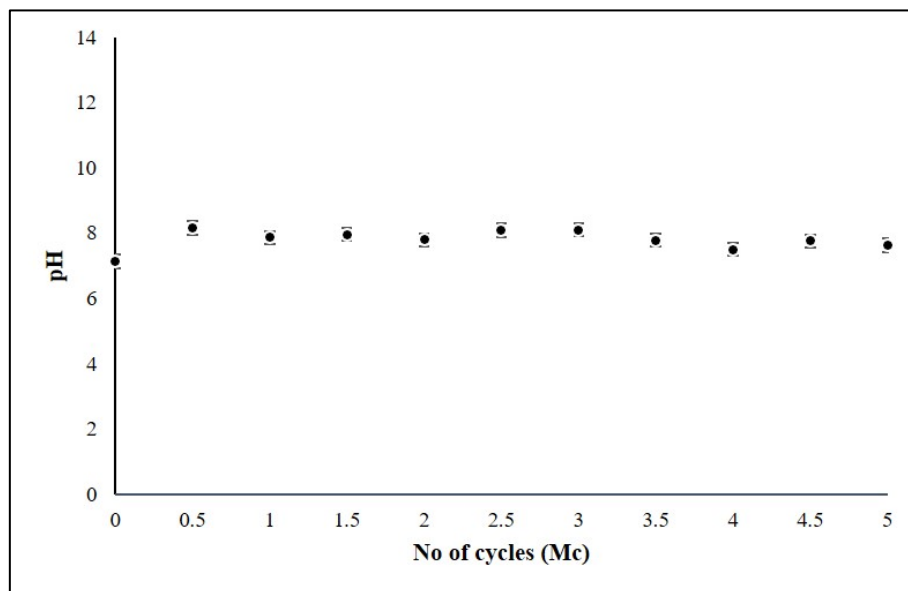


Figure 131 pH of the lubricant measured over every 0.5Mc of the MoXLPE hip simulator test. Error bars represent \pm standard deviation.

4.7 Wettability measurement

This section gives the results from the contact angle measurements, pre-and post-hip simulator wear test of the ceramic and metallic femoral heads.

Figure 132 a) and b) shows the contact angle (CA) measurement, pre and post-test, for a ceramic femoral head used in the CoC hip simulator wear test and for a CoCrMo femoral head used in the MoXLPE hip simulator wear test, respectively. There was no statistically significant difference in the mean CA values pre and post-test for the ceramic femoral heads ($p = 0.870$), with CA values, pre-test (61.20 ± 5.23)° and post-test (61.80 ± 2.52)°. Furthermore, there was no statistically significant difference in the mean CA values pre and post-test for the CoCrMo femoral heads ($p = 0.842$), with CA values, pre-test (63.00 ± 3.37)° and post-test (62.49 ± 2.56)°.

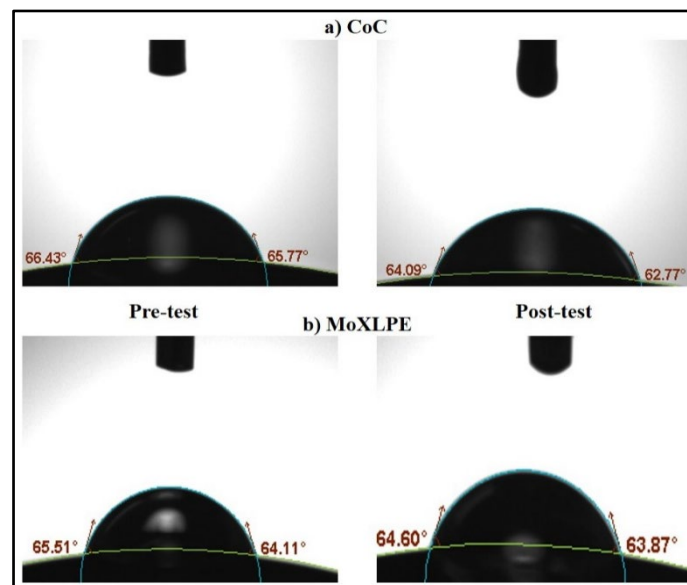


Figure 132 Contact angle measurement at the pole area of a) ceramic femoral head used in the CoC hip simulator wear test and b) CoCrMo femoral head used in the MoXLPE hip simulator wear test.

Chapter 5: Discussion

In this chapter, the experimental results are discussed, and limitations of these tests are considered.

5.1 Hip simulator wear testing of the taper-trunnion junction and bearing surfaces of modular CoC hip prostheses

This section discusses the experimental results obtained from hip simulator wear testing of the taper-trunnion junction and bearing surfaces of modular CoC hip prostheses. The necessity of testing both the taper-trunnion junction and bearing surfaces in a single test is explained. Then, the wear results and the damage pattern from the taper-trunnion junction of CoC hips are compared with results from retrieval studies. Next, the discrepancy in laboratory and clinical performance of CoC and MoP hips is described, and a possible explanation for ARMD in CoC hips is provided. Finally, wear from the bearing surfaces of CoC hips is compared with previous CoC hip simulator studies published in the literature.

This is the first long term hip simulator study to report wear generated from the taper-trunnion junction of a contemporary CoC hip joint. Retrieval studies of hip prostheses have indicated that material loss and debris formation is not only limited to the bearing surfaces but also arises from the taper-trunnion junction^{18,19,26,126,241}.

Some may suggest that it is not feasible to test both the taper-trunnion junction and the bearing surfaces in a single hip simulator test. This thesis contends that this is not only possible, but it is essential. If bearing surfaces show low wear, yet wear at the trunnion takes place, then this needs to be identified so that patients are protected, and surgeons are not led to believe in a ‘low wear’ bearing combination that causes material loss elsewhere. However, these statements are founded on the test set up, reproducing the clinical situation as closely as possible. It is postulated that the TE86 hip simulator does this, due to dynamic loading being applied to the test samples (see Figure 51) such that toggling of the femoral head on the trunnion, as seen on explanted hip prostheses^{18,19}, is reproduced.

5.1.1 Wear at the taper-trunnion junction of CoC prostheses used in the hip simulator wear test: ceramic-on-metal contact.

Based on the CoC hip simulator wear data, the Ti trunnions (total wear = 0.29mm^3) wore at a similar amount to that of the CoC bearing surfaces (total wear = 0.25mm^3). Other experimental data also indicated Ti trunnion wear. The Ti trunnion surfaces measured with a 2D contacting profilometer showed a statistically significant decrease ($p < 0.001$) in Ra post-test (see Figure 86). Moreover, the worn area of the trunnions showed a statistically significant decrease ($p < 0.001$) in 3D surface roughness (Sa) compared to that of the unworn area (see Figure 87). This decrease in surface roughness was due to an elimination of the original machining marks.

5.1.1.1 Comparison with retrieval studies

In an explant study, Langton et al. investigated the taper wear of 126 large-diameter MoM hips. Analysis of the position of the femoral taper damage suggested that a toggle effect from the femoral head was causing the damage at the taper surface¹⁹. In another explant study of modular MoM hips, Bishop et al. also suggested that the wear at the taper-trunnion junction was generated by the toggling of the CoCrMo femoral head on the stem¹⁸. As a similar wear pattern was observed in this simulator study, it is suggested that there is a similar toggling of the ceramic femoral head, as shown in Figure 133. However, in this study wear was apparent on the trunnion, likely due to the relative hardness of the ceramic compared to the Ti.

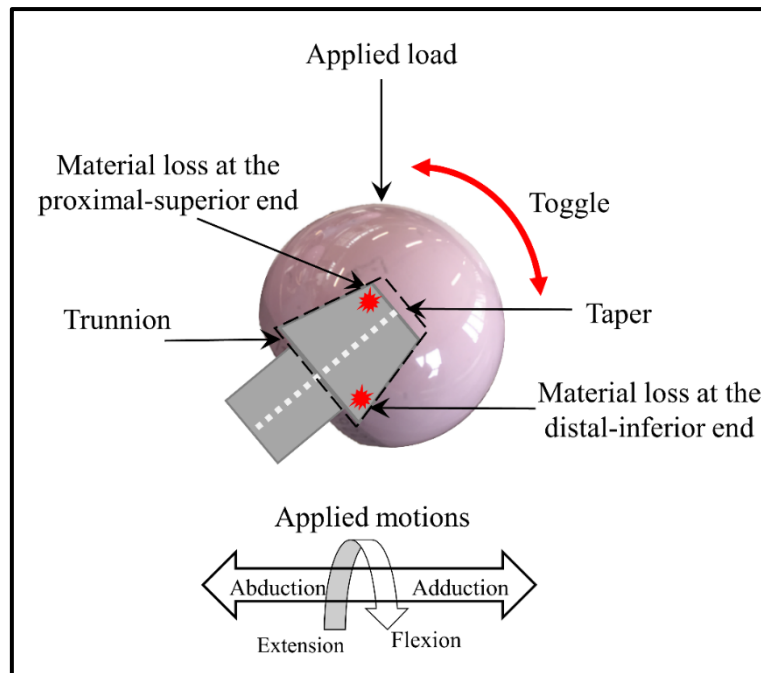


Figure 133 A test ceramic femoral head and trunnion assembly with applied load and applied motions, showing toggling and the material loss at two distinct areas (shown in red). Image from Bhalekar et al. (2018)²⁹⁵.

The femoral head tapers showed a statistically insignificant change ($p > 0.05$) in the 2D surface roughness (R_a) post-test indicating minimal material loss from the ceramic femoral tapers. A grey coloured ring, visible at the proximal end of the ceramic femoral taper, likely indicated adhesive wear from the Ti trunnion onto the ceramic femoral taper. This is in agreement with a retrieval study by Kocagoz et al., which detected metallic material transfer on the ceramic femoral taper surface of CoC and CoP retrievals²⁴¹. The same study reported no fretting corrosion or material loss at the ceramic tapers; again, this is in agreement with experimental results obtained from the present CoC hip simulator study. The retrieval study also quantified the volumetric material loss from retrieved trunnions with the wear rate ranging from 0.0-0.37 mm³/year. If one million cycles in the hip simulator are equivalent to 1 year *in vivo*³⁰⁹, then the mean wear rate (0.061 mm³/year) of the Ti trunnions obtained in the CoC hip simulator test reported here is within the range obtained from this retrieval study.

5.1.1.2 Is there a possibility that the trunnion wear in the CoC bearings is larger than that in the CoP?

Might there be a difference in taper-trunnion wear between CoC hips and CoP hips? To begin to answer this question, one should probably start by considering wear at the bearing

surfaces. Here, one would expect far less wear from CoC hips than from CoP hips. However, this result is not reflected in data from the largest joint registry in the world, the NJR. Here, CoP hips show lower revision rates than CoC hips. A possible reason could be more considerable damage at non-bearing surfaces (i.e. the taper-trunnion) of CoC hips compared to CoP. The reason being that the PE liner could act to ‘soften the blow’ of peak forces during gait and other activities. An indicative engineering comparison of a CoP hip with a CoC hip might be a mallet in comparison with a hammer. While both transmit loads, mallets are deliberately softer to lessen damage to materials. Moreover, as a load-bearing surface in biological environment, the PE subjected to static as well as dynamic loading and may behave viscoelastically at body temperature³²⁰. Examples of viscoelastic behaviours are stress relaxation, creep, fatigue, and dynamic mechanical properties. Viscoelastic behaviours are intrinsic properties of a PE compared to ceramic materials. This hypothesis should be explored in future work.

5.1.2 A possible explanation for adverse reaction to metal debris (ARMD) in CoC hip implants

Ceramic-on-ceramic hip joints, as an alternative to conventional MoP, have shown lower wear in both *in vitro*^{196,197,199-202,209,210,296} and retrieval studies^{207,208}. However, the overall risks of revision for an uncemented THR at 14 years are similar at 6.12% and 6.40% for CoC and MoP respectively⁵. The reasons for revision are multi-factorial, including infection, dislocation and fracture. However, a question that may arise is: why, particularly at longer follow-ups shown in established joint registries, the potential wear-related benefits of all-ceramic articulations do not appear to be seen. In an explant study, Milošev et al. found extensive wear on the Ti trunnion which was fitted into the ceramic femoral head of the failed prostheses³²¹. Furthermore, wear debris particles isolated from the periprosthetic tissue were shown to be the same as that of the trunnion metal alloy. A recent clinical study by Matharu et al. found more ARMD in CoC hips than MoP hips²⁴. This is in spite of there being fewer metallic components in a CoC hip than a MoP hip. The *in vitro* study described in this thesis has shown that one source of metal debris in a CoC hip is the taper-trunnion junction.

5.1.2.1 Influence of different head offsets on trunnion wear

The modularity of femoral heads and femoral stems with different offsets potentially allows surgeons to restore the natural anatomy of the hip^{82,83}. In this wear test, the same type of CoC hip prosthesis with identical neck lengths was used. In an explant study on the taper-trunnion junction of CoC, CoP and MoP hip prostheses, Kocagoz et al. found no correlation between the head offset and the material loss²⁴¹. However, Langton et al. in another explant study on large-diameter MoM hips found a positive correlation between the head offset and the material loss¹⁹. Therefore, further investigations in this area are likely to be of value.

5.1.3 Wear at the bearing surfaces of CoC joints used in the hip simulator wear test

As shown in Table 28, previous CoC hip simulator studies have not reported wear from the taper-trunnion junction and offered only wear at the bearing surfaces^{196,197,199-202,209,210,296}. The mean wear rate of the CoC joints reported in this study, $0.067 \pm 0.003 \text{ mm}^3/\text{Mc}$, is comparable to wear rates found in the literature^{196,197,199-202,209,210,296}. The Sa of the bearing surfaces showed negligible change. Pre-test values for heads and liners were 0.003 ± 0.002 and $0.005 \pm 0.001 \text{ }\mu\text{m}$ respectively, while post-test they were 0.004 ± 0.001 and $0.005 \pm 0.001 \text{ }\mu\text{m}$ respectively. These values are comparable to post-test surface roughness values from previous simulator studies^{196,197,199-202,209,210,296} as seen in Table 28. These relatively unchanged roughness measurements imply minimal wear of the ceramic bearing surfaces.

Table 28 Laboratory wear rates found for different CoC hip joints under standard testing conditions compared with this study.

Authors (year)	CoC materials	Head Size (in mm)	Surface roughness (µm)		CoC Wear rate (mm³/Mc) (Mean ± SD)	Trunnion wear rate (mm³/Mc)
			H: Heads and L: Liners			
			Pre-test	Post-test		
Smith et al ¹⁹⁶ (2001)	BIOLOX [®] <i>forte</i>	28	H: 0.001	H: 0.004	0.097 ± 0.039	Not measured
Nevelos et al ²⁰⁰ (2001)	BIOLOX [®] <i>forte</i>	28	H+L: ~ 0.005	H+L: ~ 0.005	~ 0.05	Not measured
Nevelos et al ²⁰⁹ (2001)	BIOLOX [®] <i>forte</i>	28	-	No change detected	0.09 ± 0.04	Not measured
Tipper et al ²¹⁰ (2001)	BIOLOX [®] <i>forte</i>	28	H: 0.005-0.008	No change detected	0.05 ± 0.02	Not measured
Richardson et al ¹⁹⁹ (2005)	Alumina-on-Alumina	28	-	-	< 0.01	Not measured
Essner et al ²⁰¹ (2005)	Alumina-on-Alumina	32	H+L: ~ 0.01	-	< 0.1	Not measured
Spinelli et al ²⁰² (2009)	BIOLOX [®] <i>forte</i>	36	H: 0.01 L: 0.01	H: 0.01 L: 0.01	-	Not measured
Al-Hajjar et al ¹⁹⁷ (2010)	BIOLOX [®] <i>delta</i>	36	-	H+L: ~ 0.005	0.05	Not measured
This study	BIOLOX [®] <i>delta</i>	36	H: 0.003 ± 0.002 L: 0.005 ± 0.001	H: 0.004 ± 0.001 L: 0.005 ± 0.001	0.067 ± 0.003	0.061 ± 0.015

5.2 Importance of the DL test

This section considers the importance of the DL test and employment of articulating motion in the testing of the taper-trunnion junction of modular THR.

The major difference between the CoC hip simulator and DL tests described in this thesis was that the motion (gait) was applied to the hip simulator wear test samples while no articulating motion was applied to the DL test sample. Perhaps surprisingly, there was a comparable amount of wear from the wear test samples (0.25mm^3) as from the DL sample (0.23mm^3). A possible reason could be the material loss from the bearing surfaces of the DL sample may be due to fretting wear. This has been reported previously for alumina rubbing against alumina³²² but is a topic that deserves further investigation in relation to CoC hips. Furthermore, the ASTM F1875 standard for fretting corrosion testing of modular THR employs only uniaxial dynamic loading³⁸. However, employment of articulating motion showed increased wear from the CoC hip simulator test trunnions (0.29mm^3) than from the DL test trunnion (0.05mm^3). Thus, indicating the importance of employing articulating motion in the testing of the taper-trunnion junction of modular THR.

5.3 Importance of the impaction test

This section discusses the importance of the impaction test performed on a ceramic femoral head mounted on a Ti alloy trunnion.

The impaction test was performed, in order to study the potential effect of material loss due to assembling and disassembling the femoral heads on the trunnions. The experimental results from the impaction test confirmed that the assembling/disassembling procedure did not affect either the gravimetric or surface roughness measurements for either the Ti trunnion or the taper of the ceramic femoral head. Based on the impaction test results, the assembling/disassembling procedure had no effect either the gravimetric or surface roughness measurements of the CoC hip simulator test as well. This is in agreement with Grosso et al. impaction study, which reported the assembling/disassembling procedure had no significant

damage to Ti6Al4V trunnions (Stryker) or ceramic femoral tapers (32mm BIOLOX[®] *delta*)²⁸².

5.3.1 Metal debris analysis: CoC hip simulator wear test

Titanium trunnion wear (total wear = 0.29mm³) after the CoC hip simulator wear test was indicated by experimental data, as shown in section 5.1.1. Additionally, the SEM coupled with EDX analysis of the lubricant, showed the presence of Ti (see Figure 128). Therefore, in this research study, metal debris analysis confirmed the presence of metal in the lubricant.

5.4 Hip simulator wear testing of the taper-trunnion junction and bearing surfaces of modular MoXLPE hip prostheses

This section discusses the experimental results obtained from hip simulator wear testing of the taper-trunnion junction and bearing surfaces of modular MoXLPE hip prostheses. Then, experimental results from the taper-trunnion junction of MoXLPE hips are compared with retrieval studies and other laboratory studies. Next, based on experimental results, a possible explanation for the material loss from the CoCrMo femoral taper is offered. Finally, wear from the bearing surfaces of MoXLPE hips is compared with previous relevant hip simulator studies published in the literature.

Cross-linked polyethylene (XLPE) acetabular liners are commonly used with metallic femoral heads in THR owing to their excellent laboratory and clinical performance. Nonetheless, many retrieval and case studies have exhibited that metal release from the taper-trunnion junction of modular MoP THRs can cause ARMD, leading to failure of the prostheses⁴²⁻⁴⁵. This is the first long-term hip simulator study to report material loss from the taper-trunnion junction of the most commonly used bearing combination in hip prostheses. This is essential as material loss from the taper-trunnion junction is increasingly recognised as a critical concern in contemporary THRs^{17-20,42,43,295}. It is essential to better understand the causes and progression of such material loss, testing to the same five million cycle duration as expected for bearing surfaces (ISO14242) is required.

Could material loss at the taper-trunnion junction of a MoM hip be expected to be the same at a MoP hip, given that the materials (Ti for the femoral stem and CoCrMo for the femoral head) are identical in both cases? First, it is essential to recognise that head size tends to be greater in MoM hips than MoP hips. Smith et al. reported that 79% of men fitted with a MoM THR had a cup size in the range of 46-52mm and 84% of women fitted with a MoM THR had a cup size in the range of 42–48mm, based on NJR data²². In contrast, most MoP THRs currently implanted are of 32mm and 36mm cup size⁵. Size does matter, and Smith et al. showed a direct link between increasing head size and increasing revision rate²². This is key evidence of a toggle effect leading to increased wear at the taper-trunnion junction¹⁹. A second factor is the material combination involved at the bearing surfaces. A polymeric liner might serve to compliant of peak forces during gait and other activities²⁹⁵, compared with a ‘hard-on-hard’ material combination such as MoM. Thirdly, Hothi et al. found significantly less material loss from the taper-trunnion junctions of explanted MoP THRs compared with MoM THRs of the same design²⁸⁶. Across different designs, Langton et al. have shown that wear from the taper-trunnion junction of MoP THRs is less than from MoM THRs²⁸⁵. For these reasons, material loss from the taper-trunnion junctions of MoM THRs cannot be used to predict the wear from the taper-trunnion junctions of MoP THRs.

Cook et al. reported that the toggling motion might also result in pressurisation and entrainment of debris within the fluid in the crevice, see Figure 134⁴⁵. The entraining fluid is corrosive and will additionally contain fretting debris from the proximal end of the taper-trunnion junction and proteins. The debris particles and proteins move inside the fluid and impact upon the material loss at the taper-trunnion junction allowing corrosive attack leading to MACC. The resultant metal debris and metal ions released from the taper-trunnion junction into the surrounding tissues have resulted in ARMD, the formation of the pseudotumor and the necessity for the revision surgery.

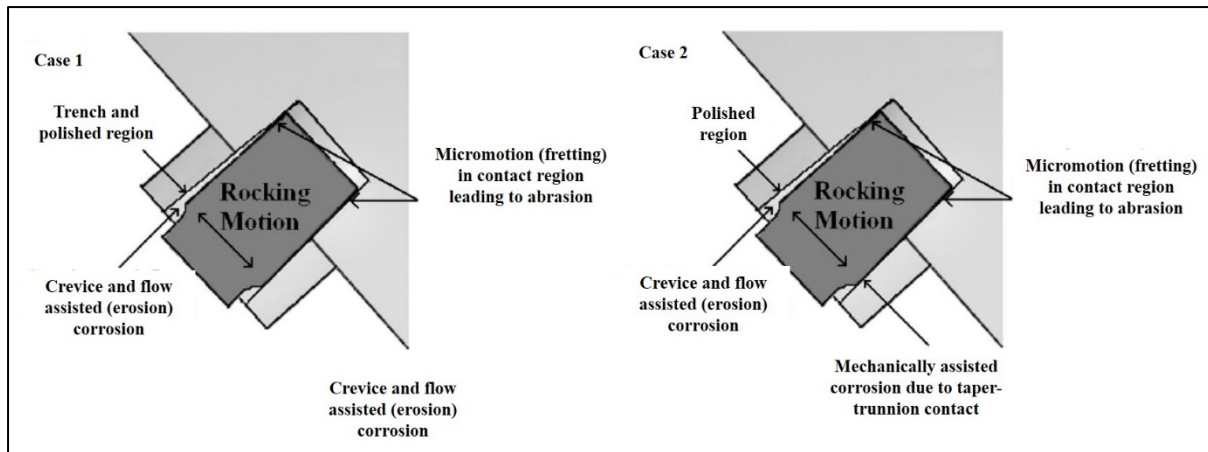


Figure 134 Schematic describing the micromotion, toggling (rocking motion) and entrainment of debris into the taper. The primary mode of damage was corrosion in case 1, and for case 2 it was due to MACC. Image adapted from Cook et al. (2013) ⁴⁵.

5.4.1 Wear of the CoCrMo femoral head: is it primarily from the bearing surface or the internal taper of the femoral head?

The experimental data from MoXLPE hip simulator study reported in this thesis shows that wear of the CoCrMo femoral heads arose mainly from the internal taper. Clearly, the heads showed a mass loss (wear). The mean volumetric wear rate of the CoCrMo femoral heads calculated using gravimetric measurements was $0.057 \pm 0.020 \text{ mm}^3/\text{Mc}$. There was no statistically significant difference ($p = 0.416$) in the mean volumetric wear rates of the CoCrMo femoral tapers calculated using gravimetric measurements ($0.057 \pm 0.020 \text{ mm}^3/\text{Mc}$) and those obtained using the CMM ($0.045 \pm 0.024 \text{ mm}^3/\text{Mc}$). Furthermore, the worn area on the CoCrMo femoral taper surface showed a statistically significant increase ($p < 0.001$) in the Sa compared to that of the unworn area. The Sa of the bearing surfaces of the femoral heads showed negligible change. Pre-test values for the femoral bearing surfaces were $0.007 \pm 0.003 \text{ } \mu\text{m}$, and post-test values were $0.008 \pm 0.003 \text{ } \mu\text{m}$. These values are in agreement with the pre-and post-test roughness values reported in the literature^{189,195,212}. These relatively unchanged roughness measurements indicate minimal damage at the bearing surfaces of the CoCrMo femoral heads. No other *in vitro* MoXLPE hip simulator studies (see Table 29) have reported wear from the metallic femoral taper^{191-193,195,198,205,211,212}.

Table 29 Laboratory wear rates for different metal-on-cross-linked (MoXLPE) hip joints under standard testing conditions compared with this study. γ : Gamma irradiation, Eb: electron beam irradiation.

Authors (year)	XLPE liner manufacturer γ or Eb in kGy	Head Size (in mm)	Surface roughness (μm)		Wear rates (mm^3/Mc)		
			H: Heads and L: Liners		(Mean \pm SD)		
			Pre-test	Post-test	XLPE liners	CoCrMo heads	Taper(T)/trunnion(Tr)
D’Lima et al¹⁹² (2003)	Durasul TM , (Eb95) Crossfire TM , (γ 75)	28	-	-	-1.5 \pm 1.6 1.6 \pm 1.3	Not measured	Not measured
Affatato et al²¹¹ (2005)	Longevity [®] , (Eb95)	28	H: 0.12-0.14	-	1	Not measured	Not measured
Dumbleton et al¹⁹¹ (2006)	Trident [®] , (γ 90)	36	-	-	3 \pm 1.3	Not measured	Not measured
Fisher et al¹⁹⁴ (2006)	Not given (Eb100)	28,36	-	-	\sim 5 (28mm) 10.6 \pm 11.4 (36mm)	Not measured	Not measured
Fisher et al²¹² (2006)	Durasul [®] Alpha	36	H: 0.006 L: 1.070	H: 0.009 L: 0.232	9.5	Not measured	Not measured
Galvin et al¹⁹⁵ (2010)	Durasul [®] Alpha	36	H: 0.006 \pm 0.001 L: 1.057 \pm 0.059	H: 0.012 \pm 0.005 L: 0.100 \pm 0.049	10.4 \pm 1.6	Not measured	Not measured
Affatato et al¹⁹⁸ (2016)	Not given [γ 75(\pm 10%)]	32	-	-	3.29	Not measured	Not measured
Partridge et al¹⁹³(2017)	Marathon [®] (γ 50)	36	-	-	8.7	Not measured	Not measured
This study	Commercially available (γ 75)	32	H: 0.007 \pm 0.003 L: 1.192 \pm 0.217	H: 0.008 \pm 0.003 L: 0.041 \pm 0.016	2.74 \pm 0.74	0.057 \pm 0.020	T: 0.045 \pm 0.024 Tr: 0.044 \pm 0.003

5.4.2 Metal release from the taper-trunnion junction of modular MoXLPE THR.

The CoCrMo femoral tapers ($0.045 \pm 0.024 \text{ mm}^3/\text{Mc}$) and Ti trunnions ($0.044 \pm 0.003 \text{ mm}^3/\text{Mc}$) showed similar volumetric wear rates in MoXLPE *in vitro* wear test. If one Mc of the *in vitro* hip simulator test is equivalent to one year *in vivo*³⁰⁹ then the mean volumetric wear rate of the CoCrMo femoral taper ($0.045 \pm 0.024 \text{ mm}^3/\text{year}$) and Ti trunnion ($0.044 \pm 0.003 \text{ mm}^3/\text{year}$) falls within the range of wear rates found in previous MoP retrieval studies which included some Corail® components in their respective cohorts^{241,286}, as shown in Table 30.

Table 30 Wear from the taper-trunnion junction of MoP THR (Ti: titanium alloy, (CoCrMo: cobalt chromium molybdenum alloy).

MoP Study	Trunnion	Wear rate (mm^3/year)		Total Volume (mm^3)	
		Femoral taper	Trunnion	Femoral taper	Trunnion
Kocagoz et al²⁴¹ (2016)	Ti (n=42)	0.02 (0-8.67)	0.00 (0-0.32)	0.04 (0-4.34)	0.00 (0-2.5)
	CoCrMo (n=8)	Median (range)	Median (range)	Median (range)	Median (range)
Hothi et al²⁸⁶ (2018)	Ti6Al4V	0.03 (0-1.07)	Not measured	0.15 (0-3.80)	Not measured
		Median (range)		Median (range)	
This Study	Ti6Al4V	0.045 ± 0.024	0.044 ± 0.003	0.22 ± 0.12	0.24 ± 0.02
		Mean \pm SD	Mean \pm SD	Mean \pm SD	Mean \pm SD

In an explant study Hothi et al. compared the material loss at the femoral tapers of MoP THR (28/32/36mm diameter) and large-diameter ($\geq 36\text{mm}$) MoM THR from a single manufacturer, both with a 12/14 taper, and reported ‘clinically insignificant’ (median 0.15mm^3) material loss from the MoP taper-trunnion junction compared to that of the MoM THR²⁸⁶. The mean time *in vivo* for the MoP THR was 4.5 years and therefore, on the basis that 1 Mc is equivalent to a year *in vivo*, of similar duration to the *in vitro* MoXLPE hip simulator study reported in this thesis. The volumetric material loss from the CoCrMo femoral tapers measured in MoXLPE hip simulator test ($0.22 \pm 0.12 \text{ mm}^3$) is within the range of MoP tapers obtained from the explant study. Kyomoto et al. tested 28mm MoXLPE in a hip simulator for 5 Mc and observed a statistically significant increase ($p < 0.01$) in post-test

surface roughness at the contacting region of the CoCrMo femoral tapers similar to that observed in this MoXLPE hip simulator study³²³. In this MoXLPE hip simulator test, damage was noted in the form of a circumferential band at the distal end of the CoCrMo femoral taper where the femoral head made physical contact with the base of the Ti trunnion. Proximal to this circumferential band, imprinting of the trunnion was observed, similar to that seen in many retrieval studies of metallic femoral tapers (MoM or MoP)^{18,19,244,283}.

Explant studies reported material loss from the femoral tapers of CoCrMo femoral heads mounted on Ti alloy trunnions^{18-20,266,276,284}. Similarly, in this MoXLPE hip simulator test, the CoCrMo femoral tapers showed material loss. A question that may arise is: why did wear arise from the harder CoCrMo alloy femoral taper when the Ti6Al4V alloy trunnion is much softer? To answer this question, Moharrami et al.³², suggested that a titanium oxide surface layer will form on the Ti6Al4V alloy trunnion, and it has a greater hardness compared with the femoral taper surface.

The lubricant employed in the wear test, dilute bovine serum, is used to replicate synovial fluid¹⁸⁷ and as such it is known to create a corrosive environment³²⁴. Consequently, the potential for corrosion within the test set up of the hip simulator was created. Despite this, the results of this study, with localised loss of material in the form of a circumferential band at the distal end of the CoCrMo femoral taper, appear to indicate that mechanical loss (wear) is of greater importance than electro-chemical (corrosion) effects.

In MoP THRs, metal release and associated pseudotumour formation leading to failure have been previously reported^{42,45,148}. In this *in vitro* test, hip simulator wear testing was undertaken on 32mm diameter MoXLPE hips. There is the possibility that femoral head diameter size is linked to clinical performance. The expectation is that larger head diameter sizes result in fewer dislocations^{270,271}. However, there are concerns that larger head diameter sizes are related to more significant damage at the taper-trunnion-junction in MoP hips. Kurtz et al. reported no associated increased risk of fretting corrosion damage in large-diameter CoCrMo femoral heads compared to small-diameter (< 36mm) femoral heads using a semi-quantitative scoring on explanted MoXLPE THRs³²⁵. In contrast to this, Balso et al. conducted a semi-quantitative scoring study on explanted MoP THRs and reported the possibility of accelerated fretting damage due to increased femoral head size⁸⁶. Additionally,

Craig et al. reported increased serum metal ion levels in large-diameter MoP hips compared with small-diameter from a single manufacturer³²⁶. Furthermore, the NJR shows higher revision rates for MoP hips ≥ 36 mm head diameter⁵. Therefore, pseudotumor formation in MoP THRs is perhaps associated with increased bearing diameter size. Coincidentally, explant studies also reported an increased material loss in large-diameter MoM THRs^{18-20,23,126}.

In this present study of 32mm diameter femoral heads, visual and microscopic inspection of the CoCrMo femoral tapers did not show the presence of toggle damage. Cook et al. observed toggle damage on retrieved large-diameter (≥ 36 mm) MoP hips⁴⁵. Interestingly, retrieval studies noted the presence of toggle damage, mainly in large-diameter MoM THRs^{18,19}. Therefore, the smaller (32mm diameter) head size could be the reason for the absence of the toggle damage in this present hip simulator study.

5.4.3 Metal ion analysis: MoP hip simulator wear test

In the MoXLPE hip simulator wear test, CoCrMo femoral tapers and Ti alloy trunnions showed similar volumetric wear rates, see Figure 122. Moreover, lubricant metal ion analysis from the MoXLPE hip simulator test showed elevated Co, Cr and Ti ions compared with the unused lubricant. Therefore, in this research study, metal debris analysis confirmed the presence of metal in the lubricant.

5.4.4 Radial clearance and its effect on the wear

It is clear from Hamrock-Dowson equation (see Equation VI), that to promote fluid-film lubrication it is essential to increase the radius of the femoral head ($R_{femoral\ head}$) and to reduce the radial clearance ($R_{acetabular\ liner} - R_{femoral\ head}$)²²⁰. The increase in wear linked with the higher radial clearance⁶¹. In CoC THRs, reduced radial clearance lead to large contact areas and low stresses at the bearing surfaces. These combine with an extremely low surface finish at the bearing surfaces leads to an increase in the minimum lubricant film thickness that is developed when the patient walks with associated reductions in surface asperities and wear⁶¹. This increased lubricant film thickness at the bearing surfaces of the CoC THRs may reduce the stress acting at the taper-trunnion junction. Whereas in the MoP THRs due to relatively high surface roughness of PE acetabular liner than the finely polished metal femoral head, the

radial clearance does not improve the lubrication significantly¹⁶⁵. Therefore, for understanding the complex tribological mechanisms in terms of friction, wear and lubrication at the taper-trunnion junctions are essential to optimise the design in terms of radial clearance.

5.4.5 The SEM coupled with EDX analysis of the CoCrMo femoral tapers

5.4.5.1 The present hip simulator study vs MoP explant studies

The material loss from the CoCrMo femoral taper was supported by SEM coupled with EDX analysis on D1. Additionally, a strong O peak and reduced Co peak present on the D1 (see Figure 114) support the concept of the release of Co and formation of a mixed oxide rich passivation layer on the damaged area. An elemental X-ray map taken on D1 indicated the removal of Co from the CoCrMo surface, leaving behind a mixed oxide surface (see Figure 116). Arnholt et al. reported the presence of a discontinuous chromium-rich oxide layer on the CoCrMo femoral tapers of explanted modular MoP THRs²⁵⁴. Zeng et al. characterised the oxide film on the CoCrMo tapers of explanted MoP THRs and confirmed the presence of chromium oxide³²⁷. As similar evidence is observed in this hip simulator study, the mixed oxide present on the femoral tapers may be a chromium-rich oxide layer. Furthermore, the presence of an O peak on the damaged area observed in this study was in agreement with an explant study by Hall et al. that reported accumulation of oxidised material debris on the CoCrMo femoral tapers³⁴. Hall et al. also reported adhesion of Ti6Al4V trunnion debris on the CoCrMo femoral taper as shown by the presence of Ti, Al and V elements on the EDX spectrum. These elements; Ti, Al and V (see Figure 115) were also found via EDX analysis in this present study alongside alloying elements on the CoCrMo femoral taper, from the elemental X-ray map (see Figure 117), which is suggestive of adhesion of Ti6Al4V from the trunnion.

5.4.5.2 The present hip simulator study vs other in vitro studies

Fischer et al. performed an *in-vitro* fretting test involving two CoCrMo alloy pins in contact with a Ti6Al4V alloy cylinder with diluted bovine calf serum (30g/L) as the lubricant²⁵⁵.

They reported that CoCrMo alloy predominantly wears by releasing Co into the lubricant while Ti6Al4V alloy mainly wears by the generation of the particles that stay in the “tribomaterial”. Furthermore, Fischer et al. also observed the presence of Ti and O on the damaged area of CoCrMo pins and noted an increase in the Cr/Co ratio (0.89). In this present hip simulator test, the elemental X-ray maps showed the absence of Co on D1 (see Figure 116) indicating wear from CoCrMo femoral taper and the presence of Ti, Al and V on D2 (see Figure 117) indicating adhesive wear from the Ti6Al4V trunnion. Furthermore, the numbers obtained from the spot EDX analysis showed the strong presence of O in D1 and a strong presence of alloying elements of Ti6Al4V trunnion present on D2 compared to U and polished area (see Table 27). The release of Co from the damaged area was indicated by an increase in the Cr/Co ratio (1.09) compared to the polished CoCrMo surface (Cr/Co ratio 0.39) in spot EDX data again showing CoCrMo femoral wears preferentially by releasing Co into the serum. Therefore, the EDX results obtained on the CoCrMo femoral tapers used in this present hip simulator study were seen to be in good agreement with Fischer et al.’s *in vitro* experiment. Similar phenomena of Co-release were observed in an *in vitro* study by Kyomoto et al. who used a hip simulator for testing 28mm MoXLPE hips for semi-quantitative analysis involving visual scoring, wear debris analysis and the surface morphological characterisation but not the quantification of the material loss from the femoral taper³²³. Their EDX results on the CoCrMo femoral taper showed the presence of strong O and Ti peaks at the distal end of the CoCrMo femoral taper, reporting that the Co concentration was over 30 times higher than the Cr concentration in the lubricant after 5Mc. Again, the SEM coupled with EDX analysis observed in this current hip simulator study for the CoCrMo femoral tapers (see Figure 114 and Figure 115) exhibits the similarity with the results reported by Kyomoto et al. Although the results obtained in this research work were in agreement with *in vitro* studies performed by Fischer et al.²⁵⁵ and Kyomoto et al.³²³, EDX results are semi-quantitative results. Therefore, the EDX results should not be taken to define mechanisms responsible for the material loss at the taper-trunnion junction. Additional chemical analytical testing such as X-ray diffraction (XRD) and X-ray Photoelectron Spectroscopy (XPS)³² should be required to investigate the multivariable process responsible for the material loss at the taper-trunnion junction of modular THRs.

5.4.6 The appearance of imprint damage on the CoCrMo femoral tapers.

Explant studies have reported imprinting damage on the CoCrMo femoral taper surfaces as a result of the micro-grooved topography of trunnions^{19,34,254,328}. A similar imprinting pattern was observed visually and microscopically on the CoCrMo femoral tapers subject to the hip simulator test (see Figure 111). Therefore, again, the similarity with explant studies was shown.

It has been suggested that the imprinting damage is the result of a mechanical (fretting)³²⁹ or an electrochemical³²⁸ process. Thus, the exact mechanism of the imprinting damage is unclear. Hall et al. suggested that the rougher surface topography of the micro-grooved trunnions and associated contact stresses can contribute to the imprinting damage^{34 329}. It has been speculated that the imprinting damage may alter the local environment by the ingress of joint fluid due to the widening of the crevices³³⁰. Langton et al. speculated on the potential of accelerated wear on the femoral taper due to imprinting damage¹⁹. Additionally, Hall et al. reported the possibility of significant material loss due to imprinting damage³³¹.

5.4.7 A possible explanation for the material loss from the CoCrMo femoral taper

In this hip simulator study, MoXLPE hips were mounted anatomically, and diluted new-born-calf serum was used to replicate synovial fluid¹⁸⁷, which is known to produce a corrosive environment³²⁴. Consequently, the potential for corrosion within all stations of the hip simulator was created. Despite this corrosive environment, the results of this study, with a localised damaged area in the form of a circumferential band at the distal end of the CoCrMo femoral taper, shows that wear is more important than corrosion.

When the dynamic loading and articulating motion (i.e. gait) is applied to the hip prosthesis, the taper-trunnion junction experiences ‘fretting’. As a result of this ‘fretting’ motion, the protective oxide layers on the taper-trunnion junction interfaces can be breached due to ‘abrasion’, leading to ‘fretting wear’. It has been reported that damaged areas with scratching perpendicular to and interrupting machining marks on the femoral taper and/or wearing away of the machining marks were considered to be implications of fretting^{30,257}. In this hip simulator study, SEM images (see Figure 112) showed that the majority of the damage was

perpendicular to circumferential machining marks on the CoCrMo femoral tapers, thus indicating fretting. In this hip simulator study, SEM coupled with EDX analysis showed the presence of metal debris from Ti6Al4V trunnions on CoCrMo femoral taper surface (see Figure 115 and Figure 117). Therefore, discolouration or black debris seen visually at the distal end of CoCrMo femoral tapers indicated adhesion of metal debris from Ti6Al4V trunnions, not corrosion of the surface.

Furthermore, it has been suggested that the ‘fretting corrosion’ process is a particular type of ‘tribocorrosion’ which comprises of synergistic effects between mechanical and electrochemical processes leading to irreversible damage at the taper-trunnion junction^{33,263,332,333}. In the patient's body, the THR is continuously exposed to a ‘tribological event’ (joint articulation) in the presence of ‘corrosive’ physiological fluid³³⁴. This has led to use of the term ‘tribocorrosion’ somewhat indiscriminately to describe the material loss at the taper-trunnion junction.

There is the possibility that femoral head size is associated with clinical performance of hip prostheses. Smith et al. showed the direct link between increasing femoral head size and increasing revision rates in stemmed MoM THRs²². The femoral head size of MoP THRs has increased over the years, but they have not reached the diameters of MoM THRs. In the context of large-diameter femoral heads, the NJR reported the range of 36mm to 44mm for MoP whereas 36mm to 54mm for MoM hips¹⁰⁰. However, there are concerns reported by explant studies that increased femoral head sizes are associated with greater material loss at the taper-trunnion junction of MoP THRs^{45,86,335}. Moreover, the NJR demonstrated higher revision rates for large-diameter MoP hips. Hence, the clinical performance of MoP THRs is perhaps associated with increased femoral head size. Since the head size does matter, then this again implies a more mechanical (wear) process rather than an electrochemical (corrosion) mechanism is responsible for the damage of the taper-trunnion junction interfaces.

Hip simulators have been used for quantification of the material loss from the bearing surfaces of hip prostheses due to combined movement and loading. In this present hip simulator test, the material loss from CoCrMo femoral tapers was quantified along with quantification of the material loss from the bearing surfaces of MoXLPE joints. However,

further chemical analysis is essential to evaluate the multivariable mechanism responsible for the material loss at the CoCrMo femoral tapers.

5.4.8 Wear at the bearing surfaces of cross-linked polyethylene liners

As shown in Table 29, the mean volumetric wear rate of the XLPE liners, 2.74 ± 0.74 mm³/Mc, falls within the range of wear rates found in previous MoXLPE hip simulator studies^{191-193,195,198,205,211,212}. The surface roughness (Sa) of the bearing surface of the XLPE liners showed a significant decrease post-test ($p < 0.001$). This finding was supported visually by the elimination of the original machining marks from the bearing surfaces of the XLPE liners (see Figure 124). The decrease in the roughness and consequent removal of the machining marks are consistent with previous *in vitro* studies which tested MoXLPE hips under standard (i.e. non-‘adverse’) conditions^{195,205,212}.

There is the potential of an additional source of *in vitro* PE wear at the backside of the acetabular liner and the pelvic insert holder. However, microscopic examination revealed minimal damage and the presence of the original circumferential machining marks (see Figure 127) at the backside of the XLPE liner indicating minimal, if any, wear. This result fits with other studies. Reyna et al. compared the wear on the backside of PE (non-XLPE and XLPE) liners used in a hip simulator test and retrieved liners using a semi-quantitative scoring method and reported similar wear scores for both groups³³⁶. Furthermore, Kurtz et al. in 3D finite element models showed at least three orders of magnitude less volumetric wear rates from the backside of the liner compared to the volumetric wear rate estimates at the articulating bearing surface³³⁷.

5.5 Metal debris analysis

The significance of elevated Co and Cr ions in the body has been previously described in the literature^{28,338-340}. There is a very limited amount of literature available on the clinical significance of elevated Ti ions following THRs. While it may be that CoCrMo wear particles are more cytotoxic than Ti alloy wear particles³⁴⁰, the history of hip arthroplasty from Charnley onwards has shown that the generation of volumes of wear debris should be

avoided. Moreover, Ti wear from joint replacements has been shown to induce aneuploidy *in vitro* and *in vivo*³⁴¹. Dalal et al. reported that Ti particles induce less toxicity than CoCrMo alloy particles³⁴⁰. However, *in vitro* animal model studies have shown that Ti particles in high levels are potentially carcinogenic³⁴². Furthermore, Haynes et al. reported that wear particles generated from Ti alloy implants could cause increased release of the mediator responsible for the bone resorption process in an animal model³⁴³. Furthermore, the potential links of Ti wear debris to metallosis in children fitted with spinal implants have recently been described³⁴⁴. Several recent studies have reported elevated Ti ions in the body following implantation of different types of modular THR³⁴⁵⁻³⁴⁷. Unpublished work at the McMinn centre reported significant elevation in Ti ions in the patients with CoC hips mounted on uncemented Ti stems, see Figure135³⁴⁸. However, the femoral head diameter is unknown; therefore, no direct comparisons can be made.

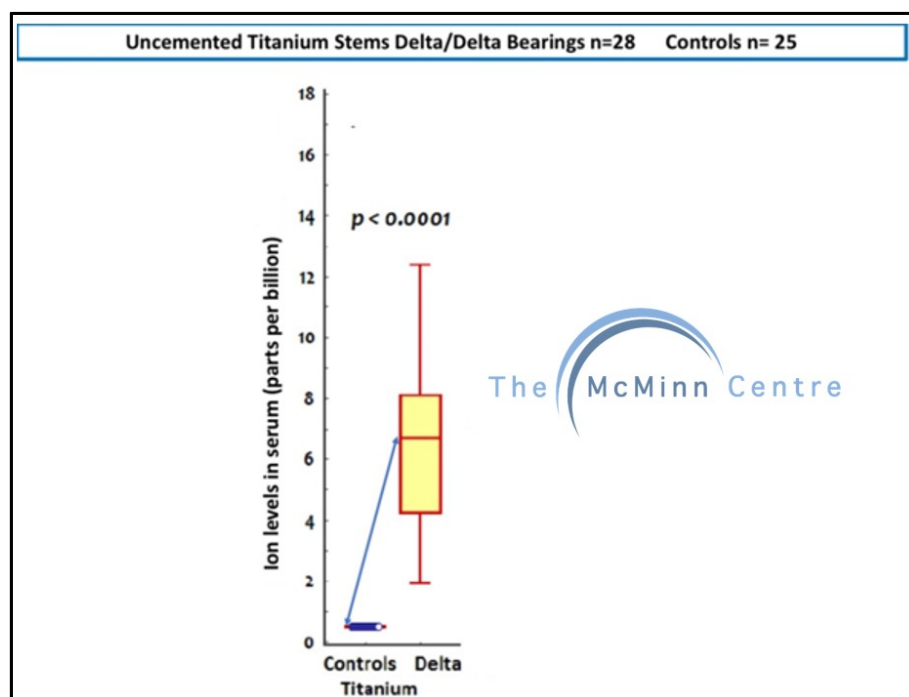


Figure135 Box plot from an unpublished work from the McMinn centre indicating statistically significant elevation Ti ion concentration in the patients with CoC THRs mounted on Ti trunnions³⁴⁸.

Gofton et al. reported elevated serum Ti ion levels in a short-term (2 years) follow up study of small diameter MoXLPE THRs with a Ti alloy modular femoral stem and neck³⁴⁵.

Furthermore, Nam et al. investigated serum metal ion concentration at 5 years following MoXLPE, ceramic-on-XLPE and oxinium-on-XLPE modular THRs with a Ti alloy stem³⁴⁷. Analysis of metal ion concentration suggested that Ti ion levels remained consistently

elevated whatever the femoral head material. Therefore, the *in vitro* results presented in this thesis, which show Ti wear, are consistent with these clinical studies which have measured increased Ti ion levels after THRs, which include Ti trunnions. However, there is no established threshold beyond which Ti serum metal ion concentrations are known to be toxic in patients with a THR³⁴⁶.

5.6 Importance of lubricant pH measurement

The slight increase in the pH of the lubricant after every 0.5Mc was in agreement with the MoXLPE hip simulator test reported by Kyomoto et al.³²³. They suggested that the release of carbon dioxide gas from the lubricant was responsible for the increase in the pH.

Interestingly, Kyomoto et al. also reported that the metal ions released from the metallic taper were increased at an accelerated rate compared with pH³²³. It is claimed that the metal ion release and oxide re-passivation of the taper-trunnion surfaces can lead to localised pH drop and further corrosion (see section 2.6.1)^{248,252}. A question that may arise is: why did the pH of the lubricant show a slight increase when metal ions release was increased? Milošev et al. reported that the influence of metal ions released after joint replacement on the pH of the synovial fluid is neutralised by the buffering capacity of the human synovial fluid, which maintains the pH at the physiological level¹⁸⁸. In this current hip simulator wear test, diluted bovine serum (21g/L) was used as a lubricant due to its similarities in pH, salt levels and protein concentration to synovial fluid^{173,349}. Therefore, the slight increase in the pH of the lubricant found in this study was maybe due to the neutralisation of an acidic environment by the buffering capacity of the diluted lubricant. Furthermore, Milošev et al. also concluded that the pH measurement in synovial fluid rather than on explanted THR component shows a more reliable method of collecting data¹⁸⁸. Hence, it is suggested that the accepted view that oxide re-passivation of the taper-trunnion surfaces can lead to localised pH drop *in vivo* and further corrosion at the taper-trunnion junction should be re-examined.

5.7 Comparison of the metallic material loss from the taper-trunnion junction of contemporary CoC and MoXLPE THRs subject to a controlled hip simulator tests

In this thesis, total metallic material loss after five million cycles from CoC hip simulator test was 0.29mm^3 (Ti trunnions) whereas MoXLPE hip simulator test it was 0.62mm^3 [CoCrMo tapers (0.38mm^3) + Ti trunnions (0.24mm^3)]. These results, supported findings of an explant study by Kurtz et al. which reported that by employing ceramic femoral heads, metal release from the taper-trunnion junction of CoCrMo femoral heads ‘may be mitigated but not eliminated’²⁵⁷. Kocagoz et al. reported ten times higher material loss from the taper-trunnion junction of CoCrMo group (MoP THRs, $n = 50$) compared with the ceramic group (CoP THRs, $n = 41$ and CoC THRs, $n = 9$) in an explant study²⁴¹. However, the results obtained in this thesis suggested that the total metallic material loss from the taper-trunnion junction of CoCrMo heads was approximately doubled compared to ceramic heads. In the ceramic group of Kocagoz et al., majority of the explants were CoP whereas in present thesis CoC THRs were tested in the hip simulator. This could provide a possible explanation for the difference in the metallic material loss between Kocagoz et al. explant study and CoC hip simulator test as described in section 5.1.1.2.

5.8 Importance of wettability measurement of the femoral heads

Kubiak et al. reported a strong correlation between the wettability of surfaces and the surface roughness²²⁵. In these hip simulator studies, the CA of ceramic (BIOLOX[®] *delta*) and CoCrMo femoral heads showed minimal change. Pre-test values for the ceramic femoral heads were $(61.20 \pm 5.23)^\circ$, and post-test values were $(61.80 \pm 2.52)^\circ$. Pre-test values for the CoCrMo femoral heads were $(63.00 \pm 3.37)^\circ$, and post-test values were $(62.49 \pm 2.56)^\circ$. Additionally, the Sa of ceramic femoral heads and CoCrMo femoral heads showed negligible change pre and post-test. Therefore, minimal change in both CA and Sa, pre and post-test supports the work of Kubiak et al. Interestingly, in the MoXLPE hip simulator test, the Sa of the bearing surface of the XLPE liners showed a significant decrease post-test ($p < 0.001$). However, due to the shape of the acetabular liner, CA measurement on the acetabular bearing surfaces could not be performed, and this is acknowledged as a limitation to this study.

5.9 Limitations

These *in vitro* tests had a number of limitations.

- In CoC hip simulator test, there were only three CoC bearing surfaces. Two further samples were required for the DL test and the impaction test, both of which were fundamental to this investigation. As these samples were all the latest fourth generation of ceramic BIOLOX[®]*delta*, obtaining such samples for independent testing was both challenging and expensive as this project was unfunded. For this reason, there were only three CoC bearing surfaces.
- The trunnions of actual Corail[®] (DePuy Synthes, UK) femoral stems could not be used as these could not be sourced and would anyway lack sufficient material from which to manufacture the double-ended trunnions employed in the hip simulator. Instead, titanium surrogates had to be manufactured.
- In the case of ceramic components, there is potential for wear to occur at the ceramic-metal interface on the backside of the acetabular liner and pelvic insert holder of the simulator. Due to the current design of the simulator, an acetabular shell cannot be accommodated. However, the simulator will be redesigned so that an acetabular shell can be incorporated in future tests.
- Impaction force and number of impactions were not measured during the tests reported in this thesis. However, the author (RMB) undertook all impactions and employed a consistent technique.
- Analysis of metal ion concentration within the lubricant used in the CoC hip simulator test was not undertaken. In part, this was because the wear was so low that such an analysis would be challenging.
- The visual markings observed at the ceramic femoral tapers in the CoC hip simulator test were removed using Sidol cleaner to minimise the effect of metal transfer that would affect the gravimetric measurements. Therefore, ceramic femoral heads were not sectioned. Additionally, tooling required to cut the ceramics were not available in the laboratory.
- Analysis of metallic or polymeric wear particles present within the lubricant used in MoXLPE hip simulator test was not carried out. However, analysis of metal ion concentration within the lubricant used in MoXLPE hip simulator test was performed. To the authors' best knowledge, no MoP retrieval studies have measured volume loss from the taper-trunnion junction and metal ion concentration in the same study. Furthermore,

the volume loss reported from the taper-trunnion junction of the MoP hips used in the present hip simulator test are in agreement with those from previous MoP retrieval studies.

- Pre and post-test CA measurements were not performed on the acetabular liners. This is due to the light source being blocked by the concave design of the acetabular liners.
- The chemical analysis using the XPS and XRD on the CoCrMo femoral was not performed due to unavailability of the funding required to perform these expensive chemical analytical techniques.
- The friction and lubrication measurements at the bearing surface of CoC and MoP THRs were not performed. However, the material loss from both taper-trunnion junction and bearing surfaces reported for the first time by this research. The TE-86 is anatomical hip joint ‘wear’ simulator. However, the simulator will be redesigned so that friction measurement can be incorporated in future tests.
- Corrosion testing was not performed in this research work as it would have been challenging to employ electrodes and wiring to each station of the hip simulator subject to articulating motions, for the measurement of the corrosion currents. In the ASTM-1875, applying corrosion testing methods would have been more accessible due to the absence of physiological walking motion³⁸. However, this present research has shown the importance of employing the articulating motion for the investigation of the material loss at the taper-trunnion junction.
- Knowledge of the contact mechanics of the taper-trunnion junction is crucial for predicting the stability of THR and the prevention of micromotion²⁴². Unfortunately, due to limited time scale contact mechanics and related measurements were not considered in this research work. However, they have been suggested for future work.
- Lastly, the surface roughness of the trunnions used in MoXLPE hip simulator test was not measured as previous explant studies showed that the material loss arises mainly from the CoCrMo alloy femoral tapers rather than the Ti alloy trunnion, when CoCrMo/Ti alloy combinations are used for the taper-trunnion junction.

Chapter 6: Conclusions and suggestions for further work

6.1 Conclusions

The aim of this research work to quantify the material loss, if any, at the taper trunnion junction of modular CoC and MoP THR's under physiological walking cycle. In order to achieve this aim, multi-station hip simulator testing of modular hips mounted on titanium (Ti) alloy trunnions was undertaken under standard physiological walking cycle, replicating the clinical scenario as closely as possible. Listed below are some key findings and answers to the research questions which are divided into subsections:

6.1.1 The material loss at the taper-trunnion junction of contemporary CoC hips shown in a multistation hip simulator

- In the CoC hip simulator wear test, based on the gravimetric measurements, bearing surface wear rates (total wear = 0.25 mm^3) were similar to those of the trunnions (total wear = 0.29 mm^3).
- This metallic wear debris may provide an explanation for the ARMD reported in CoC hip arthroplasty and for the similarity in clinical performance between CoC and MoP hips.
- Furthermore, based on the wear pattern observed, toggling of the ceramic femoral head was seen on the trunnion, which also shows good agreement with *ex vivo* studies.
- Moreover, SEM coupled with EDX analysis of wear debris within the lubricant confirmed the presence of Ti.
- Therefore, an explanation for wear-related failures in CoC THR's, despite the low wear arising at the bearing surfaces, may now exist; namely that Ti wear particles are generated from the trunnion.
- No other long-term hip simulator studies have measured wear at the taper-trunnion junction of modular CoC hips
- Research question: In CoC articulating components, comprised of purely ceramics, where is the metal debris coming from?

Answer: Based on the CoC hip simulator test, the answer to the research question is the material loss from titanium trunnion (ceramic-on-metal contact)

6.1.2 *The necessity of employing articulating motion for the quantification of material loss from the taper-trunnion junction*

- Employment of physiological walking motion indicated increased wear from the CoC hip simulator test trunnions (0.29 mm^3) compared with the DL test trunnion (0.05 mm^3).
- This result reinforces the importance of employing physiological walking motion in the testing of the taper-trunnion junction of modular THRs.
- Research question: Dynamic loading and articulating motion vs dynamic only loading, does the material loss at the taper-trunnion junction change?

Answer: Yes. There was five times increase in the material loss after employment of dynamic loading and articulating motion.

6.1.3 *The material loss at the taper-trunnion junction of contemporary MoXLPE hips shown in a multistation hip simulator*

- In the MoXLPE hip simulator wear test, based on the gravimetric, volumetric, and surface roughness measurements, the wear of the CoCrMo femoral heads arose mainly from the internal taper.
- The CoCrMo femoral tapers (0.22 mm^3) and Ti trunnions (0.24 mm^3) showed similar volumetric wear in this *in vitro* wear test. The wear from the XLPE liners (14.28 mm^3) was similar to that seen in other *in vitro* studies.
- Moreover, the imprinting damage seen on the CoCrMo femoral tapers also showed good agreement with *ex vivo* studies.
- Furthermore, analysis of wear debris within the lubricant using ICPMS confirmed the presence of Co, Cr and Ti elements. This metallic wear debris may provide an explanation for the ARMD reported in MoP hip arthroplasty.

- Research question: In MoP articulating components, comprised of metal and softer polymer contact, where is the metal debris originating from?

Answer: Based on MoXLPE hip simulator test, the answer to the research question is, the material loss from the taper-trunnion junction (CoCrMo on Ti contact).

6.1.4 Summary

This research work presented the first long-term *in vitro* hip simulator tests to report a material loss from the taper-trunnion junction of contemporary CoC and MoP THRs. The volumetric wear rates of Ti trunnions from the CoC hip simulator study, CoCrMo femoral tapers and Ti trunnions from the MoXLPE hip simulator study showed a good match with *ex vivo* studies. Toggling of the ceramic femoral head on the trunnion, imprinting of the trunnion and SEM coupled with EDX analysis on the CoCrMo femoral tapers again demonstrated good correlations with explant studies. Additionally, wear rates of the bearing surfaces of the CoC and MoP hip joints reported in this research, are comparable to wear rates found in the literature. Therefore, the hip simulator tests are fundamentally valid.

This research work quantified the material loss at the taper-trunnion junction of modular CoC and MoP THRs. Additionally, results obtained from SEM coupled with EDX in this study demonstrated similarity with other *in vitro* and *ex vivo* studies. The release of Co from the damaged area was indicated by an increase in the Cr/Co ratio (1.09) compared to the polished CoCrMo surface (Cr/Co ratio 0.39) in spot EDX data again showing the CoCrMo femoral taper wears preferentially by releasing Co into the serum. However, these results were based on the semi-quantitative analysis. Based on the results, the mechanisms responsible for the material loss at the CoCrMo femoral tapers involves a multivariable process. Further chemical analysis and corrosion testing will be required to understand these mechanisms.

In conclusion, metallic material loss from the taper-trunnion junctions of CoC and MoP THRs may provide an explanation for the ARMD reported in the literature for these THRs. These hip simulator studies confirm the necessity of measuring taper-trunnion junction wear in pre-clinical testing using the hip simulator to avoid ARMD and further increase the longevity of modular hip prostheses.

6.2 Implications

The taper-trunnion junction of the modular hips should be examined rigorously under clinically relevant test conditions prior to implanting in the patients^{27,36,265,294,295}. This research demonstrated the need for measuring taper-trunnion junction wear in pre-clinical testing. There are over thirty types of taper-trunnion designs in use because each implant manufacturer employs its specifications for manufacturing³⁵⁰. Nowadays, the laboratories of almost every one of the major orthopaedic companies and several universities worldwide possess hip joint simulators¹⁶⁶. Therefore, new designs of taper-trunnion junctions should be tested before implantation using hip simulators, as explained in this thesis.

6.3 Suggestions for further work

This research has established a methodology for quantification and assessment of the material loss from the taper-trunnion junction of modular THR's using a hip simulator. Since no other long-term hip simulator studies have measured wear at the taper-trunnion junction of non-MoM THR's, there is potential for far more hip simulator testing. Such as using different head sizes, different bearing surfaces material combinations, trunnions with different metals (CoCrMo or SS), dimensions (see Table 15) and surface finish (smooth or micro-grooved). A few suggested hip simulator tests using the methodology presented in this thesis are as follows:

1. Hip simulator study using 36mm CoP mounted on Ti alloy trunnions should be conducted and the results compared to determine the difference, if any, in taper-trunnion wear between CoC and CoP hips
2. Since the wear performance of MoP THR's is associated with increased femoral head size, a hip simulator study using ≥ 36 mm MoP mounted on Ti alloy trunnions should be undertaken and the result compared with those in this thesis.
3. Hip simulator studies using CoCrMo alloy instead of Ti alloy trunnions as it would be interesting to know how much trunnion wear occurs with a CoCrMo v CoCrMo alloy combination

4. For the understanding of the chemical analysis on the CoCrMo femoral tapers subject to hip simulator test, XRD and XPS analysis should be performed. The results obtained using these chemical analyses should be utilised along with the wear, surface roughness, EDX measurements techniques to investigate the multivariable process responsible for the material loss at the CoCrMo femoral taper.
5. Finite element model should be created of the taper-trunnion assembly replicating the same prostheses properties, applied dynamic loading and articulating motion used in the hip simulator to investigate the local topography, contact pressure and plastic strain as reported by Lundberg et al²⁴². The results obtained using the finite element and hip simulator tests will be compared for the understanding of the contact mechanics at the taper-trunnion junction.
6. Friction and lubrication measurement at the bearing surfaces should be performed to investigate the effect of lubrication regime, if any, on the material loss at the taper-trunnion junction of the modular THRs

In addition to the above-mentioned testing, the current hip simulator should be redesigned so that an acetabular shell can be incorporated to investigate material loss at the acetabular shell and backside of the acetabular liner interface.

References

1. Learmonth ID, Young C, Rorabeck C. The operation of the century: total hip replacement. *Lancet* 2007;370(9597):1508-1519.
2. Kurtz S, Ong K, Lau E, Mowat F, Halpern M. Projections of primary and revision hip and knee arthroplasty in the United States from 2005 to 2030. *Journal of Bone and Joint Surgery - Series A* 2007;89(4):780-785.
3. Nemes S, Gordon M, Rogmark C, Rolfson O. Projections of total hip replacement in Sweden from 2013 to 2030. *Acta Orthopaedica* 2014;85(3):238-243.
4. Pilz V, Hanstein T, Skripitz R. Projections of primary hip arthroplasty in Germany until 2040. *Acta Orthopaedica* 2018;89(3):308-313.
5. NJR. The National Joint Registry for England, Wales, Northern Ireland and the Isle of Man: 15th annual report. 2018.
6. AOANJRR. Australian Orthopaedic Association National Joint Replacement Registry (AOANJRR), Annual Report 2018; 2018.
7. Brach del Prever EM, Bistolfi A, Bracco P, Costa L. UHMWPE for arthroplasty: Past or future? *Journal of Orthopaedics and Traumatology* 2009;10(1):1-8.
8. Kurtz S, Medel FJ, Manley M. (iii) Wear in highly crosslinked polyethylenes. *Current Orthopaedics* 2008;22(6):392-399.
9. Ingham E, Fisher J. Biological reactions to wear debris in total joint replacement. *Proceedings of the Institution of Mechanical Engineers, Part H: Journal of Engineering in Medicine* 2000;214(1):21-37.
10. Schmalzried TP, Jasty M, Harris WH. Periprosthetic bone loss in total hip arthroplasty. Polyethylene wear debris and the concept of the effective joint space. *Journal of Bone and Joint Surgery - Series A* 1992;74(6):849-863.
11. Jacobs JJ, Shanbhag A, Glant TT, Black J, Galante JO. Wear Debris in Total Joint Replacements. *JAAOS - Journal of the American Academy of Orthopaedic Surgeons* 1994;2(4).
12. Oral E, Muratoglu OK. Vitamin E diffused, highly crosslinked UHMWPE: a review. *International Orthopaedics* 2011;35(2):215-223.
13. Fisher J, Jennings LM, Galvin AL. Wear of Highly Crosslinked Polyethylene against Cobalt Chrome and Ceramic femoral heads. In: Benazzo F, Falez F, Dietrich M, editors; 2006 2006//; Darmstadt. Steinkopff. p 185-188.
14. Gopinathan P. The Hard on Hard Bearings in THA - Current concepts. *Journal of orthopaedics* 2014;11(3):113-116.

15. Scholes SC, Joyce TJ. Ceramic-On-Ceramic Joints: A Suitable Alternative Material Combination? In: Pignatello R, editor. *Advances in Biomaterials Science and Biomedical Applications*. Rijeka: InTech; 2013. p Ch. 21.
16. Jacobs JJ, Gilbert JL, Urban RM. Corrosion of metal orthopaedic implants. *Journal of Bone and Joint Surgery - Series A* 1998;80(2):268-282.
17. Gilbert JL, Buckley CA, Jacobs JJ. In vivo corrosion of modular hip prosthesis components in mixed and similar metal combinations. The effect of crevice, stress, motion, and alloy coupling. *Journal of Biomedical Materials Research* 1993;27(12):1533-1544.
18. Bishop N, Witt F, Pourzal R, Fischer A, Rüttschi M, Michel M, Morlock M. Wear patterns of taper connections in retrieved large diameter metal-on-metal bearings. *Journal of Orthopaedic Research* 2013;31(7):1116-1122.
19. Langton DJ, Sidaginamale R, Lord JK, Nargol AVF, Joyce TJ. Taper junction failure in large-diameter metal-on-metal bearings. *Bone & Joint Research* 2012;1:56-63.
20. Matthies AK, Racasan R, Bills P, Blunt L, Cro S, Panagiotidou A, Blunn G, Skinner J, Hart AJ. Material loss at the taper junction of retrieved large head metal-on-metal total hip replacements. *Journal of Orthopaedic Research* 2013;31(11):1677-1685.
21. Langton DJ, Jameson SS, Joyce TJ, Gandhi JN, Sidaginamale R, Mereddy P, Lord J, Nargol AVF. Accelerating failure rate of the ASR total hip replacement. *The Journal of Bone and Joint Surgery. British volume* 2011;93-B(8):1011-1016.
22. Smith AJ, Dieppe P, Vernon K, Porter M, Blom AW. Failure rates of stemmed metal-on-metal hip replacements: analysis of data from the National Joint Registry of England and Wales. *The Lancet* 2012;379(9822):1199-1204.
23. Nassif NA, Nawabi DH, Stoner K, Elpers M, Wright T, Padgett DE. Taper design affects failure of large-head metal-on-metal total hip replacements. *Clinical Orthopaedics and Related Research* 2014;472(2):564-571.
24. Matharu GS, Pandit HG, Murray DW, Judge A. Adverse reactions to metal debris occur with all types of hip replacement not just metal-on-metal hips: a retrospective observational study of 3340 revisions for adverse reactions to metal debris from the National Joint Registry for England, Wales, Northern Ireland and the Isle of Man. *BMC Musculoskeletal Disorders* 2016;17(1):1-12.
25. D L, R S, J L, T J, S N, A N. Metal debris release from taper junctions appears to have a greater clinical impact than debris released from metal on metal bearing surfaces. *Orthopaedic Proceedings* 2013;95-B(SUPP_1):28-28.
26. Pastides PS, Dodd M, Sarraf KM, Willis-Owen CA. Trunnionosis: A pain in the neck. *World Journal of Orthopaedics* 2013;4(4):161-166.
27. Esposito CI, Wright TM, Goodman SB, Berry DJ. What is the Trouble With Trunnions? *Clinical Orthopaedics and Related Research* 2014;472(12):3652-3658.

28. Sidaginamale RP, Joyce TJ, Bowsher JG, Lord JK, Avery PJ, Nargol AVF, Langton DJ. The clinical implications of metal debris release from the taper junctions and bearing surfaces of metal-on-metal hip arthroplasty. *The Bone & Joint Journal* 2016;98-B(7):925-933.
29. Pourzal R, Catelas I, Theissmann R, Kaddick C, Fischer A. Characterization of wear particles generated from CoCrMo alloy under sliding wear conditions. *Wear* 2011;271(9):1658-1666.
30. Goldberg JR, Gilbert JL, Jacobs JJ, Bauer TW, Paprosky W, Leurgans S. A multicenter retrieval study of the taper interfaces of modular hip prostheses. *Clinical Orthopaedics and Related Research* 2002(401):149-161.
31. Cooper HJ, Della Valle CJ. Large diameter femoral heads. *The Bone & Joint Journal* 2014;96-B(11_Supple_A):23-26.
32. Moharrami N, Langton DJ, Sayginer O, Bull SJ. Why does titanium alloy wear cobalt chrome alloy despite lower bulk hardness: A nanoindentation study? *Thin Solid Films* 2013;549:79-86.
33. Oladokun A, Pettersson M, Bryant M, Engqvist H, Persson C, Hall R, Neville A. Fretting of CoCrMo and Ti6Al4V alloys in modular prostheses. *Tribology - Materials, Surfaces & Interfaces* 2015;9(4):165-173.
34. Hall DJ, Pourzal R, Lundberg HJ, Mathew MT, Jacobs JJ, Urban RM. Mechanical, chemical and biological damage modes within head-neck tapers of CoCrMo and Ti6Al4V contemporary hip replacements. *Journal of Biomedical Materials Research - Part B Applied Biomaterials* 2018;106(5):1672-1685.
35. Hallab NJ, Messina C, Skipor A, Jacobs JJ. Differences in the fretting corrosion of metal-metal and ceramic-metal modular junctions of total hip replacements. *Journal of Orthopaedic Research* 2004;22(2):250-259.
36. Bingley R, Martin A, Manfredi O, Nejadhamzeeigilani M, Oladokun A, Beadling AR, Siddiqui S, Anderson J, Thompson J, Neville A and others. Fretting–corrosion at the modular tapers interface: Inspection of standard ASTM F1875-98. *Proceedings of the Institution of Mechanical Engineers, Part H: Journal of Engineering in Medicine* 2018;232(5):492-501.
37. Panagiotidou A, Meswania J, Osman K, Bolland B, Latham J, Skinner J, Haddad FS, Hart A, Blunn G. The effect of frictional torque and bending moment on corrosion at the taper interface: An in vitro study. *Bone and Joint Journal* 2015;97-B(4):463-472.
38. ASTM International. ASTM F1875 Standard Practice for Fretting Corrosion Testing of Modular Implant Interfaces: Hip Femoral Head-Bore and Cone Taper Interface. West Conshohocken, PA; 2014.
39. ISO7206-6. Implants for surgery – partial and total hip joint prostheses – part 6: endurance properties testing and performance requirements of neck region of stemmed femoral components. International Organization for Standardization (ISO) 2013.

40. Affatato S, Leardini W, Zavalloni M. Hip Joint Simulators: State of the Art. In: Benazzo F, Falez F, Dietrich M, editors; 2006 2006//; Darmstadt. Steinkopff. p 171-180.
41. Smith SL, Joyce TJ. 10 - A hop, skip, and a jump: Towards better wear testing of hip implants. In: Friis E, editor. Mechanical Testing of Orthopaedic Implants: Woodhead Publishing; 2017. p 183-206.
42. Cooper HJ, Della Valle CJ, Berger RA, Tetreault M, Paprosky WG, Sporer SM, Jacobs JJ. Corrosion at the head-neck taper as a cause for adverse local tissue reactions after total hip arthroplasty. *Journal of Bone and Joint Surgery - Series A* 2012;94(18):1655-1661.
43. Lindgren JU, Brismar BH, Wikstrom AC. Adverse reaction to metal release from a modular metal-on-polyethylene hip prosthesis. *Journal of Bone and Joint Surgery - Series B* 2011;93 B(10):1427-1430.
44. Eltit F, Assiri A, Garbuz D, Duncan C, Masri B, Greidanus N, Bell R, Sharma M, Cox M, Wang R. Adverse reactions to metal on polyethylene implants: Highly destructive lesions related to elevated concentration of cobalt and chromium in synovial fluid. *Journal of Biomedical Materials Research - Part A* 2017;105(7):1876-1886.
45. Cook RB, Bolland BJRF, Wharton JA, Tilley S, Latham JM, Wood RJK. Pseudotumour formation due to tribocorrosion at the taper interface of large diameter metal on polymer modular total hip replacements. *Journal of Arthroplasty* 2013;28(8):1430-1436.
46. Drake RL, Vogl, A.W., Mitchell, A.W.M. *Gray's Anatomy for Students*. Philadelphia, PA: Churchill Livingstone; 2010.
47. Byrne D, J. Mulhall K, Baker J. *Anatomy & Biomechanics of the Hip*; 2010.
48. Gray H. *Anatomy of the Human Body*. Bartleby.com. 2000 ed. Philadelphia: Lea & Febiger; 1918.
49. Meyer H, Mueller T, Goldau G, Chamaon K, Ruetschi M, Lohmann CH. Corrosion at the cone/taper interface leads to failure of large-diameter metal-on-metal total hip arthroplasties. *Clinical Orthopaedics and Related Research* 2012;470(11):3101-3108.
50. Byrne D.P. MKJ, Baker J.F. *Anatomy & Biomechanics of the Hip*. The Open Sports Medicine Journal 2010;4:51-57.
51. Mazzucco DC. Variation in joint fluid composition and its effect on the tribology of replacement joint articulation: Massachusetts Institute of Technology; 2003.
52. Fam H, Bryant J, Kontopoulou M. Rheological properties of synovial fluids. *Biorheology* 2007;44(2):59-74.
53. McCarty DJ. Synovial fluid. In *Arthritis allied conditions: a text book of rheumatology*. Baltimore: Williams and Williams; 1997.

54. Binette J, Schmid K. The proteins of synovial fluid: A study of the $\alpha 1/\alpha 2$ globulin ratio. *Arthritis & Rheumatism: Official Journal of the American College of Rheumatology* 1965;8(1):14-28.
55. Harsha AP, Joyce TJ. Challenges associated with using bovine serum in wear testing orthopaedic biopolymers. *Proceedings of the Institution of Mechanical Engineers, Part H: Journal of Engineering in Medicine* 2011;225(10):948-958.
56. Fang H-W, Shih M-L, Zhao J-H, Huang H-T, Lin H-Y, Liu H-L, Chang C-H, Yang C-B, Liu H-C. Association of polyethylene friction and thermal unfolding of interfacial albumin molecules. *Applied Surface Science* 2007;253(16):6896-6904.
57. Liao YS, Benya PD, McKellop HA. Effect of protein lubrication on the wear properties of materials for prosthetic joints. *Journal of Biomedical Materials Research* 1999;48(4):465-473.
58. Saari H, Santavirta S, Nordström D, Paavolainen P, Kontinen Y. Hyaluronate in total hip replacement. *The Journal of rheumatology* 1993;20(1):87-90.
59. Decker B, McKenzie BF, McGuckin WF, Slocumb CH. Comparative distribution of proteins and glycoproteins of serum and synovial fluid. *Arthritis & Rheumatism: Official Journal of the American College of Rheumatology* 1959;2(2):162-177.
60. Yao J, Laurent M, Johnson T, Blanchard C, Crowninshield R. The influences of lubricant and material on polymer/CoCr sliding friction. *Wear* 2003;255(1-6):780-784.
61. Stewart TD, Hall RM. Erratum to “Basic biomechanics of human joints: Hips, knees and the spine” [Current Orthopaedics (2006) 20, 23–31]. *Orthopaedics and Trauma* 2010;24(2):170.
62. Woolf AD, Pfleger B. Burden of major musculoskeletal conditions. *Bulletin of the World Health Organization* 2003;81(9):646-656.
63. Altman RD, Gold GE. Atlas of individual radiographic features in osteoarthritis, revised. *Osteoarthritis and Cartilage* 2007;15:A1-A56.
64. Arthritis_Foundation. What Is Arthritis? [Available from: <https://www.arthritis.org/about-arthritis/understanding-arthritis/what-is-arthritis.php>]. Volume 2019.
65. NHS. National Health Services (NHS) Overview- Arthritis [Available from: <https://www.nhs.uk/conditions/arthritis/>].
66. Versus_Arthritis. What is osteoarthritis? [Available from: <https://www.versusarthritis.org/about-arthritis/conditions/osteoarthritis/>]. 2018.
67. Kanis JA, Melton Iii LJ, Christiansen C, Johnston CC, Khaltsev N. The diagnosis of osteoporosis. *Journal of Bone and Mineral Research* 1994;9(8):1137-1141.

68. Ginaldi L, Di Benedetto MC, De Martinis M. Osteoporosis, inflammation and ageing. *Immunity & Ageing* 2005;2(1):14.
69. Miller D, Meyer C, R P. A Barn Door: Fractured Neck of Femur. *The Internet Journal of Orthopedic Surgery* 2005; 3(2).
70. Dhanwal DK, Dennison EM, Harvey NC, Cooper C. Epidemiology of hip fracture: worldwide geographic variation. *Indian journal of orthopaedics* 2011;45(1):15.
71. Sambrook P, Cooper C. Osteoporosis. *The Lancet* 2006;367(9527):2010-2018.
72. Nephew S. Smith & Nephew Launches the CONQUEST FN™ Femoral Neck Fracture System, a Fresh Approach to Hip Preservation Versus Current Treatment Options [Available from: <http://www.smith-nephew.com/news-and-media/media-releases/news/smith-nephew-launches-the-conquest-fn-femoral-neck-fracture-system-a-fresh-approach-to-hip-preservation-versus-current-treatment-options/#>].
73. Edgar C, Einhorn TA. Treatment of Avascular Necrosis of the Femoral Head With Drilling and Injection of Concentrated Autologous Bone Marrow. *Techniques in Orthopaedics* 2011;26(1):2-8.
74. Koo K-H, Kim R, Ko G-H, Song HR, Jeong S-T, Cho S-H. Preventing collapse in early osteonecrosis of the femoral head. A randomised clinical trial of core decompression. *The Journal of bone and joint surgery. British volume* 1995;77(6):870-874.
75. Wang B-L, Sun W, Shi Z-C, Zhang N-F, Yue D-B, Guo W-S, Xu S-Q, Lou J-N, Li Z-R. Treatment of nontraumatic osteonecrosis of the femoral head with the implantation of core decompression and concentrated autologous bone marrow containing mononuclear cells. *Archives of orthopaedic and trauma surgery* 2010;130(7):859-865.
76. Steinberg ME, Larcom PG, Strafford B, Hosick WB, Corces A, Bands RE, Hartman KE. Core decompression with bone grafting for osteonecrosis of the femoral head. *Clinical Orthopaedics and Related Research®* 2001;386:71-78.
77. Orthoinfo. From American Academy of Orthopaedic Surgeons: Osteonecrosis of the Hip [Available from: <https://orthoinfo.aaos.org/en/diseases--conditions/osteonecrosis-of-the-hip>]. Volume 2019.
78. Aldinger PR, Thomsen M, Mau H, Ewerbeck V, Breusch SJ. Cementless Spotorno tapered titanium stems: excellent 10-15-year survival in 141 young patients. *Acta Orthopaedica Scandinavica* 2003;74(3):253-258.
79. Teloken MA, Bissett G, Hozack WJ, Sharkey PF, Rothman RH. Ten to fifteen-year follow-up after total hip arthroplasty with a tapered cobalt-chromium femoral component (tri-lock) inserted without cement. *JBJS* 2002;84(12):2140-2144.
80. ASTM International. ASTM F2068-15 Standard Specification for Femoral Prostheses—Metallic Implants. West Conshohocken, PA: ASTM International; 2015.

81. Mattei L, Di Puccio F, Piccigallo B, Ciulli E. Lubrication and wear modelling of artificial hip joints: A review. *Tribology International* 2011;44(5):532-549.
82. Hozack WJ, Mesa JJ, Rothman RH. Head—neck modularity for total hip arthroplasty: Is It Necessary? *The Journal of Arthroplasty* 1996;11(4):397-399.
83. Archibeck MJ, Cummins T, Carothers J, Junick DW, White RE. A Comparison of Two Implant Systems in Restoration of Hip Geometry in Arthroplasty. *Clinical Orthopaedics and Related Research®* 2011;469(2):443-446.
84. Stryker. The ABG™II Modular Anatomic Reconstruction. Volume 2019; 2007.
85. Zimmer. Zimmer M/L Taper Hip Prosthesis with Kinectiv Technology. 2011.
86. Del Balso C, Teeter MG, Tan SC, Howard JL, Lanting BA. Trunnionosis: Does Head Size Affect Fretting and Corrosion in Total Hip Arthroplasty? *The Journal of Arthroplasty* 2016;31(10):2332-2336.
87. Heiney JP, Battula S, Vrabec GA, Parikh A, Blice R, Schoenfeld AJ, Njus GO. Impact magnitudes applied by surgeons and their importance when applying the femoral head onto the Morse taper for total hip arthroplasty. *Archives of Orthopaedic and Trauma Surgery* 2009;129(6):793-796.
88. ASTM International. F3018-17 Standard Guide for Assessment of Hard-on-Hard Articulation Total Hip Replacement and Hip Resurfacing Arthroplasty Devices. West Conshohocken, PA; 2017.
89. Orthoworld. Orthopaedic Industry Annual Report®. Volume 2019: Orthoworld; 2019.
90. Szostakowski B, Jagiello J, Skinner JA. ArtiFacts: Ivory Hemiarthroplasty: The Forgotten Concept Lives On. *Clinical Orthopaedics and Related Research®* 2017;475(12):2850-2854.
91. Smith-Petersen M. Evolution of mould arthroplasty of the hip joint. *The Journal of bone and joint surgery. British volume* 1948;30(1):59-75.
92. Wiles P. The surgery of the osteo-arthritic hip. *British Journal of Surgery* 1958;45(193):488-497.
93. Charnley J. Arthroplasty of the hip. A New Operation. *The Lancet* 1961;277(7187):1129-1132.
94. Waugh W. John Charnley: The Man and the Hip. London: Springer-Verlag; 1990.
95. Kurtz S, Manley M. CHAPTER 61 - Cross-Linked Polyethylene. In: Hozack WJ, Parvizi J, Bender B, editors. *Surgical Treatment of Hip Arthritis*. Philadelphia: W.B. Saunders; 2009. p 456-467.
96. Furnes O, Lie S, Espehaug B, Vollset S, Engesaeter L, Havelin L. Hip disease and the prognosis of total hip replacements: a review of 53 698 primary total hip replacements reported to the Norwegian arthroplasty register 1987–99. *The Journal of bone and joint surgery. British volume* 2001;83(4):579-579.

97. Chana R, Facek M, Tilley S, Walter WK, Zicat B, Walter WL. Ceramic-on-ceramic bearings in young patients: Outcomes and activity levels at minimum ten-year follow-up. *Bone and Joint Journal* 2013;95 B(12):1603-1609.
98. Campbell R, Rothman R. Charnley low-friction total hip replacement. *American Journal of Roentgenology* 1971;113(4):634-641.
99. ISO7206-1. Implants for surgery. Partial and total hip joint prostheses. Classification and designation of dimensions. Geneva, Switzerland: International Organization for Standardization (ISO); 2009.
100. The National Joint Registry for England, Wales, Northern Ireland and the Isle of Man, 15th Annual Report - Prostheses used in hip, knee, ankle, elbow and shoulder replacement procedures 2017. 2018.
101. Affatato S. 4 - Contemporary designs in total hip arthroplasty (THA). In: Affatato S, editor. *Perspectives in Total Hip Arthroplasty*: Woodhead Publishing; 2014. p 46-64.
102. Bergmann CP, Stumpf A. Biomaterials. In: Bergmann C, Stumpf A, editors. *Dental Ceramics: Microstructure, Properties and Degradation*. Berlin, Heidelberg: Springer Berlin Heidelberg; 2013. p 9-13.
103. Williams D. *The Williams Dictionary of Biomaterials*: Liverpool University Press; 1999.
104. ISO6474-2. Implants for surgery. Ceramic materials. Composite materials based on a high-purity alumina matrix with zirconia reinforcement. Geneva, Switzerland: International Organization for Standardization (ISO); 2019.
105. Goodman SB, Gómez Barrena E, Takagi M, Konttinen YT. Biocompatibility of total joint replacements: A review. *Journal of Biomedical Materials Research Part A* 2009;90A(2):603-618.
106. Yan Y, Neville A, Dowson D. Tribo-corrosion properties of cobalt-based medical implant alloys in simulated biological environments. *Wear* 2007;263(7-12 SPEC. ISS.):1105-1111.
107. ASTM International. ASTM F75-18 Standard Specification for Cobalt-28 Chromium-6 Molybdenum Alloy Castings and Casting Alloy for Surgical Implants (UNS R30075). West Conshohocken, PA: ASTM International; 2018.
108. ASTM International. ASTM F1537-11 Standard Specification for Wrought Cobalt-28Chromium-6Molybdenum Alloys for Surgical Implants (UNS R31537, UNS R31538, and UNS R31539). West Conshohocken, PA: ASTM International; 2011.
109. Valero-Vidal C, Casabán-Julián L, Herraiz-Cardona I, Igual-Muñoz A. Influence of carbides and microstructure of CoCrMo alloys on their metallic dissolution resistance. *Materials Science and Engineering: C* 2013;33(8):4667-4676.
110. Liao Y, Hoffman E, Wimmer M, Fischer A, Jacobs J, Marks L. CoCrMo metal-on-metal hip replacements. *Physical Chemistry Chemical Physics* 2013;15(3):746-756.

111. Clemow AJT, Daniell BL. Solution treatment behavior of Co-Cr-Mo alloy. *Journal of Biomedical Materials Research* 1979;13(2):265-279.
112. Kinbrum A, Unsworth A. The wear of high-carbon metal-on-metal bearings after different heat treatments. *Proceedings of the Institution of Mechanical Engineers, Part H: Journal of Engineering in Medicine* 2008;222(6):887-895.
113. Ulrich SD, Seyler TM, Bennett D, Delanois RE, Saleh KJ, Thongtrangan I, Kuskowski M, Cheng EY, Sharkey PF, Parvizi J. Total hip arthroplasties: what are the reasons for revision? *International orthopaedics* 2008;32(5):597-604.
114. Bozic KJ, Kurtz SM, Lau E, Ong K, Vail TP, Berry DJ. The epidemiology of revision total hip arthroplasty in the United States. *JBJS* 2009;91(1):128-133.
115. Bobyn JD, Mortimer ES, Glassman AH, Engh CA, Miller JE, Brooks CE. Producing and Avoiding Stress Shielding: Laboratory and Clinical Observations of Noncemented Total Hip Arthroplasty. *Clinical Orthopaedics and Related Research®* 1992;274:79-96.
116. Engh CA, Bobyn J, Glassman AH. Porous-coated hip replacement. The factors governing bone ingrowth, stress shielding, and clinical results. *The Journal of bone and joint surgery. British volume* 1987;69(1):45-55.
117. Wang K. The use of titanium for medical applications in the USA. *Materials Science and Engineering: A* 1996;213(1-2):134-137.
118. Sumner DR, Galante JO. Determinants of stress shielding. *Clin. Orthop. Relat. Res* 1991;274:202-212.
119. Royhman D, Yuan J, Shokuhfar T, Takoudis C, Sukotjo C, Mathew M. Tribocorrosive behaviour of commonly used temporomandibular implants in a synovial fluid-like environment: Ti-6Al-4V and CoCrMo. *Journal of Physics D: Applied Physics* 2013;46(40):404002.
120. Semlitsch M. Titanium alloys for hip joint replacements. *Clinical Materials* 1987;2(1):1-13.
121. Park B, Kim YK. Metallic biomaterials. *Balance* 2003;1:50.
122. Barão VA, Mathew MT, Assunção WG, Yuan JCC, Wimmer MA, Sukotjo C. Stability of cp-Ti and Ti-6 Al-4 V alloy for dental implants as a function of saliva pH—an electrochemical study. *Clinical oral implants research* 2012;23(9):1055-1062.
123. Raju S, Chinnakkannu K, Puttaswamy MK, Phillips MJ. Trunnion Corrosion in Metal-on-Polyethylene Total Hip Arthroplasty: A Case Series. *JAAOS - Journal of the American Academy of Orthopaedic Surgeons* 2017;25(2):133-139.
124. Oldani C, Dominguez A. Titanium as a Biomaterial for Implants. *Recent advances in arthroplasty: InTechOpen*; 2012.

125. Agins HJ, Alcock NW, Bansal M, Salvati EA, Wilson Jr PD, Pellicci PM, Bullough PG. Metallic wear in failed titanium-alloy total hip replacements. A histological and quantitative analysis. *Journal of Bone and Joint Surgery - Series A* 1988;70(3):347-356.
126. Langton DJ, Jameson SS, Joyce TJ, Hallab NJ, Natsu S, Nargol AVF. Early failure of metal-on-metal bearings in hip resurfacing and large-diameter total hip replacement: A consequence of excess wear. *Journal of Bone and Joint Surgery - Series B* 2010;92(1):38-46.
127. Langton D, Joyce T, Jameson S, Lord J, Van Orsouw M, Holland J, Nargol A, De Smet K. Adverse reaction to metal debris following hip resurfacing: the influence of component type, orientation and volumetric wear. *The Journal of bone and joint surgery. British volume* 2011;93(2):164-171.
128. De Steiger RN, Hang JR, Miller LN, Graves SE, Davidson DC. Five-year results of the ASR XL acetabular system and the ASR hip resurfacing system: An analysis from the Australian Orthopaedic Association National Joint Replacement Registry. *Journal of Bone and Joint Surgery - Series A* 2011;93(24):2287-2293.
129. NJR. The National Joint Registry for England, Wales, Northern Ireland and the Isle of Man: Metal-on-metal hip implants. Volume 2019.
130. Boutin P. Alumina and its use in surgery of the hip. (Experimental study). *La Presse medicale* 1971;79(14):639-640.
131. Masson B. Emergence of the alumina matrix composite in total hip arthroplasty. *International Orthopaedics* 2009;33(2):359-363.
132. Dalla Pria P. Evolution and new application of the alumina ceramics in joint replacement. *European Journal of Orthopaedic Surgery and Traumatology* 2007;17(3):253-256.
133. Kuntz M. Validation of a New High Performance Alumina Matrix Composite for use in Total Joint Replacement. *Seminars in Arthroplasty* 2006;17(3):141-145.
134. Zimmer. Ceramic-on-Ceramic - Scientific Information BIOLOX delta Ceramic. Volume 2019.
135. CeramTec. BIOLOX® Advanced Ceramics. [Available from: <https://www.ceramtec.com/ceramic-materials/biolox/delta/>].
136. Isaac GH, Dowson D, Wroblewski BM. An Investigation into the Origins of Time-Dependent Variation in Penetration Rates with Charnley Acetabular Cups—Wear, Creep or Degradation? *Proceedings of the Institution of Mechanical Engineers, Part H: Journal of Engineering in Medicine* 1996;210(3):209-216.
137. Kurtz SM. UHMWPE biomaterials handbook: ultra high molecular weight polyethylene in total joint replacement and medical devices: Academic Press; 2009.

138. Oral E, Christensen SD, Malhi AS, Wannomae KK, Muratoglu OK. Wear Resistance and Mechanical Properties of Highly Cross-linked, Ultrahigh-Molecular Weight Polyethylene Doped With Vitamin E. *Journal of Arthroplasty* 2006;21(4):580-591.
139. Kurtz SM, Dumbleton J, Siskey RS, Wang A, Manley M. Trace concentrations of vitamin E protect radiation crosslinked UHMWPE from oxidative degradation. *Journal of Biomedical Materials Research Part A* 2009;90A(2):549-563.
140. Zagra L, Gallazzi E. Bearing surfaces in primary total hip arthroplasty. *EFORT open reviews* 2018;3(5):217-224.
141. Campbell P, Shen F-W, McKellop H. Biologic and tribologic considerations of alternative bearing surfaces. *Clinical Orthopaedics and Related Research* (1976-2007) 2004;418:98-111.
142. NICE. National Institute for Health and Care Excellence. Total hip replacement and resurfacing arthroplasty for end-stage arthritis of the hip. Technology appraisal guidance [TA304]. 2014.
143. Ulrich SD, Seyler TM, Bennett D, Delanois RE, Saleh KJ, Thongtrangan I, Kuskowski M, Cheng EY, Sharkey PF, Parvizi J and others. Total hip arthroplasties: What are the reasons for revision? *International Orthopaedics* 2008;32(5):597-604.
144. Abu-Amer Y, Darwech I, Clohisy JC. Aseptic loosening of total joint replacements: mechanisms underlying osteolysis and potential therapies. *Arthritis research & therapy* 2007;9(S1):S6.
145. Vanrusselt J, Vansevenant M, Vanderschueren G, Vanhoenacker F. Postoperative radiograph of the hip arthroplasty: what the radiologist should know. *Insights into imaging* 2015;6(6):591-600.
146. Pandit H, Glyn-Jones S, McLardy-Smith P, Gundle R, Whitwell D, Gibbons CLM, Ostlere S, Athanasou N, Gill HS, Murray DW. Pseudotumours associated with metal-on-metal hip resurfacings. *Journal of Bone and Joint Surgery - Series B* 2008;90(7):847-851.
147. Kwon Y-M, Glyn-Jones S, Simpson D, Kamali A, McLardy-Smith P, Gill H, Murray D. Analysis of wear of retrieved metal-on-metal hip resurfacing implants revised due to pseudotumours. *The Journal of bone and joint surgery. British volume* 2010;92(3):356-361.
148. Whitehouse MR, Endo M, Zachara S, Nielsen TO, Greidanus NV, Masri BA, Garbuz DS, Duncan CP. Adverse local tissue reactions in metal-on-polyethylene total hip arthroplasty due to trunnion corrosion: The risk of misdiagnosis. *Bone and Joint Journal* 2015;97-B(8):1024-1030.
149. Persson A, Eisler T, Bodén H, Krupic F, Sköldenberg O, Muren O. Revision for Symptomatic Pseudotumor After Primary Metal-on-Polyethylene Total Hip Arthroplasty with a Standard Femoral Stem. *JBJS* 2018;100(11):942-949.

150. Engh CA, Ho H. Metal-on-metal hip arthroplasty: does early clinical outcome justify the chance of an adverse local tissue reaction? *Clinical Orthopaedics and Related Research*® 2010;468(2):406-412.
151. Schmalzried TP. The future of hip resurfacing. *Orthopedic Clinics* 2011;42(2):271-273.
152. Plummer DR, Berger RA, Paprosky WG, Sporer SM, Jacobs JJ, Della Valle CJ. Diagnosis and Management of Adverse Local Tissue Reactions Secondary to Corrosion at the Head-Neck Junction in Patients With Metal on Polyethylene Bearings. *Journal of Arthroplasty* 2016;31(1):264-268.
153. Fillingham YA, Della Valle CJ, Bohl DD, Kelly MP, Hall DJ, Pourzal R, Jacobs JJ. Serum Metal Levels for Diagnosis of Adverse Local Tissue Reactions Secondary to Corrosion in Metal-on-Polyethylene Total Hip Arthroplasty. *Journal of Arthroplasty* 2017;32(9):S272-S277.
154. Waterson HB, Whitehouse MR, Greidanus NV, Garbuz DS, Masri BA, Duncan CP. Revision for adverse local tissue reaction following metal-on-polyethylene total hip arthroplasty is associated with a high risk of early major complications. *The Bone & Joint Journal* 2018;100-B(6):720-724.
155. Abdulkarim A, Ellanti P, Motterlini N, Fahey T, O'Byrne JM. Cemented versus uncemented fixation in total hip replacement: a systematic review and meta-analysis of randomized controlled trials. *Orthopedic reviews* 2013;5(1).
156. Maggs J, Wilson M. The relative merits of cemented and uncemented prostheses in total hip arthroplasty. *Indian journal of orthopaedics* 2017;51(4):377.
157. Zhang C, Yan CH, Zhang W. Cemented or cementless fixation for primary hip arthroplasty—evidence from The International Joint Replacement Registries. *Annals of Joint* 2017;2(10).
158. Nayak N, Mulliken B, Rorabeck C, Bourne R, Robinson E. Osteolysis in cemented versus cementless acetabular components. *The Journal of arthroplasty* 1996;11(2):135-140.
159. Thien TM, Chatziagorou G, Garellick G, Furnes O, Havelin LI, Mäkelä K, Overgaard S, Pedersen A, Eskelinen A, Pulkkinen P. Periprosthetic femoral fracture within two years after total hip replacement: analysis of 437,629 operations in the nordic arthroplasty register association database. *JBJS* 2014;96(19):e167.
160. Pauli W. God made the bulk; surfaces were invented by the devil. *Springer Series in Materials Science*. Volume 232; 2016. p 149-156.
161. Jost P. Lubrication (tribology) : education and research; a report on the present position and industry's needs. In: Science DoEa, editor. Great Britain; 1966.
162. Dowson D, Wright V. *Bio-tribology*. 1973; London. The Institute of Petroleum, The Institution of Mechanical Engineers, and the British Society of Rheology. p 81–88.

163. ASTM_International. ASTM G40-17 Standard Terminology Relating to Wear and Erosion. West Conshohocken, PA,: ASTM International.
164. Burwell JT, Strang CD. On the empirical law of adhesive wear. *Journal of Applied Physics* 1952;23(1):18-28.
165. Jin ZM, Stone M, Ingham E, Fisher J. (v) Biotribology. *Current Orthopaedics* 2006;20(1):32-40.
166. Affatato S, Spinelli M, Zavalloni M, Mazzega-Fabbro C, Viceconti M. Tribology and total hip joint replacement: Current concepts in mechanical simulation. *Medical Engineering and Physics* 2008;30(10):1305-1317.
167. McGee MA, Howie DW, Costi K, Haynes DR, Wildenauer CI, Percy MJ, McLean JD. Implant retrieval studies of the wear and loosening of prosthetic joints: a review. *Wear* 2000;241(2):158-165.
168. Brown TD, Lundberg HJ, Pedersen DR, Callaghan JJ. 2009 Nicolas Andry Award: clinical biomechanics of third body acceleration of total hip wear. *Clinical orthopaedics and related research* 2009;467(7):1885-1897.
169. Archard JF. Contact and rubbing of flat surfaces. *Journal of Applied Physics* 1953;24(8):981-988.
170. Hutchings I, Shipway P. 5 - Sliding wear. In: Hutchings I, Shipway P, editors. *Tribology (Second Edition)*: Butterworth-Heinemann; 2017. p 107-164.
171. Lancaster JK. Dry bearings: a survey of materials and factors affecting their performance. *Tribology* 1973;6(6):219-251.
172. Trommer RM, Maru MM. Importance of preclinical evaluation of wear in hip implant designs using simulator machines. *Revista Brasileira de Ortopedia (English Edition)* 2017;52(3):251-259.
173. ISO14242-2. Implants for surgery — Wear of total hip-joint prostheses Part 2: Methods of measurement. Geneva, Switzerland: International Organization for Standardization (ISO); 2016.
174. Katz A, Redlich M, Rapoport L, Wagner H, Tenne R. Self-lubricating coatings containing fullerene-like WS₂ nanoparticles for orthodontic wires and other possible medical applications. *Tribology Letters* 2006;21(2):135-139.
175. Clarke IC. Wear of Artificial Joint Materials I: Friction and Wear Studies: Validity of Wear-Screening Protocols. *Engineering in Medicine* 1981;10(3):115-122.
176. Bragdon C, O'connor D, Lowenstein J, Jasty M, Syniuta W. The importance of multidirectional motion on the wear of polyethylene. *Proceedings of the Institution of Mechanical Engineers, Part H: Journal of Engineering in Medicine* 1996;210(3):157-165.

177. Wright K, Scales J. Stanmore hip joint simulators for study of total hip joint replacements. *Evaluation of Artificial Joints*; Dowson, D., Wright, D., Eds 1977:9-17.
178. Duff-Barclay I, Spillman D. Paper 10: total human hip joint prostheses—a laboratory study of friction and wear. 1966. SAGE Publications Sage UK: London, England. p 90-103.
179. Linn FC. Lubrication of animal joints: I. The arthrotripsometer. *JBJS* 1967;49(6):1079-1098.
180. Scales JT, Kelly P, Goddard D. Friction torque studies of total joint replacements: the use of a simulator. *Annals of the rheumatic diseases* 1969;28(Suppl 5):30.
181. Dowson D, Walker PS, Longfield MD, Wright V. A joint simulating machine for load-bearing joints. *Medical and biological engineering* 1970;8(1):37-43.
182. Clarke IC. Wear of artificial joint materials. IV. Hip joint simulator studies. *Engineering in Medicine* 1981;10(4):189-198.
183. Whittle MW. *Gait analysis: an introduction*: Butterworth-Heinemann; 2014.
184. Rajtůková V, Michalíková M, Bednarčíková L, Balogová A, Živčák J. Biomechanics of lower limb prostheses. *Procedia Engineering* 2014;96:382-391.
185. Paul J. Paper 8: forces transmitted by joints in the human body. 1966. SAGE Publications Sage UK: London, England. p 8-15.
186. Soares dos Santos MP, Ferreira JA, Ramos A, Simões JA, Morais R, Silva NM, Santos PM, Reis MC, Oliveira T. Instrumented hip joint replacements, femoral replacements and femoral fracture stabilizers. *Expert review of medical devices* 2014;11(6):617-635.
187. ISO14242-1. Implants for surgery — Wear of total hip-joint prostheses Part 1: Loading and displacement parameters for wear-testing machines and corresponding environmental conditions for test. International Organization for Standardization (ISO). Geneva, Switzerland; 2014.
188. Milošev I, Levašič V, Vidmar J, Kovač S, Trebše R. pH and metal concentration of synovial fluid of osteoarthritic joints and joints with metal replacements. *Journal of Biomedical Materials Research Part B: Applied Biomaterials* 2016;105(8):2507-2515.
189. Saikko V. A 12-station anatomic hip joint simulator. *Proceedings of the Institution of Mechanical Engineers, Part H: Journal of Engineering in Medicine* 2005;219(6):437-448.
190. Kaddick C, Wimmer MA. Hip simulator wear testing according to the newly introduced standard ISO 14242. *Proceedings of the Institution of Mechanical Engineers, Part H: Journal of Engineering in Medicine* 2001;215(5):429-442.

191. Dumbleton JH, D'Antonio JA, Manley MT, Capello WN, Wang A. The basis for a second-generation highly cross-linked UHMWPE. *Clinical Orthopaedics and Related Research* 2006(453):265-271.
192. D'Lima DD, Hermida JC, Chen PC, Colwell Jr CW. Polyethylene cross-linking by two different methods reduces acetabular liner wear in a hip joint wear simulator. *Journal of Orthopaedic Research* 2003;21(5):761-766.
193. Partridge S, Tipper JL, Al-Hajjar M, Isaac GH, Fisher J, Williams S. Evaluation of a new methodology to simulate damage and wear of polyethylene hip replacements subjected to edge loading in hip simulator testing. *Journal of Biomedical Materials Research - Part B Applied Biomaterials* 2018;106(4):1456-1462.
194. Fisher J, Jin Z, Tipper J, Stone M, Ingham E. Tribology of alternative bearings. *Clinical orthopaedics and related research* 2006;453:25-34.
195. Galvin AL, Jennings LM, Tipper JL, Ingham E, Fisher J. Wear and creep of highly crosslinked polyethylene against cobalt chrome and ceramic femoral heads. *Proceedings of the Institution of Mechanical Engineers, Part H: Journal of Engineering in Medicine* 2010;224(10):1175-1183.
196. Smith SL, Unsworth A. An in vitro wear study of alumina-alumina total hip prostheses. *Proceedings of the Institution of Mechanical Engineers, Part H: Journal of Engineering in Medicine* 2001;215(5):443-446.
197. Al-Hajjar M, Leslie IJ, Tipper J, Williams S, Fisher J, Jennings LM. Effect of cup inclination angle during microseparation and rim loading on the wear of BIOLOX® delta ceramic-on-ceramic total hip replacement. *Journal of Biomedical Materials Research - Part B Applied Biomaterials* 2010;95 B(2):263-268.
198. Affatato S, Freccero N, Taddei P. The biomaterials challenge: A comparison of polyethylene wear using a hip joint simulator. *Journal of the Mechanical Behavior of Biomedical Materials* 2016;53:40-48.
199. Richardson HA, Clarke IC, Williams P, Donaldson T, Oonishi H. Precision and accuracy in ceramic-on-ceramic wear analyses: Influence of simulator test duration. *Proceedings of the Institution of Mechanical Engineers, Part H: Journal of Engineering in Medicine* 2005;219(6):401-405.
200. Nevelos JE, Ingham E, Doyle C, Nevelos AB, Fisher J. The influence of acetabular cup angle on the wear of "BIOLOX Forte" alumina ceramic bearing couples in a hip joint simulator. *Journal of Materials Science: Materials in Medicine* 2001;12(2):141-144.
201. Essner A, Sutton K, Wang A. Hip simulator wear comparison of metal-on-metal, ceramic-on-ceramic and crosslinked UHMWPE bearings. *Wear* 2005;259(7-12):992-995.
202. Spinelli M, Affatato S, Corvi A, Viceconti M. Ceramic-on-ceramic vs. metal-on-metal in total hip arthroplasty (THA): Do 36-mm diameters exhibit comparable wear performance? *Materialwissenschaft und Werkstofftechnik* 2009;40(1-2):94-97.

203. Smith SL, Unsworth. A comparison between gravimetric and volumetric techniques of wear measurement of UHMWPE acetabular cups against zirconia and cobalt-chromium-molybdenum femoral heads in a hip simulator. *Proceedings of the Institution of Mechanical Engineers, Part H: Journal of Engineering in Medicine* 1999;213(6):475-483.
204. Ali M, Al-Hajjar M, Partridge S, Williams S, Fisher J, Jennings LM. Influence of hip joint simulator design and mechanics on the wear and creep of metal-on-polyethylene bearings. *Proceedings of the Institution of Mechanical Engineers, Part H: Journal of Engineering in Medicine* 2016;230(5):389-397.
205. Fisher J, Jin Z, Tipper J, Stone M, Ingham E. Presidential guest lecture: Tribology of alternative bearings. *Clinical Orthopaedics and Related Research* 2006(453):25-34.
206. Liu F, Fisher J. Effect of an edge at cup rim on contact stress during micro-separation in ceramic-on-ceramic hip joints. *Tribology International* 2017;113:323-329.
207. Lusty PJ, Watson A, Tuke MA, Walter WL, Walter WK, Zicat B. Orientation and wear of the acetabular component in third generation alumina-on-alumina ceramic bearings: An analysis of 33 retrievals. *Journal of Bone and Joint Surgery - Series B* 2007;89(9):1158-1164.
208. Walter WL, Insley GM, Walter WK, Tuke MA. Edge loading in third generation alumina ceramic-on-ceramic bearings: Stripe wear. *Journal of Arthroplasty* 2004;19(4):402-413.
209. Nevelos JE, Ingham E, Doyle C, Nevelos AB, Fisher J. Wear of HIPed and non-HIPed alumina-alumina hip joints under standard and severe simulator testing conditions. *Biomaterials* 2001;22(16):2191-2197.
210. Tipper JL, Firkins PJ, Besong AA, Barbour PSM, Nevelos J, Stone MH, Ingham E, Fisher J. Characterisation of wear debris from UHMWPE on zirconia ceramic, metal-on-metal and alumina ceramic-on-ceramic hip prostheses generated in a physiological anatomical hip joint simulator. *Wear* 2001;250-251(PART 1):120-128.
211. Affatato S, Bersaglia G, Rocchi M, Taddei P, Fagnano C, Toni A. Wear behaviour of cross-linked polyethylene assessed in vitro under severe conditions. *Biomaterials* 2005;26(16):3259-3267.
212. Fisher J, Jennings LM, Galvin AL. Wear of Highly Crosslinked Polyethylene against Cobalt Chrome and Ceramic femoral heads. In: F. B, F. F, M. D, editors; 2006; Rome. Steinkopff Verlag.
213. Glyn-Jones S, Thomas GER, Garfjeld-Roberts P, Gundle R, Taylor A, McLardy-Smith P, Murray DW. The John Charnley Award: Highly Crosslinked Polyethylene in Total Hip Arthroplasty Decreases Long-term Wear: A Double-blind Randomized Trial. *Clinical Orthopaedics and Related Research* 2014;473(2):432-438.
214. Devane PA, Horne JG, Ashmore A, Mutimer J, Kim W, Stanley J. Highly Cross-Linked Polyethylene Reduces Wear and Revision Rates in Total Hip Arthroplasty: A

- 10-Year Double-Blinded Randomized Controlled Trial. *Journal of Bone and Joint Surgery - American Volume* 2017;99(20):1703-1714.
215. Hanna SA, Somerville L, McCalden RW, Naudie DD, MacDonald SJ. Highly cross-linked polyethylene decreases the rate of revision of total hip arthroplasty compared with conventional polyethylene at 13 years' follow-up. *Bone and Joint Journal* 2016;98B(1):28-32.
 216. Keeney JA, Martell JM, Pashos G, Nelson CJ, Maloney WJ, Clohisy JC. Highly cross-linked polyethylene improves wear and mid-term failure rates for young total hip arthroplasty patients. *HIP International* 2015;25(5):435-441.
 217. Rabinowicz E. *Friction Wear of Materials*. New York: John Wiley and Sons; 1965.
 218. Scholes S, Unsworth A. Comparison of friction and lubrication of different hip prostheses. *Proceedings of the Institution of Mechanical Engineers, Part H: Journal of Engineering in Medicine* 2000;214(1):49-57.
 219. Johnson KL, Greenwood JA, Poon SY. A simple theory of asperity contact in elastohydro-dynamic lubrication. *Wear* 1972;19(1):91-108.
 220. Hamrock BJ, Dowson D. Elastohydrodynamic Lubrication of Elliptical Contacts for Materials of Low Elastic Modulus I—Fully Flooded Conjunction. *J Lubr Technol Trans ASME* 1978;100(2):236-245.
 221. Brockett C, Williams S, Jin Z, Isaac G, Fisher J. Friction of total hip replacements with different bearings and loading conditions. *Journal of Biomedical Materials Research Part B: Applied Biomaterials: An Official Journal of The Society for Biomaterials, The Japanese Society for Biomaterials, and The Australian Society for Biomaterials and the Korean Society for Biomaterials* 2007;81(2):508-515.
 222. Jin ZM, Dowson D, Fisher J. Analysis of fluid film lubrication in artificial hip joint replacements with surfaces of high elastic modulus. *Proceedings of the Institution of Mechanical Engineers, Part H: Journal of Engineering in Medicine* 1997;211(3):247-256.
 223. Jin Z, Dowson D, Fisher J. Fluid film lubrication in natural hip joints. *Tribology Series: Elsevier*; 1993. p 545-555.
 224. Young T. III. An essay on the cohesion of fluids. *Philosophical transactions of the royal society of London* 1805(95):65-87.
 225. Kubiak KJ, Wilson MCT, Mathia TG, Carval P. Wettability versus roughness of engineering surfaces. *Wear* 2011;271(3-4):523-528.
 226. Asmatulu R. Highly Hydrophilic Electrospun Polyacrylonitrile/ Polyvinylpyrrolidone Nanofibers Incorporated with Gentamicin as Filter Medium for Dam Water and Wastewater Treatment; 2016. 38-56 p.
 227. Zisman WA. Relation of the equilibrium contact angle to liquid and solid constitution. *ACS Publications*; 1964.

228. Borruto A, Marrelli L, Palma F. The Difference of Material Wettability as Critical Factor in the Choice of a Tribological Prosthetic Coupling Without Debris Release. *Tribology Letters* 2005;20(1):1-10.
229. Salehi A, Aldinger P, Sprasue J, Hunter G, Bateni A, Tavana H, Neumann AW. Dynamic contact angle measurements on orthopaedic ceramics and metals. 2003. p 98-102.
230. Gispert MP, Serro AP, Colaço R, Saramago B. Friction and wear mechanisms in hip prosthesis: Comparison of joint materials behaviour in several lubricants. *Wear* 2006;260(1-2):149-158.
231. Triantafyllopoulos GK, Elpers ME, Burket JC, Esposito CI, Padgett DE, Wright TM. Otto Aufranc Award: Large Heads Do Not Increase Damage at the Head-neck Taper of Metal-on-polyethylene Total Hip Arthroplasties. *Clinical Orthopaedics and Related Research* 2016;474(2):330-338.
232. Jani SC, Sauer WL, McLean TW, Lambert RD, Kovacs P. Fretting corrosion mechanisms at modular implant interfaces. *Modularity of Orthopedic Implants: ASTM International*; 1997.
233. Ashkanfar A, Langton DJ, Joyce TJ. A large taper mismatch is one of the key factors behind high wear rates and failure at the taper junction of total hip replacements: A finite element wear analysis. *Journal of the Mechanical Behavior of Biomedical Materials* 2017;69:257-266.
234. Morlock M, Bishop N, Huber G. *Biomechanics of Hip Arthroplasty*. 2011. p 11-24.
235. Morlock MM. The taper disaster-how could it happen? *Hip International* 2015;25(4):339-346.
236. Mueller U, Braun S, Schroeder S, Sonntag R, Kretzer JP. Same same but different? 12/14 stem and head tapers in total hip arthroplasty. *The Journal of arthroplasty* 2017;32(10):3191-3199.
237. Hernigou P, Queinnec S, Lachaniette CHF. One hundred and fifty years of history of the Morse taper: from Stephen A. Morse in 1864 to complications related to modularity in hip arthroplasty. *International orthopaedics* 2013;37(10):2081-2088.
238. Jeremy L. Gilbert SAMSS. *Corrosion of Modular Tapers in Total Joint Replacements: A Critical Assessment of Design, Materials, Surface Structure, Mechanics, Electrochemistry, and Biology Modularity and Tapers in Total Joint Replacement Devices*. West Conshohocken, PA: ASTM International; 2015. 192-223 p.
239. Elkins JM, Callaghan JJ, Brown TD. Stability and trunnion wear potential in large-diameter metal-on-metal total hips: a finite element analysis. *Clinical Orthopaedics and Related Research®* 2014;472(2):529-542.
240. Banerjee S, Cherian JJ, Bono JV, Kurtz SM, Geesink R, Meneghini RM, Delanois RE, Mont MA. Gross Trunnion Failure After Primary Total Hip Arthroplasty. *The Journal of Arthroplasty* 2015;30(4):641-648.

241. Kocagoz SB, Underwood RJ, Macdonald DW, Gilbert JL, Kurtz SM. Ceramic heads decrease metal release caused by head-taper fretting and corrosion. *Clinical Orthopaedics and Related Research* 2016;474(4):985-994.
 242. Lundberg HJ, Ha NQ, Hall DJ, Urban RM, Levine BR, Pourzal R. Contact mechanics and plastic deformation at the local surface topography level after assembly of modular head-neck junctions in modern total hip replacement devices. 2015. p 59-82.
 243. Hothi HS, Eskelinen AP, Berber R, Lainiala OS, Moilanen TPS, Skinner JA, Hart AJ. Factors Associated With Trunnionosis in the Metal-on-Metal Pinnacle Hip. *Journal of Arthroplasty* 2017;32(1):286-290.
 244. Hothi HS, Kendoff D, Lausmann C, Henckel J, Gehrke T, Skinner J, Hart A. Clinically insignificant trunnionosis in large-diameter metal-on-polyethylene total hip arthroplasty. *Bone and Joint Research* 2017;6(1):52-56.
 245. Brown SA, Hughes PJ, Merritt K. In vitro studies of fretting corrosion of orthopaedic materials. *Journal of Orthopaedic Research* 1988;6(4):572-579.
 246. Urban RM, Jacobs JJ, Gilbert JL, Galante JO. Migration of corrosion products from modular hip prostheses. Particle microanalysis and histopathological findings. *Journal of Bone and Joint Surgery - Series A* 1994;76(9):1345-1359.
 247. Jacobs JJ, Urban RM, Gilbert JL, Skipor AK, Black J, Jasty M, Galante JO. Local and distant products from modularity. *Clinical Orthopaedics and Related Research* 1995(319):94-105.
 248. Gilbert JL, Jacobs JJ. The mechanical and electrochemical processes associated with taper fretting crevice corrosion: A review ASTM Special Technical Publication 1997;1301:45-59.
 249. Gilbert J, Jacobs J. The Mechanical and Electrochemical Processes Associated with Taper Fretting Crevice Corrosion: A Review
- Modularity of Orthopedic Implants. West Conshohocken, PA: ASTM International; 1997. 45-59 p.
250. Davies A, Willert H, Campbell P, Learmonth I, Case C. An unusual lymphocytic perivascular infiltration in tissues around contemporary metal-on-metal joint replacements. *JBJS* 2005;87(1):18-27.
 251. Mali SA. Mechanically assisted crevice corrosion in metallic biomaterials: a review. *Materials Technology* 2016;31(12):732-739.
 252. Brown SA, Flemming CAC, Kawalec JS, Placko HE, Vassaux C, Merritt K, Payer JH, Kraay MJ. Fretting corrosion accelerates crevice corrosion of modular hip tapers. *Journal of applied biomaterials* 1995;6(1):19-26.
 253. Swaminathan V, Gilbert JL. Fretting corrosion of CoCrMo and Ti6Al4V interfaces. *Biomaterials* 2012;33(22):5487-5503.

254. Arnholt C, Underwood R, MacDonald DW, Higgs GB, Chen AF, Klein G, Hamlin B, Lee GC, Mont M, Cates H and others. Microgrooved surface topography does not influence fretting corrosion of tapers in total hip arthroplasty: Classification and retrieval analysis. In: Greenwald A, Kurtz S, Lemons J, Mihalko W, editors. *Modularity and Tapers in Total Joint Replacement Devices*, STP1591-EB. West Conshohocken, PA: ASTM Special Technical Publication; 2015. p 99-112.
255. Fischer A, Janssen D, Wimmer MA. The Influence of Molybdenum on the Fretting Corrosion Behavior of CoCr/TiAlV Couples. *Biotribology* 2017;11:8-19.
256. Royhman D, Patel M, Runa MJ, Wimmer MA, Jacobs JJ, Hallab NJ, Mathew MT. Fretting-corrosion behavior in hip implant modular junctions: The influence of friction energy and pH variation. *Journal of the Mechanical Behavior of Biomedical Materials* 2016;62:570-587.
257. Kurtz S KS, Hanzlik J. Do Ceramic Femoral Heads Reduce Taper Fretting Corrosion in Hip Arthroplasty? A Retrieval Study. *Clinical Orthopaedics and Related Research* 2013;471:3270–3282.
258. Cook SD, Barrack RL, Clemow AJ. Corrosion and wear at the modular interface of uncemented femoral stems. *The Journal of Bone and Joint Surgery. British volume* 1994;76-B(1):68-72.
259. Hothi HS, Matthies AK, Berber R, Whittaker RK, Skinner JA, Hart AJ. The Reliability of a Scoring System for Corrosion and Fretting, and Its Relationship to Material Loss of Tapered, Modular Junctions of Retrieved Hip Implants. *The Journal of Arthroplasty* 2014;29(6):1313-1317.
260. Hothi HS. Response to Letter to the Editor on “Factors Associated With Trunnionosis in the Metal-on-Metal Pinnacle Hip”. *The Journal of Arthroplasty* 2017;32(3):1044-1045.
261. Mathew MT, Runa MJ, Laurent M, Jacobs JJ, Rocha LA, Wimmer MA. Tribocorrosion behavior of CoCrMo alloy for hip prosthesis as a function of loads: A comparison between two testing systems. *Wear* 2011;271(9):1210-1219.
262. Berry DJ, Abdel MP, Callaghan JJ, Members of the Clinical Research G. What are the current clinical issues in wear and tribocorrosion? *Clinical orthopaedics and related research* 2014;472(12):3659-3664.
263. Kwon Y-M, Rossi D, MacAuliffe J, Peng Y, Arauz P. Risk Factors Associated With Early Complications of Revision Surgery for Head-Neck Taper Corrosion in Metal-on-Polyethylene Total Hip Arthroplasty. *The Journal of Arthroplasty* 2018;33(10):3231-3237.
264. Jacobs JJ, Cooper HJ, Urban RM, Wixson RL, Della Valle CJ. What Do We Know About Taper Corrosion in Total Hip Arthroplasty? *The Journal of Arthroplasty* 2014;29(4):668-669.

265. Hussenbocus S, Kosuge D, Solomon LB, Howie DW, Oskouei RH. Head-neck taper corrosion in hip arthroplasty. *BioMed research international* 2015;2015:758123-758123.
266. Langton DJ, Sidaginamale RP, Joyce TJ, Meek RD, Bowsher JG, Deehan D, Nargol AVF, Holland JP. A comparison study of stem taper material loss at similar and mixed metal head-neck taper junctions. *Bone and Joint Journal* 2017;99B(10):1304-1312.
267. ASTM International. NACE/ASTMG193-12d Standard Terminology and Acronyms Relating to Corrosion. West Conshohocken, PA; 2012.
268. Mistry JB, Chughtai M, Elmallah RK, Diedrich A, Le S, Thomas M, Mont MA. Trunnionosis in total hip arthroplasty: a review. *Journal of Orthopaedics and Traumatology* 2016;17(1):1-6.
269. Sultan AA, Cantrell WA, Khlopas A, Berger RJ, Sodhi N, Molloy RM, Krebs VE, Mont MA. Evidence-Based Management of Trunnionosis in Metal-on-Polyethylene Total Hip Arthroplasty: A Systematic Review. *The Journal of Arthroplasty* 2018;33(10):3343-3353.
270. Howie DW, Holubowycz OT, Middleton R, Allen B, Brumby S, Chehade M, Clarnette R, Comley A, Mintz A, Montgomery R and others. Large femoral heads decrease the incidence of dislocation after total hip arthroplasty: A randomized controlled trial. *Journal of Bone and Joint Surgery - Series A* 2012;94(12):1095-1102.
271. Garbuz DS, Masri BA, Duncan CP, Greidanus NV, Bohm ER, Petrak MJ, Della Valle CJ, Gross AE. The Frank Stinchfield Award: Dislocation in Revision THA: Do Large Heads (36 and 40 mm) Result in Reduced Dislocation Rates in a Randomized Clinical Trial? *Clinical Orthopaedics and Related Research®* 2012;470(2):351-356.
272. Witt F, Bosker B, Bishop N, Ettema H, Verheyen C, Morlock M. The relation between titanium taper corrosion and cobalt-chromium bearing wear in large-head metal-on-metal total hip prostheses: a retrieval study. *JBJS* 2014;96(18):e157.
273. Goldberg Jay R, Gilbert Jeremy L. In vitro corrosion testing of modular hip tapers. *Journal of Biomedical Materials Research Part B: Applied Biomaterials* 2002;64B(2):78-93.
274. AltimedJSC. Ceramic femoral head [Available from: http://www.altimed.by/en/products/hips/heads/biolox_delta_head/].
275. Ashkanfar A, Langton DJ, Joyce TJ. Does a micro-grooved trunnion stem surface finish improve fixation and reduce fretting wear at the taper junction of total hip replacements? A finite element evaluation. *Journal of Biomechanics* 2017.
276. Brock TM, Sidaginamale R, Rushton S, Nargol AVF, Bowsher JG, Savisaar C, Joyce TJ, Deehan DJ, Lord JK, Langton DJ. Shorter, rough trunnion surfaces are associated with higher taper wear rates than longer, smooth trunnion surfaces in a contemporary large head metal-on-metal total hip arthroplasty system. *Journal of Orthopaedic Research* 2015;33(12):1868-1874.

277. Pennock AT, Schmidt AH, Bourgeault CA. Morse-type tapers: Factors that may influence taper strength during total hip arthroplasty. *The Journal of Arthroplasty* 2002;17(6):773-778.
278. Ouellette ES, Shenoy AA, Gilbert JL. The seating mechanics of head-neck modular tapers in vitro: Load-displacement measurements, moisture, and rate effects. *Journal of Orthopaedic Research* 2017;36(4):1164-1172.
279. Mali S, Gilbert J. Correlating fretting corrosion and micromotions in modular tapers: test method development and assessment. *Modularity and Tapers in Total Joint Replacement Devices: ASTM International*; 2015.
280. Ford M, Harkess J, Mihalko W. Orthopaedic Surgeon Modularity Utilization and Surgical Technique Considerations in the Face of Implant Corrosion. *Modularity and Tapers in Total Joint Replacement Devices: ASTM International*; 2015.
281. Rehmer A, Bishop NE, Morlock MM. Influence of assembly procedure and material combination on the strength of the taper connection at the head-neck junction of modular hip endoprostheses. *Clinical Biomechanics* 2012;27(1):77-83.
282. Grosso MJ, Jang ES, Longaray J, Buell S, Alfonso E, Shah RP. Influence of Assembly Force and Distraction on the Femoral Head-Taper Junction. *The Journal of Arthroplasty* 2018;33(7, Supplement):S275-S279.
283. Higgs GB, MacDonald DW, Gilbert JL, Rimnac CM, Kurtz SM, Chen AF, Klein GR, Hamlin BR, Lee GC, Mont MA and others. Does Taper Size Have an Effect on Taper Damage in Retrieved Metal-on-Polyethylene Total Hip Devices? *Journal of Arthroplasty* 2016;31(9):277-281.
284. Hothi HS, Whittaker RK, Meswania JM, Blunn GW, Skinner JA, Hart AJ. Influence of stem type on material loss at the metal-on-metal pinnacle taper junction. *Proceedings of the Institution of Mechanical Engineers, Part H: Journal of Engineering in Medicine* 2015;229(1):91-97.
285. Langton DJ, Wells SR, Joyce TJ, Bowsher JG, Deehan D, Green S, Nargol AVF, Holland JP. Material loss at the femoral head taper. *The Bone & Joint Journal* 2018;100-B(10):1310-1319.
286. Hothi HS, Eskelinen AP, Henckel J, Kwon YM, Blunn GW, Skinner JA, Hart AJ. Effect of Bearing Type on Taper Material Loss in Hips From 1 Manufacturer. *Journal of Arthroplasty* 2018;33(5):1588-1593.
287. Landolt D, Mischler S, Stemp M. Electrochemical methods in tribocorrosion: a critical appraisal. *Electrochimica acta* 2001;46(24-25):3913-3929.
288. Mathew M, Uth T, Hallab N, Pourzal R, Fischer A, Wimmer M. Construction of a tribocorrosion test apparatus for the hip joint: validation, test methodology and analysis. *Wear* 2011;271(9-10):2651-2659.

289. Mischler S. Triboelectrochemical techniques and interpretation methods in tribocorrosion: a comparative evaluation. *Tribology International* 2008;41(7):573-583.
290. Barril S, Mischler S, Landolt D. Electrochemical effects on the fretting corrosion behaviour of Ti6Al4V in 0.9% sodium chloride solution. *Wear* 2005;259(1-6):282-291.
291. Barril S, Mischler S, Landolt D. Influence of fretting regimes on the tribocorrosion behaviour of Ti6Al4V in 0.9 wt.% sodium chloride solution. *Wear* 2004;256(9-10):963-972.
292. Schaaff P. The Role of Fretting Damage in Total hip Arthroplasty with Modular Design Hip Joints-Evaluation of Retrieval Studies and Experimental Simulation Methods. *Journal of Applied Biomaterials and Biomechanics* 2004;2(3):121-135.
293. Raji Halimat Y, Shelton Julia C. Prediction of taper performance using quasi static FE models: The influence of loading, taper clearance and trunnion length. *Journal of Biomedical Materials Research Part B: Applied Biomaterials* 2018;0(0).
294. Bobyn J, Tanzer M, J. Krygier J, R. Dujovne A, Emerson Brooks C. Concerns With Modularity in Total Hip Arthroplasty; 1994. 27-36 p.
295. Bhalekar RM, Smith SL, Joyce TJ. Wear at the taper-trunnion junction of contemporary ceramic-on-ceramic hips shown in a multistation hip simulator. *J Biomed Mater Res B Appl Biomater* 2019;107(4):1199-1209.
296. Affatato S, Traina F, Toni A. Microseparation and stripe wear in alumina-on-alumina hip implants. *International Journal of Artificial Organs* 2011;34(6):506-512.
297. Saikko H-GP. Low wear and friction in alumina/alumina total hip joints: A hip simulator study. *Acta Orthopaedica Scandinavica* 1998;69(5):443-448.
298. Ratner BD HA, Schoen FJ. An introduction to materials in medicine. Amsterdam: Elsevier Academic Press; 2004.
299. Langton D, Ahmed I, Avery P, Bone M, Cooke N, Deehan D, Duffy P, Foguet P, Green S, Holland J and others. Investigation of Taper Failure in a Contemporary Metal-on-Metal Hip Arthroplasty System Through Examination of Unused and Explanted Prostheses. *The Journal of bone and joint surgery. American volume* 2017;99(5):427-436.
300. Bhalekar RM, Smith SL, Joyce TJ. Hip simulator testing of the taper-trunnion junction and bearing surfaces of contemporary metal-on-cross-linked-polyethylene hip prostheses. *Journal of Biomedical Materials Research Part B: Applied Biomaterials* 2019;0(0).
301. Clarke IC. Wear of artificial joint materials I. Friction and wear studies: Validity of wear-screening protocols. *Engineering in Medicine* 1981;10(3):115-122.

302. Black J, Hastings GW. Handbook of Biomaterials Properties. UK: Chapman and Hall; 1998.
303. Ammann AA. Inductively coupled plasma mass spectrometry (ICP MS): a versatile tool. *Journal of mass spectrometry* 2007;42(4):419-427.
304. Harrington CF, McKibbin C, Rahanu M, Langton D, Taylor A. Measurement of titanium in hip-replacement patients by inductively coupled plasma optical emission spectroscopy. *Annals of Clinical Biochemistry* 2017;54(3):362-369.
305. Harrison CL, Thomson AI, Cutts S, Rowe PJ, Riches PE. Research Synthesis of Recommended Acetabular Cup Orientations for Total Hip Arthroplasty. *The Journal of Arthroplasty* 2014;29(2):377-382.
306. Kadaba MP, Ramakrishnan HK, Wootten ME. Measurement of lower extremity kinematics during level walking. *Journal of Orthopaedic Research* 1990;8(3):383-392.
307. Isacson J, Gransberg L, Knutsson E. Three-dimensional electrogoniometric gait recording. *Journal of Biomechanics* 1986;19(8):627-635.
308. Calonius O, Saikko V. Force track analysis of contemporary hip simulators. *Journal of Biomechanics* 2003;36(11):1719-1726.
309. Schmalzried TP, Szuszczewicz ES, Northfield MR, Akizuki KH, Frankel RE, Belcher G, Amstutz HC. Quantitative assessment of walking activity after total hip or knee replacement. *Journal of Bone and Joint Surgery - Series A* 1998;80(1):54-59.
310. Saikko V. Effect of Lubricant Protein Concentration on the Wear of Ultra-High Molecular Weight Polyethylene Sliding Against a CoCr Counterface. *Journal of Tribology* 2003;125(3):638-642.
311. Saikko V. A Hip Wear Simulator with 100 Test Stations. *Proceedings of the Institution of Mechanical Engineers, Part H: Journal of Engineering in Medicine* 2005;219(5):309-318.
312. Wang A, Polineni, V. K., Essner, A., Stark, C., Dumbleton, J. H. Quantitative analysis of serum degradation and its effect on the outcome of hip joint simulator wear testing on UHMWPE.; 1999, February; Anaheim, California. p 73.
313. Bone MC, Sidaginamale RP, Lord JK, Scholes SC, Joyce TJ, Nargol AVF, Langton DJ. Determining material loss from the femoral stem trunnion in hip arthroplasty using a coordinate measuring machine. *Proceedings of the Institution of Mechanical Engineers, Part H: Journal of Engineering in Medicine* 2015;229(1):69-76.
314. Al-Hajjar M, Fisher J, Ltipper J, Williams S, Jennings LM. Wear of 36-mm BIOLOX delta ceramic-on-ceramic bearing in total hip replacements under edge loading conditions. *Proceedings of the Institution of Mechanical Engineers, Part H: Journal of Engineering in Medicine* 2013;227(5):535-542.
315. Lord JK, Langton DJ, Nargol AVF, Joyce TJ. Volumetric wear assessment of failed metal-on-metal hip resurfacing prostheses. *Wear* 2011;272(1):79-87.

316. Hutchings I, Shipway P. 2 - Surface topography and surfaces in contact. In: Hutchings I, Shipway P, editors. *Tribology (Second Edition)*: Butterworth-Heinemann; 2017. p 7-35.
317. ISO25178-2. Geometrical product specifications (GPS). Surface texture. Areal. Terms, definitions and surface texture parameters. Geneva, Switzerland: International Organization for Standardization (ISO); 2012.
318. ISO4288. Geometric Product Specification (GPS) — Surface texture — Profile method: Rules and procedures for the assessment of surface texture ICS. Geneva, Switzerland: International Organization for Standardization (ISO); 1998.
319. Joyce TJ, Langton DJ, Jameson SS, Nargol AVF. Tribological analysis of failed resurfacing hip prostheses and comparison with clinical data. *Proceedings of the Institution of Mechanical Engineers, Part J: Journal of Engineering Tribology* 2009;223(3):317-323.
320. Deng M, Uhrich KE. Viscoelastic Behaviors of Ultrahigh Molecular Weight Polyethylene Under Three-Point Bending and Indentation Loading. *Journal of Biomaterials Applications* 2010;24(8):713-732.
321. Milošev L, Antolič V, Minović A, Cör A, Herman S, Pavlovčič V, Campbell P. Extensive metallosis and necrosis in failed prostheses with cemented titanium-alloy stems and ceramic heads. *Journal of Bone and Joint Surgery - Series B* 2000;82(3):352-357.
322. Stachowiak GB, Stachowiak GW. Fretting wear and friction behaviour of engineering ceramics. *Wear* 1995;190(2):212-218.
323. Kyomoto M, Shoyama Y, Saiga K, Moro T, Ishihara K. Reducing fretting-initiated crevice corrosion in hip simulator tests using a zirconia-toughened alumina femoral head. *Journal of Biomedical Materials Research Part B: Applied Biomaterials* 2017;0(0).
324. Karimi S, Nickchi T, Alfantazi A. Effects of bovine serum albumin on the corrosion behaviour of AISI 316L, Co–28Cr–6Mo, and Ti–6Al–4V alloys in phosphate buffered saline solutions. *Corrosion Science* 2011;53(10):3262-3272.
325. Kurtz SM, MacDonald DW, Gilbert JL, Mont MA, Klein G, Chen A, Kraay M, Hamlin B, Rimnac CM. Is taper fretting corrosion a threat to the clinical performance of large-diameter hips with highly crosslinked polyethylene bearings? ; 2015. p 45-58.
326. Craig P, Bancroft G, Burton A, Collier S, Shaylor P, Sinha A. Raised levels of metal ions in the blood in patients who have undergone uncemented metal-on-polyethylene Trident–Accolade total hip replacement. *The Bone & Joint Journal* 2014;96-B(1):43-47.
327. Zeng P, Rainforth WM, Cook RB. Characterisation of the oxide film on the taper interface from retrieved large diameter metal on polymer modular total hip replacements. *Tribology International* 2015;89:86-96.

328. Van Citters DW, Martin AJ, Currier JH, Park SH, Edidin AA. Factors related to imprinting corrosion in modular head-neck junctions. In: Greenwald A, Kurtz S, Lemons J, Mihalko W, editors. *Modularity and Tapers in Total Joint Replacement Devices*, STP1591. West Conshohocken, PA: ASTM Special Technical Publication; 2015. p 83-98.
329. Pourzal R, Hall D, Lundberg H, Mathew MT, Urban R, Jacobs J. The impact of micro-motion and micro-structure on modular junction corrosion in hip arthroplasties *Orthopaedic Proceedings* 2019;101-B(SUPP_4):104-104.
330. Pourzal R, Hall DJ, Ehrich J, McCarthy SM, Mathew MT, Jacobs JJ, Urban RM. Alloy Microstructure Dictates Corrosion Modes in THA Modular Junctions. *Clinical orthopaedics and related research* 2017;475(12):3026-3043.
331. Hall D, McCarthy S, Ehrich J, Urban R, Fischer A, Jacobs J, Lundberg H, Pourzal R. Imprinting and Column Damage on CoCrMo Head Taper Surfaces in Total Hip Replacements. *Imprinting and Column Damage on CoCrMo Head Taper Surfaces in Total Hip Replacements*; 2018.
332. Landolt D, Mischler S, Stemp M. Electrochemical methods in tribocorrosion: a critical appraisal. *Electrochimica Acta* 2001;46(24):3913-3929.
333. Landolt D, Mischler S, Stemp M, Barril S. Third body effects and material fluxes in tribocorrosion systems involving a sliding contact. *Wear* 2004;256(5):517-524.
334. Mathew MT, Srinivasa Pai P, Pourzal R, Fischer A, Wimmer MA. Significance of Tribocorrosion in Biomedical Applications: Overview and Current Status. *Advances in Tribology* 2009;2009:12.
335. Dyrkacz RMR, Brandt JM, Ojo OA, Turgeon TR, Wyss UP. The influence of head size on corrosion and fretting behaviour at the head-neck interface of artificial hip joints. *Journal of Arthroplasty* 2013;28(6):1036-1040.
336. Puente Reyna AL, Jäger M, Floerkemeier T, Frecher S, Delank KS, Schilling C, Grupp TM. Backside Wear Analysis of Retrieved Acetabular Liners with a Press-Fit Locking Mechanism in Comparison to Wear Simulation In Vitro. *BioMed research international* 2016;2016:8687131.
337. Kurtz SM, Ochoa JA, Hovey CB, White CV. Simulation of initial frontside and backside wear rates in a modular acetabular component with multiple screw holes. *Journal of Biomechanics* 1999;32(9):967-976.
338. Hartmann A, Hannemann F, Lützner J, Seidler A, Drexler H, Günther KP, Schmitt J. Metal Ion Concentrations in Body Fluids after Implantation of Hip Replacements with Metal-on-Metal Bearing - Systematic Review of Clinical and Epidemiological Studies. *PLoS ONE* 2013;8(8).
339. Langton DJ, Sidaginamale RP, Joyce TJ, Natu S, Blain P, Jefferson RD, Rushton S, Nargol AVF. The clinical implications of elevated blood metal ion concentrations in asymptomatic patients with MoM hip resurfacings: a cohort study. *BMJ Open* 2013;3(3).

340. Dalal A, Pawar V, McAllister K, Weaver C, Hallab NJ. Orthopedic implant cobalt-alloy particles produce greater toxicity and inflammatory cytokines than titanium alloy and zirconium alloy-based particles in vitro, in human osteoblasts, fibroblasts, and macrophages. *Journal of Biomedical Materials Research - Part A* 2012;100 A(8):2147-2158.
341. Daley B, Doherty AT, Fairman B, Case CP. Wear debris from hip or knee replacements causes chromosomal damage in human cells in tissue culture. *Journal of Bone and Joint Surgery - Series B* 2004;86(4):598-606.
342. Angle CR. 4 - Organ-Specific Therapeutic Intervention. In: Goyer RA, Klaassen CD, Waalkes MP, editors. *Metal Toxicology*. Boston: Academic Press; 1995. p 71-110.
343. Haynes DR, Rogers SD, Hay S, Percy MJ, Howie DW. The differences in toxicity and release of bone-resorbing mediators induced by titanium and cobalt-chromium-alloy wear particles. *Journal of Bone and Joint Surgery - Series A* 1993;75(6):825-834.
344. Joyce TJ, Smith SL, Rushton PRP, Bowey AJ, Gibson MJ. Analysis of Explanted Magnetically Controlled Growing Rods From Seven UK Spinal Centers. *Spine* 2018;43(1):E16-E22.
345. Gofton W, Beaulé PE. Serum Metal Ions with a Titanium Modular Neck Total Hip Replacement System. *The Journal of Arthroplasty* 2015;30(10):1781-1786.
346. Levine BR, Hsu AR, Skipor AK, Hallab NJ, Paprosky WG, Galante JO, Jacobs JJ. Ten-Year Outcome of Serum Metal Ion Levels After Primary Total Hip Arthroplasty: A Concise Follow-up of a Previous Report*. *JBJS* 2013;95(6):512-518.
347. Nam D, Keeney JA, Nunley RM, Johnson SR, Clohisy JC, Barrack RL. Metal Ion Concentrations in Young, Active Patients Following Total Hip Arthroplasty with the Use of Modern Bearing Couples. *The Journal of Arthroplasty* 2015;30(12):2227-2232.
348. McMinn D. The McMinn Centre- New Materials for Hip Resurfacing: Why choose X-linked poly on metal? Volume 2019; 2018.
349. Parkes M, Myant C, Cann PM, Wong JSS. The effect of buffer solution choice on protein adsorption and lubrication. *Tribology International* 2014;72:108-117.
350. Wassef AJ, Schmalzried TP. Femoral taperosis: an accident waiting to happen? *The bone & joint journal* 2013;95 B(11 Suppl A):3-6.

Appendix A

Protocol for the cleaning and weighing procedures

Disassemble all THR samples from the hip simulator. Following steps should be followed for gravimetric measurement procedure.

1. Wear blue nitrile gloves from here

- i) Vibrate for **10** min in deionised water;
- ii) Rinse in deionised water;
- iii) Vibrate for **10** min in 100 mL of ultrasonic cleaner and 500 mL of deionised water;
- iv) Rinse in deionised water;
- v) Vibrate for **10** min in deionised water;
- vi) Rinse in deionised water;
- vii) Vibrate for **3** min in deionised water;
- viii) Rinse in deionised water.

Note:

- If ceramic samples are used for hip simulator testing, then use Sidol cleaner (as per CeramTec instructions) to remove any visual marking seen at the ceramic femoral tapers and the backside of the ceramic liners before above-mentioned steps.

2. Wear indigo nitrile gloves from here

- i) Dry all samples carefully using lint-free tissue;
- ii) Dry all samples with a jet of filtered inert gas;
- iii) Soak isopropanol for 5 min \pm 15 sec;
- iv) Dry all samples carefully using lint-free tissue;
- v) Dry all samples with a jet of filtered inert gas;
- vi) Air dry all samples for 30 mins;
- vii) Dry all samples with a jet of filtered inert gas;
- viii) Weigh all samples in order, taking a minimum of 3 readings for each sample, blast with a jet of filtered inert gas before placing in balance.

3. Lubricant bath and hip simulator components cleaning

- i) Wash all hip simulator components and polymeric casings in tap water with detergent. Items can be scrubbed gently with cloth or plastic bristle brush;
- ii) Rinse in tap water, ensuring the detergent is removed completely;
- iii) Rinse in deionised water;
- iv) Allow to dry.

Appendix B

A protocol for the geometric wear measurement of the femoral tapers and trunnions using the coordinate measuring machine

A coordinate measuring machine (CMM, Legex 322, Mitutoyo, UK) in combination with a custom-designed MATLAB program (MathWorks) were used for geometric wear analysis of the taper-trunnion junction. A 0.5mm ruby probe was used throughout the project. The CMM uses MCOSMOS, (Mitutoyo) software for scanning of the femoral tapers and trunnions, with the help of customised “2016 Taper scan” and “Trunnions” program respectively. Each specimen was scanned for a minimum of three times for repeatability.

Both programs work in the following three stages:

Stage 1: Identification of the first coordinate system.


Stage 2: Generation of a perfect theoretical cone representing the original perfect unworn surface (either femoral taper or trunnion)


Stage 3: Measurement of the entire surface and comparison the data points with the perfect cone to determine any deviations, which represent volumetric wear.

Appendix C


Bhalekar RM, Smith SL, Joyce TJ. “Wear at the taper-trunnion junction of contemporary ceramic-on-ceramic hips shown in a multistation hip simulator.” *Journal of Biomedical Materials Research Part B Applied Biomaterials*. 2019;107(4):1199-209.

**Journal of
Biomedical Materials Research**
PART B APPLIED BIOMATERIALS

Society For
Biomaterials


Original Research Report |  Full Access




Wear at the taper-trunnion junction of contemporary ceramic-on-ceramic hips shown in a multistation hip simulator

Rohan M. Bhalekar, Simon L. Smith, Thomas J. Joyce 

First published: 05 September 2018 | <https://doi.org/10.1002/jbm.b.34213> | Cited by: 1

[Find @ Newcastle University](#)

 SECTIONS

 PDF  TOOLS  SHARE

Abstract

Ceramic-on-ceramic (CoC) total hip replacements (THR) have a substantially lower wear rate than metal-on-polyethylene (MoP) hips, as shown by hip simulator testing. However, the revision rates of CoC and MoP hips are comparable. To try and explain this discrepancy the wear, at both the bearing surfaces and taper-trunnion interface of 36 mm BIOLOX Δ CoC THRs, mounted on 12/14 titanium (Ti6Al4V) trunnions was investigated using a hip simulator ($n = 3$) and a dynamically loaded CoC sample in a separate test station. Wear was assessed gravimetrically and surface roughness measurements of the articulating and taper surfaces taken at regular intervals. Scanning electron microscopy, surface roughness, and gravimetric measurements of trunnions was performed. After 5 million cycles, the mean total wear from the ceramic articulating surfaces was 0.25 mm³ from the hip simulator test, and that from the titanium trunnions was 0.29 mm³. This metal wear may provide an explanation for adverse reaction to metal debris found in contemporary CoC hip joints. It is therefore vital to consider taper-trunnion wear in preclinical testing of artificial hip joints. © 2018 Wiley Periodicals, Inc. *J Biomed Mater Res Part B: Appl Biomater* 107B: 1199–1209, 2019.

Available online: <https://onlinelibrary.wiley.com/doi/full/10.1002/jbm.b.34213>

Appendix D

Bhalekar RM, Smith SL, Joyce TJ. “Hip simulator testing of the taper-trunnion junction and bearing surfaces of contemporary metal-on-cross-linked-polyethylene hip prostheses.”
Journal of Biomedical Materials Research Part B Applied Biomaterials. 2019;0(0). (in press)

**Journal of
Biomedical Materials Research**
PART B APPLIED BIOMATERIALS

Society For
Biomaterials

Original Research Report |  Full Access |

Hip simulator testing of the taper-trunnion junction and bearing surfaces of contemporary metal-on-cross-linked-polyethylene hip prostheses

Rohan M. Bhalekar, Simon L. Smith, Thomas J. Joyce 

First published: 29 March 2019 | <https://doi.org/10.1002/jbm.b.34374>

Find @ Newcastle University

All authors have read and approved the final submitted manuscript.
This article is published with the permission of the Controller of HMSO and the Queen's Printer for Scotland.

 SECTIONS  PDF  TOOLS  SHARE

Abstract

Adverse reaction to metal debris released from the taper-trunnion junction of modular metal-on-polyethylene (MoP) total hip replacements (THRs) is an issue of contemporary concern. Therefore, a hip simulator was used to investigate material loss, if any, at both the articulating and taper-trunnion surfaces of five 32-mm metal-on-cross-linked-polyethylene THRs for 5 million cycles (Mc) with a sixth joint serving as a dynamically loaded soak control. Commercially available cobalt-chromium-molybdenum femoral heads articulating against cross-linked polyethylene (XLPE) acetabular liners were mounted on 12/14 titanium (Ti6Al4V) trunnions. Weight loss (mg) was measured gravimetrically and converted into volume loss (mm^3) for heads, liners, and trunnions at regular intervals. Additionally, posttest volumetric wear measurements of the femoral tapers were obtained using a coordinate measuring machine (CMM). The surface roughness (S_a) of femoral tapers was measured posttest. After 5 Mc, the mean volumetric wear rate for XLPE liners was $2.74 \pm 0.74 \text{ mm}^3/\text{Mc}$. The CMM measurements confirmed material loss from the femoral taper with the mean volumetric wear rate of $0.045 \pm 0.024 \text{ mm}^3/\text{Mc}$. The S_a on the worn area of the femoral taper showed a significant increase ($p < 0.001$) compared with the unworn area. No other long-term hip simulator tests have investigated wear from the taper-trunnion junction of contemporary MoP THRs. © 2019 Wiley Periodicals, Inc. J Biomed Mater Res Part B, 2019.

Available online: <https://onlinelibrary.wiley.com/doi/10.1002/jbm.b.34374>